UNCLASSIFIED

AD 431661

DEFENSE DOCUMENTATION CENTER

FOR

SCIENTIFIC AND TECHNICAL INFORMATION

CAMERON STATION, ALEXANDRIA, VIRGINIA

UNCLASSIFIED

QUARTERLY PROGRESS REPORT

No. 72

JANUARY 15, 1964

MASSACHUSETTS INSTITUTE OF TECHNOLOGY
RESEARCH LABORATORY OF ELECTRONICS
CAMBRIDGE, MASSACHUSETTS

The Research Laboratory of Electronics is an interdepartmental laboratory in which faculty members and graduate students from numerous academic departments conduct research.

The research reported in this document was made possible in part by support extended the Massachusetts Institute of Technology, Research Laboratory of Electronics, jointly by the U.S. Army (Signal Corps), the U.S. Navy (Office of Naval Research), and the U.S. Air Force (Office of Scientific Research), under Signal Corps Contract DA36-039-sc-78108, Department of the Army Task 3-99-25-001-08; and in part by Grant DA-SIG-36-039-61-G14.

Partial support for work in Plasma Dynamics is provided by the U.S. Atomic Energy Commission under Contract AT(30-1)-1842; the National Science Foundation (Grant G-24073); the U.S. Air Force (Electronic Systems Division) under Contract AF 19(604)-5992; and the U.S. Air Force (Aeronautical Systems Division) under Contract AF 33(615)-1083.

Partial support for work in Communication Sciences is provided by the National Science Foundation (Grant G-16526), the National Institutes of Health (Grant MH-04737-03), and the National Aeronautics and Space Administration (Grant NsG-496).

Additional support of specific projects is acknowledged in footnotes to the appropriate sections.

MASSACHUSETTS INSTITUTE OF TECHNOLOGY

RESEARCH LABORATORY OF ELECTRONICS

QUARTERLY PROGRESS REPORT No. 72

January 15, 1964

Submitted by: H. J. Zimmermann
G. G. Harvey

TABLE OF CONTENTS

CONTENTS

CONTENTS

COMMUNICATION SCIENCES AND ENGINEERING

CONTENTS

PERSONNEL

Administration

Professor H. J. Zimmermann, Director
Professor G. G. Harvey, Associate Director
Mister R. A. Sayers, Personnel and Business Manager

Advisory Committee

Dean G. S. Brown (Ex officio)
Professor W. W. Buechner
Professor W. B. Davenport, Jr.
Professor P. Elias
Professor G. G. Harvey
Professor A. G. Hill
Professor I. W. Sizer
Professor H. J. Zimmermann (Chairman)

R. L. E. Research Committee

Professor H. J. Zimmermann (Chairman)
Professor S. C. Brown
Professor L. J. Chu
Professor R. M. Fano
Professor M. Halle
Professor G. G. Harvey
Mister R. A. Sayers
Professor W. M. Siebert
Professor L. D. Smullin
Professor M. W. P. Strandberg
Professor P. D. Wall
Professor J. R. Zacharias

Faculty

Algazi, V. R.
Allis, W. P. (Absent)
Arden, D. N.
Barrett, A. H.
Bekefi, G.
Bers, A.
Billman, K. W.
Bitter, F.
Bose, A. G.
Brazier, Mary A. B. (Visiting)
Brown, G. A.
Brown, S. C.
Carabateas, E. N.
Chomsky, A. N.
Chu, L. J.
Cooper, R. S.
Dennis, J. B.
Dupree, T. H.
Eden, M.
Edgerton, H. E.
Elias, P.
Fano, R. M.
Fiocco, G.
Fodor, J. A.
Freedman, S. I.
Gallager, R. G.
Garland, C. W. (Absent)
Getty, W. D.
Graham, J. W.
Gyftopoulos, E. P.
Hall, J. L., II
Halle, M.
Hammes, G. G.
Harvey, G. G.
Hatsopoulos, G. N. (Absent)
Haus, H. A.
Heinz, J. M.
Heiser, W. H.
Hennie, F. C., III
Hill, A. G.
Hoffman, M. A.
Huang, T. S.
Ingard, K. U.
Jackson, W. D.
Jacobs, I. M.
Jakobson, R.
Katz, J. J.
Kerrebrock, J. L.
King, J. G.
Kinsey, J. L.
Klima, E. S.
Kyhl, R. L.
Lee, H. B.
Lee, Y. W.
Lettvin, J. Y.
Lidsky, L. M.
Liu, C. L.
Manders, A. M.
Mason, S. J.
Matthews, G. H.
McCune, J. E.
Meissner, H. P.
Minsky, M. L.
More, T., Jr.
Nottingham, W. B.
Oates, G. C.
Peake, W. T.
Penfield, P. L., Jr.
Penhune, J. P.
Perry, C. H.
Pfeiffer, R. R.
Postal, P.
Putnam, H.
Rafuse, R. P.
Reiffen, B. (Visiting)

PERSONNEL

Faculty (continued)

Reynolds, J. M.
Rose, D. J.
Rosenblith, W. A.
Ruina, J. P.
Samuel, A. L. (Visiting)
Schetzen, M.
Schreiber, W. F.
Schwab, W. C.
Searle, C. L.
Shannon, C. E.
Shapiro, A. H.
Siebert, W. M.
Smith, J. L., Jr.
Smullin, L. D.
Stevens, K. N.
Stickney, R. E.
Stiglitz, I. C.
Stockham, T. G., Jr.
Strandberg, M. W. P.
Teager, H. M.
Thornton, R. D.
Tretiak, O. J.
Troxel, D. E.
Van Trees, H. L.
Wall, P. D.
Warren, B. E.
Waugh, J. S. (Absent)
Weiss, T. F.
Whitehouse, D. R.
Wozencraft, J. M.
Young, L. R.
Zacharias, J. R.
Zimmermann, H. J.

Instructors

Alter, R.
Andersen, J.
Briggs, R. J.
Bruce, J. D.
Crystal, T. H. (Absent)
Dean, L. W., III
East, D. A.
Gray, P. R.
Huibonhoa, R.
Ingraham, J. C.
Katona, P. G.
Kincaid, T. G.
Kliman, G. B.
Koskinen, M. F.
Krishnayya, J. G. (Absent)
Landsman, E.
MacDonald, J. S.
Oppenheim, A. V.
Parente, R. B.
Perlmutter, D. M.
Pierson, E. S.
Shavit, A.
Spann, R. N.

Lecturers

Ferretti, E. F.
Goldstein, M. H., Jr. (Visiting)
Pitts, W. H.
Rines, R. H.

Research Associates

Barlow, J. S.
Bishop, P. O.
Cerrillo, M. V.
Dupress, J.
Durlach, N. I.
Edmonds, P.
Gesteland, R. C.
Hall, R. D.
Hermann, H. T.
House, A. S.
Jones, M. E.
Kilmer, W. L.
Reifenstein, E. C., III
Stark, L.
Szekely, G.
Thompson, E.
Yngve, V. H.

Staff Members

Andrews, John M., Jr.
Badessa, R. S.
Bates, V. J.
Bosche, Carol M.
Breon, R. K.
Brown, R. M.
Campbell, Elizabeth J.
Charney, Elinor K.
Clark, W. A., Jr. (Lincoln Laboratory)
Congleton, Ann
Crist, A. H.
Darlington, J. L.
Duffy, D. F.
Edwards, D. J.
Farley, B. G. (Lincoln Laboratory)
Gerstein, G. L.
Giberman, E.
Goodall, M. C.
Harrison, M. C.
Hewitt, J. H.
Howland, B. H. (Lincoln Laboratory)
Ingersoll, J. G.
Ingham, K. R.
Isami, Y.
Jordan, F. N.
Kannel, Muriel
Kerllenevich, N.

Staff Members (continued)

Keyes, R. V., Jr.
Kiang, N. Y-S.
Kierstead, J. D.
Kuiper, J. W.
Langbein, D.
Levin, M. I.
Levy, Rachel J.
Lindsley, V. Susan
Maling, G. C., Jr.
Marceau, C.
McCarthy, J. J.
McCulloch, W. S.
Mulligan, W. J.

O'Brien, F. J.
Öhman, S. E. G. (Fellow of the Sweden-America Foundation)
O'Rourke, Ann M.
Palfy, M. A.
Papert, S.
Pennell, Martha M.
Percival, W. K.
Pitts, W. H.
Rosebury, F.

Ryan, L. W.
Saltalamacchia, A. J.
Sandel, T. T. (Lincoln Laboratory)
Sayers, R. A.
Smith, P. L.
Thomas, Helen L.
Vidale, Eda B.
Viertel, J. J.
Vlaardingerbroek, M. T.
Weingrad, J. S.
Wendt, R. H.
Willke, H. L., Jr.

Visitors

Baldwin, H. A.
Bendall, L. K. (Postdoctoral Fellow – Social Science Research Council Study Fellow)
Chayen, M. J. (Visiting Scholar)
Cunningham, J. E.
Fohl, T.
Frenk, S. (Postdoctoral Fellow of the John Simon Guggenheim Memorial Foundation)
Hancox, R.
Huggins, A. W. F. (R. L. E. Postdoctoral Fellow)
Ikushima, K.
Keyser, S. J.

Kornacker, K. (Postdoctoral Fellow of the National Institutes of Health)
Lehtinen, Meri (Visiting Scholar)
Lindblom, B. E. F. (Fellow of the Wenner-Bren Foundation for Anthropological Research)
Menyuk, Paula (Postdoctoral Fellow of the National Institutes of Health)
Molnar, C. E.
Moore, G. P. (Postdoctoral Fellow of the National Academy of Science)

Nadezhkin, V. V. (Visiting Scholar)
Pickard, W. F. (Postdoctoral Fellow of the National Institutes of Health)
Prange, E. A.
Rondeau, G.
Schiff, Helga (Postdoctoral Fellow – German Scientific Research Fellowship)
Tinkham, M.
Walker, D. E.
Weksel, W. (Postdoctoral Fellow of the National Science Foundation)
Wu, K. (R. L. E. Postdoctoral Fellow)

Graduate Students

Allen, R. J.
Andrews, M. L.
Arunasalam, V.
Axelrod, F. S.
Badrawi, M. T.
Baecker, R. M. (National Science Foundation Fellow)
Bar-David, I. (Israel Government Fellow)
Bartsch, R. R. (Teaching Assistant)
Bauer, R. F.

Berlekamp, E. R. (National Science Foundation Fellow)
Bever, T. G.
Black, W. L. (RCA Fellow)
Blum, M.
Bobrow, D. G.
Botha, D. G.
Brassert, W. L.
Breeding, R. J.
Brown, T. S.
Buntschuh, C. D.
Burns, S. K. (Teaching Assistant)

Bush, A. M.
Cahlander, D. A.
Capranica, R. R. (Communications Development Training Program Fellow of Bell Telephone Laboratories, Inc.)
Carson, J. F.
Chandra, A. N.
Chapman, J. C.
Chessman, M.
Clarke, J. F.
Clayton, R. J.

Graduate Students (continued)

Clemens, J. K.
Coccoli, J. D.
Coggins, J. L.
Colburn, H. S. (National Science Foundation Fellow)
Collins, L. D. (National Science Foundation Fellow)
Crimi, G. F.
Cuvaj, C.
Dethlefsen, R.
Diamond, B. L.
Disbrow, J. R. (Teaching Assistant)
Domen, J. K.
Donaldson, R. W. (Teaching Assistant)
Dunn, F. E. (National Science Foundation Fellow)
Dym, H.
Ebert, P. M. (National Science Foundation Fellow)
Edwards, R. K.
Ellis, J. R., Jr.
Epstein, M. R.
Erman, J. E.
Evans, S. A.
Falconer, D. D.
Fessenden, T. J.
Fetz, E. E.
Flannery, D. L. (General Motors Fellow)
Fleury, P. A. (National Science Foundation Fellow)
Forney, G. D., Jr. (National Science Foundation Fellow)
Fraser, J. B.
Froeschle, T. A.
Fukomoto, A.
Gadzuk, J. W.
Garosi, G. A.
Gaut, N. E. (NASA Fellow)
Gentle, K. W. (National Science Foundation Fellow)
Gerry, E. T.
Ghosh, S. K.
Glaser, J. (National Science Foundation Fellow)
Glenn, W. H., Jr. (Hughes Aircraft Fellow)
Golub, R.
Graham, D. N. (Teaching Assistant)
Gramenopoulos, N. (Teaching Assistant)
Grams, G. W. (Ford Fellow)
Grayzel, A. I.
Greata, J. M. (Teaching Assistant)
Greenblatt, S. (Teaching Assistant)
Gronemann, U. F.
Guinan, J. J., Jr. (National Science Foundation Fellow)
Guttrich, G. L.
Hall, Barbara C. (National Science Foundation Fellow)
Halverson, W. D.
Hart, T. P.
Hartenbaum, B. A.
Hegblom, E. R.
Henke, W. L. (Teaching Assistant)
Heywood, J. B.
Holsinger, J. L.
Hooper, E. B., Jr.
Hsi, C-F. G. (U.S. AEC Fellow)
Hsieh, H. Y.
Ivie, E. L. (Teaching Assistant)
Iwadare, Y. (RCA Fellow)
Jameson, P. W.
Johnston, W. D., Jr.
Kachen, G. I., Jr. (U.S. AEC Fellow)
Kellen, P. F.
Kinzer, T. J., III (National Defense Education Act Fellow)
Kiparsky, R. P. V.
Kniazzeh, A. G. F.
Kocher, D. G.
Koerber, K. C.
Koons, H. C.
Kronquist, R. L.
Kukolich, S. G.
Kuroda, S. Y. (Whitney Fellow)
Kurtz, D. C.
Kusse, B. R.
Langendoen, D. T.
Lee, K. S.
Lenoir, W. B. (Teaching Assistant)
Lercari, R. F.
Levine, R. C. (Teaching Assistant)
Levison, W. H.
Lewis, T. B.
Lieberman, M. A. (National Science Foundation Fellow)
Lightner, T. M. (National Defense Foreign Language Fellow)
Little, R. G.
Llewellyn-Jones, D. T.
Lou, D. Y-S.
Lubin, B. T.
Lutz, M. A.
Maidique, M. A.
Manheimer, W. M.
Mark, R. G.
Marks, R. E. (Teaching Assistant)
Mattison, E. M.
Mayo, J. W.
McCawley, J. D. (National Science Foundation Fellow)
McMorris, J. A., II
McNary, C. A.
Mendell, L.
Mermelstein, P.
Michael, J. A. (Public Health Service Fellow)
Mills, J. D.
Moran, J. M., Jr. (Sloan Fellow)
Morse, D. L.
Moses, J.
Mozzi, R. L.
Murphy, R. A. (National Science Foundation Fellow
Nelsen, D. E.
Niessen, C. W. (National Science Foundation Fellow)
Nolan, J. J., Jr. (Teaching Assistant)
Norton, L. M.
Nowak, R. T.

Graduate Students (continued)

Offenberger, A. A. (Whitney Fellow)
Olsen, J. H.
Otte, R. F.
Patt, M. A. (RCA Fellow)
Pauwels, H. J. E. H. (Belgium-American Educational Foundation Fellow)
Peters, P. S., Jr.
Petrie, L. M., Jr.
Pilc, R. (Bell Telephone Laboratories Fellow)
Pollak, R. K.
Porter, R. P.
Prabhu, V. K. (Teaching Assistant)
Pruslin, D. H.
Puri, S. (Teaching Assistant)
Qualls, C. B.
Redi, O.
Renard, R. H.
Reznek, S. R.
Rich, M. A.
Rizzo, J.
Robertson, C. G.
Rogers, A. E. E.
Rogoff, G. L.
Rook, C. W., Jr.
Rosenbaum, P. S.
Rowe, A. W.
Sachs, M. B. (Teaching Assistant)
Sandberg, A. A.
Savage, J. E.
Schaffer, M. J. (National Science Foundation Fellow)
Schane, S. A. (Teaching Assistant)
Schneider, H. M. (Teaching Assistant)
Schuler, C. J., Jr.
Shah, J. C.
Shimony, U.
Simon, R. W.
Simpson, J. I.
Sklar, J. R.
Slater, T. S.
Smythe, D. L., Jr. (Teaching Assistant)
Snow, K. D. (Teaching Assistant)
Solbes, A.
Spangler, P. S.
Spoor, J. H.
Staelin, D. H.
Stanley, R. J. (National Science Foundation Fellow)
Steele, D. W.
Steinbrecher, D. H.
Stewart, C. C.
Strahm, N. D. (National Science Foundation Fellow)
Sutherland, W. R. (National Science Foundation Fellow)
Taub, A. (National Institutes of Health Fellow)
Taylor, M. G.
Theodoridis, G.
Thomae, I. H. (National Science Foundation Fellow)
Thornburg, C. O., Jr.
Tomlinson, R. S.
Tse, F. Y-F.
T'sou, C. L.
Turner, J. H. (I. T. T. Fellow)
Ulvang, W. F.
Vanderweil, R. G.
Wagner, C. E.
Ward, R. L. (IBM Fellow)
Wiener, S. D. (National Science Foundation Fellow)
Welch, J. R.
Whitman, E. C.
Wickelgren, Barbara G. (National Science Foundation Fellow)
Wiederhold, M. L.
Wien, G. E.
Winett, J. M.
Wissmiller, J. C.
Witting, H. L.
Witting, J. M. (I. T. T. Fellow)
Woo, J. C.
Wright, B. L. (National Science Foundation Fellow)
Yarnell, C. F.
Yudkin, H. L.
Zeidenbergs, J. (Sperry Fellow)
Zeiders, G. W., Jr.
Zieger, H. P.
Zuber, B. L.
Zwicky, A. M., Jr. (National Defense Education Act Fellow)

Undergraduates

Aaron, A. M.
Brincko, A. J.
Broadley, W. H.
Brown, P. B.
Buckman, A. B.
Carpenter, R. A.
Chang, G. D. Y.
Chang, K.
Cheng, J.
Chiodi, W. R.
Deininger, C. C.
Der Sarkisian, S. F.
Eggers, T. W.
Elliot, J. L.
Gibson, E. J.
Gill, G. Y.
Haney, D. L.
Jensen, E. R.
Keiser, K. K.
Kalman, J. S.
Knobe, B. S.
Luconi, F.
Mann, C. A., Jr.
Moxon, E. C.
Norris, P. E.
Norris, R. B., Jr.
O'Halloran, W. F., Jr.
Perrolle, P. M.
Pettigrew, D. D., Jr.
Politzer, P. A.
Sanders, R. D.
Schmidt, R. A., Jr.
Shook, G. K., II
Siemens, P. J.
Smith, D. P., Jr.
Stampfel, J. P., Jr.
Steele, G. R.
Walpert, G. A.
Wan, A. C. M.
Weidner, M. Y.

PERSONNEL

Senior Thesis Students

Abzug, C.
Alusic, D. J.
Barron, M. B.
Bennett, J. G.
Bowman, H. W.
Brown, D. G.
Brownell, J. H.
Burnett, G. J.
Chrisman, B. L.
Clay, A. W. W., Jr.
Coldwell, J. A.
Diamond, S. M.
Erickson, S. A., Jr.
Fertel, Jeanne H.
Friedlander, S. B.
Gallant, J. M.
Gerhart, D. E.
Greenberg, A. J.
Harlem, G. S.
Hawk, T. L.
Herbert, T. J.
Hirsch, M. S.
Irwin, G. M.
Katyl, R. H.
Laurence, C. L.
Lipes, R. G.
McCarthy, D. J.
McCowan, D. W.
McGaughy, J. P., Jr.
Moter, J. T.
Murray, M. J.
Ng, L. C.
Okereke, S. A.
Pappalardo, A. N.
Prather, J. F.
Savin, N. J.
Shulsinger, A.
Smith, D. F.
Staecker, P. W.
Sterling, S. A.
Strober, Janet K.
Teich, A. H.
Veneklasen, L. H.
Wactlar, H. A.
Weinstein, A. A.
Yuille, D. L.

Assistants and Technicians

Aquinde, P.
Arnold, Jane B.
Babcock, E. B.
Barrett, J. W.
Barrows, F. W.
Beaton, Catherine M.
Bella, C. J.
Berg, A. E.
Booker, D. M. M.
Butler, R. E., Jr.
Chase, Arbella P.
Colby, Betsy F.
Connolly, J. T.
Cook, J. F.
Cranmer, R. E.
Crist, F. X.
DiPietro, P. J.
Engler, R. R.
Fitzgerald, E. W., Jr.
Fontaine, C. L.
Gay, H. D.
Grande, Esther D.
Greenwood, E. L.
Gregor, C. A.
Haywood, K. A.
Karas, P.
Kelly, M. A.
Kirkpatrick, Patti I.
Lewis, R. R.
Linehan, J.
Major, Diane
Massey, L. N.
McKenzie, J. A.
McLean, J. J.
Merrill, E. G.
Misail, M. L.
Neal, R. W.
North, D. K.
Papa, D. C.
Peck, J. S.
Proteau, J-C.
Pyle, Cynthia M.
Rowe, T. A.
Saunders, Marjorie A.
Schwabe, W. J.
Sears, A. R.
Shane, Carolyn S.
Sprague, L. E.
Stevens, J. A.
Thompson, J. B.
Tortolano, A. J.
Volkmann, Ruth
Yaffe, M. A.
Yee, F. Q.

Document Room

Hewitt, J. H.
Hurvitz, Rose S.
Luster, Faith L.
Myers, Alberta L.

Drafting Room

Navedonsky, C. P., Foreman
Donahue, J. B.
Morss, Dorothy H.
Porter, Jean M.
Rollins, I. E.

PERSONNEL

Machine Shop

Keefe, J. B., Foreman
Aalerud, R. W.
Barnet, F. J.
Bletzer, P. W.
Brennan, J.
Bunick, F. J.
Cabral, M., Jr.
Carter, C. E.
Gibbons, W. D.
Harvey, A. O.
Ives, D. W.
Liljeholm, F. H.
MacDonald, J. R.
Marshall, J. J.
Muse, W. J.
Reimann, W.
Ryan. J. F.
Sanromá, J. B.
Shmid, E.
Smart, D. A.
Tucker, C. L.
Wentworth, W. G., Jr.

Secretaries

Attix, E. Patricia
Barron, Gladys G.
Bertozzi, Norma
Blais, Gisele G.
Carbone, Angelina
Cavanaugh, Mary C.
Chapman, Carol A.
Cheever, Beatrice J.
Cohen, Phyllis J.
Cummings, Jane F.
Docos, Dorothea H.
Dordoni, Joan M.
Epstein, Elinor F.
Fuller, Ruth D.
Geller, Elaine J.
Giles, Natalie M.
Gordon, Linda S.
Iverson, Alice I.
Johnson, Barbara A.
Johnson, Christine
Kaloyanides, Venetia
Kruckemeyer, Ann S.
Lannoy, Doris E.
Laurendeau, Carole A.
Loeb, Charlotte G.
Mackenzie, Jean E.
May, Nancy A.
McCarthy, Barbara L.
McEntee, Doris C.
Milan, Marilyn A.
Murray, Maureen P.
Owens, Mary Ellen
Parenteau, Joan C.
Petone, Rosina C.
Scalleri, Mary B.
Smith, Clare F.
Solomon, Cynthia
Staffiere, Rose Carol
Thorne, Jutta
Toebes, Rita K.
Townley, Madeline S.
Weisel, Linda E.

Technical Typists

Barnes, R. A.
Fleming, Patricia L.
Levin, L.
Levine, R. I.
Rabkin, W. I.

Stock Rooms

Doiron, E. J., Foreman
Audette, A. G.
Cardia, P. F.
Haggerty, R. H.
Joyce, T. F.
Legier, D. O.
Lucas, W. G.
McDermott, J. F.
Pacitto, H. T.
Riley, J. F.
Sharib, G.
Sincuk, J., Jr.

Technicians' Shop

Lorden, G. J., Foreman
D'Amico, C. R.
Fownes, Marilyn R.
Lander, H. J.
MacDonald, K. B.

Tube Laboratory

Staff

Rosebury, F.
Ryan, L. W.

Glass Blowers

DiGiacomo, R. M.
Doucette, W. F.

Technicians

Aucella, Alice A.
Griffin, J. L.
Leach, G. H., Jr.
MacDonald, A. A.

PUBLICATIONS AND REPORTS

MEETING PAPERS PRESENTED

International Symposium on High-Temperature Technology (sponsored by Stanford Research Institute), Monterey, California

September 8-11, 1963

W. B. Nottingham, Emitter Materials for High-Temperature Energy Conversion

International Scientific Radio Union General Assembly, Tokyo, Japan

September 9-20, 1963

A. G. Bose, A Two-State Modulation System

J. M. Wozencraft and R. S. Kennedy, Coding and Communication

American Chemical Society Fall Meeting, New York

September 11, 1963

G. G. Hammes, Relaxation Spectra of Enzymatic Reactions

Fifth International Congress of Slavists, Sofia, Bulgaria

September 17-24, 1963

M. Halle, On Cyclically Ordered Rules in the Russian Conjugation Systems of Slavic Languages (in Russian)

Physics Seminar, University of New Hampshire, Durham, New Hampshire

October 3, 1963

S. C. Brown, Infrared Studies of High-Density Plasmas (invited)

American Electroencephalographic Society Meeting, San Francisco, California

October 7-9, 1963

J. S. Barlow, Some Preliminary Observations on Evoked Responses and Perception of Visual Stimuli in Man (invited)

Thermionic Converter Specialist Conference (sponsored by IEEE), Gatlinberg, Tennessee

October 7-9, 1963

W. B. Nottingham, Voltage-Current Data Interpreted in Relation to the Theory of the Isothermal Cesium Diode

H. L. Witting and E. P. Gyftopoulos, Volume Ionization Processes in Cesium Converters

Institute of Electrical and Electronic Engineers, Boston Section Meeting, Boston, Massachusetts

October 8, 1963

W. A. Rosenblith, Engineering and the Sciences of Life and Man (invited)

Fifth IBM Medical Symposium, Endicott, New York

October 11, 1963

W. A. Rosenblith, The Use of Computational Techniques in the Study of Brain Function (invited)

Sixteenth Annual Gaseous Electronics Conference, Mellon Institute, Pittsburgh, Pennsylvania

October 16-18, 1963

K. U. Ingard, G. Bekefi, and K. W. Gentle, Effect of Gas Flow on Electrical Properties of a Positive Column

IEEE Joint Meeting, Professional Groups on Nuclear Science, Microwave Theory and Techniques, and Electron Devices, Boston, Massachusetts

October 23, 1963

A. Bers, Electron Beam-Plasma Interaction for Fusion (invited)

National Electronics Conference, Chicago, Illinois

October 28-30, 1963

R. P. Rafuse, Recent Developments in Parametric Multipliers

NEREM Conference, Boston, Massachusetts

November 4-6, 1963

H. H. Woodson, Magnetohydrodynamic Power Generation

Associated Mid-West Universities, Argonne National Laboratory Conference on Direct Conversion, Lemont, Illinois

November 5, 1963

W. D. Jackson, Review of MHD Power Generation (invited)

Acoustical Society of America Meeting, University of Michigan, Ann Arbor, Michigan

November 6-9, 1963

J. L. Hall II, Binaural Interaction in the Accessory Superior Olivary Nucleus of the Cat

T. F. Weiss, Response of a Model of the Peripheral Auditory System to Sinusoidal Stimuli

American Physical Society, Division of Plasma Physics Fifth Annual Meeting, San Diego, California

November 6-9, 1963

A. Bers and R. J. Briggs, Criteria for Determining Absolute Instabilities and Distinguishing between Amplifying and Evanescent Waves

R. J. Briggs and A. Bers, Electron-Beam Interactions with Ions in a Hot Plasma

T. H. Dupree, Theory of Radiation Emission and Absorption in Plasma

W. D. Getty, High-Perveance Electron Beam-Plasma Interaction

L. M. Lidsky, Orbit Stability in the Corkscrew

D. L. Morse, Low-Frequency Instabilities of a Partially Ionized Plasma in a Magnetic Field

D. L. Morse, Plasma Rotation in a Hollow-Cathode Discharge

D. J. Rose, L. M. Lidsky, and E. Thompson, Radiation Enhancement in an Optical Thomson Scattering Experiment

L. D. Smullin, The Beam Plasma Discharge (invited)

Physics Colloquium, Dartmouth College, Hanover, New Hampshire

November 14, 1963

S. C. Brown, Far Infrared Studies of Gas Discharge Plasmas (invited)

16th Annual Conference on Engineering in Medicine and Biology, Baltimore, Maryland

November 18-20, 1963

M. Eden and P. Mermelstein, Mathematical Models for the Dynamics of Handwriting Generation

W. H. Levison, G. O. Barnett, and W. D. Jackson, Nonlinear Analysis of the Pressoreceptor Reflex System

Sechenov Centennial Celebration, Academy of Sciences, Moscow, U.S.S.R.

November 24-30, 1963

W. A. Rosenblith, D. A. Fessard, J. Massion, and R. D. Hall, Cortical and Thalamic Responses to Somatic Stimulation in Awake and Asleep Cats (invited)

American Physical Society, Division of Plasma Physics Meeting, Cambridge, Massachusetts

November 26, 1963

N. Gothard, W. D. Jackson, and J. F. Carson, Preliminary Experiments with a Liquid-Metal MHD Waveguide

W. D. Jackson and M. H. Reid, Experimental Study of Induction-Coupled Liquid-Metal MHD Channel Flow

JOURNAL ARTICLES ACCEPTED FOR PUBLICATION

(Reprints, if available, may be obtained from the Document Room, 26-327, Research Laboratory of Electronics, Massachusetts Institute of Technology, Cambridge 39, Massachusetts.)

F. T. Barath, A. H. Barrett, J. Copeland, D. E. Jones, and A. E. Lilley, The Mariner II Microwave Radiometer Experiment and Results (Astron. J.)

A. Bers, Electron Beam-Plasma Interaction for Fusion (The Reflector)

M. Clarke, Jr. and P. Milner, Dependence of Timbre upon Tonal Loudness Produced by Musical Instruments (J. Audio Eng. Soc.)

T. H. Dupree, Kinetic Theory of Plasma and the Electromagnetic Field (Phys. Fluids)

JOURNAL ARTICLES ACCEPTED FOR PUBLICATION (continued)

M. Eden, Human Information Processing (IEEE Trans. PGIT)

J. A. Fodor, Review of "Questions of Meaning" by L. Antal (Language)

W. D. Getty and L. D. Smullin, The Beam-Plasma Discharge: Build-up of Oscillations (J. Appl. Phys.)

W. J. C. Grant and M. W. P. Strandberg, Derivation of Spin Hamiltonians by Tensor Decomposition (J. Phys. Chem. Solids)

G. G. Hammes and M. L. Morrell, A Study of Ni(II) and Co(II) Phosphate Complexes (J. Am. Chem. Soc.)

H. A. Haus, Review of "Topics in the Theory of Random Noise" by R. L. Stratonovick (Gordon and Breach Science Publishers, New York, 1963) (Proc. IEEE)

J. J. Katz and J. A. Fodor, A Reply to Dixon's "A Trend in Semantics" (Linguistics)

C. L. Liu, The Memory Orders of States of an Automaton (J. Franklin Inst.)

A. P. Paul, A. S. House, and K. N. Stevens, Automatic Reduction of Vowel Spectra: An Analysis-by-Synthesis Method and Its Evaluation (J. Acoust. Soc. Am.)

L. Stark, M. Okajima, G. Whipple, and S. Yasui, Computer Pattern Recognition Techniques: Some Results with Real Electrocardiographic Data (IEEE Trans. Biomedical Electronics)

L. Stark and L. R. Young, Variable Feedback Experiments Supporting a Discrete Model for Eye-Tracking Movements (IEEE Trans. (PGHFE) Special Manual Control Issue)

S. Weinreb, A. H. Barrett, M. L. Meeks, and J. C. Henry, Radio Observations of OH in the Interstellar Medium (Nature)

D. R. Whitehouse and H. B. Wollman, Plasma Diffusion in a Magnetic Field (Phys. Fluids)

LETTERS TO THE EDITOR ACCEPTED FOR PUBLICATION

J. A. Bellisio, C. Freed, and H. A. Haus, Noise Measurements on Gaseous Optical Maser Oscillators (J. Appl. Phys.)

W. H. Heiser, Magnetohydrodynamic Shock Waves and Magnetically Driven Shock Tubes (Phys. Fluids)

S. G. Kukolich, Ammonia Maser with Separated Oscillating Fields (Proc. IEEE)

O. Redi and H. H. Stroke, Spins and Nuclear Moments of Hg^{203} (Phys. Letters (Amsterdam))

W. F. Schreiber, The Effect of Scanning Speed on the Signal/Noise Ratio of Camera Tubes (Proc. IEEE)

TECHNICAL REPORTS PUBLISHED

(These and previously published technical reports, if available, may be obtained from the Document Room, 26-327, Research Laboratory of Electronics, Massachusetts Institute of Technology, Cambridge 39, Massachusetts.)

414 Laszlo Tisza and P. M. Quay, The Statistical Thermodynamics of Equilibrium

416 Joseph L. Hall II, Binaural Interaction in the Accessory Superior Olivary Nucleus of the Cat – An Electrophysiological Study of Single Neurons

417 William D. Rummler, Optimum Noise Performance of Multiterminal Amplifiers

418 Thomas F. Weiss, A Model for Firing Patterns of Auditory Nerve Fibers

419 Michael A. Arbib, Hitting and Martingale Characterizations of One-Dimensional Diffusions

SPECIAL PUBLICATIONS

W. P. Allis and J. L. Delcroix, Notions générales sur la théorie macroscopique des ondes dans les Plasmas (Seminar, University of Paris, September 1962)

A. G. Bose, A Two-State Modulation System (Proc. 1963 Western Electronic Show and Convention, Los Angeles, California, August 20-23, 1963)

J. B. Dennis, Distributed Solution of Network Programming Problems (Proc. Allerton Conference on Circuits and Systems, University of Illinois, Urbana, Illinois, November 15-17, 1963)

H. A. Haus and J. A. Mullen, Noise in Optical Maser Amplifiers (Proc. Symposium on Optical Masers, Polytechnic Institute of Brooklyn, New York, April 16-18, 1963)

W. S. McCulloch, Studies in Carbohydrate Metabolism and Its Regulation in Health and Disease of the Central Nervous System (Ann. New York Acad. Sci.)

D. R. Whitehouse, Diagnostics and Communications (Proc. Third Annual Symposium on the Engineering Aspects of Magnetohydrodynamics, Gordon and Breach, Science Publishers, Ltd., New York)

Proceedings of the VIth International Conference on Ionization Phenomena in Gases, Orsay (S-et-O), France, September 1, 1963. The following papers are included:

H. Fields and G. Bekefi, Relaxation Rate of Electrons to Equilibrium

J. C. Ingraham and S. C. Brown, Electron Energy Decay in the Helium Afterglow

P. W. Jameson and D. R. Whitehouse, Electron Energy Streaming in a Collisionless Plasma

D. T. Llewellyn-Jones, S. C. Brown, and G. Bekefi, Far Infrared Electron Density Measurements

J. F. Waymouth, Perturbation of a Plasma by a Probe

Introduction

This report, the seventy-second in a series of quarterly progress reports issued by the Research Laboratory of Electronics, contains a review of the research activities of the Laboratory for the three-month period ending November 30, 1963. Since this is a report on work in progress, some of the results may not be final.

Following our custom of the past several years, in this issue of January 15, 1964 we preface the report of each research group with a statement of the objectives of the group. These summaries of our aims are presented in an effort to give perspective to the detailed reports of this and ensuing quarters.

RADIO PHYSICS

I. MOLECULAR BEAMS*

Prof. J. R. Zacharias
Prof. J. G. King
Prof. C. L. Searle
Prof. K. W. Billman
R. S. Badessa
V. J. Bates
R. Golub
G. L. Guttrich
W. D. Johnston, Jr.
S. G. Kukolich
F. J. O'Brien
R. W. Simon
C. O. Thornburg, Jr.

RESEARCH OBJECTIVES

Three kinds of research are pursued in the molecular beams group:

1. High-precision studies of atomic and molecular radiofrequency spectra, an example being the study of the rotational spectrum of HF.

2. The development and intercomparison of atomic frequency standards. The two-cavity ammonia maser and the ammonia molecule decelerator are examples. The CS electric resonance studies mentioned in our "Research Objectives" in Quarterly Progress Report No. 68 (page 25) have been abandoned, because of insufficient signal-to-noise ratio. Work is also being done to determine the system properties of a cesium beam tube, and to develop complementary electronics to realize its latent frequency stability. These new clocks and others of different types will be intercompared by using the computer facilities at M. I. T. in order to check for possible variations in rate with epoch.

3. Experiments that apply parts of these techniques to interesting problems in any area of physics, as in the following list:
   (a) measurement of the velocity of light in terms of atomic standards,
   (b) search for a charge carried by molecules,
   (c) an experiment on an aspect of continuous creation.

These problems are well advanced. In an earlier phase are the following experiments:
   (d) the velocity distribution of He atoms from liquid He,
   (e) experiments with slow electrons (10^{-6} ev).

J. R. Zacharias, J. G. King, C. L. Searle

A. CESIUM BEAM TUBE INVESTIGATION

In Quarterly Progress Report No. 70 (pp. 59-60) it was reported that measurements made on two atomic clocks (incorporating Type 1001 cesium beam tubes) showed that the frequency stability falls far short of the results that might be expected on the basis of the tests of the electronic apparatus described in Quarterly Progress Report No. 69 (pp. 17-21). It was suggested that the instability was caused by a component that would not influence the results of these electronic tests such as faults in the beam tubes themselves or in the modulators used to frequency-modulate the X-band excitation signal. Since plans had already been made to replace the Type 1001 beam tubes by the improved Type 2001, investigation during the past quarter has been confined to a detailed study of the modulators and the errors that they might introduce. The results of this study not only indicate that distortion was being introduced by this particular modulator design, but also showed that a modulator capable of maintaining the low distortion required in this application for long periods of time would be difficult to realize in a practical design.

*This work was supported in part by Purchase Order DDL BB-107 with Lincoln Laboratory, a center for research operated by Massachusetts Institute of Technology, with the support of the U.S. Air Force under Contract AF 19(628)-500.

Because square-wave phase modulation can be generated easily with low distortion, we are now studying the properties of systems that have modulation of this type. We have termed it "Frequency Impulse Modulation" to avoid confusion with the square-wave frequency-modulation system that we have been describing in recent quarterly reports. Whereas for square-wave frequency modulation we utilized gating in an attempt to minimize certain undesirable characteristics of the beam-tube transients, the new method of modulation provides a method for removing the basic cause of these undesirable characteristics. In so doing it causes the output frequency of the atomic clock to depend to a greater extent upon the cesium atom itself, thereby achieving accuracy, as well as stability. Specifically, frequency impulse modulation provides a means for detecting the existence of a cavity error θ by observing the beam-tube output while it is in actual operation as a frequency-stabilization device. It therefore permits continuous instrumentation to correct for this error.

The approximate transition probability of a beam tube with separated oscillating fields in the vicinity of resonance is given by

$$P_{p,q} = \sin^2 \frac{2b\ell}{v_n} \cos^2 \frac{(\omega_o-\omega) L}{2v_n}, \tag{1}$$

where ω_o (hereafter called the "true" cesium frequency) is the frequency of the Cs^{133} hyperfine transition (4,0-3,0) for the magnetic field that is being used, ℓ is the length of each of the microwave exciting cavities, L is the distance between the two cavities, b is proportional to the RF amplitude, and v_n is the particle velocity.

We have assumed in this equation that the oscillating fields in the two cavities are exactly in phase, a condition that in practice is hard to achieve. If the two cavities are out of phase by an angle θ, then the frequency-dependent part of the beam-tube output in the vicinity of resonance can be expressed as

$$V_o = A'(v_n) \cos \left[\frac{(\omega_o - \omega) L}{v_n} + \theta\right] \tag{2}$$

$$= A'(v_n) \cos (a+\theta), \tag{3}$$

where

$$a = \frac{(\omega_o - \omega) L}{v_n}.$$

Note that the quantities a and θ are identical as far as their effect upon the output is concerned. The peak output is not obtained at cesium frequency, but at the frequency for which $a = -\theta$. If we plot the output voltage from Eq. 2 as a function of $(\omega_o-\omega)$, the cosine function would have a period $\Delta\omega = \frac{2\pi v_n}{L}$ and a central peak at a frequency $(\omega_o-\omega) = -\frac{\theta v_n}{L}$. Since these quantities are both functions of particle velocity, summation of a family of these curves to represent the effect of a velocity distribution would be the summation

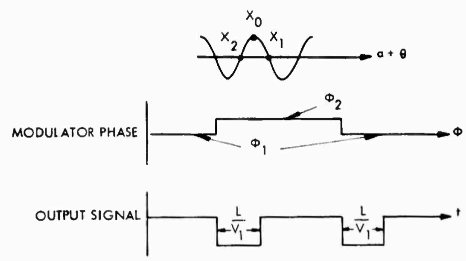

Fig. I-1. Monovelocity (v_1), $(\omega_o-\omega)$ = 0, θ = 0.

of a group of cosine functions that differ both in period and position. The result is the familiar Ramsey pattern that, for θ = 0, would be symmetrical about the cesium frequency $(\omega_o-\omega) = 0$.

Let us first consider the case of a monovelocity beam with rf excitation at the cesium frequency and no cavity phase error (that is, $\alpha=0$, $\theta=0$). The operating point will be at the exact peak of the cosine function as shown by position X_o in Fig. I-1. If we then apply an abrupt step of phase to the rf excitation, the atoms that had left the first cavity before the phase step, on entering the second cavity, see a phase offset equal to this step. The result will be a sudden drop of the operating point to a lower point on the cosine function, say, to position X_1 (shown for a 90° step). If we maintain this new phase, ϕ_2, undisturbed, the operating point will remain for a while at position X_1, then return abruptly to the steady-state position X_o after all of the atoms that are present between the two cavities at the time of the step have left the interaction space, that is, after an interval L/v_1. If we then apply a second phase step, thereby returning the radio frequency to its original phase ϕ_1, the operating point will again drop to a lower point on the cosine function, but this time on the opposite side of the peak. As before, if we maintain this phase undisturbed, the operating point will drop back abruptly to the position on the peak after an interval equal to the transit time between the cavities. This is shown by the waveforms of Fig. I-1. If the phase steps (or frequency impulses) are generated by a square wave, the output waveform will consist of a series of identical rectangular pulses occurring at twice the rate of the modulation. Hence no odd harmonics of the modulating rate would exist.

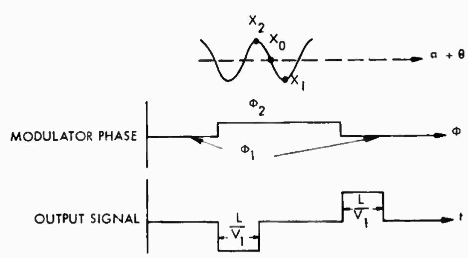

Fig. I-2. Monovelocity (v_1), $(\omega_o-\omega) = \frac{\pi}{2}\frac{v_1}{L}$, $\theta = 0$.

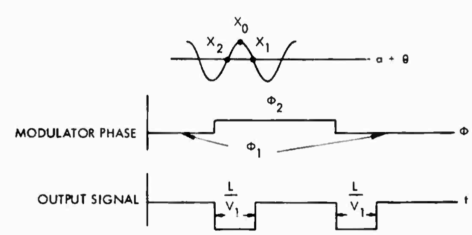

Fig. I-3. Monovelocity (v_1), $(\omega_o-\omega) = -\theta\frac{v_1}{L}$, $\theta \neq 0$.

If the rf excitation frequency is now changed so that $(\omega_o - \omega) = \frac{\pi}{2}\frac{v_1}{L}$, the output waveform will consist of a series of alternating negative and positive rectangular pulses as shown in Fig. I-2. Such a waveform contains odd harmonics of the modulating signal (including a strong fundamental) which could be used as a control quantity by passing the output signal through a synchronous detector. If we had chosen to operate at a frequency located

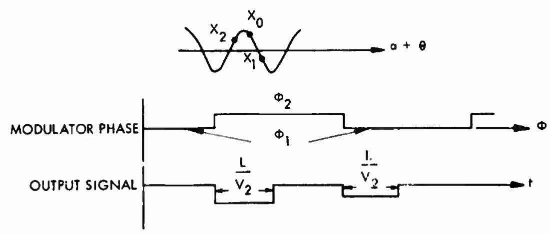

Fig. I-4. Monovelocity (v_2), $(\omega_o - \omega) = -\theta\frac{v_1}{L}$, $\theta \neq 0$.

on the other side of cesium resonance, the output waveform would be the exact negative of the one shown and thus would also provide sense information.

Next, let us assume that there is a cavity tuning error θ, and that the frequency of the rf excitation is such that $(\omega_o - \omega) = -\frac{\theta v_1}{L}$, that is, $a = -\theta$. Under these conditions, the steady-state operating point is again at the exact peak of the cosine function, as shown in Fig. I-3. Square-wave phase modulation produces here an output waveform that is

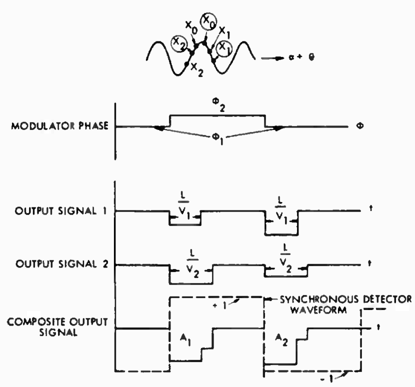

Fig. I-5. Dual velocity, $-\frac{\theta v_1}{L} < (\omega_o - \omega) < \frac{\theta v_2}{L}$, $\theta \neq 0$.

free of odd harmonics of the modulating frequency, and hence, in the absence of knowledge regarding the existence of cavity error, would give the erroneous information that the excitation was at cesium frequency.

If, however, we assume a different velocity, v_2, but maintain the same rf excitation frequency $(\omega_o - \omega) = -\frac{\theta v_1}{L}$, then the operating point will fall to one side of the peak as shown in Fig. I-4. It is obvious that odd harmonics of the modulating rate exist in the output waveform. Thus a frequency-stabilization loop would call for correction of the rf excitation frequency.

If the beam tube has particles of both v_1 and v_2, then the loop must find some compromise condition, for example, such as the one illustrated in Fig. I-5, in which the operating points corresponding to v_2 have been circled for clarity. The condition of lock requires that the operating points be placed so that the corresponding output waveform gives zero average voltage when applied to the loop synchronous detector. If the synchronous detector reference is positioned as shown by the dotted line in Fig. I-5, this imposes the condition that area A_1 = area A_2. By geometrical procedures, it can be shown that stabilization for the case illustrated in Fig. I-5 will occur at the frequency $(\omega_o - \omega)$ which satisfies the relationship

$$\frac{1}{v_1} \sin \left[(\omega_o - \omega) \frac{L}{v_1} + \theta\right] + \frac{1}{v_2} \sin \left[(\omega_o - \omega) \frac{L}{v_2} + \theta\right] = 0. \tag{4}$$

By inspection, it is seen that $(\omega_o - \omega)$ must lie between $-\frac{\theta v_1}{L}$ and $-\frac{\theta v_2}{L}$. Thus the cavity error θ will still cause an inaccuracy to exist. If we extend the analysis to the general case of n velocities, in which the relative density of particles of velocity v_n is denoted D_n, we obtain

$$\sum \frac{D_n}{v_n} \sin \left[(\omega_o - \omega) \frac{L}{v_n} + \theta\right] = 0. \tag{5}$$

Notice that no term involving the size of the phase step is present in this expression; thus it appears that frequency impulse modulation causes the frequency of lock to be independent of modulation level.

Of special interest in Fig. I-5 is the fact that the part of the output waveform associated with the positive phase step is not identical in shape to that part associated with the negative step. This indicates that odd harmonics are still present, even though the condition area A_1 = area A_2 causes an average voltage of zero to occur at the output of the synchronous detector. Thus as we tune the rf excitation through resonance, the odd harmonics will reach a minimum at some frequency, but will not go to zero as long as there is a cavity error θ. The synchronous detector output voltage, on the other hand, will go through zero whenever the areas enclosed by its positive and negative half-periods are equal.

The consequences of having odd harmonics in the output waveform that merely go through a minimum as a function of the rf excitation frequency are twofold. First, it causes the position of lock of the loop to become dependent upon the phase of the synchronous detector reference. This is evident from Fig. I-5, for, since A_1 and A_2 have different shapes, a choice of synchronous detector reference slightly to the right of the one shown would cause somewhat different areas to be enclosed, and would make the loop call for correction. Second, the existence of these residual odd harmonics gives

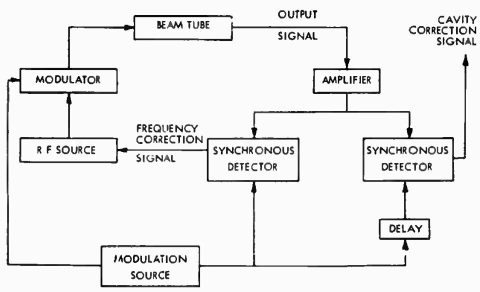

Fig. I-6. Double-loop servo system for locking to true cesium frequency.

valuable evidence that the cavity is, indeed, out of adjustment, and permits us to take measures to correct it, thereby eliminating both the dependence of lock upon the position of the synchronous detector reference and the error caused by having a detuned cavity. A double-loop system for accomplishing this might take the form shown in Fig. I-6. One loop is used for tuning the rf excitation and is essentially the conventional loop used for frequency stabilization. Its synchronous detector reference could be in phase with the modulating signal. The second loop is used for trimming the phase of the cavities and has a synchronous detector reference delayed somewhat from the first. Some interaction between the two loops will occur, but the final point of stabilization will be at a frequency and a cavity tuning for which the average voltage from both synchronous detectors is zero. This, however, can only occur when successive half-periods of the output waveform are identical, a condition that occurs only at cesium frequency with perfectly tuned cavities.

What we have said regarding the undesirability of residual odd harmonics is true for all stabilization loops, regardless of the type of modulation used. In sinusoidal modulation (for which the effect is termed "quadrature"), as well as in other types, it is characterized by output waveforms with minute differences of shape between successive half-periods. In the past the cause of this difference has often been the distortion in the waveform of the phase modulation of the rf excitation, a distortion that might be so low that it defies direct measurement and still be significant enough to completely override the contribution caused by moderate cavity detuning. Since the waveforms used in

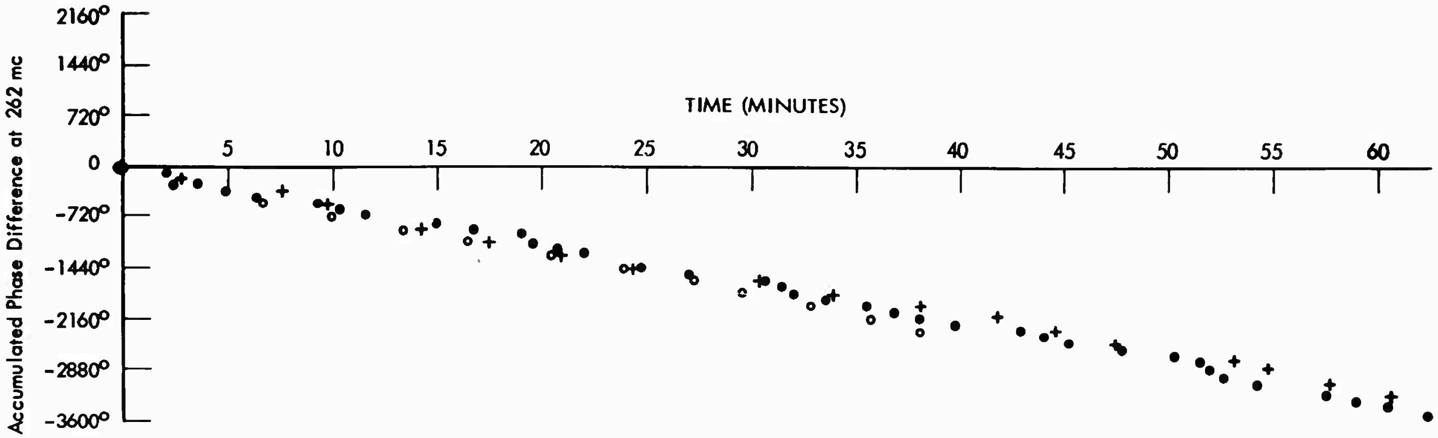

•• December 5, 1963	Average Frequency Offset 1.00×10^{-11}	Frequency Stability* 6×10^{-13}	for 63 min Average
++ December 6, 1963 a.m.	Average Frequency Offset 0.94×10^{-11}	Frequency Stability 7×10^{-13}	for 60 min Average
∘∘ December 6, 1963 p.m.	Average Frequency Offset 1.08×10^{-11}	Frequency Stability 8.4×10^{-13}	for 38 min Average

$$\text{* Frequency Stability} = \frac{\text{Peak to Peak Phase Deviation from Average Frequency Offset}}{360^\circ \times \text{Measurement Frequency} \times \text{Averaging Time}}$$

Fig. I-7. Preliminary measurements made on the cesium clocks by using the double-loop system.

frequency impulse modulation are of a type that are easily obtainable to meet virtually any distortion specification (the phase modulator, for example, operates at essentially two discrete points on its characteristic), the presence of any "quadrature" effect can safely be assumed to result from the action of the beam tube itself.

The most significant advantages of frequency impulse modulation will now be summarized.

1. Frequency impulse modulation produces waveforms that are conducive to extremely low modulation distortion. This permits using the presence of residual odd harmonics as a guide for correcting cavity phase error and achieving lock to the true cesium frequency.

2. The stabilization frequency of a loop with frequency impulse modulation is independent of modulation level, even when the presence of uncorrected cavity error produces a Ramsey pattern that is unsymmetrical.

3. Since frequency impulse modulation derives all of its information from observation of the effect of applying phase steps to the RF excitation, the period of repetition of these steps need be no longer than that required to accommodate the resultant transients. This tends to yield high permissible modulation rates, which is a desirable feature from a practical standpoint, particularly when long beam tubes are used.

Two atomic clocks incorporating Type 2001 cesium beam tubes have been assembled with control loops for which frequency impulse modulation is used. Since no provision exists in these beam tubes for electronic correction of cavity tuning, a system of waveform correction has been devised which is based on the principles outlined above and has been incorporated in a control loop to serve as a temporary substitute for the cavity correction loop. The measurements that we have made are preliminary, but they seem to confirm the desirability of this type of modulation.

Examination of the data presented in Fig. I-7 shows a frequency stability somewhat better than one part in 10^{12} for averaging times of approximately one hour. The first test was made during one afternoon. After its completion, the clocks were shut down until the following morning when they were restarted for the second test. The third test was taken approximately 24 hours after the first. Care was taken to reset the C field currents to the same level for each test, but an improved method for setting these fields is under consideration for future measurements.

R. S. Badessa, V. J. Bates, C. L. Searle

B. AMMONIA MASER WITH SEPARATED OSCILLATING FIELDS

The 3-2 inversion transition in ammonia was observed by means of a molecular beam maser with two microwave cavities separated by 36 cm. The resulting resonance shows the typical Ramsey[1] shape with several peaks, the width of these peaks being determined by the separation of the microwave cavities.

This device is similar to the original ammonia maser[2] in physical construction but differs in that this device does not oscilalte spontaneously and the linewidth is much narrower, since it depends on the separation of the microwave cavities. Using separated cavities has the additional feature of greatly reducing Doppler effects that would be encountered with a single long cavity. The two-cavity maser is shown in Fig. I-8.

Microwave power is injected into the first cavity, and a microwave receiver is connected to the second cavity. Both cavities have open ends to that some of the microwave power from the first cavity is coupled into the second cavity. The conditions are similar to those described by Ramsey[1] for resonance with separated oscillating fields, except that here the transition probability is not measured by deflection of the beam but by observing the additional power delivered to the microwave receiver by the ammonia molecules.

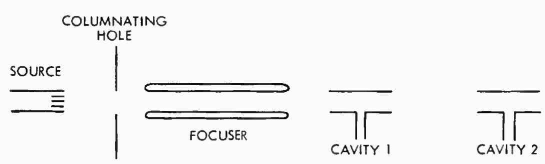

Fig. I-8. The maser.

Feynman[3] has shown that any ensemble of two level noninteracting systems may be described by the equations of motion of the magnetic moment of a spin $\frac{1}{2}$ particle in a magnetic field. This allows us to use the analysis of the magnetic case by Ramsey[1] to describe the interaction of the ammonia beam with the RF fields. For the ammonia beam the only physical axis in the representation given above is the axis along which the beam passes, since the oscillating electric field is in this direction.

If we use this description we see that the RF field in the first cavity produces an effect that is analogous to rotating the moment by $\pi/2$ about the RF field direction in magnetic resonance. That is, the transition probability in the first cavity is nearly 1/2, and the beam has a coherent oscillating electric polarization as it leaves the first cavity. In the space between the cavities the RF field is very small (the Q of the cavities is 1200), so that this polarization oscillates unperturbed at the ammonia inversion frequency. If the frequency of the fields in both cavities resulting from the injected signal is very near the inversion frequency, the oscillating polarization in the beam and the field in the second cavity will be in phase as the beam passes through the second cavity. Consequently, the field in the second cavity will increase the total transition probability and hence also increase the power level in the second cavity, which is coupled to the microwave receiver.

If the frequency of the RF fields in the cavities is slightly off the ammonia frequency, the oscillating polarization in the beam will become progressively farther out of phase with the RF power injected into the cavities as the beam passes from the first cavity to the second. If this phase difference becomes $\pm\pi$, the RF field in the second cavity will reduce the total transition probability and thus the beam will absorb power from the second cavity. This condition will produce the first minima on either side of the main resonance peak.

If the beam velocity is v and the cavity separation is L, the accumulated phase difference will be π when $\Delta\omega = \frac{\pi}{T} = \frac{\pi v}{L}$ or when $\Delta f = \frac{1}{2}\frac{v}{L}$. If the effects of the beam velocity distribution are properly taken into account, then $\Delta f \cong 0.6\frac{v}{L}$ and other maxima are reduced with respect to the main peak.[1]

We may also note from this description that if the RF field in the second cavity is phase-shifted by π with respect to the rf field in the first cavity, this will appear as a frequency error of approximately Δf_o, the linewidth of the molecular resonance. Thus $\frac{\delta f}{\Delta f_o} = \frac{\delta\phi}{\pi}$.

One way of obtaining a phase shift $\delta\phi$ is to detune the second cavity. Near the center of the cavity resonance this shift is $\frac{2\delta\phi}{\pi} = \frac{\delta f_c}{\Delta f_c}$, where δf_c is the cavity detuning, and Δf_c the width of the cavity resonance. Thus the shift of the observed resonance resulting from cavity detuning is $\frac{\delta f}{\Delta f_o} = \frac{\delta\phi}{\pi} = \frac{\delta f_c}{\Delta f_c}$. This effect is similar to the "cavity-pulling" formula for a single-cavity maser[4] and also occurs in a conventional Ramsey molecular beam apparatus.

In a thorough analysis of a two-cavity maser Basov and Oraevskii[5] have also suggested that this experiment would be possible.

In our experiment the beam is produced by a crinkle-foil source. A four-pole electric field, 22 cm long, focuses the upper-state molecules into the cavities. The upper inversion-state molecules then pass through two TM_{010} mode microwave cavities 10 cm long and separated by 36 cm. The frequency of the stimulating signal injected into the first cavity is varied, and the power delivered by the second cavity to the microwave receiver as a function of frequency is measured. The injected signal is frequency modulated at 165 cps, and a phase-sensitive detector is used to obtain the first

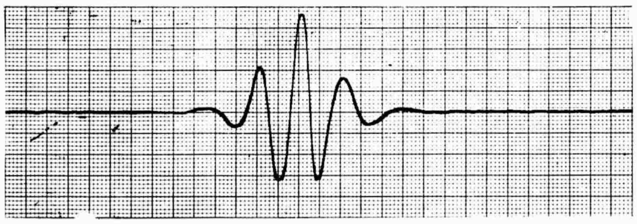

Fig. I-9. Derivative of Ramsey resonance pattern with $\pi/2$ phase shift between the rf fields in the cavities.

derivative of the resonance. The first derivative of the resonance for $\pi/2$ phase difference between the cavities is shown in Fig. I-9.

The observed linewidth is approximately 1 kc, and the resonance pattern is the typical Ramsey curve. In a preliminary experiment the frequency of the ammonia 3-2 inversion line was measured with respect to a National 1001 cesium clock. The measured frequency is 22, 834, 184, 850 ± 100 cps. This is in agreement with 22, 834. 18 mc obtained by Shimoda and Kondo.[6] In this frequency measurement the output voltage from the phase-sensitive detector was used as the error signal in a servo loop to control the frequency of the microwave power injected into the first cavity. The resetability from one day to the next was a few parts in 10^9. The principal source of this inaccuracy is believed to be variations of the cavity temperatures, which are not yet sufficiently well stabilized. Since the present cavities are silver, the variations in thermal tuning could be sufficient to account for these deviations. The focuser voltage on this device was changed from 12 kv to 24 kv and the frequency of the resonance changed by less than one part in 10^8.

Since for larger cavity separation this device may have a very narrow linewidth, it should be possible to construct a molecular resonance clock of useful stability.

S. G. Kukolich

References

1. N. F. Ramsey, Molecular Beams (Oxford University Press, London, 1956), Chap. 5.

2. J. P. Gordon, H. J. Zeiger, and C. H. Townes, Phys. Rev. 99, 1264 (1955).

3. R. P. Feynman, F. L. Vernon, and R. W. Hellwarth, J. Appl. Phys. 28, 49 (1957).

4. K. Shimoda, T. C. Wang, and C. H. Townes, Phys. Rev. 102, 1308 (1956).

5. N. G. Basov and A. N. Oraevskii, Soviet Phys. – JETP 15, 1062 (1962).

6. K. Shimoda and K. Kondo, J. Phys. Soc. Japan 15, 1125 (1960).

II. MICROWAVE SPECTROSCOPY*

Prof. M. W. P. Strandberg
Prof. R. L. Kyhl
Dr. J. M. Andrews
A. Fukumoto
R. Huibonhoa
J. G. Ingersoll
J. D. Kierstead
J. W. Mayo
H. J. E. H. Pauwels
S. Reznek
W. J. Schwabe
J. Shah
S. Sterling
A. Teich

RESEARCH OBJECTIVES

Our major emphasis is now focused on studies of the metallic and semiconducting states. This extremely broad area is one of current worldwide interest and investigation. Our specialized interest lies in interactions within the electron "plasma" and between the electron plasma and the lattice phonons. We now have considerable experience and facility in the generation and use of microwave phonons (coherent sound waves in the kilomegacycle frequency range), and, in particular, sound-attenuation measurements in metals and superconductors will be an important activity. Other studies in the microwave frequency range include surface impedance measurements (both phonon and electromagnetic impedance) and investigation of phonon amplification mechanisms in semiconductors. Related studies at optical frequencies in which a gas laser is used continue.

This program represents a continuation of the shift away from electron paramagnetic resonance in crystals which was our major interest during the past several years. A problem in paramagnetic cross relaxation which must be resolved before we can leave this area of research is described in this report. Apparatus for paramagnetic resonance measurements in solids and gases is still operative and is being used by our own personnel and by members of other laboratories.

M. W. P. Strandberg, R. L. Kyhl

A. ULTRASONIC ATTENUATION IN SUPERCONDUCTING METALS AT RADIO AND MICROWAVE FREQUENCIES

This report is a summary of a Ph. D. thesis submitted to the Department of Physics, M. I. T., October 28, 1963.

Ultrasonic attenuation by conduction electrons in soft superconductors has been studied as a function of temperature, magnetic field, and frequency. A derivation is presented of the electronic contribution to the ultrasonic attenuation coefficient α_n of metals in the normal state, which follows closely the kinetic approach of Pippard[1] except that quantities involving the product of the ultrasonic frequency ω and the electronic mean-free time τ are not neglected. The same results as those obtained by Pippard are obtained for all cases in which α_n is sufficiently large to be observable. The quantum theory of superconductivity is worked out in detail by following the original Bardeen-Cooper-Schrieffer (BCS) derivation,[2] except for the introduction of the improved mathematical devices proposed by Bogolyubov[3] and Valatin.[4] In particular, the statistical operator of Valatin serves to simplify the calculation of α_s/α_n which is worked out for the case in which the phonon frequency is less than the superconducting energy gap. An analysis of ultrasonic attenuation in superconductors in the intermediate state is presented, based

*This work was supported in part by Purchase Order DDL BB-107 with Lincoln Laboratory, a center for research operated by Massachusetts Institute of Technology, with the support of the U. S. Air Force under Contract AF 19(608)-500.

upon the assumption of an average magnetization throughout the volume of the metal. Particular attention has been paid to the phenomenon of supercooling; in this research a modified form of the mathematical model of Faber[5] was followed.

Experiments were carried out at 0.165 Gc, 0.910 Gc, and 9.17 Gc. Analysis of the temperature-dependent data at 0.910 Gc indicates a close agreement with the BCS theory. The magnetic-field dependence of the ultrasonic attenuation coefficient supports the conclusions of the theoretical treatment, thereby indicating an effective demagnetizing coefficient of the sample that exhibits the proper orientation dependence, and yielding critical field values whose temperature dependence is in close agreement with the data of other investigators. The temperature dependence of the supercooling phenomenon exhibits the same sort of behavior that is anticipated from theoretical considerations, and the conclusions regarding the size of the nucleation centers that trigger the phase transition are numerically consistent with the values obtained by Faber, who employed a different experimental method. The frequency dependence of α_n agrees qualitatively with the prediction of Pippard. It was not possible to observe ultrasonic attenuation at 9.17 Gc; this is attributed to the fact that the sample faces were many wavelengths out of parallel at this frequency. Recommendations for further research are offered.

J. M. Andrews, Jr.

References

1. A. B. Pippard, Phil. Mag. 46, 1104 (1955).
2. J. Bardeen, L. N. Cooper, and J. R. Schrieffer, Phys. Rev. 108, 1175 (1957).
3. N. N. Bogolyubov, Nuovo cimento 7, 794 (1958).
4. J. G. Valatin, Nuovo cimento 7, 843 (1958).
5. T. E. Faber, Proc. Roy. Soc. (London) A214, 392 (1952).

B. CROSS RELAXATION IN RUBY

In 1962, certain experimental paradoxes in our measurements of cross relaxation in typical ruby maser crystals were reported.[1]

More accurate measurements have been made and have disclosed the nature of some of the discrepancies. Our original results on 0.05 per cent ruby near 27° orientation, 4400 gauss, for which 2, 3, and 4 quantum levels (Chang-Siegman notation) are equally spaced, are shown in Fig. II-1. These results are consistent with those of other experimenters, except for the presence of additional time constants as shown. At low temperatures and low chromium concentration, we have $T_2 < T_{12} < T_1$; we are referring to the time constants for spin-spin relaxation, cross relaxation, and spin-lattice relaxation, respectively. The effect of spin-spin relaxation was observable, although not plotted in Fig. II-1. If we "burn a hole" in the inhomogeneously broadened ruby

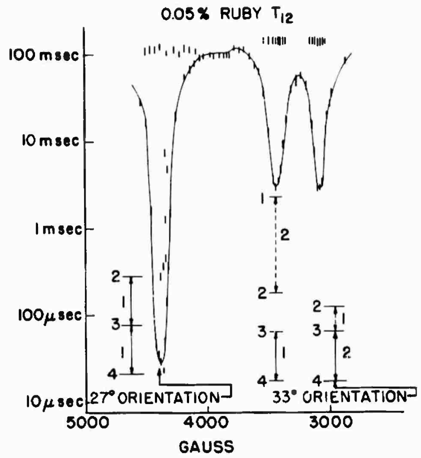

Fig. II-1. Relaxation time of ruby 3-4 transition near 30° orientation. Frequency, 9 Gc.

resonance lines with a magnetron pulse, the hole fills in within a few microseconds, and we might assume that thermal equilibrium is established within each energy level in a time of that order.

The new surprising result is that the cross relaxation is not properly describable by a time constant, but that equilibrium among the three not quite equally spaced levels is approached approximately as $t^{-1/2}$ with time. We must have a distribution of cross-relaxation times. The crystals are of laser quality and show no evidence of inhomogeneous effects in spin-lattice relaxation so that it does not seem possible to ascribe the effect to inhomogeneity in magnetic field or c-axis wander. Thus it appears that the cross relaxation proceeds between quantum levels that are not themselves in thermal equilibrium. It is true that one chromium site in the lattice differs from another in the disposition of nearest neighbors and of aluminum nuclear spins, but the observed microsecond time constant should average over the sites. Probably we have an interesting example of nonergodic behavior. The resulting theoretical puzzle is being analyzed.

R. L. Kyhl

References

1. Research on Paramagnetic Resonances, Sixth Quarterly Progress Report on Contract DA36-039-sc-87376, Research Laboratory of Electronics, M. I. T., May 15, 1962, pp. 40-46.

C. ENERGY CONSERVATION OF HYPERSONIC WAVES IN SEMICONDUCTORS

Amplification of sound waves in semiconductors through interactions with electrons drifting under the influence of a D. C. electric field and having velocity v_d greater than the velocity v_s of the sound wave was discovered some time ago.[1,2] As a coupling mechanism one may either have piezoelectric coupling or deformation potential coupling. Experiments have been successful on piezoelectric materials (CdS) at frequencies at which it is possible to work at room temperature, that is, up to 600 Mc.[3,4] For higher frequencies it is necessary to work at liquid-helium temperature. The lack of piezoelectric semiconductors with appropriate conduction properties at these temperatures makes it necessary to use the deformation potential coupling, which is much weaker than the piezoelectric coupling, but becomes more important as the frequency increases. Experiments at 9 Gc on n-type InSb of carrier concentration 10^{14} cm^{-3} performed in our laboratory have not been successful thus far. We might mention, however, that theoretically an amplification of 10 db/cm is expected at power densities described by 10 amp/20 mm^2 and 10 volts/cm. We computed also that in GaAs (piezoelectric) amplification of 70 db/cm should be possible at slightly higher power densities. But we would require very pure samples (10^{14} cm^{-3}). We do not know whether or not these are available.

The coupling mechanism between a sound wave traveling in the z direction and drifting electrons can be described one-dimensionally by the equations:

$$D = \epsilon E + P$$

$$T = cS + F,$$

in which D is the electric induction, E the electric field, T the stress, S the strain, ϵ the dielectric constant, and c the elastic constant. P is a (longitudinal) polarization and F a stress on the lattice. P and F are the coupling terms and are related by energy relations. It is known that in piezoelectric semiconductors $P = eS$ and $F = -eE$, in which e is the piezoelectric constant. A rather simple theory[2] has been formulated for this kind of coupling at lower frequencies. The deformation potential is described by $P = -(C\epsilon/q)(\partial S/\partial z)$, in which C is a constant and q the electronic charge. We have found that F has to be $-(C\epsilon/q)(\partial E/\partial z)$. This expression provides a theory for the deformation potential which is analogous in formalism with one given by White[2] for the piezoelectric coupling. It leads to the important result that amplification through the deformation potential coupling in a given material under given conditions is more important than through piezoelectric coupling at $\omega > \omega_{cr} = v_s eq/\epsilon C$, the ratio being $(\omega/\omega_{cr})^2$. For InSb this critical frequency should be ≤ 10 Gc, with $e \leq 0.025$ C/m^2; for GaAs, piezoelectric amplification is 25 times stronger at 10 Gc; for CdS, 3600 times.

In trying to derive an expression for F, we developed some energy conservation principles, which may have some didactical value. If a sound wave travels through a conducting crystal, the energy appears under different forms: electromagnetic energy, acoustical energy of the lattice, kinetic energy of the electrons and heat (incoherent acoustical energy of the lattice). We shall try to find the relations between these different forms of energy. We use the following notation: E, H, D, B, ϵ, μ, international symbols for electromagnetic fields; J, current density; P, polarization; T, stress; S, strain; c, elastic constant; F, coupling stress; v, velocity of the electrons; v_d, drift velocity of the electrons; u, velocity of the lattice; u_D, displacement of the lattice; m_c, effective mass of the carriers; q, electronic charge; ρ, resistivity or specific weight; N, carrier density; N_o, density of donors; E_F, Fermi energy; f, density of particles per unit volume in position and velocity space; τ, relaxation time. All fields have a D. C. term and an A. C. term of the form $\exp j(\omega t-kz)$.

1. Electromagnetic Energy

We have $D = \epsilon E + P$. From curl $E = -\mu\partial H/\partial t$ and curl $H = \frac{\partial}{\partial t}(\epsilon E+P) + J$, after dot multiplication with $-H$ and E, respectively, we obtain in the usual manner

$$-\text{div}\,(E\times H) = \frac{\partial}{\partial t}\left(\frac{\epsilon E^2}{2} + \frac{\mu H^2}{2}\right) + E\cdot\frac{\partial P}{\partial t} + J\cdot E. \tag{1}$$

It can be shown that for sound waves the A. C. part of div $(E\times H)$ can be neglected.

2. Coherent Motion of the Lattice

For simplicity we treat the problem one-dimensionally. We have $T = cS + F$. From $\partial T/\partial z = \rho\partial^2 u_D/\partial t^2$, with $u = \partial u_D/\partial t$ and $S = \partial u_D/\partial z$, we obtain

$$\rho\frac{\partial u}{\partial t} = \frac{\partial T}{\partial z} \qquad \text{and} \qquad \frac{\partial S}{\partial t} = \frac{\partial u}{\partial z}.$$

After multiplication with u and T, respectively, we obtain

$$\frac{\partial}{\partial t}\left(\frac{1}{2}\rho u^2\right) + \frac{\partial}{\partial t}\left(\frac{1}{2}cS^2\right) + F\frac{\partial S}{\partial t} = \frac{\partial}{\partial z}(uT). \tag{2}$$

3. Kinetic Energy of the Electrons

Let us first give an introductory calculation based on the equation of motion.

$$m_c\frac{dv}{dt} = -qE - \frac{m_c(v-u)}{\tau}, \tag{3}$$

in which v is the average velocity of the electrons. We assume that τ is independent of the thermal velocity of the electrons. The assumption of completely inelastic scattering is related to the assumption $v \ll v_{th}$. This equation also assumes that the wavelength is large compared with the mean-free path, since we have not taken an integral of E over the trajectory of the particle. After taking the dot product with $Nv = Nu + N(v-u)$, we obtain

$$N\frac{d}{dt}\frac{1}{2}mv^2 = E\cdot J - \frac{m}{\tau}N(v-u)^2 - \frac{mu}{\tau}\left(\frac{J}{-q} - Nu\right)$$
$$= E\cdot J - \rho(J+Nuq)^2 + \frac{mu}{q\tau}(J+Nuq). \tag{4}$$

We made use of the expression $J = -Nqv$, we omitted the index c of m_c, and we replaced

$m/N q^2\tau$ by the resistivity ρ. The left-hand side of this equation can be transformed to $\frac{\partial}{\partial t}\left(\frac{1}{2}mv^2N\right) + \nabla \cdot \left(\frac{1}{2}mv^2Nv\right)$ by making use of the facts that $v = v(r,t)$ and thus $dv/dt = (\partial v/\partial t) + v \cdot (\partial/\partial r)v$, that $N = N(r,t)$, and that the continuity equation for the number of particles is $\partial N/\partial t + \nabla \cdot (Nv) = 0$. Equation 4 thus becomes

$$\frac{\partial}{\partial t}\left(\frac{1}{2}mv^2N\right) + \nabla \cdot \left(\frac{1}{2}mv^2Nv\right) = E \cdot J - \rho(J+Nqu)^2 + \frac{mu}{q\tau}(J+Nqu). \tag{5}$$

The interpretation of (5) is as follows: The rate of increase per unit time of the energy density, plus the power flow from a unit volume, is balanced by the energy taken from the electromagnetic energy minus the energy lost to the scattering centers in incoherent and coherent form. The last term of the right-hand side of (5) can be understood by writing it as $u \cdot Nm(v-u)/\tau$, which is the product of the velocity of the scattering centers and the force exerted on them by the electrons.

Given Eq. 3, one can derive (5). Its interpretation is correct if v should be the real velocity of the electrons, not its average. We therefore develop a more exact calculation based on the Boltzmann transport equation in the presence of the sound wave and the D. C. electric field.

$$\frac{\partial f}{\partial t} + v \cdot \frac{\partial f}{\partial r} + \frac{-qE}{m} \cdot \frac{\partial f}{\partial v} = \frac{f_s - f}{\tau}, \tag{6}$$

with $f = f(r,v,t)$ = perturbed distribution,

f_s = equilibrium distribution centered around the velocity of the scattering centers and adapted to the local electron density given by

$f_s = f_o[v-u(r,t), E_F(r,t)]$.

We now define

electron density, $N = \int f\, d^3v$

current density, $J = -\int qfv\, d^3v = -N\bar{v}q$

pressure tensor of electron gas, $\overline{\overline{P}} = \int mvvf\, d^3v$.

After integration of (6) over v-space, we get

$$\frac{\partial N}{\partial t} + \nabla \cdot (N\bar{v}) = \frac{N - N}{\tau} = 0. \tag{7}$$

We have assumed that τ and the force $(-qE/m)$ are velocity-independent. After multiplication of (6) with v and integration over v-space, we get

$$\frac{\partial}{\partial t}(N\bar{v}) + \nabla \cdot \frac{\overline{\overline{P}}}{m} - \frac{qE}{m}(-N) = \frac{Nu + J/q}{\tau}. \tag{8}$$

We made use of

$$E_i \int \frac{\partial f}{\partial v_i} v_j \, d^3v = E_i \int \frac{\partial (fv_j)}{\partial v_i} d^3v - E_i \int f \frac{\partial v_j}{\partial v_i} d^3v$$

$$= 0 - E_i \int f \delta_{ij} \, d^3v = -E_j N.$$

We shall now transform and linearize Eq. 8 in the perturbation. The index 0 will indicate the unperturbed quantities. We assume that $\int fv_i^2 \, d^3v = \frac{1}{3} \int fv^2 \, d^3v$ for $i = 1, 2, 3$, and that $\int fv_iv_j \, d^3v = 0$ for $i \neq j$. This implies that the electron gas cannot exert shear stresses; we also have neglected $\overline{v}^2$ with respect to $\overline{v^2}$, which is a second-order error. If we assume that this average $\int fv^2 \, d^3v$ is only dependent on the local position of the Fermi level, and not on other properties of the perturbation, we may set

$$\frac{P}{m} = \frac{1}{3} \int fv^2 \, d^3v = \phi(N), \tag{9}$$

so that $\nabla \cdot \overline{\overline{P}}/m = \nabla P/m = \phi'(N) \nabla N$. We now give an example of linearization:

$$N\overline{v} = (N_o+n)(\overline{v}_o+\tilde{\overline{v}}) = (N_o+n)\overline{v} = N_o\overline{v} + \ldots .$$

In the same way $(\partial/\partial t)(J/-q)$, $\phi'(N) \nabla N$, qEN/m, Nu, and $J/-q$ are replaced by $N_o\partial\overline{v}/\partial t$, $\phi'(N_o) \nabla N$, qEN_o/m, N_ou, and $N_o\overline{v}$, respectively. Thus from Eq. 8, after multiplication with m/N_o, we obtain

$$m\frac{\partial\overline{v}}{\partial t} + m \frac{\phi'(N_o)}{N_o} \nabla N = -qE + (u-v) \, m/\tau. \tag{10}$$

Dot multiplication of (10) by Nv and multiplication of (7) by $m\phi'(N_o) N/N_o$ and adding the results gives

$$\frac{N}{2} m \frac{\partial\overline{v}^2}{\partial t} + \frac{m\phi'(N_o)}{N_o} \left[(\nabla N) \cdot N\overline{v} + N\nabla \cdot (N\overline{v}) + \frac{1}{2} \frac{\partial N^2}{\partial t}\right] = E \cdot J - \frac{mN}{\tau} (\overline{v}-u)^2 + \frac{mu}{q\tau} (J+Nqu).$$

We now define

$$\phi'(N_o) = \frac{1}{2} v_T^2,$$

and neglect third-order, so that $N\partial\overline{v}^2/\partial t = N_o\partial\overline{v}^2/\partial t$. Then we get

$$\frac{\partial}{\partial t}\left(N_o \frac{m\overline{v}^2}{2} + \frac{mv_T^2}{4} \frac{N}{N_o} N\right) + \nabla \cdot \left(\frac{mv_T^2}{2} \frac{N}{N_o} N\overline{v}\right) = E \cdot J - \rho(J+Nqu)^2 + \frac{mu}{q\tau} (J+Nqu). \tag{11}$$

The various terms in (11) are of second order in the perturbation except the second and the third terms of the right-hand side. If we set $N = N_o + n$, we get

$$\frac{\partial}{\partial t}\left(\frac{mv_T^2}{4}\,\frac{N}{N_o}\,N\right) = \frac{\partial}{\partial t}\left(\frac{mv_T^2}{2}\,N + \frac{mv_T^2}{2}\,\frac{n^2}{2N_o^2}\right)$$

or

$$\nabla\cdot\left(\frac{mv_T^2}{2}\,\frac{N}{N_o}\,N\bar{v}\right) = \frac{mv_T^2}{2}\,\nabla\cdot\left(N_o\bar{v} + 2n\bar{v} + \frac{n^2\bar{v}}{N_o}\right).$$

The first-order part of (11) thus, in fact, is

$$\frac{mv_T^2}{2}\left(\frac{\partial N}{\partial t} + \nabla\cdot N_o\bar{v}\right) = 0.$$

4. Energy Balance

From Eqs. 1, 2, and 11 we derive Fig. II-2. The electric field and the coupling

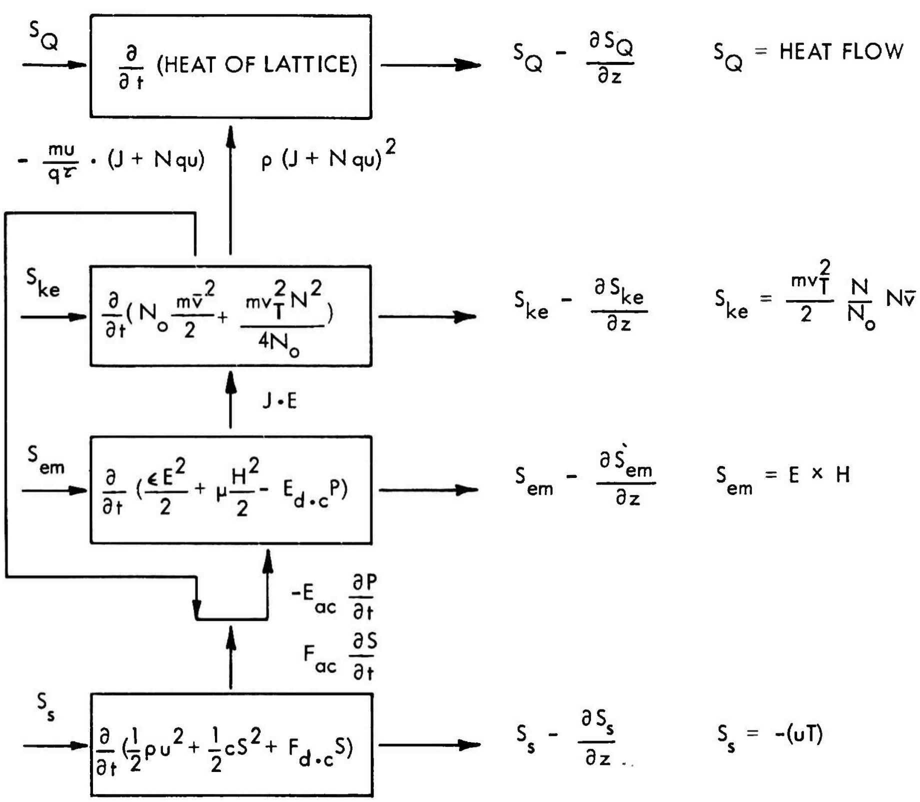

Fig. II-2. Energy balance for sound waves in semiconductors showing energy storage and power flow.

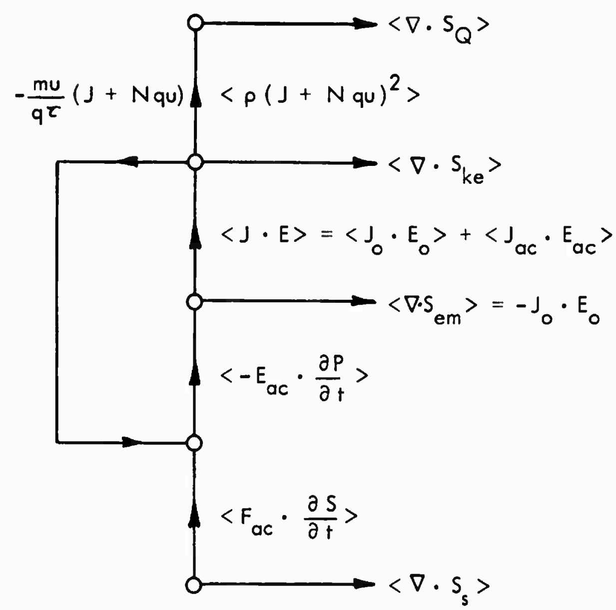

Fig. II-3. Energy balance for sound waves in semiconductors in a stationary situation.

stress F have been split into a D. C. and an A. C. part. Figure II-3 illustrates a stationary alternating situation, in which < > means the time average over one period. The term $<\nabla \cdot S_{em}>$ is split into $\nabla \cdot (E_o \times H_o)$ and the contribution of the A. C. parts. The former is equal to J_oE_o, as can be easily understood by considering a simple conducting wire; the A. C. parts can be proved to be negligible for a sound wave. We note that $<\nabla \cdot S_s>$ is negative for attenuation, and positive for amplification. At each small circle, we have a balance.

5. Applications

a. Equations of State: Piezoelectricity and Deformation Potential

Figure II-3 shows that

$$\left\langle F_{ac} \frac{\partial S}{\partial t} \right\rangle = \left\langle -E_{ac} \frac{\partial P}{\partial t} \right\rangle + \left\langle \frac{mu}{q\tau} (J+Nqu) \right\rangle .$$

If we neglect the second term on the right-hand side, we obtain

$$\left\langle F_{ac} \frac{\partial S}{\partial t} \right\rangle = \left\langle -E_{ac} \frac{\partial P}{\partial t} \right\rangle . \tag{12}$$

In the piezoelectric case we have $D = \epsilon E + P$, with $P = eS$. It can easily be seen that

(12) is satisfied if and only if $F_{ac} = -eE_{ac}$. There is no physical reason why this equation should be valid only for the A. C. components; thus $F = -eE$, and the equations of state thus are

$$D = \epsilon E + eS \qquad T = cS - eE.$$

We can verify the statement that $F\partial S/\partial t = -E\partial P/\partial t$, so that we can say that instantaneously the energy taken from the acoustical wave through the coupling force F shows up in the electromagnetic energy as the energy set free by the depolarization of the "piezoelectric" charges.

In the deformation-potential case, we have $D = \epsilon E + P$, with $P = -(C\epsilon/q)(\partial S/\partial z)$. By considering sinusoidal fields, we can again verify the conclusion that (12) is satisfied if and only if $F_{ac} = -(C\epsilon/q)(\partial E/\partial z)$, so that the equations of state are

$$D = \epsilon E - (C\epsilon/q)\partial S/\partial z \qquad T = cS - (C\epsilon/q)\partial E/\partial z.$$

In this case it can be verified that $F\partial S/\partial t = P\partial E/\partial t = \frac{\partial}{\partial t}(PE) - E\partial P/\partial t$, so that the previous statement about the instantaneous energy transfer is no longer true. Figure II-2 is only approximate.

b. Attenuation Constant

From Fig. II-3, we see that the energy taken from the sound wave is given by

$$Q = \left\langle F_{ac}\frac{\partial S}{\partial t}\right\rangle = \left\langle E_{ac}\frac{-\partial P}{\partial t}\right\rangle + \left\langle\frac{mu}{q\tau}(J+Nqu)\right\rangle = \left\langle J\cdot E\right\rangle + \left\langle\frac{mu}{q\tau}(J+Nqu)\right\rangle. \tag{13}$$

If all fields are now of the form $u = u_o \exp j(\omega t-kz)$, with $jk = \alpha + j\beta$, we get

$$2\alpha \operatorname{Re}\left(\frac{uT^*}{2}\right) = Q \tag{14}$$

from

$$-\left\langle\nabla\cdot S_s\right\rangle = \left\langle F_{ac}\frac{\partial S}{\partial t}\right\rangle = Q \qquad \text{and} \qquad S_s = -(uT).$$

The attenuation, α, is caused by the factor F in the equation $T = cS + F$, and thus in $\rho\partial u/\partial t = \partial T/\partial z$. If we calculate α by a first-order calculation, we use formula (14) but calculate Q and uT^* in the unperturbed situation. Thus from $\rho\partial u/\partial t = c\partial S/\partial z$, $T = cS$, and $\partial S/\partial t = \partial u/\partial z$, we get $v_s^2 = c/\rho$ and $S = u/v_s$.

Thus for α we obtain

$$\alpha = \frac{Q}{2\operatorname{Re}\left(\frac{uT^*}{2}\right)} = \frac{Q}{\rho|u|^2 v_s}, \tag{15}$$

with Q given by (13). This is the equation used in published results for calculations of α.

H. J. E. H. Pauwels

References

1. H. N. Spector, Phys. Rev. 127, 1084 (1962).

2. D. L. White, J. Appl. Phys. 33, 2547 (1962).

3. A. R. Hutson, J. H. McFee, and D. L. White, Phys. Rev. Letters 7, 237 (1961).

4. K. Blotekjaer and C. F. Quate, ML Report 1057, Microwave Laboratory, Stanford University, Stanford, California, July 1963.

III. RADIO ASTRONOMY*

Prof. A. H. Barrett	R. K. Breon	M. Palfy
Prof. J. W. Graham	N. E. Gaut	T. S. Slater
Prof. R. P. Rafuse	J. I. Glaser	J. H. Spoor
Prof. W. C. Schwab	J. W. Kuiper	D. H. Staelin
R. J. Allen	W. B. Lenoir	D. H. Steinbrecher
	J. M. Moran, Jr.	

RESEARCH OBJECTIVES AND SUMMARY OF RESEARCH

The research objectives of the radio astronomy group may be subdivided as follows:

1. Development of techniques for radiometry at millimeter wavelengths.
2. Observation of extraterrestrial radio sources, principally, but not exclusively, at short centimeter and millimeter wavelengths.
3. Microwave studies of the terrestrial atmosphere and surface with application to meteorological satellites.
4. A study of wide base-line interferometry at millimeter wavelengths.

During the past year work has progressed in all of these research areas, to a varying degree. Significant results have included the construction of 4.2-mm radiometer having a bandwidth of 1.8 Gc/sec, and a sensitivity of approximately 1.5°K for an integration time of 1 second. This radiometer incorporates a wide-band crystal mixer, which was also developed under this program within the past year. A digital synchronous detector has been designed and built. Work has progressed on a solid-state local oscillator, the ultimate objective being a 5-mm source of local-oscillator power. At present a high-efficiency quadrupler is in operation from 5 Gc/sec to 20 Gc/sec.

Because the over-all program is concerned with millimeter wavelengths, we must have detailed knowledge of the transmission properties of the terrestrial atmosphere. This has led to a program of atmospheric studies at wavelengths of 13, 5, and 4 mm. Observations of the 13.5-mm water-vapor line have been made over a small region centered on the resonant frequency in an attempt, thus far unsuccessful, to detect stratospheric water vapor. Further observations of the entire line will be made with a multichannel K-band radiometer that is nearing completion. A program for studying the molecular oxygen lines at high altitudes has also been started. A three-channel 5-mm radiometer has been constructed, and one balloon flight has been made. Other flights are planned for the coming year. In conjunction with observations of planetary radiation at 4-mm wavelength, measurements have also been made of atmospheric attenuation at this wavelength.

Three observing programs on extraterrestrial radiation have been initiated during the past year: (i) measurements of Venus, Taurus A, Sun, and Moon at 11.8 mm; (ii) discovery of the interstellar OH line in the absorption spectrum of Cassiopeia A at 18-cm wavelength; and (iii) observations of Jupiter and Taurus A at 4.2-mm wavelength. All of these programs will continue during the coming year, except that the K-band observations will be expanded to cover the wavelength range 16-8 mm.

In the study of wide base-line interferometry we have investigated the degree of phase coherence permitted by the terrestrial atmosphere and ionosphere as a function of frequency, and the advantages to be gained by using "clipped signals" and digital data

---

*This work was supported in part by the National Aeronautics and Space Administration (Grants NsG-250-62 and NsG-419); in part by the U.S. Navy (Office of Naval Research) under Contract Nonr-3963(02)-Task 2; and in part by Purchase Order DDL BB-107 with Lincoln Laboratory, a center for research operated by Massachusetts Institute of Technology, with the support of the U.S. Air Force under Contract AF 19(628)-500.

processing to reduce the problem of gain instability of separated amplifiers.

A 10-ft precision parabolic antenna has been put into operation on the laboratory roof and used in the 4-mm observations. The antenna is altazimuth mounted and controlled in celestial coordinates by a PDP-1 digital computer. This whole system is now in operation.

A. H. Barrett, J. W. Graham

A. A 22-Gc BALANCED, CANONICALLY TUNED VARACTOR QUADRUPLER WITH 50-mw OUTPUT POWER

To the best of the authors' knowledge the varactor multiplier that is described in this report is the first successful realization of a symmetric, multiple-diode varactor frequency multiplier at centimeter wavelengths. The quadrupler is capable of delivering a power output of more than 50 milliwatts at 22.2 Gc with an efficiency in excess of 13 per cent.

The circuit is unique in several respects. First, separation of even- and odd-harmonic power into different parts of the circuit is inherently accomplished through the use of a two-varactor balanced arrangement which increases the power-handling capability by a factor of two. Second, canonical (noninteracting) tuning is provided in the input, output, and idler circuits. Third, a combination of waveguide and coaxial elements are utilized to achieve the desired separation of harmonic and fundamental power.

The breadboard model of the quadrupler is shown in Fig. III-1. The coaxial

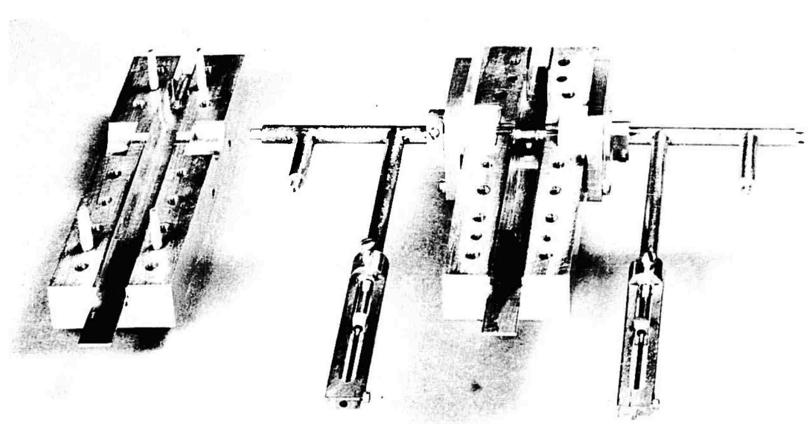

Fig. III-1. Partially exploded view of the 5.55-22.2 Gc balanced quadrupler. The two varactors are mounted across the waveguide and driven coaxially at the center point. The idlers are tuned individually by the two coaxial stubs.

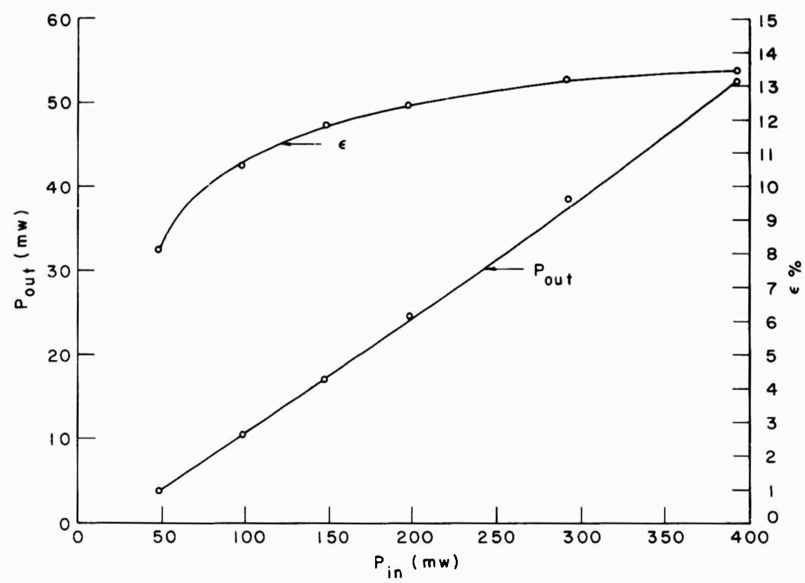

Fig. III-2. Efficiency and power output versus input power for the 5.55-22.2 Gc balanced quadrupler.

structures serve as the idler (11.1 Gc) tuning adjustments while simultaneously providing short-circuits at the guide faces at 5.55 Gc and 22.2 Gc, independently of the position of the idler tuning stubs. The third harmonic (16.65 Gc) is open-circuited at the input port by a quarter-wave series trap. The output is tuned and matched to the load with a sliding backshort and an E-H tuner (not shown), and then filtered with a simple cavity filter (to insure that all of the indicated output power is at 22.2 Gc). Input tuning is provided by coaxial, double-stub tuners. The diodes are individually biased from 1000 Ω ten-turn potentiometers supplied with 12 volts.

The power output and efficiency of the quadrupler is plotted against the input power in Fig. III-2. Note that the efficiency rapidly climbs from 8 per cent to over 10 per cent for a 3-db input-power increase from 50 mw to 100 mw and then levels off to a slow rise to 13.5 per cent at 400-mw input. Calculations have indicated that the diodes begin to overdrive at less than 80-mw input. The canonical tuning makes the adjustment of the multiplier particularly simple. Saddle points and other tuning anomalies are absent; in fact, with a very small sacrifice in efficiency, the quadrupler can be retuned for input powers ranging from 30 mw to 500 mw with bias voltage adjustment alone.

Although the experimental quadrupler employs overdriven graded-junction varactors (two matched, epitaxial GaAs varactors, Type D5047B, supplied by Sylvania Electric Products, Woburn, Mass.), the theoretical results that are available on overdriven doublers[1,2] can be used to extrapolate from the existing abrupt-junction theory.[3] If reasonable levels of idler loss and input-output circuit loss are assumed, the measured efficiency is in agreement with the theoretical efficiency. The overdrive ratio is fairly high (greater than 5:1) without appreciable conduction current (less than 1 ma/diode at 50-mw output).

Recent measurements directed toward separation of diode losses and circuit losses indicate that a considerable portion of the circuit loss is associated with the input double-stub tuners. The magnitude of this portion of the loss is approximately 3-4 db. Thus it appears that an improved input tuning structure may increase the efficiency by as much as a factor of two. A new low-loss tuning structure has been designed and construction is now in progress.

The results verify the supposition that careful attention to design, together with symmetric-circuit techniques, can remove a great deal, if not all, of the necessity of having an "agile screwdriver" for successful operation of microwave varactor multipliers. The multiplier presented no surprises other than pleasant ones and proved tractable and free of spurious oscillation.

Further results will be presented at the International Solid State Circuits Conference, to be held in Philadelphia, February 19-21, 1964, and will be published in the Conference Digest.

R. P. Rafuse, D. H. Steinbrecher

References

1. J. A. Davis, A Forward-Driven Varactor Frequency Doubler, S. M. Thesis, Department of Electrical Engineering, M. I. T., May 1963.

2. R. P. Rafuse, Recent Developments in Parametric Multipliers, Proc. National Electronics Conference, October 1963, Vol. XIX, pp. 461-470.

3. P. Penfield, Jr. and R. P. Rafuse, Varactor Multipliers (The M. I. T. Press, Cambridge, Mass., 1962).

B. DISCOVERY OF THE INTERSTELLAR 18-cm LINES OF THE HYDROXYL (OH) RADICAL

Following the detection of the 21-cm line of atomic hydrogen in the interstellar medium, Shklovsky[1] and Townes[2] both suggested that the Λ-doublet line of the $^2\Pi_{3/2}$, $J = 3/2$ state of the hydroxyl (OH) radical might be detectable. A search, in 1956, by Barrett and Lilley was unsuccessful,[3] but this search was made without the benefit of precise laboratory frequencies for the lines. In 1959, Ehrenstein, Townes, and Stevenson[4] measured the frequencies in the laboratory and obtained 1667.34 ± 0.03 mc/sec for the $F = 2 \rightarrow 2$ hyperfine line, and 1665.46 ± 0.10 mc/sec for the $F = 1 \rightarrow 1$ line.

With accurate values of the frequencies and the improved techniques that are now available, another search was undertaken, in October 1963, as a joint experiment between the Research Laboratory of Electronics and Lincoln Laboratory. M. L. Meeks, S. Weinreb, and J. C. Henry participated from Lincoln Laboratory. The experiment was performed with the 84-ft parabolic antenna at Millstone Hill Observatory, Lincoln Laboratory, M. I. T., and made use of a digital spectral-line autocorrelation radiometer that had been designed and built by Weinreb at the Research Laboratory of Electronics

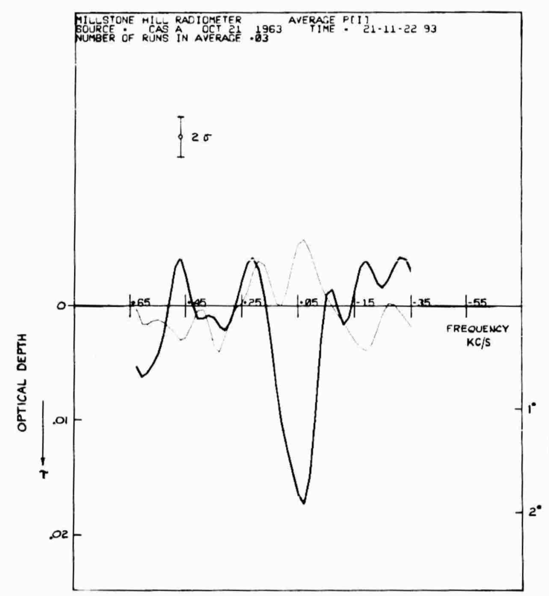

Fig. III-3. A portion of the observed 1667 mc/sec OH absorption spectrum in Cassiopeia A. The heavy line shows 8000 seconds of data taken with the antenna beam directed at Cassiopeia, and the light line shows 6000 seconds of data taken with the beam displaced slightly from Cassiopeia.

as part of his doctoral research program.[5]

Observations were conducted between October 15 and October 29, 1963, in the direction of the strong radio source Cassiopeia A, since this direction would yield the largest observable effect for the least number of OH radicals in the antenna beam. The observation frequency was corrected for the Doppler shift resulting from the motion of the earth and sun. The first night's observation gave strong evidence of a positive detection of OH absorption lines in the spectrum of Cassiopeia A, and subsequent nightly observations furnished verification. Absorption lines corresponding to both OH lines were found at 1665 mc and 1667 mc, with relative intensities in agreement with expected values. A 20-kc shift of the lines was observed between October 17 and October 29, 1963, which is in agreement with the orbital velocity of the earth and gives positive evidence that the OH was extraterrestrial. One of the absorption lines is shown in Fig. III-3.

The detection of OH provides radio astronomy with a second radio line, and will lead to many comparison studies with the galactic H distribution as determined from 21-cm research. The OH/H abundance ratio can be computed from our results, and gives values of 10^{-7}. Our preliminary results have been published.[6] Word of our discovery was communicated to radio astronomers with the result that the Australian group confirmed the detection within three weeks.

Observations of OH in other parts of the galaxy will continue at the Millstone Hill Observatory.

A. H. Barrett

References

1. I. S. Shklovsky, Doklady Akad. Nauk S. S. S. R. 92, 25 (1953).

2. C. H. Townes, International Astronomical Union Symposium No. 4, edited by H. C. van de Hulst (Cambridge University Press, London, 1957), p. 92.

3. A. H. Barrett and A. E. Lilley, Astron. J. 62, 5 (1957).

4. G. Ehrenstein, C. H. Townes, and M. J. Stevenson, Phys. Rev. Letters 3, 40 (1959).

5. S. Weinreb, A Digital Spectral Analysis Technique and Its Application to Radio Astronomy, Technical Report 412, Research Laboratory of Electronics, M. I. T., August 30, 1963.

6. S. Weinreb, A. H. Barrett, M. L. Meeks, and J. C. Henry, Nature 200, 829 (1963).

IV. FAR INFRARED SPECTROSCOPY

Prof. C. H. Perry
Jeanne H. Fertel
D. J. McCarthy
E. C. Reifenstein III
J. P. Stampfel, Jr.
H. D. Wactlar

RESEARCH OBJECTIVES

The aim of this group is to continue the study of the properties of solids in the far infrared. Transmission and reflection measurements at room temperatures of three perovskite titanates have been completed. Temperature-dependent reflection measurements in the range 77-700°K are to be undertaken on these materials above their Curie temperatures to gain further understanding of their ferroelectric behavior. With this end in view, the study is being extended to zirconates, hafnates, and other perovskites that exhibit similar properties. Current solid-state research problems also include the infrared spectra of some antiferromagnetic materials and some inorganic compounds that have low internal molecular and lattice vibrations.

The study of low-temperature detectors for the 50-1000 μ region continues in cooperation with Professor R. C. Lord of the Spectroscopy Laboratory, M. I. T.* Detector noise measurements as a function of frequency are being undertaken to study the detectivity of these bolometers and ascertain the optimum chopping frequency. The evaluation of the performance of a commercial far infrared Michelson interferometer is expected to be carried out in the near future, but this will have to await delivery of the instrument. Interferometers should inherently make better use of the available energy than conventional spectrometers; this should decrease the time for taking spectra, as well as provide better resolution. Some modifications in the instrument will be necessary in order to make reflection studies and for low-temperature measurement, but these appear to be minor.

C. H. Perry

A. FAR INFRARED REFLECTANCE AND TRANSMITTANCE OF POTASSIUM MAGNESIUM FLUORIDE AND MAGNESIUM FLUORIDE

1. Introduction

Many compounds possessing the cubic perovskite crystal structure exhibit unusual properties, such as ferroelectricity and antiferromagnetism. Knowledge of the nature of the interatomic forces in the crystal should prove extremely useful in explaining these phenomena. To make such information available, several studies[1-5] of the far infrared and Raman spectra of the perovskite titanates and the related rutile have been reported recently. Some disagreement exists concerning the interpretation of these spectra. To furnish additional data to help resolve the disagreement, and to facilitate the interpretation of the electronic absorption spectral studies of the compounds made by one of us (J. F.), research on the transmittance and reflectance spectra and the dielectric dispersion of potassium magnesium fluoride and magnesium fluoride was undertaken as a prelude to a more comprehensive study of the vibrational nature of fluoride perovskites and their "rutile" counterparts.

*This work is supported in part by the National Science Foundation (Grant G-19637).

2. Experiment

The room-temperature reflectances of potassium magnesium fluoride and magnesium fluoride were measured by using unpolarized radiation from 4000 cm^{-1} to 30 cm^{-1} relative to the reflectance of a reference mirror coated with aluminum. Measurements were also made on each material at 5 cm^{-1}, with the use of a "Carcinotron" source of 2-mm radiation at Lincoln Laboratory, M. I. T.; the samples were mounted at a 20° included-angle bond in a light pipe, and the reflectances were compared with a reference mirror in the same position. The results were in reasonably close accord with our low-frequency far infrared measurements.

The infrared reflection spectra were recorded on a Perkin-Elmer Model 521 grating double-beam spectrophotometer, equipped to scan continuously from 4000 cm^{-1} to 250 cm^{-1}. A Perkin-Elmer reflectance attachment was used in this instrument, and the reflectance data were recorded at an angle of incidence of approximately 15°. Below 400 cm^{-1}, it was necessary to flush the instrument with evaporated liquid nitrogen to remove most of the water vapor. A single-beam grating spectrometer, constructed in the M. I. T. Spectroscopy Laboratory, was used for measurements below 500 cm^{-1}.[6] This instrument was improved by complete enclosure in a vacuum case[7]; this procedure allowed water vapor to be entirely removed from the optical path and so provided smooth background spectra. Again, the angle of incidence for the reflection measurements was 15°. The samples used were grown at the Bell Telephone Laboratories, Inc. The $KMgF_3$ sample was a single crystal with a polished face approximately 0.5 inch square. The MgF_2 was not a single crystal and was more irregularly shaped, which necessitated a slight vignetting of the beam. Transmission measurements over the same range as for reflection were made on the two infrared instruments described above. The samples consisted of finely divided powders dispersed in KBr matrices for measurements above 300 cm^{-1}, and dispersed in polyethylene for measurements below 600 cm^{-1}.

3. Data Analysis

The real and imaginary parts of the complex dielectric constant, $\epsilon' = n^2 - k^2$ and $\epsilon'' = 2nk$ (where n is the refractive index, and k is the absorption coefficient) were obtained by transforming the reflectance data by using the Kramers-Kronig relation.[8] In this, the reflectivity amplitude is given by $re^{-i\theta}$, where $r = R^{1/2}$, and R and $\theta(\nu)$ are respectively the reflectance and the associated phase angle, the latter being given by

$$\theta(\nu) = \frac{2\nu}{\pi} \int_0^\infty \frac{\ln [r(\nu')]\, d\nu'}{\nu^2 - \nu'^2}.$$

The infinite integral was evaluated by representing $\ln r(\nu')$ by straight-line segments between data points and programming the relationships for use on an IBM 7090 computer at the Computation Center, M. I. T.

4. Discussion

Potassium magnesium fluoride possesses the cubic perovskite crystal structure, which belongs to the space group O_h^1 (P_{m3m})[9] and contains one molecule per unit cell. Each atom of the same element in the crystal forms an equivalent set, but the site symmetry of the fluorine atoms is D_{4h}, while that of the magnesium and potassium atoms is O_h.

In discussing the number and symmetry species of the active vibrational modes in the perovskite $BaTiO_3$, Last[1] breaks down thc twelve nontranslatory modes into one triply degenerate set of three lattice modes (F_{1u}) in which the TiO_3 group oscillates as an entity against the lattice of barium atoms and nine modes of vibration of a titanium atom surrounded by a regular octahedron of 6 half-oxygen atoms. The last are treated under the point group O_h and yield the result that there are two triply degenerate sets of F_{1u} infrared allowed modes and one triply degenerate F_{2u} infrared forbidden set of modes. Narayanan and Vedam,[4] in reporting the Raman spectrum of strontium titanate, disagree with Last's conclusion and assert that there are, in fact, 4 nontranslatory triply degenerate sets of infrared-active modes, all of which belong to species F_{1u}, and they quote Rajagopal's[10] treatment of the lattice dynamics of cubic perovskites as substantiating this contention. We feel that they have misinterpreted this work, for although Rajagopal states there are four triply degenerate fundamentals for a cubic ABO_3 structure, he does not specify to which symmetry species they belong. He does indicate, however, that his determinant of order fifteen factors into three of order five (indicating 5 triply degenerate oscillations, of which one is the acoustical or translatory mode), and furthermore that the ν_4 mode separates out. The cubic equation resulting from the removal of the translatory mode and the ν_4 vibration yields the three infrared-active vibrational modes described by Last.

We have used the following standard considerations to arrive at a conclusion that is in agreement with Last's. The number of normal modes of a particular symmetry species is given by n_i, the number of times the irreducible representation Γ_i corresponding to that species is contained in the reducible representation Γ. The group theoretical expression for n_i is

$$n_i = \frac{1}{N} \sum_{\rho} h_\rho X'_\rho(R)\, X_i(R),$$

where N is the order of the group, h_ρ the number of group operations falling under the class ρ, $X'_\rho(R)$ and $X_i(R)$ are the characters of the group operation R in the representation Γ and Γ_i, respectively, and

$$X'_\rho(R) = U_R(\pm 1 + 2\cos\phi_R).$$

Proper rotations by ϕ take the positive sign, and improper rotations take the negative sign. For point group operations, U_R is given by the number of atoms that remain invariant under operation R. For space group operations, however, which are appropriate when considering crystals, U_R is the number of atoms in the repeating unit (for crystals, the unit cell) which, for a particular operation R, contains either the appropriate rotation axis, reflection plane or inversion center. When applied to $KMgF_3$ (which has an ideal cubic perovskite structure[11]), these considerations yield $4F_{1u} + 1F_{2u}$ as the symmetry species of the normal modes, of which one F_{1u} is a translation and the F_{2u} mode is forbidden in the infrared. We find that such a conclusion is also in agreement with our experimental data. Figures IV-1 and IV-2 show the transmittance and reflectance spectra of $KMgF_3$, and Fig. IV-3 shows the real and imaginary part of the dielectric constant calculated from the reflectance data. The maxima of the imaginary part yields the true resonant frequencies, and these are listed together with assignments in Table IV-1a. While we describe the various modes as bending and stretching, we realize that they are not pure modes, and knowledge of the actual form of the vibrations must await a complete normal coordinate analysis.

For magnesium fluoride, the tetragonal crystal structure is isomorphous with

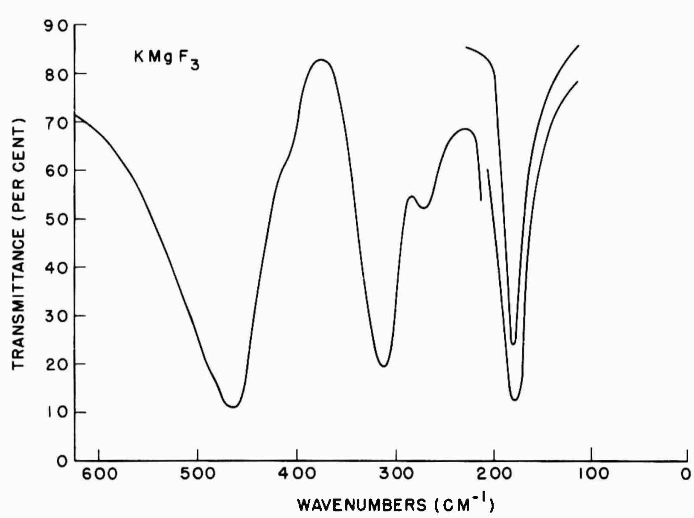

Fig. IV-1. Transmittance of $KMgF_3$ in polyethylene films.

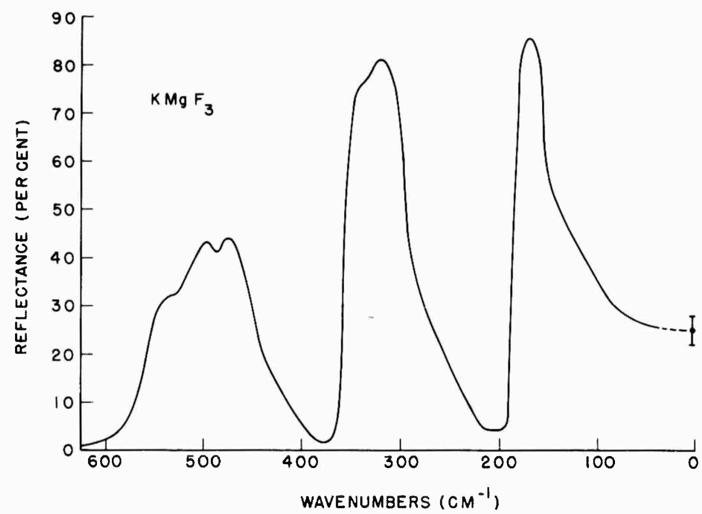

Fig. IV-2. Reflectance of $KMgF_3$.

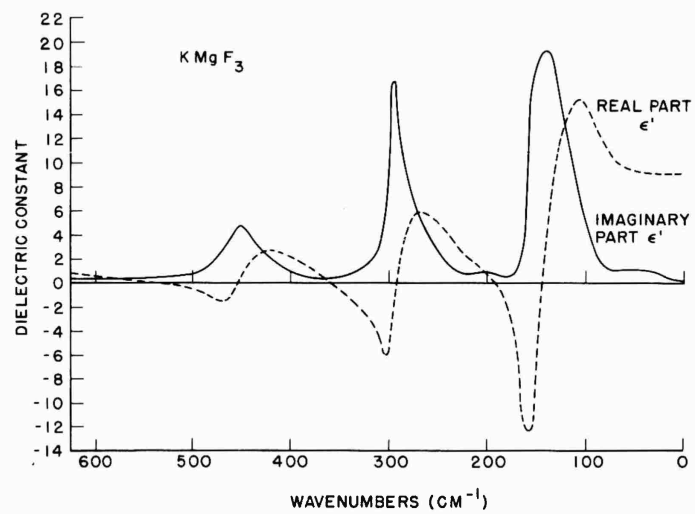

Fig. IV-3. K-K analysis of reflectance data for $KMgF_3$.

cassiterite (SnO_2), belongs to the space group D_{4h}^{14} [$P4_2/mnm$],[12] and contains two molecules of MgF_2 per unit cell. The magnesium atoms have D_{2h} site symmetry, and the fluorine atoms have C_{2v}. Using the considerations outlined above, we find that the vibrations belong to the following symmetry species of the D_{4h} space group (D_{4h}):

Table IV-1. Frequencies (in cm^{-1}) and symmetry of infrared modes obtained from K-K analysis of the reflection data for $KMgF_3$ and for MgF_2.

			(a) $KMgF_3$
ν_1	450	F_{1u}	MgF stretch
ν_2	295	F_{1u}	FMgF bend
ν_3	140	F_{1u}	K-(MgF_3) stretch (lattice mode)
			(b) MgF_2
ν_1	435	E_u	MgF stretch
ν_2	405	E_u	MgF stretch – FMgF bend
ν_3	280	E_u	pseudo lattice modes with Mg moving one way and F in the opposite direction
ν_4	265	A_{2u}	

$A_{1g} + A_{2g} + A_{2u} + B_{1g} + B_{2g} + 2B_{1u} + E_g + 3E_u$, of which only the A_{2u} and $3E_u$ modes are infrared-active. This agrees with the results of the treatment of the rutile vibrations by Narayanan[13] and Matossi.[14]

The transmission and reflection spectra and the dielectric dispersion data for MgF_2

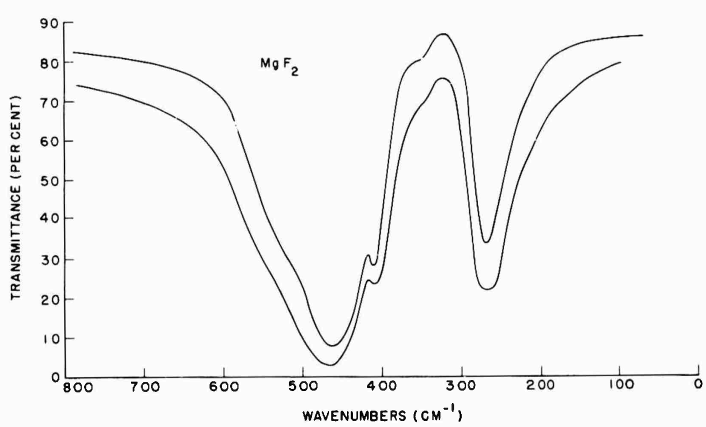

Fig. IV-4. Transmittance of MgF_2 in polyethylene films.

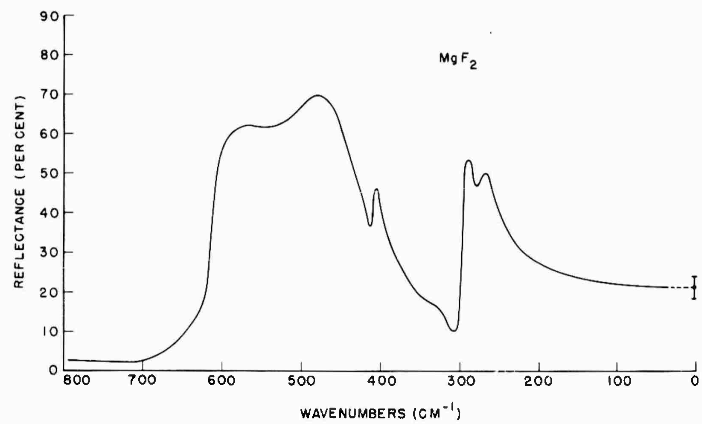

Fig. IV-5. Reflectance of MgF_2.

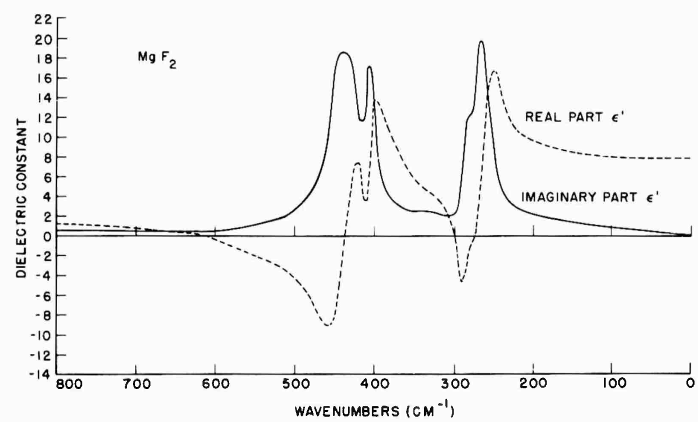

Fig. IV-6. K-K analysis of reflectance data for MgF_2.

are shown in Figs. IV-4, IV-5, and IV-6, and the resonant frequencies are listed in Table IV-1b. The A_{2u} and one of the E_u modes correspond to motions in which all of the fluorine atoms are moving together in a direction opposite to that of all the Mg atoms. There is, of course, no "lattice" mode corresponding to that for $KMgF_3$. The two remaining E_u modes can be considered as motions in which only the fluorine atoms are moving appreciably. The stretching and bending modes are more difficult to describe and less pure than for $KMgF_3$, since the fluorines in MgF_2 form an irregular octahedron around the magnesium atoms and consequently the lattice is made up of interpenetrating unit cells. Hence a mode in one cell which could be described as predominantly a stretching mode automatically gives rise to a predominantly bending mode in all of the interpenetrating cells. Again, a full description of the form of the vibrations must await a normal coordinate analysis for which the additional information regarding the frequencies of the infrared-active modes must be obtained from the Raman spectrum.

We wish to express our thanks to Professor R. C. Lord of M. I. T. for his encouragement in this work and for many helpful suggestions; to Dr. D. L. Wood of Bell Telephone Laboratories, Inc. for useful discussions; to Mr. J. Ballentyne of the Insulation Laboratory, M. I. T., for reflection measurements at 5 cm^{-1} taken at Lincoln Laboratory, M. I. T., and for the use of his K-K analysis program, and to Dr. H. J. Guggenheim and Dr. K. Knox of Bell Telephone Laboratories, Inc. for the crystal samples.

C. H. Perry, G. R. Hunt, J. Ferguson

(Dr. G. R. Hunt is now at the Air Force Cambridge Research Laboratories (CRFL), Bedford, Massachusetts. Dr. J. Ferguson is at Bell Telephone Laboratories, Inc., Murray Hill, New Jersey.)

References

1. J. T. Last, Phys. Rev. 105, 1740 (1957).
2. A. S. Barker, Jr. and M. Tinkham, Phys. Rev. 125, 1527 (1962).
3. W. G. Spitzer, R. C. Miller, D. A. Kleinman, and L. E. Howarth, Phys. Rev. 126, 1710 (1962).
4. P. S. Narayanan and K. Vedam, Physik 163, 158 (1961).
5. C. H. Perry and B. N. Khanna, Quarterly Progress Report No. 71, Research Laboratory of Electronics, M. I. T., October 15, 1963, pp. 23-32.
6. R. C. Lord and T. K. McCubbin, Jr., J. Opt. Soc. Am. 47, 689 (1957).
7. C. H. Perry, Quarterly Progress Report No. 70, Research Laboratory of Electronics, M. I. T., July 15, 1963, pp. 19-31.
8. T. S. Robinson, Proc. Phys. Soc. (London) B65, 910 (1952).
9. R. W. G. Wyckoff, Crystal Structures, Vol. 2, Chap. VIIA, 5 (Interscience Publishers, New York, n. d.).
10. A. K. Rajagopal, J. Phys. Chem. Solids 23, 633 (1962).
11. K. Knox, private communication, 1963.
12. R. W. G. Wyckoff, op. cit., Vol. 1, Chap. IV, b1.
13. P. S. Narayanan, J. Indian Inst. Sci. 32, 279 (1950).
14. F. Matossi, J. Chem. Phys. 19, 1543 (1951).

B. INFRARED ABSORPTION SPECTRA OF CRYSTALLINE K_2PtCl_4

1. Introduction

Many fundamental frequencies of inorganic molecules occur below 400 cm^{-1}. In particular, the stretching and bending frequencies of metal-halogen bonds and lattice vibrations occur in this region. We have made a preliminary investigation of K_2PtCl_4 with a view toward extending this study to other complex halides. A similar solid-state study of this molecule has been carried out recently by D. M. Adams and H. A. Gebbie,[1] using a far infrared interferometer. There is some disagreement, however, in the assignment of the infrared normal modes because we have found two additional infrared-active vibrations that were not observed by the previous authors. Owing to the presence of a center of symmetry in the unit cell of these crystals, there is a mutual exclusion rule between the infrared- and the Raman-active modes. The Raman spectra of the complex ion $(PtCl_4)^{2-}$ has been observed by H. Stammreich and R. Forneris,[2] and the assignment of the observed frequencies to the Raman-active modes can be made directly.

2. Experiment

Transmission measurements of crystalline K_2PtCl_4 suspended in polyethylene matrices[3] have been studied from 400 to 60 cm^{-1}. The measurements above 250 cm^{-1} were made on a P-E double-beam spectrophotometer, and below 250 cm^{-1} they were recorded on the single-beam vacuum far infrared instrument.[4,5] Preliminary investigation at room temperature showed a strong band at ~320 cm^{-1}, and two broad bands in the far infrared. Further experiments with samples of various thicknesses showed that the two broad bands were probably each split, and this was confirmed by transmission measurements at liquid-nitrogen temperature, with the use of the Limit Research

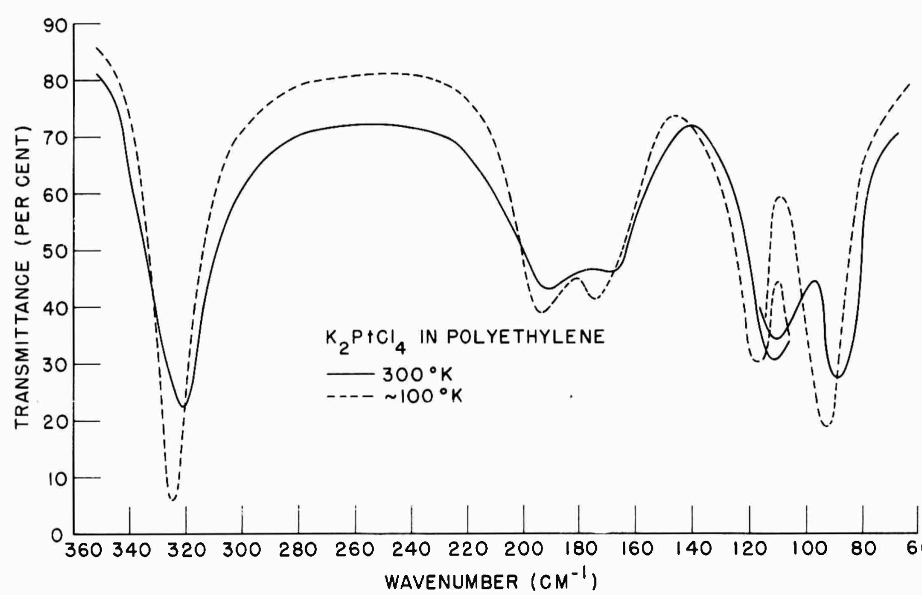

Fig. IV-7. Transmittance of K_2PtCl_4 in polyethylene from 60 cm^{-1} to 360 cm^{-1}.

Table IV-2. Internal and lattice vibrations in K_2PtCl_4. Crystal Structure D'_{4h}, one molecule per unit cell.

Frequency (cm^{-1})		Approximate intensity	Species	Selection rules	Qualitative description
300°K	100°K				
89 ± 2	91 ± 1	strong	E_u	Infrared	Lattice mode (Doubly degenerate)
110 ± 2	117 ± 2	medium	A_{2u}	Infrared	Lattice mode
164	–	weak	B_{1g}	Raman	$PtCl_4$ I. P. bending
170 ± 5	174 ± 2	weak	A_{2u}	Infrared	$PtCl_4$ O. P. bending
190 ± 5	193 ± 2	weak	E_u	Infrared	$PtCl_4$ I. P. bending
304	–	strong	B_{2g}	Raman	$PtCl_4$ I. P. anti-symmetric stretching
321 ± 1	324 ± 1	strong	E_u	Infrared	$PtCl_4$ I. P. stretching
335	–	strong	A_{1g}	Raman	$PtCl_4$ I. P. symmetric stretching
–	–	–	B_{1u}	Inactive in infrared and Raman	$PtCl_4$ O. P. bending

Corporation low-temperature cell both in the P-E 521 and in the far infrared instrument. The final results are shown in Fig. IV-7 for the sample of ~3 mg K_2PtCl_4 per square centimeter run at ~300°K and ~100°K.

3. Discussion

The vibrational spectrum of $R_n(XY_4)$ molecules belonging to the D'_{4h} space group would be expected to consist of 5 nondegenerate and two doubly degenerate fundamental modes for the $(XY_4)^{n-}$ ion. The tetragonal crystal structure[6] would cause the triply degenerate lattice modes to split into a nondegenerate and a doubly degenerate lattice mode.

Three Raman-active frequencies have been observed,[2] in full agreement with the selection rules, and the normal mode assignment can be made directly. Two doubly degenerate and one nondegenerate mode are active in the infrared, together with one degenerate and one nondegenerate lattice mode as described above. Five infrared-active vibrations have been observed in our results (see Fig. IV-7) and this is in full agreement with the selection rules. The frequencies, vibrational assignment and a short description of the motion are given in Table IV-2.

Macoll[7] gives the approximate form of these normal vibrations and the symmetry species, with which all previous workers[1,2] and the present authors agree. Adams and Gebbie,[1] however, in the assignment of their frequencies ignore the fact that they may not have been able to resolve all of the bands and also the possibility that one of the bands with which they associate an internal vibration may be a lattice mode. This

Table IV-3.

Frequency (cm^{-1})		Species	Qualitative description
Adams and Gebbie	This work		
320	321 ± 1	E_u	$PtCl_4$ I. P. stretching
183*	190 ± 5	E_u	$PtCl_4$ I. P. bending
93*	170 ± 5	A_{2u}	$PtCl_4$ O. P. bending
–	110 ± 2	A_{2u}	Lattice mode
–	89 ± 2	E_u	Lattice mode

*broad

can be seen more clearly in Table IV-3, in which our results are compared with those of Adams and Gebbie.

The complete removal of these ambiguities can only be accomplished by further measurements on materials of similar structure. Consequently, work is already in progress here on Rb_2PtCl_4 and Cs_2PtCl_4. We would expect that the cation-$(PtCl_4)$ lattice vibrations would be most changed, and we would expect to see the two lowest vibrations shift to even lower frequency, and little change in frequency for those associated with the $PtCl_4$ internal vibrations if our interpretation is correct.

Further study is proposed for the bromides of these materials, and also for PdII and AuIII (in place of the PtII), in order to determine the low internal molecular and lattice vibrations for all of these materials.

C. H. Perry, Jeanne H. Fertel

References

1. D. M. Adams and H. A. Gebbie, Spectrochim. Acta 19, 925 (1963).
2. H. Stammreich and R. Forneris, Spectrochim. Acta 16, 363 (1960).
3. C. H. Perry and B. N. Khanna, Quarterly Progress Report No. 71, Research Laboratory of Electronics, M.I.T., October 15, 1963, pp. 23-32.
4. R. C. Lord and T. K. McCubbin, Jr., J. Opt. Soc. Am. 47, 689 (1957).
5. C. H. Perry, Quarterly Progress Report No. 70, Research Laboratory of Electronics, M.I.T., July 15, 1963, pp. 19-31.
6. R. W. G. Wyckoff, Crystal Structures (Interscience Publishers, New York, n.d.).
7. A. Macoll, J. Proc. Roy. Soc. New South Wales 77, 130 (1944).

V. ELASTIC AND THERMAL PROPERTIES OF SOLIDS

Prof. C. W. Garland
R. H. Renard
C. F. Yarnell

RESEARCH OBJECTIVES

There is a variety of problems in the physics and chemistry of solids in which phonons (lattice vibrations) play an important role. The theory of lattice dynamics can be used to calculate many bulk properties of a crystalline material if appropriate interatomic force constants are known. The adiabatic elastic constants of a single crystal, which can be measured with high precision by ultrasonic pulse techniques, provide direct information about the dispersion curves and frequency spectrum at low frequencies, and thus determine the low-temperature thermal properties. They also provide a way of testing or evaluating the force constant parameters in various force models of a solid.

Recently, attention has been focussed on the elastic properties of crystals near lambda-point transitions. There are "anomalous" changes in the elastic constants of a solid near the critical temperature for an order-disorder transition; such changes are related to the detailed structural changes that occur and to the nature of the interatomic forces involved.

Experiments performed in the past year showed that there are important variations in the elastic constants of NH_4Cl around the lambda-point transition. These variations are caused partly by the change in the volume of the lattice which occurs at the lambda-point transition. To resolve these contributions, the pressure dependence of the elastic constants of NH_4Cl will be studied at several temperatures. A high-pressure system capable of achieving pressures up to 10,000 atmospheres has been built for this study. A large constant-temperature bath was built in order to obtain good control of the temperature down to -30°C. To improve the accuracy of the measurements, the ultrasonic pulse method of H. J. McSkimin was adopted. Preliminary measurements of the elastic constants of NH_4Cl as a function of pressure at room temperature have been made.

NH_4Br and K_2SnCl_6 have lambda-point transitions at a convenient temperature. Crystals of NH_4Br and K_2SnCl_6 are being grown. The elastic constants of these crystals will be measured as a function of temperature and pressure and the results compared with those for NH_4Cl.

C. W. Garland

Publications

C. W. Garland and J. R. Wilt, Infrared spectra and dipole moments of $Rh_2(CO)_4Cl_2$ and $Rh_2(CO)_4Br_2$, J. Chem. Phys. 36, 1094 (1962).

C. W. Garland and K. C. Park, Low temperature elastic constants of Gallium Arsenide, J. Appl. Phys. 33, 759 (1962).

L. L. Isaacs and C. W. Garland, Heat capacity of crystalline polyethylene from 1.8°K to 5.3°K, J. Phys. Chem. Solids 23, 311 (1962).

C. W. Garland, Infrared spectra of adsorbed molecules, PB Report 149, 515 (1962), U. S. Department of Commerce, Office of Technical Services, Washington, D. C.

D. P. Shoemaker and C. W. Garland, Experiments in Physical Chemistry (McGraw-Hill Book Company, New York, 1962).

C. W. Garland and J. S. Jones, Elastic constants of Ammonium Chloride near the lambda transition, J. Chem. Phys. (in press).

VI. GEOPHYSICS

Prof. F. Bitter
Prof. G. Fiocco
Dr. T. Fohl
Dr. H. C. Praddaude
Dr. J. F. Waymouth
R. J. Breeding
J. C. Chapman
G. W. Grams
W. D. Halverson
H. C. Koons
R. G. Little
O. Redi
C. J. Schuler, Jr.

RESEARCH OBJECTIVES

This group will be concerned with a variety of problems of geophysical interest, including laboratory investigations of the properties of matter and radiation under extreme conditions. The initial program includes two principal projects.

1. Planetary Radiation Belts

Theoretical and experimental studies will be undertaken to extend our knowledge of the interaction of charged particles in a magnetic field, especially to include conditions under which electric and magnetic forces are of comparable magnitude. These studies should have a bearing on scattering, recombination, and radiation processes in very low density plasmas.

Laboratory studies are planned for the investigation of the diffusion of charged particles in the fields of magnetic dipoles.

F. Bitter

2. Scattering of Light in the Earth's Atmosphere

Studies of the Earth's atmosphere by scattering of laser radiation will be pursued. An important part of this program will involve studying the dust layers existing at an altitude of 20 km and above. We are planning to take the apparatus to Sweden during next summer to observe noctilucent clouds.

The possibility of using Raman scattering in order to obtain profiles of density and temperature for various species in the lower atmosphere will be investigated.

The scattering cross section in the vicinity of an absorption line will be investigated experimentally with a tunable laser.

G. Fiocco

A. TRANSITION FROM PREDOMINANTLY ELECTRIC TO PREDOMINANTLY MAGNETIC BINDING IN THE HYDROGEN ATOM IN A MAGNETIC FIELD

Attempts to obtain complete solutions for the hydrogen atom in a magnetic field thus far have been only partially successful, and will not be reported now. The following simple semiclassical calculation of the effect of combined magnetic and electric forces acting on electrons in circular orbits in a hydrogen atom with the nucleus at rest indicates the kind of phenomena to be expected. For this case, for the forces, we have

$$\frac{m v^2}{r} = \frac{ke}{r^2} + evB, \tag{1}$$

and for the canonical angular momentum

$$p = n\hbar = mr^2\left(\dot{\phi} - \frac{eB}{2m}\right). \tag{2}$$

Upon eliminating the velocity, we obtain an expression for the radius

$$n^2 = \frac{r}{a} + \frac{r^4}{b^4}, \tag{3}$$

where a is the first Bohr orbit

$$a = \frac{\hbar^2}{kem} = 0.53 \times 10^{-10} \text{ meter},$$

and b is the lowest cyclotron orbit radius

$$b = \frac{3.62 \times 10^{-8} \text{ meter}}{\sqrt{B}}.$$

This case is illustrated in Fig. VI-1. For small values of r and B, the radius is independent of B. This is in accordance with the Larmor theorem, which states that, to a first approximation, magnetic fields do not distort atomic configurations, but merely produce the Larmor precession. At high fields and in large orbits in which

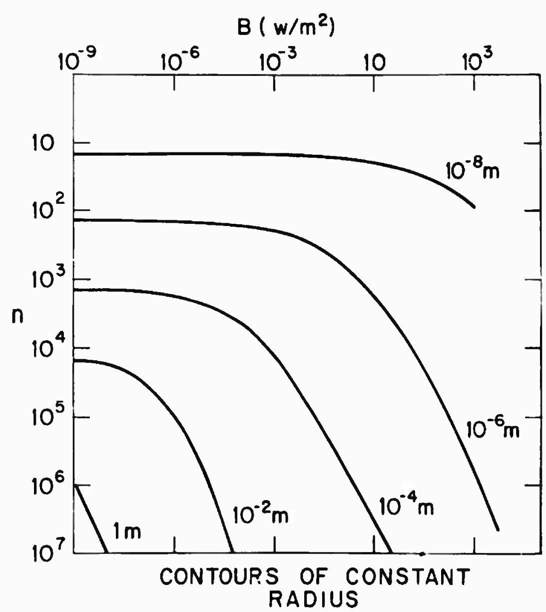

Fig. VI-1. Radius of circular Bohr orbits with magnetic quantum number $m = \pm n$ plotted as a function of n and B.

the electrostatic forces are negligible, the orbits approach the cyclotron orbits of free electrons.

The total energy of the system,

$$E = \frac{1}{2} mv^2 - \frac{ke}{r}, \tag{4}$$

may be put into the form

$$E = \pm\mu_B B\left[n \pm \sqrt{n^2 - \frac{r}{a}}\right] - \frac{1}{2}\frac{ke}{r}. \tag{5}$$

For small orbits in weak magnetic fields $n^2 = \frac{r}{a}$, and the energy is simply the zero-field energy $\pm n\mu_B B$. For large fields $\frac{r}{a} \ll n^2$, and the energy becomes

$$E = 2n\mu_B B$$

when the magnetic moment is antiparallel (diamagnetic), or zero when it is parallel (paramagnetic) to the applied field. In the diamagnetic case, the energy levels approach the cyclotron or Landau levels.

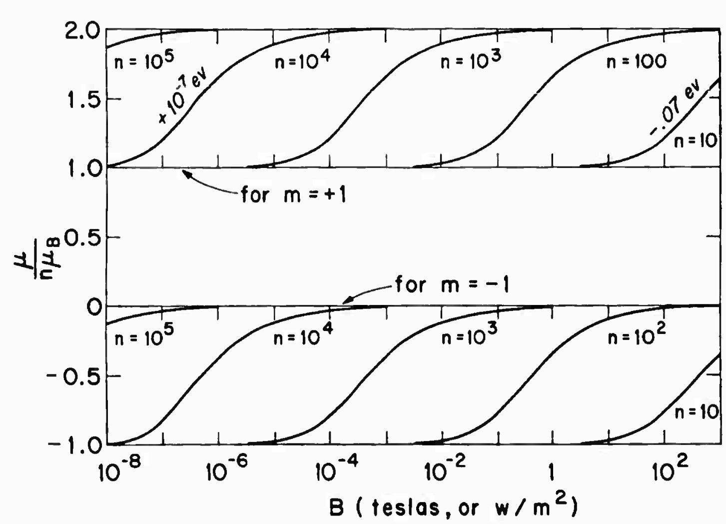

Fig. VI-2. Magnetic moment of quantized circular orbits in arbitrary magnetic fields.

The magnetic moment of the atom in these states is plotted in Fig. VI-2 in units normalized to "n" Bohr magnetons. The density of energy levels, normalized to the corresponding density of Landau levels, is plotted in Fig. VI-3. Note that the usually accepted density of states of an atom in zero magnetic field, which rises to infinity as negative

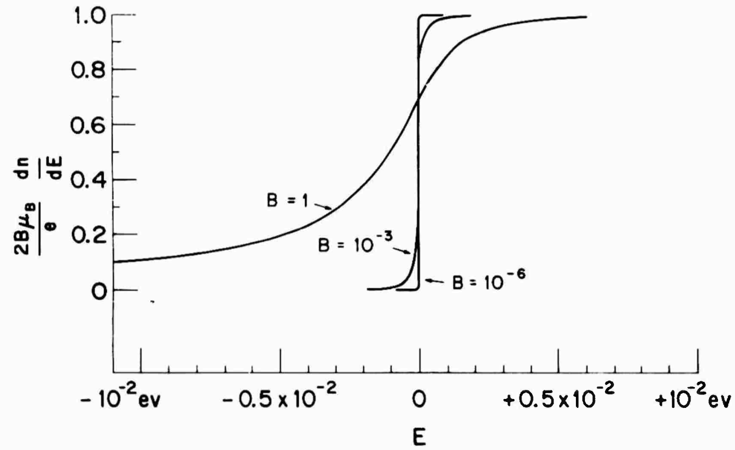

Fig. VI-3. Density of atomic-energy levels for circular diamagnetic orbits in the vicinity of the ionization potential.

energies approach the ionization potential and is zero for positive energies, is a "singular" or physically unachievable condition. In arbitrarily weak fields these particular states have a very low density for negative energies, and a constant density equal to the density of Landau levels for free electrons for positive energies.

This work was partly carried out at the Computation Center of the Massachusetts Institute of Technology.

F. Bitter

B. AN INTERPRETATION OF SOME OPTICAL RADAR RESULTS*

Recent optical radar observations of echoes from the upper atmosphere have been reported elsewhere by Fiocco and Smullin.[1] The results of several successive nights of observations indicated, among other features, weak sporadic echoes at altitudes between 110 km and 140 km; between 100 km and 110 km a noticeable reduction of the returned signal was observed. The interpretation of the results reported here has been developed in collaboration with Dr. Giusseppe Colombo, of the Smithsonian Institution Astrophysical Observatory, Cambridge, Massachusetts, and the University of Padua, Italy.

The results that are of present interest are shown in Fig. VI-4. The diagram gives the observed radar cross section per unit volume, averaged over 10-km range intervals

*This work was supported in part by the National Aeronautics and Space Administration (Grant NsG-419).

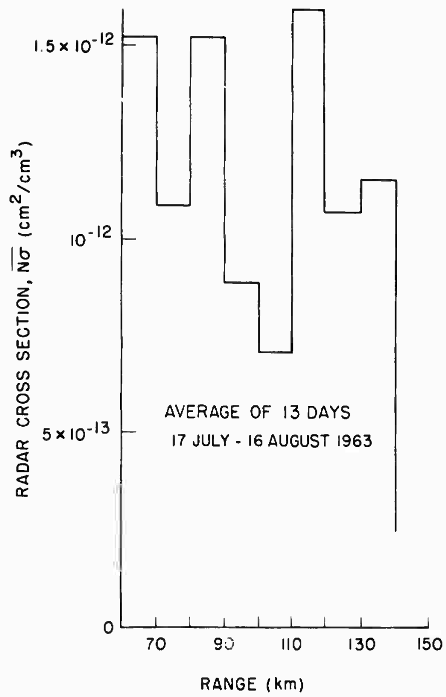

Fig. VI-4. Average of observed radar cross sections per unit volume versus range.

and over 13 nights during which observations were possible, from 17 July to 16 August 1963. The radar's wavelength is 0.694 micron.

We are concerned at present with an interpretation of the echoes obtained at heights above 100 km, that is, with the presence of maxima in the radar cross section above 100 km, and of minima between 100 km and 110 km. The diagram results from averaging the successive observations of each single night (several hundred pulses), and then averaging again the results of the 13 successive nights, giving to each night the same weight. A few remarks have to be made with regard to the accuracy of these determinations. Some measure of accuracy is provided by the amplitude of the rms background fluctuations, which is equivalent to 1.5×10^{-13} $(Z/100)^2$ cm^2/cm^3 (Z = height in km). Because of slow recovery and nonlinearity of the photodetector, the sensitivity of the receiver decreases with decreasing height. The effect is noticeable at altitudes below 90 km; the cross sections, as given in Fig. VI-4, are less accurate at this range. No correction has been introduced, since the present discussion is limited to the results of observations at higher levels. We note, however, that the echoes observed between 80 km and 90 km, at the mesopause, are indicative of cross sections much smaller than those that would be expected in noctilucent clouds,[2] and are in agreement qualitatively with the measurements of Mikirov.[3] The appearance of these echoes could be related to the same process that is responsible for the formation of the noctilucent clouds.

It seems reasonable to assume that these echoes at higher altitudes are produced by small particles, meteoroids. A knowledge of their shape and of the ratio of the size to the wavelength is therefore essential in order to establish their individual cross sections.

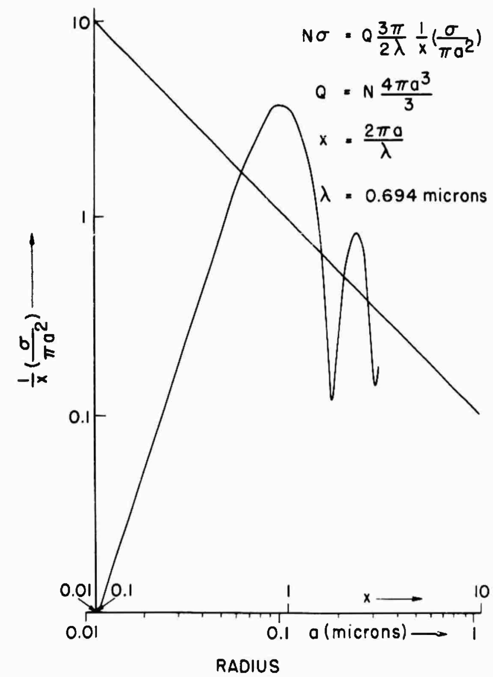

Fig. VI-5.
Radar cross section $N\sigma$ of N totally reflecting spheres of equal radius a and constant volume Q.

For a particle much larger than the wavelength the radar cross section, σ, is proportional to the geometrical cross section and independent of wavelength; for dimensions much smaller than the wavelength λ, the scattering cross section decreases with λ^{-4} dependence. In the intermediate region of sizes, large fluctuations occur. Values of the ratio $\sigma/\pi a^2$ for totally reflecting spheres are given by Van de Hulst[4] as a function of $x = 2\pi a/\lambda$. Suppose that a given volume Q is fragmented into N totally reflecting spheres of radius a, the density remaining constant. The total radar cross section of the N spheres, taken as independent scatterers, is

$$N\sigma = Q\,\frac{3\pi}{2\lambda}\,\frac{1}{x}\left(\frac{\sigma}{\pi a^2}\right). \tag{1}$$

A plot of $\frac{1}{x}\frac{\sigma}{\pi a^2}$ is shown in Fig. VI-5. As the wavelength of the radar is 0.694 micron, a reduction in size corresponds to a large increase in total cross section until an optimum size ($x \approx 1$, $a \approx 0.11$ micron) is reached beyond which the cross section decreases very rapidly. Thus one may conceive that on its flight through the atmosphere a meteoroid undergoes progressive fragmentation in such a way that the collective radar cross section of the fragments increases until an average optimum size is reached and that further breakup, at lower heights, is responsible for a successive reduction of the observed cross section.

In the real case the particles will not behave as totally reflecting scatterers; the choice of spherical shape is unfavorable because it minimizes the geometrical cross section for a given mass and is probably far from reality, since published photographs of "fluffy" particles by Hemenway and Soberman[5] indicate very complex shapes. For these filamentary shapes the radar cross section is much larger than the geometrical cross section.

Since we are interested in obtaining from the measure of the collective radar cross section an order-of-magnitude estimate of mass density and influx, but do not have any measurement of individual radar cross sections, we shall assume that at some stage in the descent the meteoroid breaks up into fragments of optimum size for observation at the radar wavelength. We shall also assume that when the optimum size is reached, the average radar cross section σ is 10 times larger than the average geometrical cross section A.

Witt, Hemenway, and Soberman[2] have collected particles from the mesopause. They found a large number of submicron particles of a size that would not be expected to scatter efficiently at wavelength $\lambda = 0.69$ micron, and that cannot exist in elliptical orbit in the solar system, because of radiation pressure.

Some conditions of a purely mechanical character, which we have formulated but will not present here, indicate that physically the following process is possible: A meteoroid, with a radius of 10 microns or more, a density between 0.1 and 0.5,[1] and entering velocity of 30 km/sec, will begin to fragment in sizes of 0.1-0.5 micron at a height of 120-140 km (which is above the height Z previously defined) if it has a crushing strength somewhat higher than 10 dynes/cm^2; these fragments of density close to one will keep breaking up in flight downward into smaller crystals, typically of 0.02-0.05 micron, at an altitude of 110-120 km, having reached a speed of approximately 10 km/sec, if they have a crushing strength of the order of 100 dynes/cm^2. The size distribution should be variable with height, and the atmosphere would be working as a "filter."

On the bases of the radar observations and of the present model of fragmentation, an attempt can be made to estimate the influx on Earth of meteoric material that is undergoing fragmentation and is of a size suitable for observation.

From the size population found by Hemenway and Soberman it can be established that most of the total mass is obtained in sizes smaller than 0.1-micron radius. According to our model, all of this material is produced by fragmentation. Thus an estimate of the flux based on these particles of larger size that are observable by optical radar at higher altitudes accounts for most of the mass obtained at lower levels. Some of the larger particles may well enter at lower speed in such a way that their contribution to the total flux will be small.

Since the experiments have been performed in a period of high meteoric activity and at night, a seasonal and diurnal rate factor affects the measurements. For the sake of obtaining an order-of-magnitude estimate, we take the yearly average of the observed difference in cross section between the maximum above 110 km and the minimum between 100 km and 110 km to be of the order of 10^{-13} cm^2/cm^3. For particles of dimensions close to optimum, we shall assume an average radar cross section of the order of 7×10^{-9} cm^2, an individual mass of the order of 2.5×10^{-14} gm, a density of 1.5, with an average radial velocity of 5 km/sec. A total influx of the order of 6×10^4 tons a day on Earth is thus obtained. It is unnecessary to emphasize the great uncertainty attached to this estimate, in view of the scarcity of experimental data and the variety of assumptions. The number obtained is, however, in agreement with other published results. For instance, it is in fair agreement, within an order of magnitude, with evaluations obtained from measurements of meteoric impact on satellites by Dubin and McCracken.[6] The hypothesis of fragmentation may account for the relatively low influxes obtained on the basis of Volz and Goody's twilight experiments.[7,8]

G. Fiocco

References

1. G. Fiocco and L. D. Smullin, Nature 199, 1275-1276 (1963).

2. G. Witt, C. L. Hemenway, and R. K. Soberman, COSPAR, 4th Space Science Symposium, Warsaw, Poland, 1963.

3. A. Ye. Mikirov, Planet. Space Sci. 11, 417-426, 1963 (translated by H. S. M. Massey from Iskusstvennye Sputniki Zemli, No. 13, 97, 1962).

4. E. C. Van de Hulst, Light Scattering from Particles (John Wiley and Sons, Inc., New York, 1957).

5. C. L. Hemenway and R. K. Soberman, Astron. J. 67, 256-266 (1962).

6. M. Dubin and C. W. McCracken, Astron. J. 67, 248-256 (1962).

7. F. E. Volz and R. M. Goody, J. Atmospheric Sci. 19, 385 (1962).

8. N. P. Carleton, J. Atmospheric Sci. 19, 424 (1962).

VII. NOISE IN ELECTRON DEVICES

Prof. H. A. Haus
Prof. P. L. Penfield, Jr.
Prof. R. P. Rafuse

RESEARCH OBJECTIVES

The purpose of the work on the noise performance of multiterminal-pair networks (Quarterly Progress Report No. 68, pages 53-59) has been to ascertain the limiting noise performance, as well as to determine appropriate measures of noise performance for amplifiers with more than two terminal pairs. This phase of the work has been completed and the results were submitted to the Department of Electrical Engineering, M.I.T., June 1963, as part of an Sc.D. thesis by W. D. Rummler. This thesis is to be published as Technical Report 417 of the Research Laboratory of Electronics, M.I.T.

Our future effort will be concentrated in three areas. The first concerns the noise performance of devices in which quantum effects are expected to be detectable or, in fact, dominant. Because amplitude noise measurements on the c.w. gaseous maser oscillator are relatively convenient to make, the theoretical and experimental work will be concentrated around this device.

(a) A quantum-mechanical analysis of the noise in optical maser oscillators will be undertaken. The purpose of the analysis is to determine the limitations of the semiclassical analysis, briefly summarized in this report.

(b) Measurements on the amplitude noise in optical maser oscillators will continue. Our intent is to determine the noise level of "quiet" optical maser oscillators by refinement of the existing apparatus.

(c) The sensitivities of various experimental methods for the determination of amplitude noise of optical waves will be compared experimentally.

The second area of interest is noise in frequency multipliers, especially those made from varactors. We hope to develop simple parameters to indicate the noisiness of a signal and of a multiplier through which this signal passes, and then to compare the noise performamce of various types of multiplier chains.

The third area of interest is the noise contribution of double-sideband degenerate parametric amplifiers in a variety of applications.

H. A. Haus, P. Penfield, Jr., R. P. Rafuse

A. ANALYSIS OF NOISE IN OPTICAL MASER OSCILLATOR

With the aid of a semiclassical analysis, Lamb[1] has shown that a gaseous laser with a Doppler-broadened line obeys equations similar to those of the van der Pol oscillator. Because of these results, it is reasonable to attempt to relate the existing work on noise in van der Pol oscillators to fluctuations in the optical maser. If one considers a maser oscillating in a single mode and if one disregards the coupling to other modes of the optical cavity, one may represent the dynamic behavior of the amplitude of the oscillation by the equivalent circuit of Fig. VII-1. The nonlinear negative conductance of the maser material has the assumed voltage dependence

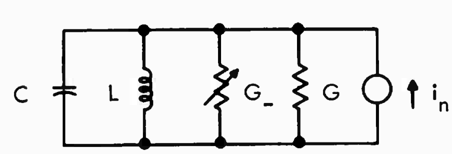

Fig. VII-1. Equivalent circuit.

$$G_{-} = G_m(1-a\langle V^2\rangle), \tag{1}$$

where the angular brackets represent a (short-)time average over a few cycles of the optical frequency, and a is a constant. The conductance G represents the losses and external loading of the optical cavity. The inductance L and capacitance C of the circuit resonate at the optical-cavity frequency ω_o; their magnitude with respect to G is determined by the "cold" cavity Q. If one intends to represent microphonics as caused by the vibration of the mirrors, an important contribution to the frequency modulation of the optical maser output, one would have to vary L and C in time, keeping their ratio fixed if the Q remains unaffected by these variations. Here we shall disregard such effects in the belief that they may not contribute to the amplitude modulation of the maser output. The noise current generator incorporates the fluctuations associated with thermal effects (negligible in the case of an optical maser) and with the emission of the active material. If one disregards changes in i_n that are due to the nonlinearities of G_{-}, one may use for it the well-known value[2-4] associated with the spontaneous emission in a linear, active material. The mean-square fluctuations within the frequency increment $\Delta\nu$ are

$$\overline{i_n^2} = \alpha 4 G_m h\nu\Delta\nu. \tag{2}$$

Here, $\alpha(\geq 1)$ is a factor accounting for the incomplete inversion in the maser medium.

$$\alpha = 1 + \frac{1}{\exp\left(\frac{h\nu}{k|T_m|}\right) - 1}, \tag{3}$$

where T_m is the (equivalent) negative temperature of the maser medium. To the equivalent circuit of Fig. VII-1 one may apply the theory of noise in a van der Pol oscillator.[5] One assumes the time dependence of the voltage

$$V(t) = R(t)\cos[\omega_o t - \theta(t)]. \tag{4}$$

Furthermore, one notes that R(t) and θ(t) are relatively slow functions of time. Finally, one treats the case of low noise, for which

$$R(t) = R_o + R_1(t). \tag{5}$$

Here,

$$R_1(t) \ll R_o$$

$$\theta(t) = \theta_o + \theta_1(t), \tag{6}$$

where $\theta_1(t)$ is a slow function. Under these assumptions, for the steady-state amplitude R_o one finds

$$R_o = \sqrt{\frac{G_m - G}{aG_m}}, \tag{7}$$

and for steady-state phase θ_o

$$\theta_o = \text{const.} \tag{8}$$

The noise terms R_1 and θ_1 satisfy the (approximate) differential equations

$$\dot{R}_1 + \frac{\omega_o}{Q'} R_1 = -\frac{1}{\omega_o C}\left\langle \frac{di_n}{dt} \sin\left(\omega_o t - \theta_o\right)\right\rangle \tag{9}$$

$$R_o \dot{\theta}_1 = -\frac{1}{\omega_o C}\left\langle \frac{di_n}{dt} \cos\left(\omega_o t - \theta_o\right)\right\rangle, \tag{10}$$

where

$$Q' = \frac{\omega_o C}{G_m - G}. \tag{11}$$

Here, Q' is the "hot Q" of the oscillator. Near threshold it varies between a value much greater than the "cold Q" to a value comparable with it. The spectra of R_1 and θ_1 can be obtained from Eqs. 2, 9, and 10. Defining the spectral density of the driving noise current generator, $W_o(\nu)$, by

$$W_o(\nu) = \frac{\overline{i_n^2}}{2\Delta \nu}, \tag{12}$$

one has

$$W_{R_1}(\nu) = \frac{\frac{1}{2} W_o}{C^2\left[\omega^2 + \omega_o^2/Q'^2\right]}, \tag{13}$$

with $\omega = 2\pi\nu$, and

$$W_{\theta_1}(\nu) = \frac{\frac{1}{2} W_o}{R_o^2 C^2} \frac{1}{\omega^2}. \tag{14}$$

A measurement with a photocell or photomultiplier on the light output of a single maser detects only $W_{R_1}(\nu)$. The mean-square fluctuation $\overline{R_1^2}$ may be obtained from the integral over all frequencies of $W_{R_1}(\nu)$. For the modulation ratio m^2 one finds

$$m^2 = \frac{\overline{R_1^2}}{R_o^2} = \frac{\alpha h \nu_o}{\frac{1}{2} R_o^2 C} \frac{G_m}{G_m - G}. \tag{15}$$

The output power may be expressed in terms of an external Q, Q_e:

$$P = \frac{1}{2} R_o^2 \frac{\omega_o C}{Q_e}. \tag{16}$$

One may assign a bandwidth $\Delta\omega_e$ to $1/Q_e$ by

$$\Delta\omega_e = \omega_o/Q_e. \tag{17}$$

Then the modulation ratio becomes

$$m^2 = \frac{\alpha\hbar\nu_o\Delta\omega_e}{P} \frac{G_m}{G_m - G}. \tag{18}$$

One can make estimates as to the magnitude of m^2. Taking the He-Ne visible maser line at 6328 Å, $\Delta\omega_e = 10^7$ mc, and an output power of 1 μw, one has

$$m^2 = \alpha \frac{G_m}{G_m - G} 1.9 \times 10^{-5}. \tag{19}$$

The factor $\alpha G_m/(G_m-G)$ is greater than unity. We believe that a value of m^2 as obtained here is within reach of achieved experimental sensitivities.

H. A. Haus

References

1. W. H. Lamb, Theory of an optical maser (to be published in Phys. Rev.).

2. M. W. Muller, Noise in a molecular amplifier, Phys. Rev. 106, 8-13 (1957).

3. R. V. Pound, Spontaneous emission and the noise figure of maser amplifiers, Ann. Phys. 1, 24-32 (1957).

4. H. A. Haus and J. A. Mullen, Noise in optical maser amplifiers, Presented at the Polytechnic Institute of Brooklyn Symposium on Optical Masers, New York, April 1963.

5. J. A. Mullen, Background noise in nonlinear oscillators, Proc. IRE 48, 1467-1473 (1960).

B. OPTIMUM NOISE PERFORMANCE OF MULTITERMINAL AMPLIFIERS

This report is an abstract of an Sc.D. thesis, Department of Electrical Engineering, M.I.T., August 19, 1963, which will appear as Technical Report 417, in January 1964.

The problem is to find the optimum noise performance that can be achieved from a linear multiterminal-pair signal source used in the most general linear way with a linear multiterminal-pair amplifier; this optimum performance is achieved at a single-output terminal-pair in a narrow band of frequencies. The most general linear way in which to use such a source and amplifier is to imbed both networks in an arbitrary linear lossless network and take the output through this network. The optimum noise performance of such a system is defined as the maximum signal-to-noise ratio that can be achieved at large exchangeable signal power. It is shown that this is a meaningful criterion for any system that is to deliver ultimately an amount of signal power considerably greater than $kT_o\Delta f$, the noise power available from a room-temperature resistor in the same bandwidth. The techniques described can be used, however, to determine the maximum signal-to-noise ratio that can be achieved at any value of exchangeable (or available) signal power.

The discussions are simplified by presenting the results in a plot with noise-to-signal ratio and the reciprocal of exchangeable signal power as coordinates — the noise-performance plane. This plot is useful for examining the noise performance of any linear system. The noise performance of a conventional two-terminal-pair amplifier is examined on this plane. Such a system defines two points in the noise-performance plane: one by the noise-to-signal ratio and exchangeable signal power of the source; and another by the noise-to-signal ratio and exchangeable signal power at the output. In terms of these two points, noise figure, exchangeable-power gain, and noise measure are given a geometrical interpretation in the noise-performance plane.

It is shown that the noise performance — signal-to-noise ratio and exchangeable signal power — that can be achieved by imbedding a multiterminal-pair source and a multiterminal-pair amplifier in an arbitrary lossless network can also be achieved by imbedding the source in an arbitrary lossless network to reduce it to a one-terminal-pair source and using this one-terminal-pair source to drive an arbitrary lossless reduction of the amplifier. Thus the optimization problem can be solved by considering separately the noise performance of the source and the noise performance of the amplifier. For this reason, the problem is attacked by considering a set of problems of increasing difficulty. First, the noise performance that can be achieved with a noisy (positive or negative) resistance used in conjunction with a one-terminal-pair source is examined. The points in the noise-performance plane that can be achieved at the output of such a system all lie on a straight line through the source point with a slope equal to the exchangeable noise power of the resistance. Subsequently, the problem of the noise performance of a multiterminal-pair amplifier used with a one-terminal-pair source is considered. After the noise performance of a multiterminal-pair source imbedded in an arbitrary lossless network has been examined, the general noise-performance problem can be solved by inspection.

With this work used as a basis, definitions are given for the noise figure, exchangeable-power gain, and noise measure of a multiterminal-pair amplifier that is used with a multiterminal-pair source. These quantities are derived and/or interpreted by comparing a system with its noiseless and "gainless" equivalent — its equivalent source network.

The optimization procedure is extended to multifrequency networks coupled in an arbitrary manner by a lossless nonlinear device that obeys the Manley-Rowe formulas. In this context, the optimum noise performance of an ideal (lossless) double-sideband parametric amplifier is examined for both the cases in which the noises in the two sidebands are uncorrelated and partially correlated.

W. D. Rummler

VIII. MAGNETIC RESONANCE

Prof. J. S. Waugh
J. D. Macomber
J. W. Riehl
D. S. Thompson
C. G. Wade

RESEARCH OBJECTIVES

The activity of this group is centered on the study of the structure and atomic dynamics of solids and fluids through experiments on nuclear and electronic magnetism. Work is under way on six specific projects.

1. Structure of Liquid Dielectrics

Nuclear spin Hamiltonians of interest in magnetic-resonance experiments can be expressed in terms of spherical tensors of rank 2, a circumstance that arises because the nuclear moments involved are magnetic dipole and electric quadrupole. The secular interactions, which give rise to shifts and splittings of the nuclear Zeeman levels, thus have scalar parts and parts that depend on the orientation of molecules through $Y_{\ell m}(\theta, \phi)$. In ordinary liquids, rapid molecular reorientation makes the anisotropic terms unobservable, inasmuch as the average of $Y_{\ell m}$ over a spherically symmetric probability distribution vanishes. In a polar liquid subjected to an electric field, however, the probability distribution is no longer exactly spherical, and one expects to see small perturbations of the nuclear-resonance spectrum which depend on electric field intensity E and temperature T as $(E/T)^2$, and also on the local order in the liquid produced by intermolecular forces. For molecules of known properties it becomes possible to measure such averages as $\overline{Y_{20}}$ through the nuclear-resonance spectrum. This information, together with a knowledge of $\overline{Y_{10}}$ obtained from dielectric studies, is expected — for the first time — to provide detailed information about the degree and type of local order produced by molecular interaction in dielectric liquids. It is also expected that such experiments will throw light on the mechanism of electrical conduction in insulating liquids. The present state of our experiments is described in this report.

J. D. Macomber, J. S. Waugh

2. Magnetic Relaxation in Gases

Nuclear relaxation in monatomic gases such as helium is exceedingly slow, a fact that has suggested the use of He^3 nuclear moments in navigational gyroscopes. We are studying the mechanisms responsible for such relaxation by performing transient magnetic-resonance experiments on gases at high pressures for which the relaxation is rapid enough to be measurable. We are even more actively studying nuclear relaxation by similar methods in simple polyatomic gases, in which there are stronger mechanisms arising from the anisotropy of the forces between colliding molecules. We are at present attempting to get a detailed picture of these forces in the simple prototype system of hydrogen deuteride gas at low temperatures. We hope, in collaboration with Professor Irwin Oppenheim, to arrive at an exact theoretical connection between nuclear relaxation times and intermolecular forces for simple systems.

C. G. Wade, J. S. Waugh

3. Transport Properties of Dense Fluids

For a long time, a great deal of theoretical attention has been devoted to the general problem of the nonequilibrium properties of liquids and dense gases. Despite the fact that diffusion, viscosity, thermal conductivity, and so forth, are among the most classical subjects of experimental physical chemistry, almost none of the work that has been done is of direct use in testing transport theory. This is because of the necessity of low temperatures and/or high pressures for obtaining high densities of fluids composed of single atoms or small molecules. Also, one would like experimental values of transport coefficients over wide ranges of temperature and density, since one would expect transport theories to do a better job of predicting the form of temperature and density dependences than of giving numerical values of the transport coefficients. Fortunately the experimental difficulties of the classical methods are largely obviated, in the case of diffusion, by the spin-echo technique of nuclear resonance. We have already used this method to study the temperature dependence of self-diffusion in liquid ethane over an extremely wide temperature range (see Quarterly Progress Report No. 64, pages 37-39). We have now completed and tested a system for extending the same type of measurements to high pressures. It will be used initially to study the experimentally convenient liquids CH_4 and C_2H_6, and will then be extended to monatomic and other polyatomic liquids.

J. W. Riehl, J. S. Waugh

4. Atomic Motion in Solids

Thermal relaxation of nuclei in solids typically occurs through the agency of magnetic dipole-dipole interactions, randomly modulated by the motions of nuclei with respect to one another. In general, it is assumed that the time autocorrelation function $G(\tau)$ describing the statistical fluctuation of these interactions $\mathscr{H}(t)$ is an exponential, described by a correlation time τ_c:

$$G(\tau) \equiv \overline{\left\langle \mathscr{H}(t)\, \mathscr{H}^*(t+\tau) \right\rangle} = \overline{|\mathscr{H}(t)|^2} \exp(-\tau/\tau_c).$$

This assumption, applied to solids whose atomic motions are thermally activated so that $\tau_c = \tau_{co} \exp(E/kT)$, has been very successful in identifying the atomic motions that occur and determining the energetic barriers E that hinder them. An example from our recent work is described in this report.

In general, where correlations exist between the motions of neighboring nuclei or where the motion is complex in character, the assumption that a single correlation time exists is certainly not correct. The nuclear relaxation time is still a measure of the correlation function, being directly related to its Fourier transform evaluated at the experimental resonance frequency. We are beginning a series of studies of relaxation in various solids with the object of mapping out the correlation function experimentally and finding out what sorts of departures from exponential behavior do occur typically. Such work requires observing the relaxation of nuclear magnetization toward equilibrium in an applied magnetic field whose strength is variable from a few to many thousand oersteds. The usual procedure is to polarize the sample in a strong field and then reduce the field quickly to the desired value. After a time, the field is restored to a large value and the remaining magnetization is measured by means of a free-induction decay or an adiabatic fast passage. Alternatively, the desired low magnetic fields can be obtained in the rotating frame by means of Solomon's "spin-locking" procedure.

J. S. Waugh

5. Electron-Spin Resonance

A good deal of interest exists in the properties of magnetically dilute solutions of transition metal ions in diamagnetic crystals, partly because of the applications of such systems to optical masers. We are carrying out some optical and X-band electron spin-resonance studies on the d^4 ion Cr^{+2} in CaF_2 and SrF_2 single crystals. The object of this work is to obtain an analysis of the Jahn-Teller effect through its influence on the

F^{19} hyperfine interaction at low temperatures. We are also carrying on some electron spin-resonance work on solutions of rare-earth metals in liquid ammonia in the hope of throwing some further light on the structure of these peculiar conducting liquids (see this report).

D. S. Thompson, J. S. Waugh

6. Mössbauer Effect

Isomer shifts and quadrupole splittings in recoilless gamma-ray spectra are known to be related to the electronic structure of solids, but the theoretical interpretation of these quantities *ab initio* is very difficult. We have done some preliminary studies of a number of solid monosubstituted ferrocyanides having a range of tetragonal crystal field strengths in an attempt to establish semiempirical criteria for the discussion of chemical bonding. This work is now dormant, but results obtained thus far are partially discussed in a paper that has been submitted to *Applied Optics*.

F. Mannis, J. S. Waugh

STATUS OF CURRENT PROJECTS

1. NUCLEAR MAGNETIC RESONANCE OF POLAR LIQUIDS IN ELECTRIC FIELDS

Detection of the small effects of dipolar interactions and anisotropy of chemical shift on the nuclear magnetic resonance (NMR) spectrum of a liquid subject to an electric field requires the greatest possible spectral resolution. In sample cells of most practical designs the applied magnetic field is made inhomogeneous by the presence of the cell structure and the sample itself, both of which have magnetic susceptibilities different from that of the surrounding air. Small currents flowing in the sample also produce inhomogeneous magnetic fields of their own. After much experimentation, we seem to have solved the first of these problems by constructing long cylindrical cells containing the sample liquid in a long cavity of rectangular cross section. The cell body is cast from an epoxy resin that has been doped with rouge until its volume diamagnetic susceptibility matches that of the sample. The electrodes are sufficiently thin that they do not appreciably distort the magnetic field. As far as the magnetostatic problem is concerned, the sample cell can then be treated as an infinite homogeneous cylinder, inside which the field is uniform. We have also tried long concentric glass cells in which the sample and electric field appear in a thin annulus. The glass is coated with a chemically inert semiconducting film (courtesy of Dr. D. W. Rice of the Corning Glass Company). Such a cell avoids, in principle, both sources of field inhomogeneity mentioned above. But it must be rapidly spun about its cylinder axis in order to average out the line broadening that arises because the relative directions of the electric and magnetic fields are different in different parts of the cell. This averaging reduces the observable effects of the electric field on the NMR spectrum by a factor of four. This, together with the complications inherent in making the necessary electrical connection to a rotating cell, have resulted in our preference for the, perhaps less elegant, parallel-plate geometry.

The above-mentioned sorts of spurious line broadening, as well as other forms of interference, always occur to some degree when a strong electric field is applied to a liquid whose steady-state NMR spectrum is being examined. Rather than trying to disentangle the desired shifts and splittings from these adventitious effects by direct examination of changes in the NMR line shape, we are now employing a sideband technique. Instead of a constant electric field, we apply an audiofrequency alternating field, $E_o \cos \omega_e t$. Its effects are conveniently described with reference to the proton resonance of CH_3NO_2, on which much of our work has been done. In the alternating field the resonance, previously a single line, splits into a triplet of intensity ratio 1:2:1 and spacing $3D_{HH}$. At the same time, sideband resonances appear at $\pm 2\omega_e$ from the main resonance. These resonances have the form of doublets of spacing $6D_{HH}$. Their amplitudes contain a component oscillating at the frequency $2\omega_e$ with intensity proportional to a product of Bessel functions: $J_o(k)\ J_1(k)$, where the modulation index k is given by $k = \text{const.} \times E_o^2/\omega_e$. These sidebands are not present at all unless the desired electric-field splitting exists, and their intensities, suitably measured with a lock-in detector operating at the frequency $2\omega_e$, measure D_{HH}. Calibration is conveniently made by comparison with a magnetic field modulation sideband of like frequency. In order to increase the time during which the weak signals can be integrated, it is convenient to lock the spectrometer into resonance by means of still another magnetic sideband, after the fashion of Freeman and Anderson.[1] The equipment for accomplishing this rather involved situation has now been built and successfully tested, although refinement still continues.

A preliminary account of this work was given at the Eighth Jugoslav Summer School of Physics, in Hercegnovi, September 1-7, 1963, and will be published in the Proceedings of this conference.

The polarization of a liquid by an electric field introduces into the spin Hamiltonian, among other things, a dipolar interaction for each pair of nuclei:

$$\mathcal{H}_d^{(ij)} = D_{ij}(\underset{\sim}{I}_i \cdot \underset{\sim}{I}_j - 3I_{zi}I_{zj}),$$

where

$$D_{ij} = \frac{\gamma_i\gamma_j\hbar^2}{r_{ij}^3}\left\langle P_2(\cos\theta_{ij})\right\rangle.$$

Here, θ_{ij} is the orientation of the internuclear vector $\underset{\sim}{r}_{ij}$ with respect to the magnetic field $\underset{\sim}{H}$. The average with respect to θ_{ij} is related to the averaging of the molecular dipole moment μ in the electric field E (described by an angle ψ) as follows:

$$\left\langle P_2(\cos\theta_{ij})\right\rangle = \left\langle P_2(\cos\psi)\right\rangle P_2(\cos a)\, P_2(\cos\beta_{ij}),$$

where α is the angle between $\underset{\sim}{E}$ and $\underset{\sim}{H}$, and β_{ij} is that between $\underset{\sim}{\mu}$ and $\underset{\sim}{r}_{ij}$. Observation of dipolar splittings in the NMR spectrum of a molecule of known structure thus permits a determination of $\left\langle P_2(\cos\psi)\right\rangle$. Both this quantity and $<\cos\psi>$, which for highly polar liquids is approximately obtainable from the dielectric constant ϵ:

$$<\cos\psi> \approx \frac{(\epsilon-1)\,E}{4\pi\mu}\left(\frac{V}{N}\right),$$

are characteristic of the angular distribution of molecules in the electric field. For a fluid without intermolecular forces, this distribution is proportional to $\exp(\mu E\cos\psi/kT)$, and leads to

$$<\cos\psi> = \frac{1}{3}\left(\frac{\mu E}{kT}\right); \qquad \left\langle P_2(\cos\psi)\right\rangle = \frac{1}{15}\left(\frac{\mu E}{kT}\right)^2.$$

In dense fluids, in which intermolecular forces are important, either of these may be made consistent with experiment if E is replaced by an "effective field" F that is imagined to represent the effects of neighboring molecules. For this concept to be physically meaningful, the same value of F must be used in both of the above-mentioned averages, and leads to the requirement

$$\eta \equiv \left\langle P_2(\cos\psi)\right\rangle / <\cos\psi>^2 = \frac{3}{5}.$$

The combination of the electric-field NMR experiment and measurements of dielectric constant thus provide a measure of the extent to which specific intermolecular forces cause the distribution function to depart from a basically independent-particle form describible by an effective field. Such departures may in fact be very large: The results obtained by Buckingham and McLauchlan[2] on the molecule p-nitrotoluene, together with the dielectric constant (estimated to be 20.5 ± 0.5 at the temperature of their NMR experiment), give $\eta \approx 4$.

The absolute value sign on this result reflects the possibility that certain rather special types of local ordering in the liquid might lead to a negative value for $P_2(\cos\psi)$. Such a situation (considered very unlikely in this case) would require a reversal of the argument by which the above-mentioned authors have determined the absolute sign of the indirect spin-spin coupling constant J_{ij}.

J. D. Macomber, J. S. Waugh

References

1. R. Freeman and W. A. Anderson, J. Chem. Phys. 37, 85; 2053 (1962).
2. A. D. Buckingham and K. A. McLauchlan, J. Chem. Soc., p. 144, May 1963.

2. NUCLEAR RELAXATION IN XENON TETRAFLUORIDE

The spin-lattice relaxation time T_1 of the F^{19} nuclei in polycrystalline XeF_4 has been measured between approximately 77°K and 400°K. (See Fig. VIII-1.) At low

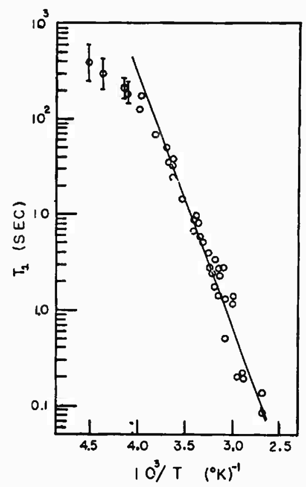

Fig. VIII-1. Spin-lattice relaxation of F^{19} in crystalline XeF_4. The relaxation time, T_1, is plotted on a logarithmic scale against the reciprocal of the absolute temperature. Measurements were made at 30 mc. The straight line is drawn for an activation energy for molecular motion of 12.0 kcal/mole.

temperatures T_1 is roughly constant at approximately 10^3 sec, but at higher temperatures it drops proportionally to exp(E/RT). The activation energy is 12.0 ± 1.5 kcal/mole. The molecular motion responsible for relaxation is evidently an activated reorientation of XeF_4 molecules in situ. These results are consistent with a previously reported line-width transition in the neighborhood of 250°K. Details have been submitted for publication to the Journal of Chemical Physics.

C. G. Wade

3. ELECTRON-SPIN RESONANCE OF METAL-AMMONIA SOLUTIONS

The well-known blue solutions of alkali metals in liquid ammonia exhibit a single sharp paramagnetic resonance absorption. This single resonance has been attributed to "solvated free electrons" formed, for example, in the reaction:

$$Na_{(metal)} + NH_{3\,(liquid)} = Na^{+}_{(in\,liq.\ NH_3)} + e^{-}_{(solvated)} + NH_{3\,(liquid)}.$$

There has been considerable speculation concerning the degree to which the metal ions and the "solvated electrons" are associated. Knight Shifts of the Na^{23} resonance indicate an appreciable spin density of "solvated electrons" at the sodium nucleus in sodium-ammonia solutions. This has led to a model that considers the electrons to be very closely associated with the sodium ions in solution — forming "expanded atoms." Indeed, concentrated solutions of metals in liquid ammonia have a metallic luster, and are very metallic in their electrical properties.

We have prepared and measured the paramagnetic resonance spectra of solutions of Europium metal in liquid ammonia. It was predicted that this rare-earth metal-ammonia system, which is qualitatively similar to alkali metal-ammonia systems, might further elucidate the electronic structure of metal-ammonia solutions, in that the Europium cations as well as the "solvated free electrons" might be expected to exhibit paramagnetic resonance absorption. This has been found to be the case.

Work is now in progress to measure the line shapes and linewidths of these paramagnetic resonance spectra of Eu-NH_3 as a function of concentration and temperature. Future work will include study of the absorption spectra of these solutions from the near infrared to the ultraviolet.

Recent experiments indicate that Eu metal may also dissolve in very pure tetrahydrofuran and dimethoxyethane, thereby giving blue solutions. It may also be possible to study metal-ammonia solutions of other rare-earth metals.

D. S. Thompson

IX. X-RAY DIFFRACTION STUDIES

Prof. B. E. Warren
R. L. Mozzi

RESEARCH OBJECTIVES

The work of this group is concentrated on the application of x-ray diffraction methods to the study of problems of interest to solid state physics. Applications of current interest are:

1. The determination of interatomic force constants and elastic-wave frequency distributions in simple structures from a measurement of the temperature diffuse scattering of x-rays. An application to gold is now in progress.

2. Measurement of long-range and short-range order parameters in binary alloys that show order-disorder changes. A new interpretation of short-range order in Cu_3Au is developing from present studies.

3. Studies of the imperfections that characterize the structure of real materials, in particular the nature of cold work in a deformed metal. Present applications are to the study of deformation in ordered Cu_3Au.

4. Development of the technique for x-ray diffraction study of the structure of non-crystalline materials. Present application is to the simple glasses SiO_2 and B_2O_3.

B. E. Warren

X. SOFT X-RAY SPECTROSCOPY

Prof. G. G. Harvey

RESEARCH OBJECTIVES

The soft x-ray spectroscopy program has as its objective the experimental study of the structure of the conduction band of electrons in a series of metals, particularly the alkalis, alkaline earths, and some of the transition metals. The filled portion of such a band can be studied by observing the emission spectrum produced by transitions from this band to the nearest available sharp levels below this band. In most metals this corresponds to an energy in the range 15-250 ev (wavelength in the range 900-50 A), so that techniques of extreme ultraviolet vacuum spectroscopy need to be used. The energy widths of these bands usually lie in the range 2-10 ev.

In order to avoid serious contamination of the metal that is being studied, an ultrahigh vacuum (5×10^{-10} Torr) spectrometer has been constructed. Another feature of the device is the elimination of the usual ruled grating as a dispersing element. Analysis of the emission spectrum is accomplished by using a neutral atomic beam from which photoelectrons are ejected after absorption of the x-rays to be analyzed. This instrument has been completed and some preliminary tests have been run.

This project is temporarily inactive because of lack of manpower.

G. G. Harvey

XI. MECHANISM OF ENZYMATIC REACTIONS*

Prof. G. G. Hammes
J. E. Erman
T. B. Lewis

RESEARCH OBJECTIVES AND SUMMARY OF RESEARCH

In recent years, considerable effort has been expended in the elucidation of biochemical mechanisms utilizing physical chemical techniques. This project, while still making use of general physical chemical techniques, is primarily concerned with kinetic studies of chemical reactions of biochemical interest. A number of techniques have been developed recently which permit the study of chemical reactions with half times as short as 5×10^{-10} sec.[1] The advantage of being able to carry out kinetic studies over an extended time range is that the entire course of a chemical reaction can be observed. Since reaction intermediates are directly detected, detailed chemical mechanisms can be obtained.

The work that is being done can be divided roughly into two catagories: the study of model systems, and the study of biological systems themselves. By studying relatively simple model systems, complex biological processes can be better understood. In this connection, studies of the interaction of metal ions with amino acids, peptides, phosphates, and polymers have been carried out[2] in an effort to understand the role of metal ions in enzymatic catalysis. Since macromolecules are necessary for almost all biological processes, chemical relaxation processes of simple polymers, polypeptides, proteins and polynucleotides are being examined, particularly with regard to the possibility of fast conformational changes.

In addition to model systems, several enzymatic systems are being studied. Results are already available in two cases, aspartic amino transferase and ribonuclease.[3,4] Some detailed information about the nature and number of reaction intermediates has been obtained. As a result, considerable insight into the elementary steps in enzyme mechanisms has been gained. Since the structure determination of macromolecules is now feasible, it should be possible ultimately to understand enzymatic mechanisms on a molecular basis.

G. G. Hammes

References

1. G. G. Hammes, Quarterly Progress Report No. 65, Research Laboratory of Electronics, M.I.T., April 15, 1962, p. 5.

2. G. G. Hammes and J. I. Steinfeld, J. Am. Chem. Soc. 84, 4639 (1962).

3. G. G. Hammes and P. Fasella, J. Am. Chem. Soc. 84, 4644 (1962).

4. R. Cathou and G. G. Hammes (in preparation).

*This research is supported in part by the National Institutes of Health (Grant RG-7803).

XII. PHYSICAL ELECTRONICS

Prof. W. B. Nottingham
J. L. Coggins
L. E. Sprague

RESEARCH OBJECTIVES

1. Theory of Energy-Conversion Electronics

The effectiveness of energy conversion by means of thermionic emission from an emitter depends upon the existence of a suitable difference in work-function between the emitter and the collector. Many aspects of the physics of electronics are involved in this application and need to be examined in considerable detail, with theory compared with experiment. Thermionic converters are, at present, very difficult to make. The application of thermionic-emission theory, gas-discharge theory, and space-charge theory all contribute to a better understanding of the phenomena found in practical converters. It is, therefore, one of our objectives to organize these various branches of physics and relate them to experimental work that is generally carried on in other laboratories.

2. Determination of Current-Voltage Characteristics of Solid-State Devices

Some studies made on transistors furnished by Fairchild Semiconductor Corporation, Mountain View, California, have shown interesting current-voltage characteristics relating the current conducted through the transistor to the emitter-to-base voltage. Quantitative measurements of these functions, as well as the transfer characteristics, are to be investigated under various operating conditions, including the control of ambient temperatures.

3. Ionization Gauge Control

Circuit devices relating to ionization gauge control experiments indicate that greater versatility would be advantageous. Development in the area of ionization gauge control will continue.

My activity in the general field of Physical Electronics at the Research Laboratory of Electronics is gradually being concluded in anticipation of my retirement at the end of the present academic year.

W. B. Nottingham

XIII. PHYSICAL ACOUSTICS*

Prof. K. U. Ingard	Dr. H. L. Willke, Jr.	J. H. Turner
Dr. L. W. Dean III	P. A. Fleury V	S. D. Weiner
Dr. G. C. Maling, Jr.	K. W. Gentle	J. M. Witting
	W. M. Manheimer	

RESEARCH OBJECTIVES

Our general objective involves the study of the emission, propagation, and absorption of sound and vibrations in matter. Specific areas of current research in fluids include generation and propagation of sound waves in ionized gases, nonlinear acoustics and shock waves, and problems dealing with acoustic and flow instabilities.

In solids the attenuation of ultrasonic waves at the order-disorder transition in alloys is being investigated.

K. U. Ingard

A. SOUND EMISSION FROM KARMAN VORTICES

The balance described previously[1] has been used to measure the drag force on a cylinder in an air stream. Of particular interest is the magnitude of the drag force when the frequency of Karman vortex shedding from the rod is coincident with a cross resonance of the duct. Some experimental data are presented in Fig. XIII-1. It can be seen that the drag force is generally proportional to V^2, where V is the mean flow velocity. When the coincidence condition described above occurs (indicated by vertical arrows in Fig. XIII-1), there is a slight increase in the drag force. The data shown are for rods 3/8 in. and 3/16 in. in diameter. It was not possible to reach flow velocities large enough to obtain the resonance condition with a rod of 0.5-in. diameter.

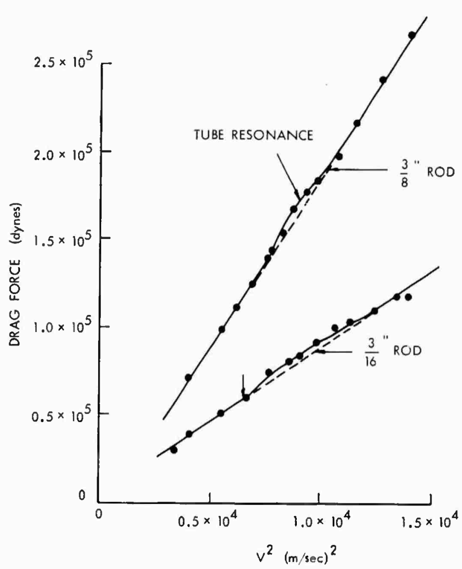

Fig. XIII-1. Drag force as a function of flow velocity for rods of 3/8-in. and 3/16-in. diameter.

Also, we found that the frequency of the radiated sound (f_s) tended to "lock in" with the cross-resonance frequency (f_t) of the tube. As the velocity past the rod of 3/8-in. diameter was decreased, f_s tended to change abruptly at 650 cps and dropped to

*This work was supported in part by the U. S. Navy (Office of Naval Research) under Contract Nonr-1841(42).

XIV. ELECTRODYNAMICS OF MOVING MEDIA

Prof. L. J. Chu
Prof. H. A. Haus
Prof. P. Penfield, Jr.

RESEARCH OBJECTIVES

We are developing the fundamental equations of electrodynamics (for both electromagnetism and dynamics) of moving and deforming material, especially dielectric and magnetic material. The ultimate goal is the determination of the macroscopic force acting on a continuum, and the distribution of that force as a function of space and time. The fundamental equations must be consistent with (a) the special theory of relativity; (b) electromagnetism of free space; (c) electromagnetism of stationary bodies; (d) relativistic continuum mechanics of solids or fluids without electromagnetic fields; (e) thermodynamic measurements of the various kinds of power flow; and (f) nonlinear material properties. Thus far we have obtained equations for nondispersive conservative media. Work is now in progress on media showing dispersion both in time and/or space. We intend to extend the equations to irreversible phenomena. Also, the connection between the equations for nonlinear media and their corresponding small-signal formulation will be explored.

Use of these equations in specific situations is contemplated (a) to illustrate the equations and the various approximations, and (b) to predict novel effects, with a view toward testing for these effects experimentally.

A history of this problem was given in Quarterly Progress Report No. 70, July 15, 1963, pp. 79-82.

L. J. Chu, H. A. Haus, P. Penfield, Jr.

A. INTERPRETATION OF RELATIVISTIC FORCE DENSITY IN MOVING POLARIZABLE AND MAGNETIZABLE MEDIA

We have previously reported[1] an expression for the relativistic force density within a moving and deforming magnetizable and polarizable conservative (isotropic) fluid in an electromagnetic field. The force density is

$$\begin{aligned}\overline{f}^k = & -\nabla\pi_o + (\overline{P}\cdot\nabla)\,\overline{E} + (\mu_o\overline{M}\cdot\nabla)\,\overline{H} + \overline{v}\times(\overline{P}\cdot\nabla)\,\mu_o\overline{H} - \overline{v}\times(\mu_o\overline{M}\cdot\nabla)\,\epsilon_o\overline{E} \\ & + \left[\frac{\partial}{\partial t}\overline{P} + \nabla\cdot(\overline{v}\,\overline{P})\right]\times\mu_o\overline{H} - \left[\frac{\partial}{\partial t}(\mu_o\overline{M}) + \nabla\cdot(\overline{v}\mu_o\overline{M})\right]\times\epsilon_o\overline{E} \\ & - \frac{\partial}{\partial t}\left[\frac{\gamma^2\overline{v}}{c^2}(\pi_o+W_o) + \overline{G}_N\right] - \nabla\cdot\left\{\overline{v}\left[\frac{\gamma^2\overline{v}}{c^2}(\pi_o+W_o) + \overline{G}_N\right]\right\}.\end{aligned} \tag{1}$$

Here, $\overline{P}$ is the polarization density, $\overline{M}$ is the magnetization density, π_o is the sum of the electrostrictive, magnetostrictive, and hydrostatic pressures as observed in the rest frame, $\overline{v}$ is the velocity of the fluid, and

$$\overline{G}_N = -\frac{\gamma^2}{c^2}\left[(\overline{v}\cdot\overline{P})(\overline{E}+\overline{v}\times\mu_o\overline{H}) + (\overline{v}\cdot\mu_o\overline{M})(\overline{H}-\overline{v}\times\epsilon_o\overline{E})\right]. \tag{2}$$

This expression has been obtained in two ways: by application of Hamilton's principle to an appropriate Lagrangian, and by the principle of virtual work applied to a fluid element in its rest frame and a subsequent relativistic transformation. For both of these derivations, thermodynamic information was used to obtain the appropriate energy function.

It is possible to obtain the same expression for the force density without the pressure term π_o from a simple model of a polarizable and magnetizable fluid without recourse to thermodynamics. This model gives insight into the significance of the various terms and, therefore, is presented here. For sake of brevity, and without loss of generality, we shall limit ourselves to a polarizable fluid because the way to include magnetization effects will be self-evident. We shall then show how the pressure term may be included phenomenologically.

We consider a fluid consisting of noninteracting electric dipoles, each of vector strength

$$\overline{p} = q\overline{\delta}, \tag{3}$$

where q is the magnitude of the charges, and $\overline{\delta}$ is the vector distance between them. We interpret the dipole strength (3) as that observed in the laboratory frame in which the dipole (its center of mass, to be precise) may possess an arbitrary velocity $\overline{v}$. If this velocity is relativistic, the dipole strength $\overline{p}$ observed in the laboratory frame is not the same as that observed in the rest frame. The dipole strengths differ because of the relativistic contraction of the component of $\overline{\delta}$ in the direction of motion. For simplicity, we assign the entire mass of the dipole to the negative-charge portion of the dipole and ascribe to it the velocity $\overline{v}(\overline{r})$. The positive charge of the dipole then moves with velocity

$$\overline{v}_+(\overline{r}) = \overline{v}(\overline{r}) + \frac{d\overline{\delta}}{dt}.$$

The forces acting on the dipoles are assumed to be long-range forces only. Thus a fluid of this kind cannot exhibit pressure or electrostrictive effects and we cannot expect to reproduce the term $\nabla\pi_o$ in Eq. 1. The net force acting on a dipole as evaluated in the laboratory frame is obtained as the vector sum of the force acting on the positive charge of the dipole and that acting on the negative charge. We must take into account the possible variations of the electric and magnetic fields over the distance $\overline{\delta}$. We obtain

$$\begin{aligned}\overline{F}_d &= q[\overline{E}(\overline{r}+\overline{\delta}) + \overline{v}_+(\overline{r}) \times \mu_o\overline{H}(\overline{r}+\overline{\delta})] - q[\overline{E}(\overline{r}) + \overline{v}(\overline{r}) \times \mu_o\overline{H}(\overline{r})] \\ &= q\overline{\delta}\cdot\nabla\overline{E} + q\overline{v} \times \mu_o(\overline{\delta}\cdot\nabla)\,\overline{H} + q\frac{d\overline{\delta}}{dt} \times \mu_o\overline{H}.\end{aligned} \tag{4}$$

The polarization density $\overline{P}$ of the dielectric fluid is the dipole strength per unit volume.

If N is the number of dipoles per unit volume, then

$$\overline{P} = Nq\overline{\delta}. \tag{5}$$

The expression for $\overline{F}_d$ in Eq. 4 can be converted into a force density per unit volume by adding the forces acting on all dipoles per unit volume

$$\overline{f}_d = N\overline{f}_d = \overline{P} \cdot \nabla\overline{E} + \overline{v} \times \mu_o\overline{P} \cdot \nabla\overline{H} + \left[\frac{\partial\overline{P}}{\partial t} + \nabla\cdot(\overline{v}\,\overline{P})\right] \times \mu_o\overline{H}. \tag{6}$$

Here, we have used the continuity law satisfied by the dipole number density

$$\frac{\partial}{\partial t}N + \nabla \cdot (\overline{v}N) = 0. \tag{7}$$

The entire force density (6) is not utilized in the acceleration of the fluid mass density (considered here to be associated with the negative charge). The binding forces between the positive and negative charges store energy. Energy in motion acquires momentum according to the relativistic transformation laws. Furthermore, a stress is introduced on a volume element dv containing the mass associated with the negative charges. Indeed, if one draws the boundaries of this volume element in the rest frame taken to be a rectangular parallelepiped, one finds that the binding forces of all those positive charges just outside the element, whose negative partners are inside the volume element, pass through the boundary. The net force passing the boundary $dy_o dz_o$ is equal to the product of the force $(q\overline{E}_o)$ within each dipole times the number of dipoles piercing this boundary $(N\delta\, dy_o dz_o)$. For the net force per unit area we have

$$\overline{n} \cdot \overline{P}_o\overline{E}_o,$$

where $\overline{n}$ is the unit vector normal to the element $dy_o dz_o$ and the subscript o indicates that the quantities are those observed in the rest frame. We conclude that the polarization of the fluid is accompanied by a stress of tensor strength $\overline{P}_o\overline{E}_o$. Relativistically, a stress in motion possesses momentum. The force density $\overline{f}_d$ in Eq. 6 must overcome the time rate of change of this momentum, that of the momentum associated with the energy stored in the dipoles, and the inertia associated with the mass of the fluid. The momentum associated with the stress energy tensor in the rest frame,

$${}^0T^p_{ij} = \left[\begin{array}{c:c} -\overline{P}_o\overline{E}_o & 0 \\ \hdashline 0 & -W_o \end{array}\right], \tag{8}$$

can be found by conventional relativistic transformation methods for a stress-energy tensor as $\overline{G}^p = \gamma^2 W_o\overline{v}/c^2 + \overline{G}_N$, where G_N is given in Eq. 2. The force density $\overline{f}^k$ producing the acceleration of the fluid is that portion of $\overline{f}_d$ that remains after the force density responsible for the total rate of change of the momentum $\overline{G}^p$ has been subtracted.

$$\bar{f}^k = \bar{f}_d - \frac{\partial}{\partial t}\bar{G}^p - \nabla\cdot(\bar{v}\bar{G}^p) = \bar{P}\cdot\nabla\bar{E} + \bar{v}\times(\bar{P}\cdot\nabla)\mu_o\bar{H} + \left[\frac{\partial\bar{P}}{\partial t} + \nabla\cdot(\bar{v}P)\right]\times\mu_o\bar{H}$$

$$-\frac{\partial}{\partial t}\left[\frac{\bar{v}}{c^2}\gamma^2 W_o + \bar{G}_N\right] - \nabla\cdot\left\{\bar{v}\left[\frac{\bar{v}}{c^2}\gamma^2 W_o + \bar{G}_N\right]\right\}. \tag{9}$$

This equation agrees with (1) if magnetization effects are omitted and π_o is set equal to zero. In this way, we have found a simple interpretation for most of Eq. 1. The generalization to a fluid exhibiting magnetization is easy. Pressure effects and electrostrictive effects can be included phenomenologically by assigning, instead of the tensor (8), a new energy momentum tensor in the rest frame

$$^0T^p_{ij} = \left[\begin{array}{c:c} \pi_o\bar{\bar{\delta}} - \bar{P}_o\bar{E}_o & 0 \\ \hdashline 0 & -W_o \end{array}\right]. \tag{10}$$

The kinetic and electrostrictive pressure contribution π_o is entered in the stress part of the rest-frame energy momentum tensor. The inclusion of π_o has two obvious consequences. First of all, it contributes through its gradient to the force density; second, it contributes to the momentum when the tensor (10) is evaluated in the laboratory frame. This is exactly the way in which the inclusion of pressure affects Eq. 1.

H. A. Haus, P. Penfield, Jr.

References

1. P. Penfield, Jr., Force of electromagnetic origin in fluids, Quarterly Progress Report No. 70, Research Laboratory of Electronics, M.I.T., July 15, 1963, pp. 82-88.

PLASMA DYNAMICS

XV. PLASMA PHYSICS*

Prof. S. C. Brown
Prof. G. Bekefi
Prof. K. U. Ingard
Prof. D. R. Whitehouse
Dr. J. C. Ingraham
M. L. Andrews
V. Arunasalam
C. D. Buntschuh
J. D. Coccoli
F. X. Crist
J. K. Domen
E. W. Fitzgerald, Jr.
D. L. Flannery
G. A. Garosi
W. H. Glenn, Jr.
E. B. Hooper, Jr.
P. W. Jameson
R. L. Kronquist
J. J. Linehan
D. T. Llewellyn-Jones
J. J. McCarthy
W. J. Mulligan
J. J. Nolan, Jr.
G. L. Rogoff
F. Y-F. Tse
B. L. Wright

RESEARCH OBJECTIVES

The aim of this group continues to be the study of the fundamental properties of plasmas. We have been placing particular emphasis on plasmas in magnetic fields, plasmas of high percentage ionization at low pressures, and most recently on a plasma showing turbulence in high-speed flow.

We are also studying ways of determining the characteristics of plasmas by means of very far infrared optics in the wavelength range 0.1-1 mm, and by means of optical lasers.

The infrared diagnostic techniques are closely correlated with our continued effort to improve the more standard microwave methods. Most of our microwave techniques at the present time involve the study of microwave radiation from plasmas, with and without magnetic fields.

Theoretical work has been concentrated on the study of waves in plasma, turbulence in flowing gases, and the statistical nature of plasmas.

S. C. Brown

A. SCATTERING OF MICROWAVES FROM "COLLECTIVE DENSITY FLUCTUATIONS" IN PLASMAS

The dispersion relation for a plasma of electrons and ions in general has two roots (normal modes). One of these normal modes is the high-frequency optical mode (the electron plasma oscillations) in which the electrons and ions move out of phase, and the other is the low-frequency acoustic mode (the ion plasma oscillations) in which the electrons and ions move in phase. If one produces a plasma in which the electrons have a steady drift velocity with respect to the ions, then the velocity distribution functions take the forms

$$f_-(v) = \frac{1}{\sqrt{2\pi}\, v_-} \exp\left[-(v-v_d)^2/2v_-^2\right] \tag{1a}$$

and

*This work was supported in part by the U.S. Atomic Energy Commission (Contract AT(30-1)-1842); and in part by the U.S. Air Force (Electronic Systems Division) under Contract AF19(604)-5992.

$$f_+(v) = \frac{1}{\sqrt{2\pi}\, v_+} \exp\left[-v^2/2v_+^2\right]. \tag{1b}$$

Here, for the electrons and ions,

$$v_\mp^2 = \frac{KT_\mp}{m_\mp}.$$

It is clear from expression (1a) that $f_-(v)$ increases as v increases for electron velocities $v \leq v_d$. If this drift velocity is large enough for the phase velocity of any one of the normal modes mentioned above to satisfy the inequality $v_p = \frac{\omega}{k} \leq v_d$, then it is possible for the waves of that normal mode to grow in amplitude.

Such a growth in the amplitude of the wave is a consequence of the transfer of the "extra" kinetic energy of those electrons whose velocities lie in the neighborhood of the phase velocity of the wave to that wave under consideration. If, furthermore, the wave frequency is sufficiently large compared with the frequency appropriate to the damping mechanism (that is, the collision frequency), then it can be shown that the growth rate of these waves can exceed unity. Thus for sufficiently large drift velocities and sufficiently low collision frequencies, it is possible to have plasma wave instabilities. It can be shown that the density-density correlation function corresponding to the "collective density fluctuations" exhibits a huge increase as the plasma from a region of stability approaches a critical point corresponding to the onset of the above-mentioned plasma wave instabilities. Consideration of the theory of electromagnetic wave scattering leads us to predict enormously increased scattering of the electromagnetic radiation from such "collective density fluctuations." In such a scattering the difference between the frequency of the scattered radiation and the frequency of the incident radiation is equal to the frequency of the wave responsible for the scattering, and the scattering cross section is approximately proportional to the potential energy of the wave responsible for the scattering.

Once the instability sets in, the amplitude of the "plasma oscillations" presumably becomes sufficiently large that nonlinear effects such as the coupling between plasma modes of different wavelengths begin to play a role. This coupling will cause the modes of lower wave numbers to decay into modes of a higher wave number. The higher wave-number modes decay, in turn, into still higher wave-number oscillations, until presumably those oscillations whose wave number is approximately equal to the reciprocal of the Debye length decay into fine-grained random or thermal motion. Since these oscillations grow by absorbing the necessary energy from the directed particle motion, we conclude that the relative drift velocity will tend to saturate near the threshold for creation of those high wave-number unstable oscillations that are capable of decaying directly into a fine-grained random or thermal motion.

Ichimaru,[1] Ichimaru, Pines, and Rostoker,[2] and Pines and Schrieffer[3] have analyzed the theory of the plasma wave instabilities in detail. They point out that the scattering of electromagnetic waves by electron density fluctuations in a plasma is determined by $S(\vec{k},\omega)$, the Fourier transform of the electron density-density correlation function. The differential cross section, $d^2\sigma/d\Omega d\omega$, for the transfer of momentum $\hbar k$ (for scattering into a solid angle $d\Omega$) and energy $h\omega$ from an electromagnetic wave to the electrons in a plasma is given by

$$\frac{d^2\sigma}{d\Omega d\omega} = \left(\frac{e^2}{m_-c^2}\right)^2 \left(1 - \frac{1}{2}\sin^2\theta\right) S(\vec{k},\omega), \tag{2}$$

where θ is the angle between the incident and scattered waves. $S(\vec{k},\omega)$ is defined as

$$S(\vec{k},\omega) = \frac{L^3}{2\pi} \int_{L^3} d\vec{r} \int_{-\infty}^{\infty} dt \left\langle n(\vec{r}\,'+\vec{r}, t'+t) n(\vec{r}\,', t')\right\rangle e^{-i(\vec{k}\cdot\vec{r}-\omega t)}, \tag{3}$$

where N is the total number of electrons in a volume L^3, $n(\vec{r},t)$ denotes the electron number density, and the angular brackets refer to a statistical average over the electron states. The measurement of the intensity of radiation scattered into a given angle yields directly the structure factor $S(\vec{k})$, which is

$$S(\vec{k}) = \frac{1}{N}\int_{-\infty}^{\infty} d\omega\, S(\vec{k},\omega). \tag{4}$$

By using the distribution functions given by Eqs. 1 in the Boltzmann-Poisson equations, Ichimaru and others[1-3] derived an expression for the longitudinal dielectric coefficient $\epsilon(\vec{k},\omega)$. By letting $\mathrm{Im}\,\epsilon[\vec{k},\omega(\vec{k})] = 0$, they obtained the boundary between the growing and damped ion acoustic waves. They represent this boundary by a curve $\vec{v}_d(\vec{k})$ in the $\vec{v}_d$-$\vec{k}$ plane, and the equation of this boundary is given by

$$v_d(k) = v_{d_1}(k) + v_{d_2}(k). \tag{5}$$

Here,

$$\frac{v_{d_1}(k)}{v_-} = \frac{(m_-/m_+)^{1/2}}{[1+(k^2/k_-^2)]^{1/2}} \left\{1 + \left(\frac{m_+}{m_-}\right)^{1/2}\left(\frac{T_-}{T_+}\right)^{3/2} \exp\left[-\frac{1}{2}\left(\frac{T_-/T_+}{1+k^2/k_-^2} + 3\right)\right]\right\} \tag{6}$$

and

$$\frac{v_{d_2}(k)}{v_-} = \sqrt{\frac{2}{\pi}}\,\frac{1}{\omega_+\tau_+}\,\frac{[1+k^2/k_-^2]^{3/2}}{k/k_-}, \tag{7}$$

where τ_+ is the relaxation time of the ions, $\omega_+ = 2\pi f_+ = (4\pi n_+ e^2/m_+)^{1/2}$, and $k_- = (4\pi n_- e^2/KT_-)^{1/2}$. Letting Re $\epsilon[\vec{k},\omega(\vec{k})] = 0$, we obtain the dispersion relation for the ion acoustic plasma oscillations:

$$\frac{f}{f_+} = \frac{\omega}{\omega_+} = \frac{k/k_-}{[1+k^2/k_-^2]^{1/2}}. \tag{8}$$

This equation can be rewritten in a convenient form

$$\frac{k_-^2}{k^2} = \left[\frac{f_+^2}{f^2} - 1\right]. \tag{9}$$

From Eqs. 5-7 we can define a critical point k_c as that wave vector for which, with increasing drift velocity $\vec{v}_d$, the ion sound wave first becomes unstable. Let $v_c = v_d(k_c)$ be the associated minimum drift velocity for instability. Using such a notation, they show that just at the onset of the ion acoustic plasma wave instability the dynamic form factor $S(\vec{k},\omega)$ and the structure factor $S(\vec{k})$ are given by

$$S_{crit}(\vec{k},\omega) = \frac{N}{\sqrt{2\pi}\, kv_-}\left[\frac{1}{\{1-[\omega(k)^2/\omega^2]\}^2 + \pi\{[(v_c-v_d)+v_1(k^2/k_-^2)]/v_-\}^2/2}\right]^{1/2} \tag{10}$$

$$S_{crit}(\vec{k}) = \frac{1}{2}\left|\frac{(m_-/m_+)^{1/2}}{\{[v_c-v_d]/v_- + (v_1/v_-)(k^2/k_-^2)\}}\right| \tag{11}$$

for $k^2 < k_-^2$ and $k_c = 0$.

For sufficiently large temperature ratios (say, $T_-/T_+ > 10$),

$$\frac{v_1}{v_-} \approx \frac{1}{2}\left\{\left[\left(\frac{T_-}{T_+}\right)^{5/2} e^{-[(T_-/T_+)+3]/2}\right] - \left(\frac{m_-}{m_+}\right)^{1/2}\right\}. \tag{12}$$

Using Eqs. 5-7 we have plotted Fig. XV-1 for a hydrogen plasma. Here $(m_-/m_+)^{1/2} \approx 1/43$. For $(T_-/T_+) \approx 25$ and $500 \leq \omega_+\tau_+ \leq 1000$ we see from Fig. XV-1 that $k_c \approx 0$, and $v_c = v_d$ for "marginal stability," and $(v_1/v_-) \approx -\frac{1}{2}(m_-/m_+)^{1/2}$. Under these conditions, $S_{crit}(\vec{k})$ of Eq. 11 reduces to the approximate form

$$S_{crit}(\vec{k}) \approx \frac{1}{(k^2/k_-^2)} = \frac{k_-^2}{k^2}. \tag{13}$$

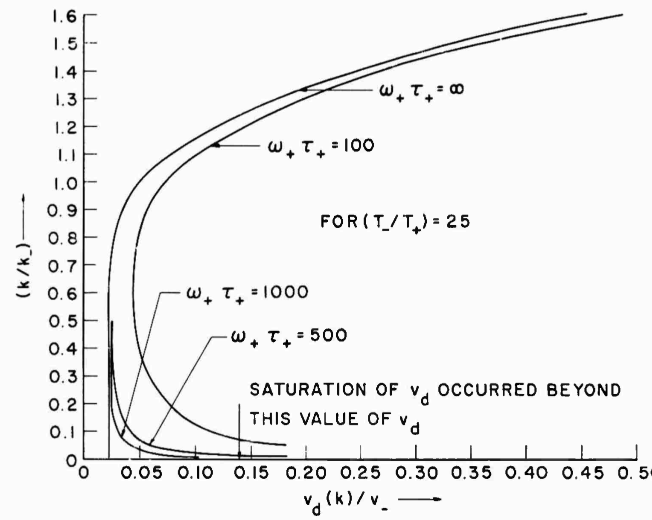

Fig. XV-1. Boundary between growing and damped waves as a function of drift velocity.

Using Eq. 9, we can go from momentum space to energy space, and, by using Eq. 13, we can define the structure factor in energy space appropriate to the critical condition:

$$S_c(f) = [(f_+^2/f^2)-1]. \tag{14}$$

If we measure the intensity of the scattered radiation collected over all angles $\theta \gg \theta_o$ around the critical angle θ_c as a function of frequency f, then, with the aid of Eq. 2, we are led to relate the total cross section $\sigma_c(f)$ to the Thomson cross section $\sigma_o = \frac{8\pi}{3}(e^2/m\_c^2)^2$ as

$$\sigma_c(f) = \sigma_o S_c(f) = \sigma_o[(f_+^2/f^2)-1] \tag{15}$$

and

$$\sigma_c(f) = \int_{-B/2}^{B/2} \left(\frac{d\sigma}{df}\right)_c df,$$

where B is the bandwidth of the detector instrument, and

$$\begin{aligned} \theta_c &= 2 \sin^{-1} (k_c/2k_i) \\ \theta_o &= 2 \sin^{-1} (k\_/2k_i). \end{aligned} \tag{16}$$

Here, k_i is the wave number that the incident radiation will have inside the plasma, and this is related to the wave number k_o of the incident radiation in free space by the relation $k_i = k_o \, \mathrm{Re}\, [\epsilon^{1/2}]$, where ϵ is the dielectric coefficient of the plasma appropriate to the incident radiation. If the plasma is in a magnetic field, ϵ will depend on the directions of $\vec{E}$ and $\vec{k}_o$ with respect to the magnetic field.[4] Furthermore, it is quite likely that condition (16) need not be satisfied in the presence of a uniform magnetic field $\vec{B}$, since the vector potential for such a $\vec{B}$ field may be written as $\vec{A} = \frac{1}{2} \vec{B} \times \vec{r} + \vec{\nabla} f(r)$, where f(r) is any arbitrary function of the coordinate. This arbitrariness in $\vec{A}$ generally allows us to ignore the momentum conservation relations, since the canonical momenta of electrons and ions responsible for the wave are also arbitrary to some extent when a magnetic field is present.

The scattered power is given by

$$P_s(f) = n_- \sigma_c(f)\,(\text{volume of scatterer})\left(\frac{\text{incident power}}{\text{area}}\right). \tag{17}$$

It is interesting to note from Eqs. 15 and 17 that for $f^2 \ll f_+^2$

$$\sigma_c(f) \sim \frac{n}{f^2} \tag{18}$$

and

$$P_s(f) \sim \frac{n^2}{f^2}, \tag{19}$$

in which we have used the reasonable assumption that $n_- \approx n_+ \approx n$ (say).

The discharge current is generally given by

$$(J/\text{area}) = j = nev_d. \tag{20}$$

If the drift velocity saturates and the area remains constant, then Eqs. 18-20, for $f^2 \ll f_+^2$, give

$$\sigma_c(f) \sim (J/f^2) \tag{21}$$

and

$$P_s(f) \sim (J^2/f^2). \tag{22}$$

It should be noted that this analysis assumes that the drift velocity is in the direction of $\vec{k}$ of the ion acoustic wave responsible for the scattering.

The experimental arrangement is illustrated in Fig. XV-2. The over-all length of the discharge tube used for the production of the plasma is approximately 15 cm, and the diameter of the Pyrex plasma tube is approximately 2 cm. The distance between the two probes on either side of the scattering volume is approximately 6.5 cm. The cathode is an oxide-coated tungsten spiral. The shield around the cathode is a cylindrical can of molybdenum. The shield is tied to one of the cathode leads and insulated from the other cathode lead by an insulation bead. The face of the water-cooled anode is of stainless steel and the rest of it is of copper. A magnetic field of 2290 gauss was applied parallel to the axis of the discharge tube with the aid of an electromagnet.

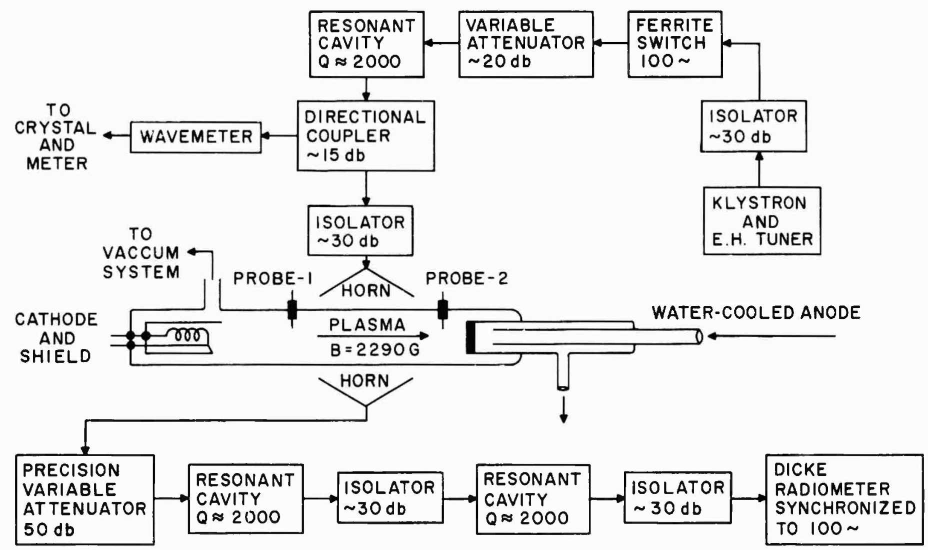

Fig. XV-2. Experimental arrangement.

In the actual experiment the discharge tube was initially evacuated to a pressure of 10^{-7} mm Hg, and hydrogen gas from a litre bottle attached to the vacuum system was admitted into the discharge tube until the pressure was 80 μ Hg as read by the McLeod gauge. The maximum discharge current used for the measurement was 1 amp. Readings were taken for discharge currents in steps of 1/10 amp. The voltage across the two probes was measured for each current. This voltage varied from 19 volts to 25 volts as the discharge current was increased from 0.1 amp to 0.3 amp, but remained relatively constant (within ±2 volts of 26 volts) for the range 0.3-1.0 amp. There were no visible dark spaces in the discharge. In appearance the plasma is of cylindrical shape, with a 4-mm diameter, and extends from cathode to anode.

The incident X-band microwave power was supplied by a Varian X-13 klystron, and the incident frequency was varied from 9140 mc to 9380 mc by steps of approximately 8 mc for the purposes of scanning the scattered spectrum. With the aid of the directional coupler, wavemeter, crystal, and meter in the incident line, the frequency of the incident power was read directly in megacycles, and the incident power was held constant as the frequency spectrum was scanned. The Dicke radiometer and all of the resonant cavities in the detector line were tuned to a fixed frequency of 9255 mc. The incident power of approximately 90 mw (only 1/36 of this power reaches the plasma because of attenuation of approximately 16 db in the line) was modulated in the line by the ferrite switch at 100 cps, and the radiometer was synchronized to this modulation frequency. With the aid of the three resonant cavities, each of $Q \approx 2000$, we were able to avoid any direct pickup as the incident frequency was brought to approximately 7 mc on each side of the detector frequency. The horns used in the incident and detector lines are X-band to C-band transitions. The $\vec{E}$ and $\vec{k}$ vectors of both the incident and detector lines were kept perpendicular to the uniform magnetic field of 2290 gauss.

The ion density, $n_+ \approx n$, was determined from the ratio (slope/intercept) = f_+^2 of the straight-line graph in Fig. XV-6. The electron density $n_- \approx n$, measured by determining the plasma "cutoff" condition of the extraordinary wave, was found to agree reasonably with this value of the ion density. The drift velocity was then calculated with the aid of Eq. 20. Also, from the knowledge of the measured values of E/p, where p is the pressure, the drive velocity was calculated. The value of the drift velocity as given by Eq. 20 was found to be five times larger than that given by E/p measurements. With the aid of Sanborn C. Brown's data,[5] under the assumption that the ions are approximately ten times hotter than the background gas (that is, $T_+ \approx \frac{1}{4}$ ev), we estimated the values of T_-/T_+, $\tau_+ = 1/\nu_+$, and ν_-. The bandwidth of the radiometer was measured by comparing a known fraction of the klystron power with that of a standard noise tube of known radiation temperature: $P = kTB$.

Experimental data are summarized below.

<u>Data and Results</u>

Gas	Hydrogen
Pressure of gas	$\approx 80\ \mu$ Hg
Plasma electric field $\vec{E}$	≈ 4 volts/cm
$\therefore$ E/p	≈ 50 volts/cm-mm Hg
Variation in E/p as current was varied from 0.1 amp to 0.3 amp	≈ 10 volts/cm-mm Hg
Variation in E/p as current was varied from 0.3 amp to 1.0 amp	≈ 4 volts/cm-mm Hg
Diameter of the cylindrical plasma column	≈ 0.4 cm
Scattering length of plasma column	≈ 5 cm
Total length of plasma column	≈ 11 cm

<u>Data and Results</u> (continued)

Magnetic field, $\vec{B}$	2290 gauss
$\therefore$ The electron-cyclotron frequency f_b	6400 mc
The ion plasma frequency f_+ calculated from Fig. XV-6. Here, J is the total discharge current in amperes	$140\sqrt{J}$ mc
$\therefore$ The electron plasma frequency f_-	$\approx 6000\sqrt{J}$ mc
$\therefore$ The electron density $n_- \approx n$	$\approx 4.5 \times 10^{11}$ J/cm^3
For incident frequency of 9200 mc, the plasma cutoff condition for extraordinary wave occurred at	≈ 0.9 amp
For the electron plasma frequency f_- this gives	$\approx 5400\sqrt{J}$ mc
Drift velocity calculated by using n_- and Eq. 20	$\approx 1.1 \times 10^8$ cm/sec
Drift velocity calculated by using E/p and Fig. 3.2 of S. C. Brown[5]	$\approx 2 \times 10^7$ cm/sec
Electron temperature T_- calculated by using E/p and Fig. 3.53 of S. C. Brown[5]	≈ 6 volts
$\therefore$ $v_- = \left(\frac{KT_-}{m_-}\right)^{1/2}$	$\approx 1.45 \times 10^8$ cm/sec
The value of (v_d/v_-) was in the range	$0.14 \lesssim (v_d/v_-) \lesssim 0.76$
(T_-/T_+), by assuming $T_+ \approx \frac{1}{4}$ volt	≈ 24
$\nu_+ = \frac{1}{\tau+}$ for $T_+ \approx \frac{1}{4}$ volt by using Fig. 1.50 of S. C. Brown[5]	≈ 1.2 mc
$\therefore$ $\omega_+\tau_+ = 2\pi f_+\tau_+$	$\approx 730\sqrt{J}$
Power sent out by klystron ($\approx$16 db loss on line)	≈ 90 mw
Incident power for scattering	≈ 2.5 mw
Measured bandwidth B of radiometer	≈ 0.75 mc

In Fig. XV-3 we have plotted the scattering cross section $\sigma_c(f)$ as a function of (f/f_+) as given by the theoretical equation (15), and in the same figure we have shown the experimental measurements of $\sigma_c(f)$, in which the point corresponding to $\sigma_c(f) = 400\ \sigma_o$ was fitted to the theoretical curve. In plotting the data taken at currents of 0.3, 0.4, 0.5, 0.6, 0.7, 0.8, 0.9, and 1.0 amp, we have made use of Eq. 21 and the relation that $f_+ \sim \sqrt{J}$. This graph seems to confirm the correctness of Eqs. 15 and 21. In Fig. XV-4

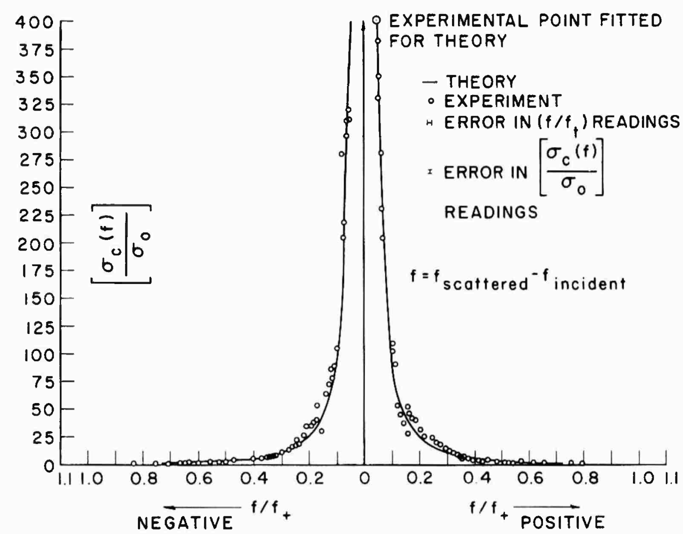

Fig. XV-3. Scattering cross section $\sigma_c(f)$ as a function of wave frequency f.

we have plotted the scattered power as a function of the square of the discharge current for given frequency difference between the incident and scattered frequencies. In Fig. XV-4a, the frequency of the scattered radiation is less than that of the incident radiation, and in Fig. XV-4b, the scattered radiation is of higher frequency than the incident radiation. In Fig. XV-5, we have plotted the slopes of the straight-line graphs of Fig. XV-4 as a function of $1/f^2$, where f is the difference between the incident and scattered frequencies. These graphs in Figs. XV-4 and XV-5 seem to confirm the correctness of Eq. 22 reasonably well.

In Fig. XV-6 we have plotted the scattered power as a function of $1/f^2$ for a discharge current of 1.0 amp. Using the relation

$$f_+^2 = \left(\frac{n_+ e^2}{\pi m_+}\right) = \left(\frac{\text{slope}}{\text{intercept on } P_s \text{ axis}}\right)$$

for the straight-line graph in Fig. XV-6, we calculated the ion plasma frequency f_+ and the ion density $n_+ \approx n$.

From Eqs. 15, 17, and 20 one can show that for $f^2 < f_+^2$

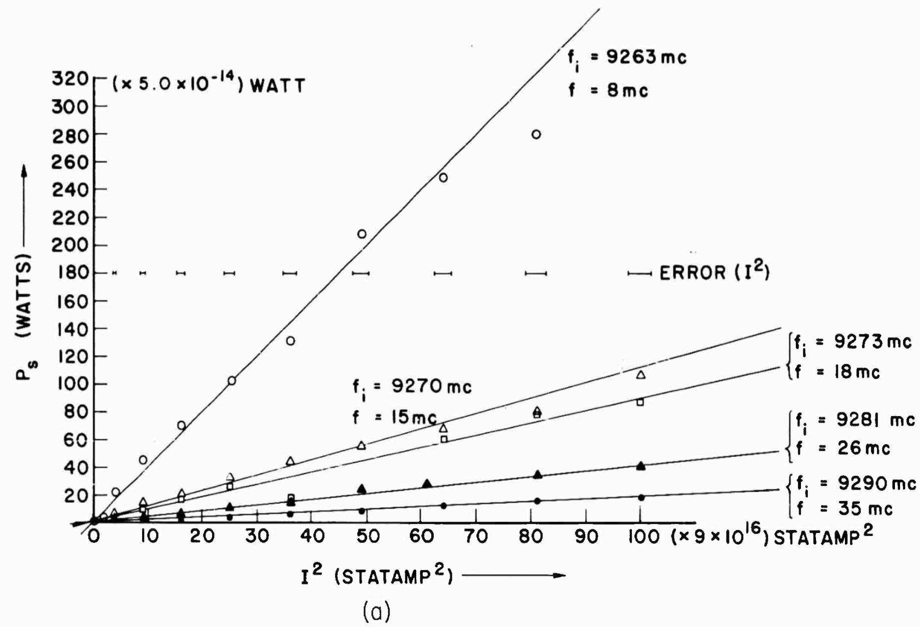

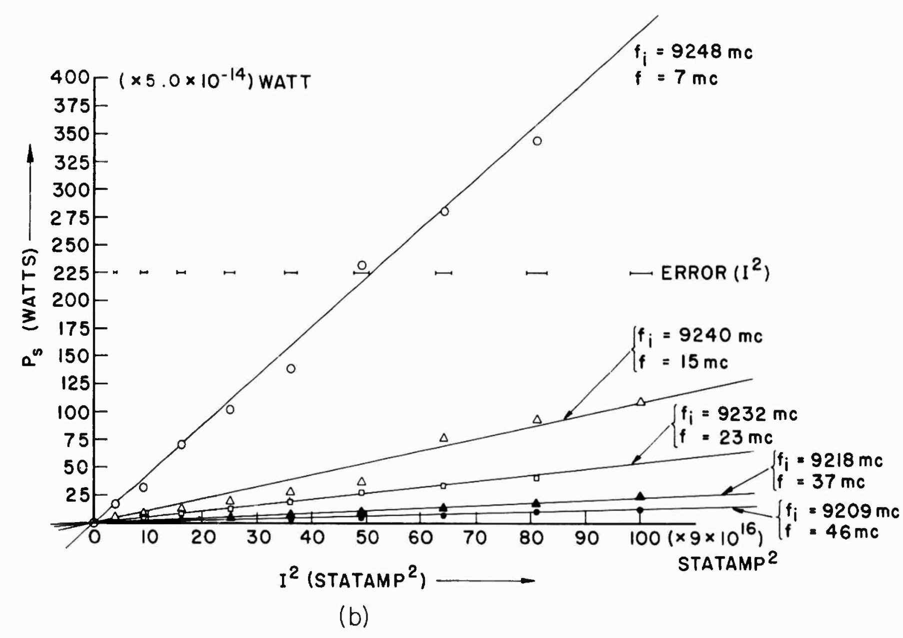

Fig. XV-4. Scattered power vs square of the discharge current J. (a) Scattered frequency less than incident frequency. (b) Scattered frequency greater than incident frequency.

$$P_s(f) = \left[\frac{4\sigma_o(\text{incident power})}{\pi^2 m_+ d^3 v_d^2}\right]\left(\frac{J^2}{f^2}\right), \tag{23}$$

where d is the diameter of the cylindrical plasma column. Using Eq. 23 and the slope of the graph in Fig. XV-5, we get

$$\sigma_o \approx \begin{cases} 5.90 \times 10^{-24}\ \text{cm}^2 & \text{if } v_d \approx 2 \times 10^7\ \text{cm/sec} \\ 1.79 \times 10^{-22}\ \text{cm}^2 & \text{if } v_d \approx 1.1 \times 10^8\ \text{cm/sec.} \end{cases}$$

But the actual value of the Thomson cross section $\sigma_o = \frac{8\pi}{3}(e^2/m_-c^2)^2 \approx 6.6 \times 10^{-25}\ \text{cm}^2$.

This analysis of the experimental results seems to indicate that the measured scattering cross section $\sigma_m(f)$ satisfies the relation

$$\sigma_m(f) = \delta\sigma_c(f) = \delta\sigma_o\left[\frac{f_+^2}{f^2} - 1\right], \tag{24}$$

where the enhancement factor δ is not a function of f or f_+. Comparing Eq. 24 with the theoretically calculated equation (15) for "marginal stability," we see that this enhancement factor δ is a measure of the level of the ion plasma oscillations which exists at steady state with respect to that at the "marginal stability." Therefore this enhancement factor δ is a measure of the nonlinear coupling between the plasma modes

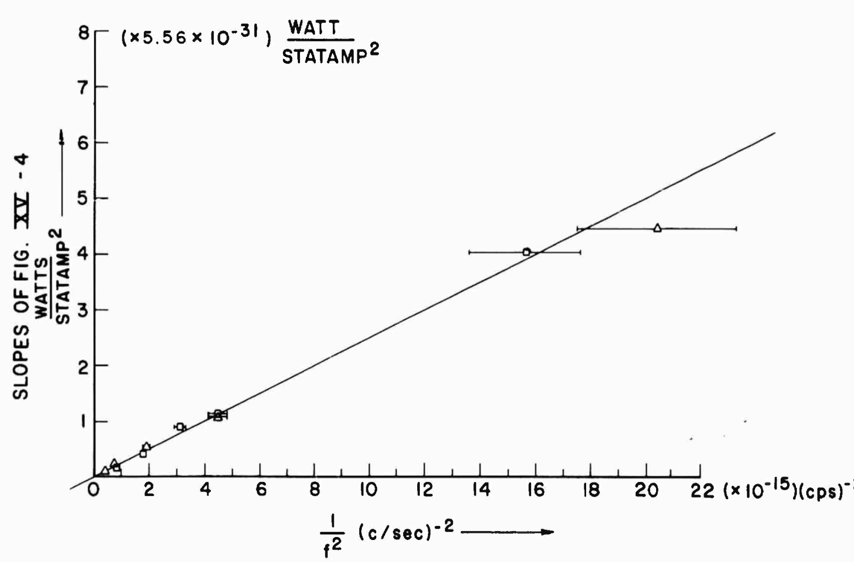

Fig. XV-5. Slopes of Fig. XV-4a and 4b versus $1/f^2$.

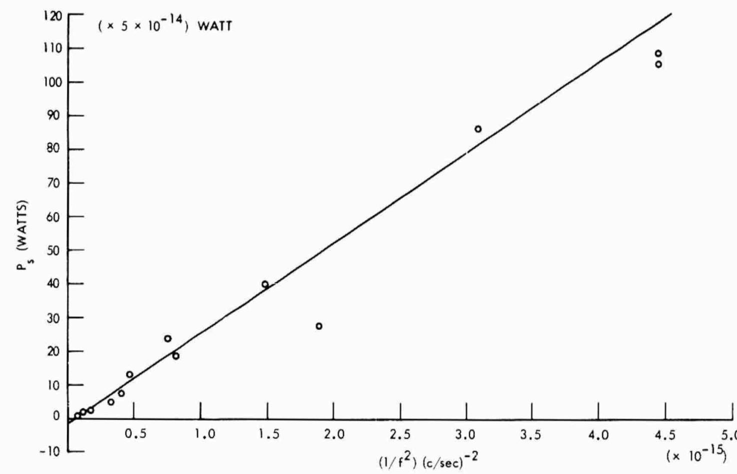

Fig. XV-6. Scattered power versus $1/f^2$ for 1.0-amp discharge current.

of different wavelengths. For a given value of the relative drift velocity $v_d \gtrsim v_c$, the weaker are the nonlinear effects, the larger is the portion of the available drift energy going into the plasma oscillations. Thus if the nonlinear effects are very weak, one will expect this enhancement factor δ to be very much larger than unity, since the plasma will reach a steady state far beyond the conditions of "marginal stability," and if the nonlinear effects are very strong δ will be equal to unity, since the plasma will reach a steady state almost at the conditions of "marginal stability." Our experimental results yield

$$\delta \approx \begin{cases} 9.0 & \text{if } v_d \approx 2 \times 10^7 \text{ cm/sec} \\ 270 & \text{if } v_d \approx 1.1 \times 10^8 \text{ cm/sec.} \end{cases}$$

Thus the experimental measurement of δ seems to indicate that the nonlinear coupling between the plasma modes of different wavelengths is not too strong.

The results presented in Figs. XV-3, XV-4, and XV-5 seem to be in reasonable agreement with the theory of Ichimaru,[1] and Ichimaru, Pines, and Rostoker.[2] The experimental verification of Eq. 22, along with the observed approximate constancy of the value of E/p as the discharge current was varied from 0.3 amp to 1.0 amp, seems to indicate that the drift velocity tends to saturate. From the measured value of this saturation drift velocity and Fig. XV-1, we are led to conclude that the saturation of drift velocity occurs near the threshold for the creation of unstable oscillations of wave numbers $k \approx 1.2k_-$. This seems to be reasonable in the light of the qualitative arguments presented by Pines and Schrieffer.[3]

In conclusion, we wish to point out that Newcomb[6] has shown that in the presence of a magnetic field Eq. 8 takes the form

$$\frac{\omega^2}{\omega_+^2} \approx \frac{k^2/k_-^2}{1 + k^2/k_-^2} + \frac{\Omega^2 \sin^2 \alpha}{\omega_+^2},$$

where $\Omega = (eB/m_+c)$ is the ion-cyclotron frequency and α is the angle between $\vec{k}$ and $\vec{B}$. For regions of interest to us here $\Omega^2/\omega_+^2 \ll k^2/k_-^2$, and therefore the correction term to Eq. 8 is negligible. Furthermore, in our experiment $\alpha \approx 0$, and thus the correction term to Eq. 8 is approximately zero.

V. Arunasalam

References

1. S. Ichimaru, Ann. Phys. 20, 78-118 (1962).

2. S. Ichimaru, D. Pines, and N. Rostoker, Phys. Rev. Letters 8, 231 (1962).

3. D. Pines and J. R. Schrieffer, Phys. Rev. 124, 1387-1400 (1961).

4. W. P. Allis, S. J. Buchsbaum, and A. Bers, Waves in Anisotropic Plasmas (The M.I.T. Press, Cambridge, Mass., 1963).

5. S. C. Brown, Basic Data of Plasma Physics (The Technology Press of the Massachusetts Institute of Technology, Cambridge, Mass., and John Wiley and Sons, Inc., New York, 1959).

6. W. A. Newcomb, Ion Oscillations in a Magnetic Field, Report UCRL-4941, Livermore, California, July 30, 1957.

B. SCATTERING FROM PLASMA OSCILLATIONS IN THE PRESENCE OF AN INHOMOGENEOUS MAGNETIC FIELD

Electromagnetic radiation has been scattered from a plasma in an inhomogeneous magnetic field. Under those plasma conditions for which the plasma contains strong oscillations, a large enhancement of the scattering cross section has been found as a result of the presence of the inhomogeneous field. When an electromagnetic wave is scattered from a plasma, the scattered frequencies correspond to the sum and differences of the incident frequency and the frequencies of the plasma oscillations. In the presence of an inhomogeneous field the dispersion relation can contain resonances both at the incident and at the scattered frequencies, thereby giving rise to a large increase in the scattering cross section.

1. Plasma and Plasma Oscillations

The plasma used in the experiment was a cesium hot cathode discharge.[1] The pressure of the cesium was 0.1-5 μ Hg and was controlled by the temperature of the discharge tube. The discharge was approximately 1 meter long, and the cathode was an oxide-coated ribbon. The phenomena of interest occurred for discharge currents of a few milliamperes, or electron densities of approximately $10^8/\text{cm}^3$, and for external magnetic fields of approximately 1000 gauss.

The plasma had three different modes of operation. The first mode was one in which the plasma was electrically very quiet. This mode existed only for low cesium pressures ($\lesssim 0.2\ \mu$ Hg), and for low discharge currents ($\lesssim 2$ ma). The voltage across the meter-long discharge tube was typically 10 volts in this mode of operation.

The second mode of operation was most easily observed as a transition from the first mode as the discharge current was raised. Strong oscillations appeared in the current, and the voltage across the discharge tube jumped to over 400 volts. The frequency of the oscillations (~15 kc) and the values of the critical electric and magnetic fields causing the transition suggest that the second mode was a rotational instability,[2,3] with a wavelength twice the length of the discharge tube. This mode did not exist for pressures above 0.15 μ.

The third mode similarly occurred as a transition from the second, although at cesium pressures above approximately 0.2 μ Hg it was the only mode that was observed. If the current through the discharge was increased while the discharge was in the second mode, the voltage across the discharge abruptly dropped to 14-20 volts. The discharge current in this mode was characterized by strong oscillations in the 10-50 kc frequency range. Although there is no concrete evidence to verify the nature of these oscillations, their frequencies fall in the range of ion acoustic waves.[4]

Also, oscillations in the frequency range 10-100 mc were observed in mode 3 with the aid of a spectrum analyzer. These are the oscillations from which the scattering occurred (see section 3). Because of the frequencies involved, it seems likely that these oscillations were electron oscillations.

2. Emission and Absorption of the Plasma

The interaction of radiation with the plasma was studied by radiometer techniques such as that illustrated in Fig. XV-7. The frequencies used were between 2500 mc and 3100 mc. The plasma was immersed in the magnetic field formed by coils spaced 6 inches apart. This spacing caused a ripple of approximately 3 per cent in the magnetic field.

The cyclotron emission of the plasma is shown in Fig. XV-8. The line shape and line width were caused by the inhomogeneities in the magnetic field. At the pressures used, the collision broadening was estimated to be less than one-tenth of the inhomogeneity broadening.

Absorption measurements were made, and line shapes similar to the emission shape were obtained. The transmission of the plasma was also measured as a function of the DC conductivity of the plasma, and is illustrated for the mode 1 and mode 3 operations

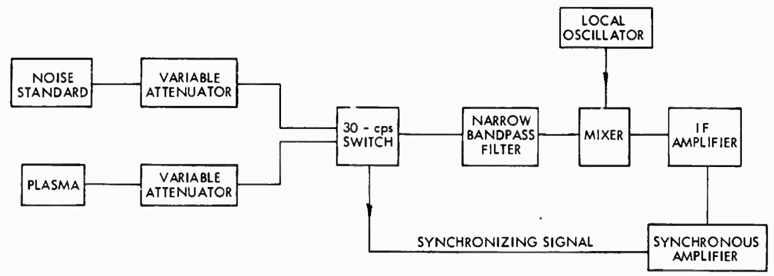

Fig. XV-7. Microwave bridge to measure plasma radiation. Bandwidth of the system, 2 mc. Similar bridge arrangements were used to measure absorption and scattering by the plasma. Plasma was a 1-inch positive column passed through an S-band waveguide at 6°.

(Fig. XV-9). The absorption of the plasma while in mode 2 operation was very small, as would be expected.

As may be seen in Fig. XV-9, absorption was proportional to the current in both mode 1 and mode 3 operation, thereby indicating that the electron density was proportional to the current. The change in slope of the curves for the two cases, however,

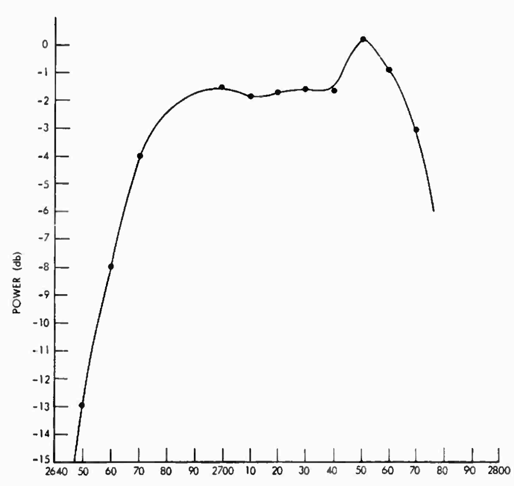

Fig. XV-8. Cyclotron emission from plasma. At 0 db the electron temperature is 10^4°K. Magnet current, 31.35 amps.

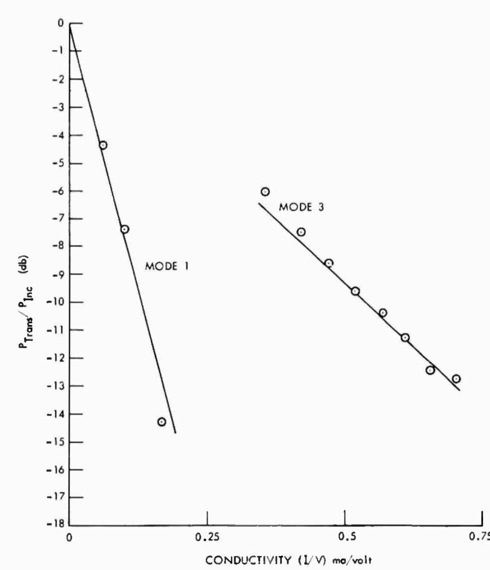

Fig. XV-9. Transmitted power. Cesium pressure, 0.18 μ Hg; frequency, 2705 mc; magnet current, 31.35 amps.

suggests that the electron diffusion mechanism in the plasma changes. This is as expected, for there were strong oscillations in the third mode, which should lead to an enhanced diffusion, although not of the magnitude of that encountered in mode 2.

3. Electromagnetic Scattering

If a signal with a frequency within the cyclotron line was passed through the plasma, there was a strong scattering of radiation. The scattering occurred in all frequencies within the broad resonance, and occurred for all incident frequencies within the resonance (Fig. XV-10). The total scattered energy was approximately one part in 10^6 of

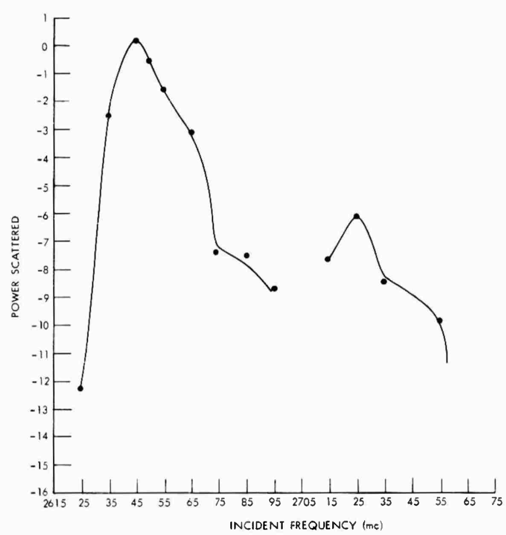

Fig. XV-10.
Scattered power. Measuring frequency, 2705 mc; magnet current, 31.35 amps.

the incident energy.

It can be seen easily that the plasma should resonate both for radiation within the cyclotron line and for scattering within the line. Consider an incident electric field with frequency ω_{inc}. Then, if there are density oscillations in the plasma the Boltzmann equation may easily be solved in the cold-plasma approximation for scattering into a frequency ω. Substituting this solution in the wave equation, for radiation in a waveguide of width a, one finds

$$\frac{d^2E_x}{dz^2}+\left[-\left(\frac{\pi}{a}\right)^2+\frac{\omega^2}{c^2}-\frac{\omega_p^2}{c^2}\,\frac{(1+i\nu_c/\omega)}{\left(1+\frac{i\nu_c}{\omega}\right)^2-\frac{\omega_B^2(z)}{\omega^2}}\right]E_x=\frac{1}{c^2}\,\frac{(1+i\nu_c/\omega)}{\left(1+\frac{i\nu_c}{\omega}\right)^2-\frac{\omega_B^2(z)}{\omega^2}}\,E_x^1(z,\omega_{inc})\,\omega_p^2(z,\omega-\omega_{inc}). \qquad (1)$$

Here, $\omega_p^2(z,\omega-\omega_{inc})$ is the "plasma frequency" corresponding to the oscillating density, and $\omega_B(z) = \dfrac{eB_z(z)}{m}$. The density is assumed to be uniform across the waveguide, and the radial magnetic field is neglected. With these approximations the scattering term contains the same resonance as the dispersion relation.

If the collision frequency is small enough, the resonance on the right-hand side will "pick out" the oscillations at those values of z for which

$$\omega_B^2(z) = \omega^2 - \nu_c^2. \tag{2}$$

Thus, if there is one resonance, the scattered field will be a measure of the oscillations at one point within the plasma; if there are two resonances, at two points, and hence the two-point correlation function is measured. If there are more resonant points, higher order correlation functions can be measured.

The precise calculation of the scattering requires the solution of Eq. 1, with the proper boundary conditions. The magnetic-field configuration for the scattering discussed earlier is too complicated to find an analytic solution; thus a detailed comparison of the experiment and theory has not been attempted. An approximate solution to the equation for the case of a linear variation in magnetic field has been obtained, however,

$$\frac{E_s(\omega_s)}{E_o(\omega_s)} = \frac{\pi i}{2c^2}\left|\frac{z_s\omega_s}{\omega_B^1(z_s)}\right| \omega_p^2(z_o,\omega_s-\omega_i)\left\{\frac{z_s - z_i - i\nu_c/\omega_B^1(z_i)}{-z_i - i\nu_c/\omega_B^1(z_i)}\right\} e^{i(k_i-k_s)z_o}$$

$$\times F\left(\frac{i\omega_p^2}{4k\omega_B^1(z_s)\,\omega_s}\,\Big|\,1\,\Big|\,2ik\left(L - z_s - \frac{i\nu_c}{\omega_B^1(z_s)}\right)\right) \frac{F\left(\dfrac{i\omega_p^2}{4k\omega_B^1(z_i)\,\omega_s}\,\Big|\,1\,\Big|\,2ik\left(z_o - z_1 - \dfrac{i\nu_c}{\omega_B^1(z_i)}\right)\right)}{F\left(\dfrac{i\omega_p^2}{4k\omega_B^1(z_i)\,\omega_s}\,\Big|\,1\,\Big|\,-2ik\left(z_1 + \dfrac{i\nu_c}{\omega_B^1(z_i)}\right)\right)} \tag{3}$$

In this equation E_s is the field scattered at a frequency ω_s, and E_o is the transmitted field, if a field of the same amplitude as the incident field, but with frequency ω_s, is passed through the plasma. z_s is the point at which ω_s resonates, and z_i is the point at which the incident frequency, ω_i, resonates. $\omega_B^1(z)$ is the derivative of the cyclotron frequency. k is the wave vector in the absence of a plasma, and thus

$$k_s^2 = \frac{-\pi^2}{a^2} + \frac{\omega_s^2}{c^2} \text{ and } k_i^2 = \frac{-\pi^2}{a^2} + \frac{\omega_i^2}{c^2}.$$

The function F is the confluent-hypergeometric function.[5]

The experimental dependence of the scattered radiation on such parameters as the plasma frequency, the slope of the magnetic field, and so forth, will be compared with Eq. 3 for the case of a single resonance. If the comparison indicates that the approximations used in deriving Eq. 3 are valid, a similar result will be used to determine the correlation function of the oscillations causing the scattering. Study of the low-frequency oscillations, as well as any coupling between these oscillations and the higher frequency oscillations from which the scattering occurs, will be continued.

E. B. Hooper, Jr.

References

1. J.C. Terlouw, Arc discharge in cesium vapor, Quarterly Progress Report No. 63, Research Laboratory of Electronics, M.I.T., October 15, 1961, pp. 5-8.

2. B. B. Kedomscv and A. V. Nedospasov, J. Nuclear Energy 1, Part C, 230 (1960).

3. F. C. Hoh and B. Lehnert, Phys. Rev. Letters 7, 75 (1961).

4. T. H. Stix, The Theory of Plasma Waves (McGraw-Hill Book Company, Inc., New York, 1962), pp. 41-43.

5. P. M. Morse and H. Feshbach, Methods of Theoretical Physics (McGraw-Hill Book Company, Inc., New York, 1953), pp. 550-554, 671-673.

C. ELECTROMAGNETIC COMPRESSION

Attempts are being made to produce a low-pressure plasma by electron-cyclotron resonance breakdown. It is hoped that by using two cavities the electromagnetic compression forces will confine the plasma between the two cavities.

According to the theories of Boot[1] and Hall[2] these forces should approach infinity in the vicinity of cyclotron resonance. From a physical standpoint, we know that this cannot be. Their method utilizes an average over one period of the RF field, whereas it is known that the particle's perpendicular velocity experiences a beat phenomenon of frequency $\omega - \omega_b$. We therefore would like to use a different approach that will be valid in the vicinity of resonance. We also would like to observe the effect of an initial velocity, ignored in previous treatments.

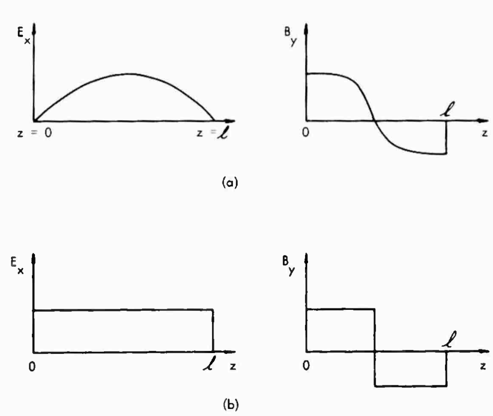

Fig. XV-11.
Electromagnetic fields. (a) Physical fields. (b) Idealized model.

Without a computer it is impossible to perform a calculation of the particles' trajectory inside a cavity. We therefore have made a model of the fields inside the cavity which corresponds roughly to the actual fields but, however, does not satisfy Maxwell's equations. The physical fields are those of a TE_{111}-mode cylindrical cavity. Our field model consists of a uniform electric field in the x-direction with a uniform magnetic field in the y-direction in each half of the cavity. But in each half it has a different sign. (See Fig. XV-11.) Also, we assume another set of fields at right angles to those described above, with a 90° phase shift, so that we have right circular polarization, an assumption that is physically realizable. At present we shall be concerned only with the fields in one-half of the cavity, it being assumed for the present that most of the reflected particles will be reflected before they reach the middle, or not at all. The electric fields in the model can be represented in the following form:

$$\begin{aligned} &E_x(t) + jE_y(t) = E\, e^{j\omega t} \\ &B_x(t) + jB_y(t) = -\frac{k}{\omega} E\, e^{j\omega t}, \qquad 0 < z < \frac{\ell}{2},\ k = \frac{\pi}{\ell} \\ &\vec{E}(t) = \vec{B}(t) = 0 \qquad z < 0 \\ &\vec{B}_o = \hat{i}_z B_o. \end{aligned} \tag{1}$$

Defining $w(t) = v_x(t) + jv_y(t)$, we can write the equation of motion of an electron

$$\frac{d}{dt} w(t) - j\omega_b w(t) = -\frac{e}{m} E\, e^{j\omega t}. \tag{2}$$

The solution is

$$w(t) = \frac{-\frac{eE}{m}}{j(\omega - \omega_b)} \left(e^{j\omega t} - e^{j\omega_b t}\right) + v_{\perp o}\, e^{j\omega_b t + j\theta}, \tag{3}$$

where $v_{\perp o}$ is the perpendicular velocity at $t = 0$.

The z-acceleration can be computed from the Lorentz force.

$$\frac{dv_z(t)}{dt} = -\frac{e}{m} (\vec{v} \times \vec{B})_z = \frac{e}{m} \operatorname{Im} w(t)(B_x + jB_y)^*. \tag{4}$$

Using our solution for $w(t)$, we can integrate this equation to obtain $z(t)$.

$$\begin{aligned} z(t) = v_{zo} t &- \frac{k}{\omega\delta\omega} \left(\frac{eE}{m}\right)^2 \frac{t^2}{2} - \frac{k}{\omega\delta\omega} \left(\frac{eE}{m}\right)^2 \left(\frac{1 - \cos \delta\omega t}{(\delta\omega)^2}\right) \\ &- \frac{k}{\omega\delta\omega} \frac{eE}{m} v_{\perp o} \left[\cos\theta \left(\frac{\sin \delta\omega t}{\delta\omega} - t\right) + \sin\theta \left(\frac{1 - \cos \delta\omega t}{\delta\omega}\right)\right], \end{aligned} \tag{5}$$

where $\delta\omega = \omega - \omega_b$. The second term on the right-hand side represents the time-averaged force computed by Hall's method; the fourth term is not included in the usual treatments. If $t \gg \frac{1}{\delta\omega}$, Eq. 5 can be approximated by

$$z(t) \approx v_{zo}t - \frac{k}{\omega\delta\omega}\frac{eE}{m}t\left[\frac{eE}{m}\frac{t}{2} - v_{\perp o}\cos\theta\right]. \tag{6}$$

Equation 6 can be solved for the time and place at which the particle stops.

$$z(t_s) \equiv \frac{eE}{m\omega}\frac{k}{\delta\omega} = \frac{m}{2e}\left(v_{zo} + \sqrt{\frac{\Omega}{\delta\omega}}v_{\perp o}\cos\theta\right)^2, \tag{7}$$

where

$$\Omega \equiv \frac{k}{\omega}\frac{eE}{m} = \frac{eB_{RF}}{m}. \tag{8}$$

Equation 7 can be represented graphically (see Fig. XV-12). To find the stopping distance, lay off v_{zo} and $\cos\theta\sqrt{\frac{\Omega}{\delta\omega}}v_{\perp o}$, go to the parabola, and read off the ordinate

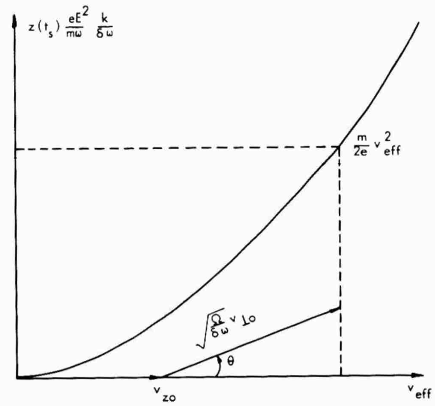

Fig. XV-12. Stopping distance in an applied field, E.

given in normalized stopping distance.

With reference to Eq. 5, we note that if $\delta\omega T \ll \frac{\pi}{2}$ to first order, then there is no time-averaged force because of the forced motion of the particle. This condition corresponds to that for $\omega \approx \omega_b$. It predicts that a large force will be observed only after a very long time and the closer to resonance the longer that time will be.

P. W. Jameson

References

1. H. A. H. Boot, S. A. Self, and R. B. R-Shersby-Harvie, J. Electronics and Control 4, 434-453 (1958).

2. R. B. Hall, Large Signal Behavior of Plasmas, Sc. D. Thesis, Department of Electrical Engineering, M.I.T., September 1960.

D. ANOMALOUS PULSED EMISSION AND ABSORPTION BY A XENON PLASMA AT THE ELECTRON-CYCLOTRON FREQUENCY

Anomalous microwave radiation from xenon, argon, and krypton plasmas in a magnetic field was observed by Tanaka et al.[1] This radiation appeared in the form of a large, very narrow line of radiation at the electron-cyclotron frequency in the pressure range 0.1-5.0 mm Hg. It was suggested by Tanaka et al.[1] that the radiation was a manifestation of the negative radiation temperature predicted by Bekefi, Hirshfield, and Brown[2] and by Twiss.[3]

We have observed several additional features in the emission and absorption of radiation at the cyclotron frequency by a xenon plasma.

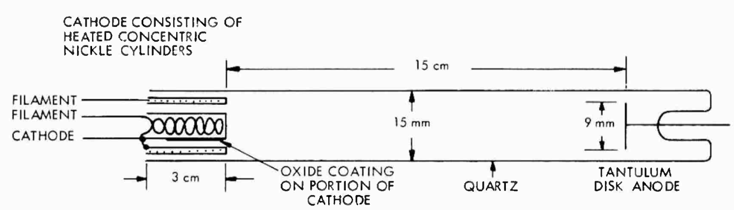

Fig. XV-13. Xenon plasma discharge tube.

The discharge tube is shown in Fig. XV-13. The cathode is similar in construction to the cathode described by Tanaka et al.[1] The anode-to-cathode separation in our discharge tube is 15 cm. The tube diameter is 15 mm. The discharge tube is immersed in the magnetic field of a solenoid. The tube axis coincides with the direction of the magnetic field. The spatial variation in the magnetic field within the volume occupied by the discharge tube is less than 3 gauss per thousand. The measurement was made with a Bell incremental gaussmeter.

The discharge tube passes through the narrow side of a section of S-band waveguide. The microwave electric vector, the direction of propagation, and the external magnetic field are mutually perpendicular.

The pressure of the xenon gas in the discharge tube was measured with a mercury MeLeod gauge. A cold trap filled with Dry Ice and acetone was located between the discharge tube and the McLeod gauge to eliminate mercury vapor from the discharge.

The plasma emission was measured with an S-band radiometer operating synchronously at a 30-cps modulation frequency. The radiometer operated at a fixed frequency of $\omega/2\pi$ = 3262 mc. The bandwidth of the radiometer IF amplifier was 2 mc. Precision attenuators were used to balance the radiation in the plasma arm against that from an argon noise standard with a radiation temperature of 10,600°K.

The absorption coefficient of the plasma was inferred by measuring the power transmitted through the plasma from an external source. At very low power levels, comparable with the plasma emission level, measurements were performed with the radiometer. The power from the external source was modulated at the synchronous frequency of 30 cps. The plasma emission was not modulated and therefore did not contribute. At high power levels (milliwatts) the radiation was detected by a crystal detector and displayed on an X-Y recorder as a function of the magnetic field. At intermediate power levels (10^{-11}-10^{-8} watt) the signal-to-noise ratio was good enough that the output of the radiometer IF amplifiers could be used without synchronous detection.

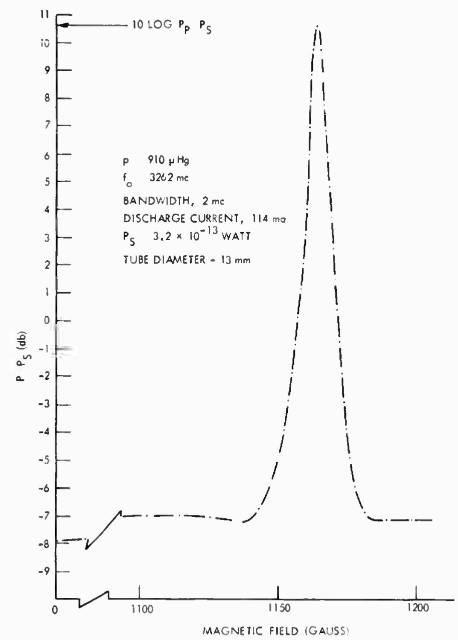

Fig. XV-14. Radiometer measurements of the anomalous cyclotron radiation of a xenon plasma as a function of magnetic field at a fixed microwave frequency.

Figure XV-14 is a typical set of emission data. The ratio of the power radiated from the plasma to that radiated by the noise standard, P/P_S, is presented as a function of the magnetic field at constant discharge current I_d, and constant pressure p. The radiation confirms the features reported by Tanaka et al.[1] It is very narrow, approaching the lower limit imposed by the nonuniformity of the magnetic field. In Fig. XV-14 the amplitude is 17 db above the normal plasma radiation and 11 db above the noise source. This is not as intense as that reported by Tanaka et al.[1] We observed that the amplitude was very sensitive to the orientation of the discharge tube in the magnetic field. In some cases we observed amplitudes 30 db above the normal plasma radiation. Nor did this appear to be a maximum, but further flexing of the glass discharge tube attached to the glass vacuum system seemed unadvisable. Most of the measurements that we shall report were taken with the discharge tube in an in unstrained position. It appears that the position of the cathode surface is important in determining the nature of the nonthermal distribution of electrons near the cathode. The radiation from a xenon discharge containing a flat cathode surface oriented normal to the external magnetic field did not display the narrow-line radiation. When the tube was turned through a small angle the narrow-line cyclotron radiation was detected, although it was small in amplitude. Thus, it appears important that the electrons near the cathode should be subjected to an acceleration at right angles to the magnetic field.

The amplitude of the narrow-line radiation is denoted as P_P. A typical plot of P_P/P_S as a function of discharge current I_d at constant pressure and frequency is shown in Fig. XV-15. The value of the discharge current at which the largest amplitude occurs

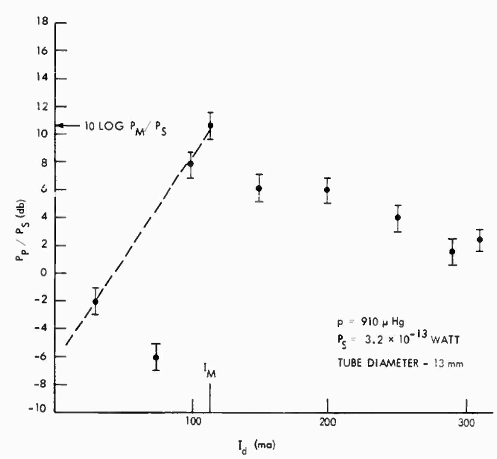

Fig. XV-15.

Radiometer measurements of amplitude of anomalous cyclotron radiation of a xenon plasma as a function of discharge current at constant pressure and microwave frequency.

is denoted I_M and the largest amplitude is denoted P_M.

If the collision frequency is assumed to have the form

$$\nu = a\, p\, v^{h-1},$$

where a and h are constants and v is the electron velocity, then the intensity of radiation from a tenuous plasma containing monoenergetic electrons[1] is

$$I_\omega = \frac{3}{3-h}\left[1 - \exp\left(-\frac{3-h}{3}\frac{\omega_p^2 L}{c\nu_o}\right)\right] B_\omega, \tag{1}$$

where $\omega = \omega_b$ (ω_b is the electron-cyclotron frequency), and B_ω is the black-body intensity at a temperature equal to the average energy of the plasma electrons.

With h = 4.05 for xenon and L = 1 cm, the value of the exponent in Eq. 1 is positive and greater than unity for most values of electron density, temperature, and collision frequency occurring in these experiments. With the value p = 900 μ Hg in Fig. XV-15, Eq. 1 can be approximated by

$$10 \log \frac{P_P}{P_S} = C + 3.035 \times 10^{-10} \frac{m}{P_c\sqrt{V}}. \tag{2}$$

Here, M is the electron density (electrons/cm^3), P_c is the collision probability, and

$$C = 10 \log 2.857 \frac{T_e}{T_S}, \tag{3}$$

where T_e is the electron temperature and T_S is the noise source temperature.

The dashed line in Fig. XV-15 in the range of discharge currents from 0 ma to 110 ma represent Eq. 2 when

$$\frac{m_o}{P_c\sqrt{V}} = 4.71 \times 10^{10}, \quad \frac{T_e}{T_S} = 1.5 \tag{4}$$

where m_o is the value of the electron density oocurring at I_d = 100 ma. If the value h = 4.46 supplied by Tanaka et al. is used,

$$\frac{m_o}{P_c\sqrt{V}} = 3.3 \times 10^{10}, \quad \frac{T_e}{T_S} = 1.1.$$

When the electron density is approximately 10^{11} cm^{-3} the plasma frequency is equal to the fixed frequency of the radiometer. The assumption of a reflectionless plasma employed in the derivation of Eq. 1 is not valid at this and higher densities. As the plasma becomes highly reflecting the emission should decrease. The amplitude of the narrow cyclotron line diminishes (Fig. XV-15) when the discharge current is increased beyond the value I_M = 110 ma. Several data points in Fig. XV-15 do not fall close to the dashed lines. Further experimental investigation is continuing to establish the P_P vs I_d curves for different pressures.

In Fig. XV-15 the value of the discharge current denoted I_M is believed to correspond to the condition $\omega_P = \omega$.

The electron density is a function of the ratio $I_d/(E/p)$. The discharge current required to maintain a fixed value of electron density decreases as the pressure increases. In Fig. XV-16 the discharge current required to hold the density at the constant value corresponding to $\omega_P = \omega$, that is, I_M, decreases with increasing pressure above 500 μ Hg. The behavior of I_M as a function of pressure below 500 μ Hg is not understood at present.

In Fig. XV-16 of Tanaka et al.[1] the value of I_M is 600 ma at a pressure of 260 μ Hg. This is approximately triple our value, as it should be, since their radiometer

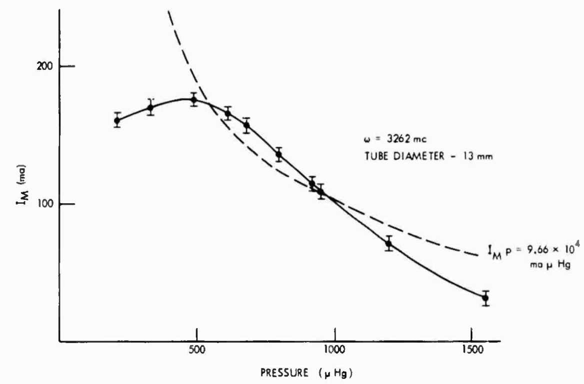

Fig. XV-16. Discharge current for a maximum radiated power as a function of xenon gas pressure.

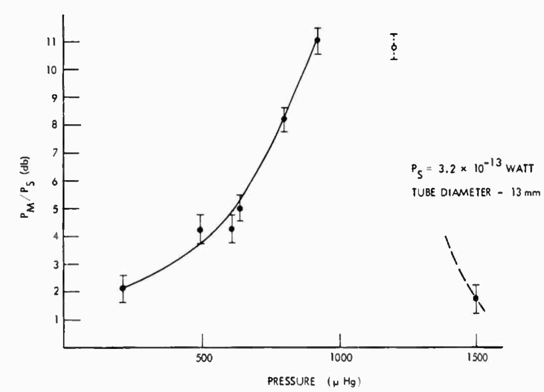

Fig. XV-17. Radiometer measurements of the maximum power radiated in the anomalous cyclotron radiation of a xenon plasma as a function of the gas pressure.

frequency is triple ours.

The value of P_P is a maximum at I_M, and is denoted P_M. P_M is plotted against pressure in Fig. XV-17. On the basis of Eq. 1 the amplitude of the narrow emission line should decrease with increasing pressure. Figure XV-17 shows the amplitude of P_M increasing with pressure in the range 200-1000 μ Hg. An uncertain experimental observation indicates that the value of P_M is fairly constant in the pressure range 1000-1200 μ Hg. Above 1200 μ Hg the value of P_M decreases rapidly with pressure. Several factors should be considered to obtain an adequate theoretical description of

Fig. XV-17. The electron temperature decreases with increasing gas pressure (cf. Brown[4]). Thus the number of electrons found at favorably low Ramsauer energies would increase with increasing pressure, thereby enhancing the emission. The rate of thermalization of the electron gas, however, also increases with pressure. Therefore, at higher pressure the amplitude of nonthermal radiation should decrease with increasing pressure.

Nonsynchronous observation of the output of the IF amplifier of the radiometer revealed that the narrow cyclotron line emission was pulsed rather than continuous. These pulses are so intense ($\sim 10^{-11}$–10^{-9} watt) that it is not necessary to use synchronous detection. The relative amplitude of these pulses as a function of magnetic field conform to the line shape shown in Fig. XV-14. That is, intense pulses occur only over a very narrow range of magnetic field.

A cw microwave signal was generated by a klystron mounted with several variable attenuators in a shielded box. The power output could be varied between 10^{-13} watt and 10^{-2} watt. The cw signal was modulated at 30 cps and transmitted through the plasma. The plasma emission was unmodulated.

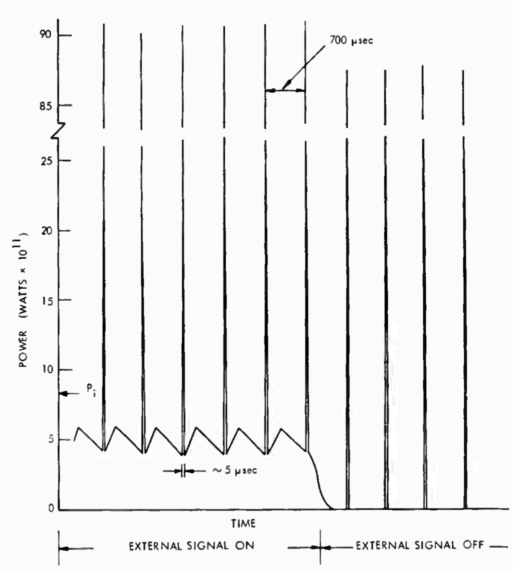

Fig. XV-18.
Power radiated by a xenon plasma at the cyclotron frequency as a function of time; power transmitted through the plasma from an external source. I_d = 25 ma; p = 500 μ Hg; $\omega = \omega_b$; IF bandwidth = 2 mc; P_i = incident power of external signal.

Figure XV-18 shows a period of time in which the klystron signal is incident on the plasma followed by a period in which the klystron signal is blocked off. The unmodulated plasma radiation is always present. The normal plasma radiation is too small, at this scale, to be seen, but the pulses are impressive. By careful adjustment of the discharge current the pattern of pulses could be made stationary with respect to the modulating frequency and displayed on an oscilloscope. Figures XV-18, XV-19, and XV-20 are drawn from photographs of the oscilloscope patterns. The pulses occur at 700-μsec intervals when the discharge current is 25 ma and the gas pressure is 500 μ Hg. The width of the pulses was estimated to be less than 5 μsec. Variation between the amplitude of individual pulses was, at most, only a few per cent. No amplification of the transmitted part of the cw signal is evident. The detected power appears to be the sum of the plasma-attenuated cw signal plus the plasma generated pulses.

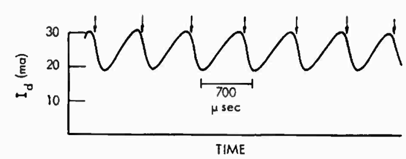

Fig. XV-19. Xenon plasma discharge current versus time. Arrows indicate time and current at occurrence of anomalous cyclotron radiation pulses.

Synchronous detection of the transmitted part of the modulated cw signal (with the plasma emission unmodulated) has not shown any tendency for the plasma to amplify external signals. Measurements were taken over the range from 10^{-13} watt to 10^{-2} watt.

Figure XV-18 further reveals that the transmitted cw signal is not constant in time. There is a saw-toothed oscillation with the same period as the plasma pulses. This variation in the absorption of the cw signal is due to a variation in the plasma density. Figure XV-19 shows the time variation of the discharge current. The arrows indicate the time and current values at which the plasma emits pulses. The discharge tube and a 100-ohm external resistor are in series with a constant voltage source. As the current (and density of electrons) increases, the voltage across the discharge decreases. $I_dR_{EXT} + V_d =$ constant. The electron temperature is probably a minimum when the pulses are emitted. A large inductance was placed in series with the discharge tube in order to maintain a constant discharge current. The pulses from the plasma persisted, but at random intervals.

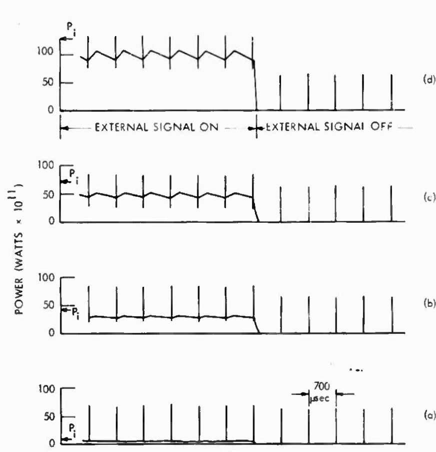

Fig. XV-20. Anomalous cyclotron pulses and transmitted portion of a P_i watt incident external signal.

Figure XV-20 shows the occurrence of absorption 'pulses' in the transmitted cw signal as the strength of the incident signal is increased. In the presence of

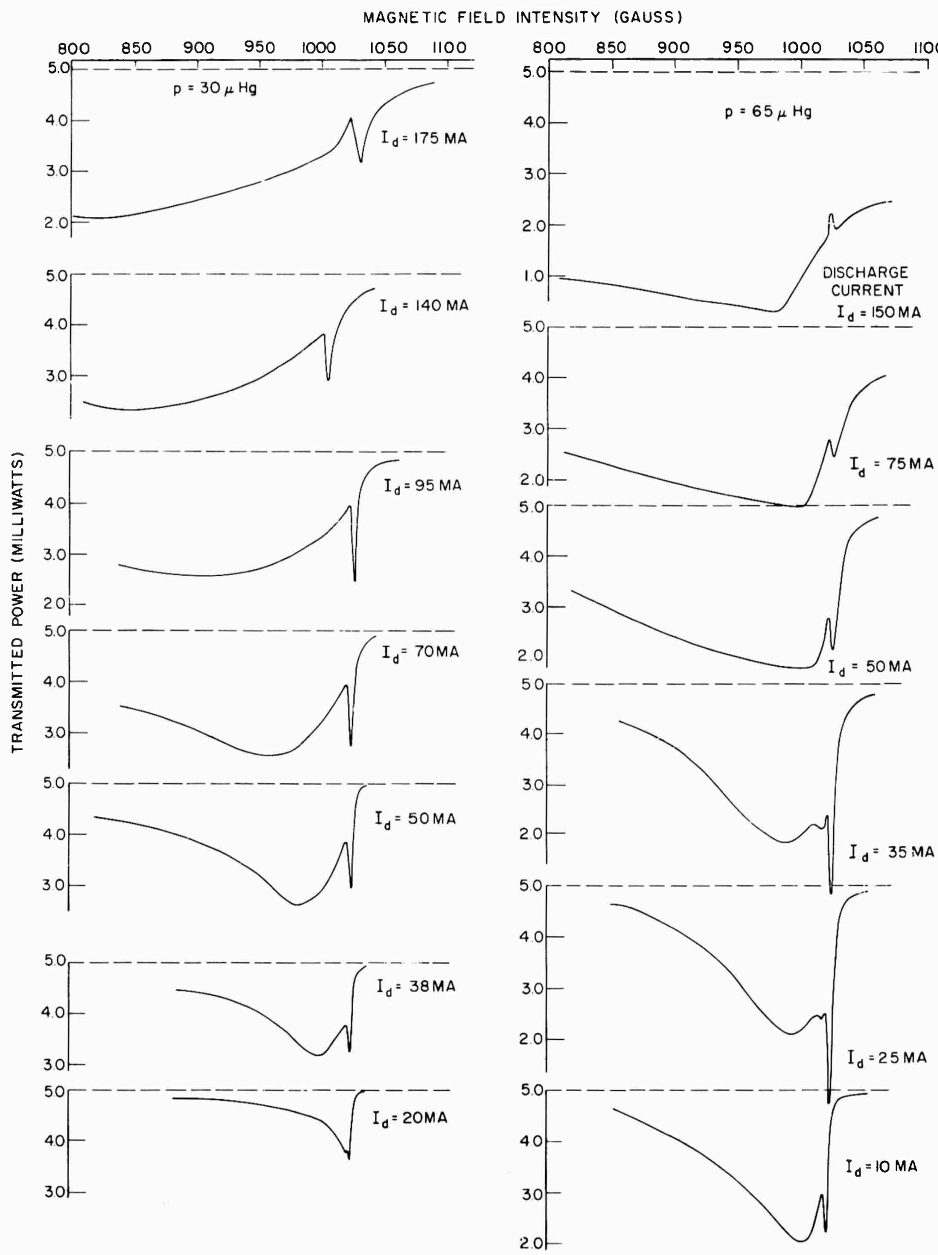

Fig. XV-21. Absorption of milliwatt microwave power by a xenon plasma as a function of magnetic field. Incident power = 5 mw.

an external signal the amplitude of the emitted pulse decreases while the amplitude of the absorption pulse increases with increasing signal. The time sequence of the two pulses has not been determined.

Figure XV-21 shows the power transmitted through the plasma as a function of magnetic field at milliwatt incident power. The narrow absorption line at the cyclotron frequency appears superimposed on a much broader 'normal' cyclotron absorption. The spectrum flattens out at higher discharge currents as the plasma approaches black-body conditions.

These experiments were repeated with helium. Helium does not contain a Ramsauer minimum in its electron collision cross section. The narrow-line cyclotron emission and absorption were not detected.

Many additional experiments are being undertaken. They will employ various gases, with and without Ramsauer minima. The radiation and absorption by these discharges will be measured in cavities, as well as in waveguides.

To summarize, intense pulses of radiation were observed in a xenon plasma. They occurred over a very narrow range of cyclotron frequencies centered at the fixed frequency of the detector. Synchronous detection of the transmitted portion of externally generated signals at levels comparable with the normal radiation from the plasma did not reveal amplification or additional absorption of the signal by the plasma. With the external signal comparable with the pulse height of the narrow-line emission, a narrow absorption line at the cyclotron frequency appears. This narrow absorption line is present when the external signal level is milliwatts.

No conclusive theoretical explanation for these phenomena are offered at this time. If the narrow-line radiation is due to amplification of the plasma radiation, the amplifier appears to be operating at saturation or poorly coupled to the external signal because no amplification of external signals has been detected. Another possibility is that there may occur a condition in which a large fraction of the electrons attain energies at the Ramsauer minimum. Since $P_c = 4$ at the minimum, they would radiate a very narrow line. The Ramsauer resonance is narrow and the electron lifetime at the minimum would be short. If the plasma were driven by a large external signal, this group of electrons would contribute to a narrow absorption line.

J. D. Coccoli

References

1. S. Tanaka, K. Mitani, and H. Kubo, Experiments on the Negative Radiation Temperature at Cyclotron Resonance in Cold Plasma, Research Report IPPJ-6, Institute of Plasma Physics, Nagoya University, Japan, February 1963.

2. G. Bekefi, J. Hirshfield, and S. C. Brown, Phys. Fluids 4, 173 (1961); Phys. Rev. 122, 1037 (1961).

3. R. Q. Twiss, Australian J. Phys. 11, 564 (1958).

4. S. C. Brown, Basic Data of Plasma Physics (The Technology Press of the Massachusetts Institute of Technology, Cambridge, Mass., and John Wiley and Sons, Inc., New York, 1959); Special Technical Report No. 2, Research Laboratory of Electronics, M.I.T., August 17, 1959.

XVI. PLASMA ELECTRONICS*

Prof. L. D. Smullin
Prof. H. A. Haus
Prof. A. Bers
Prof. W. D. Getty
Prof. P. Penfield, Jr.
Prof. D. J. Rose
Prof. T. H. Dupree
Prof. L. M. Lidsky
Prof. E. P. Gyftopoulos
R. R. Bartsch
W. L. Brasser
R. J. Briggs
T. S. Brown
J. F. Clarke
P. Edmonds
S. A. Evans
T. J. Fessenden
E. T. Gerry
R. Hancox
B. A. Hartenbaum
C. F. G. Hsi
H. Y. Hsieh
G. I. Kachen
B. Kusse
M. A. Lieberman
L. N. Lontai
J. D. Mills
D. L. Morse
A. A. Offenberger
L. M. Petrie, Jr.
S. Puri
C. G. Robertson
P. S. Spangler
G. Theodoridis
E. Thompson
P. B. Ulrich
M. T. Vlaardingerbroek
C. E. Wagner
H. L. Witting
J. C. Woo

RESEARCH OBJECTIVES AND SUMMARY OF RESEARCH

1. Plasmas for Electrical Energy Conversion

This group is concerned with the synthesizing or design of particular plasma systems to perform specific functions. The research program described below is concerned primarily with the plasma as a component of a power generator: either controlled thermonuclear fusion or magnetohydrodynamic. To implement this program, we are studying several methods of producing and containing dense, hot plasmas. We are also concerned with the collective behavior of plasmas of finite dimensions, and are studying possible means of energy extraction. Thus we are led to the investigation of waves in plasma waveguides and their stability, and of millimeter oscillations induced by drifting plasmas in semiconductors.

(a) Beam-Plasma Discharge

During the past year we have made considerable progress toward gaining a detailed understanding of the dynamics of the beam-plasma discharge (BPD). From study of the time behavior of the radiofrequency spectrum radiated by the discharge, we have clarified our ideas about the interaction mechanisms, and we have evidence of direct excitation of the ions by the beam, at the ion plasma frequency. Our studies of the loss mechanisms have uncovered a "rotating spoke" instability. The newest beam-plasma discharge device has a hollow, high-perveance, electron beam. It generates a plasma density $>2 \times 10^{13}/\text{cm}^3$ in a neutral gas background of $2 \times 10^{12}/\text{cm}^3$, X-rays with energy >100 kv with a voltage of 7-10 kv. During the coming year we shall pay particular attention to the excitation of ion plasma oscillations as a means of heating the ions.

L. D. Smullin, W. D. Getty

(b) Electron-Cyclotron Resonant Discharge

We have placed in operation a medium-power device. Pulsed RF power 50 kw peak, 50-100 watts avg, is used to excite a cylindrical cavity, 15 inches in diameter, at

*This work was supported in part by the National Science Foundation (Grant G-24073); and in part by Purchase Order DDL BB-107 with Lincoln Laboratory, a center for research operated by Massachusetts Institute of Technology, with the support of the U.S. Air Force under Contract AF 19(628)-500.

3000 mc. The average x-radiation just outside the cavity is ~5 r/m, and energies >1 Mev are observed. Diamagnetic probe signals indicate that a relatively high β plasma is produced. Low-frequency oscillations (~10-30 mc) are radiated by the plasma during the interpulse period.

During the coming year we shall study the parametric behavior of the electron-cyclotron resonance discharge (ECRD) with special emphasis on the mechanisms for transferring energy from the electrons to the ions.

L. D. Smullin, T. J. Fessenden

(c) Beam-Induced Ion Plasma Oscillations

Experiments on the beam-plasma discharge have indicated that the electron beam can induce oscillations at ω_{pi}, if the electrons are hot enough. In these new experiments we are using a medium-power electron-cyclotron resonance discharge (ECRD) to produce a plasma with hot electrons. Into this plasma we fire an electron beam, and we shall examine the spectrum of the induced oscillations.

L. D. Smullin, M. T. Vlaardingerbroek, M. A. Lieberman

(d) Theory of Active and Passive Anisotropic Waveguides

This research will proceed along two lines.

(i) Development of small-signal energy and momentum-conservation principles that are applicable to the linearized equations of anisotropic waveguides in the absence of loss will be undertaken to obtain criteria for the stability or amplifying nature of the waves in these systems.

(ii) Analysis of specific waveguides of present interest, and determination of their dispersion characteristics will be carried out.

The dispersion characteristics may also be used to test the general criteria obtained from the conservation principles.

A. Bers, H. A. Haus, P. Penfield, Jr.

2. Highly Ionized Plasma and Fusion Research

Studies that are applicable to controlled nuclear fusion assume many forms. Our activities, for the most part, are involved with plasmas: plasma kinetic theory, plasma production by injection, nonadiabatic particle motions, stability and turbulence, and interaction with coherent radiation. Our other activities (energy extraction and tritium regeneration through a surrounding blanket, superconducting magnetic-field structures for plasma confinement), while motivated by the thought of controlled fusion, have wider applicability.

(a) Interaction of Coherent Radiation and Plasmas

Study of the following physical problems, by means of pulsed high-intensity laser beams, continues:

(i) Thomson scattering from free electrons in an electron beam, as a diagnostic tool for study of beam structure;

(ii) Thomson scattering from free electrons in an almost fully ionized plasma (ion density 10^{13}-10^{14}/cm^3, neutral density 10^{11}-10^{12}/cm^3);

(iii) Photoionization of excited atoms in a plasma, and related phenomena;

(iv) Measurement of the plasma correlation structure, by means of scattering through angles $\theta \approx$ (laser wavelength/2π Debye length); and

(v) Light-suppression and light-collection techniques to optimize the methods involved in experiments of this general nature.

E. Thompson, L. M. Lidsky, D. J. Rose

(b) Plasma Kinetic Theory

Our research in plasma kinetic theory is concentrated in two general areas. The first is concerned with the derivation of "reasonably" simple but "reasonably" exact equations to provide a complete description of plasma behavior. The starting point has usually been a set of generalized hierarchy equations that includes the transverse electromagnetic field. The second phase of the program is directed toward obtaining interesting solutions to the fundamental equations to second order in the plasma parameter. General formulas for the approach to equilibrium, including expressions for radiation emission and absorption, have been derived.

T. H. Dupree

(c) Nonadiabatic Motion of Particles

Our studies of charged-particle trapping by injection into nonadiabatic systems are being extended to include the general problem of weakly nonadiabatic motion in various magnetic structures of practical interest. This work will include study of particle "unwinding" devices, and minimum-field plasma-confinement configurations.

L. M. Lidsky, D. J. Rose

(d) Plasma Turbulence and Stability

The structure of plasma columns in axial magnetic fields is being studied theoretically and experimentally, with a view toward applying concepts of turbulent motion to the analysis of their behavior. New minimum-field confinement configurations will be applied to these plasma columns and possibly to differently produced plasmas, to decrease the level of turbulent instability at the plasma-vacuum interface.

D. J. Rose, L. M. Lidsky

(e) Ion Beam

With the advent of Lorentz dissociation of excited molecular beams and Lorentz ionization of excited atomic beams, we are extending our low-divergence high-current ion-beam studies to include measurements of the efficiency of production of excited atomic and molecular beams and their subsequent ionization and dissociation.

E. Thompson

(f) Superconducting Magnet

Modifications of our superconducting magnet assembly to remove a thermal contact have been completed. Analysis of, and introspection concerning, the present design of large superconducting magnets, based upon experience gained thus far, lead us to quite different design concepts. A new configuration will be detailed during the coming year. A propos of superconducting magnet systems, in general, we remark that the newer minimum-field configurations for more stable plasma confinement are exceedingly expensive in terms of magnetic field energy; the plasma is also kept relatively remote from the field sources. These requirements, in our opinion, will be satisfied by superconducting magnet systems, and by no other kind.

D. J. Rose, L. M. Lidsky

(g) Thermonuclear-Blanket Studies

We have shown that if confinement of a controlled-fusion plasma is possible, the nuclear and other facts of nature will permit regeneration of the tritium that is necessary for a D-T reaction, probably with a small safety margin. Principal extensions of this study will be

(i) Calculation of transport, neutron flux, and tritium regeneration in finite systems,

(ii) Experimental measurement of tritium production and of energy deposition (by means of gamma rays) in a cylindrical blanket mock-up with point neutron source,

(iii) Study of the physical and engineering feasibility (or nonfeasibility) of a fast pulsed controlled fusion system.

D. J. Rose, I. Kaplan

(h) Cesium Plasmas

Properties of low-energy cesium plasmas and formation of molecular ions through excited cesium-atom collisions have been investigated with promising results.[1,2]

Intermetallic adsorption systems have been studied during the past year. Heats of desorption and rates of emission of cesium and other metallic atoms and ions desorbed from partially covered surfaces have been derived theoretically.[3-6] State functions for partially covered intermetallic surfaces have also been derived.

Work on these subjects, together with experimental studies of cesium ion-beam neutralization schemes, will continue.[7]

E. P. Gyftopoulos

References

1. H. Witting, Concentration of excited states in a low-energy cesium plasma, Quarterly Progress Report No. 70, Research Laboratory of Electronics, M.I.T., July 15, 1963, pp. 153-162.

2. H. Witting and E. P. Gyftopoulos, Volume Ionization Processes in Cesium Converters, presented at the Thermionic Converter Specialist Conference, Gatlinburg, Tennessee, October 7-9, 1963.

3. J. D. Levine and E. P. Gyftopoulos, Adsorption Physics of Metals Partially Coated by Metallic Films, Proc. Twenty-third Annual Conference on Physical Electronics, M.I.T., March 1963, pp. 239-249.

4. J. D. Levine, Adsorption Physics of Metals Partially Coated by Metallic Films, Ph.D. Thesis, Department of Nuclear Engineering, M.I.T., April 1963.

5. J. D. Levine and E. P. Gyftopoulos, Adsorption physics of metals partially coated by metallic particles, Part I – Desorption energies (to be published in Surface Science).

6. J. D. Levine and E. P. Gyftopoulos, Adsorption physics of metals partially coated by metallic particles, Part II – Desorption, vaporization and sublimation rates (to be published in Surface Science).

7. G. C. Theodoridis, Space-Charge neutralization experiment, Quarterly Progress Report No. 70, Research Laboratory of Electronics, M.I.T., July 15, 1963, pp. 164-167.

A. BEAM-PLASMA DISCHARGES

1. SYSTEM A: RADIOFREQUENCY SIGNALS RADIATED BY BEAM-PLASMA DISCHARGE

This report summarizes our observations of the radio frequencies emitted by the beam-plasma discharge. Three observations are particularly striking. First, strong microwave oscillations occur in several narrow bands of frequencies. Second, microwave frequencies continue to be emitted for as long as 15 μsec after the beam pulse has ended. Third, strong VHF signals are observed at frequencies corresponding to the ion-plasma frequency.

With either the wideband "video" detector or the narrow-band detector,[1] the microwave oscillations (5.5 kmc to 15 kmc) always appear as spikes in time. In many cases the duration of the spike appears to be limited by the bandwidth of the detector. Typically, a spike is 0.1-0.2 μsec in duration, Fig. XVI-1b. At low magnetic fields (less than 250 gauss) the spikes occur more or less continuously during the entire beam-plasma discharge. At higher magnetic fields, the spikes occur in groups that vary in duration from 10 μsec to 50 μsec.[1] The strength of these oscillations varies along the axis. It is much stronger (10-100 times stronger) near the gun than at the collector, Fig. XVI-2. The same dependence has been found in both hydrogen and helium.

By comparing the outputs of two wideband "video" detectors that respond in different frequency ranges (the X-band detector covers a range of 7-10 kmc, the Ku-band detector covers a range of 10-14 kmc), it has been found that the oscillations in these two bands are anticoincident. Figure XVI-1c shows a correlogram of the Ku-signal and the X-signal. A 5-μsec sample of the radio frequency is taken during each beam pulse, and the photograph is an exposure over 100 pulses. Figure XVI-1b shows a time-expanded view of the Ku-signal and X-signal, illustrating the anticoincident characteristics.

Using the spectrum analyzer, we found that strong microwave oscillations occur in several narrow bands of frequencies which are distinctly separated by intervals of very weak or no oscillations. A parametric mapping of the instantaneous frequency and intensity during the beam-plasma discharge is under way. Preliminary investigations show that at higher beam powers the bands move toward high frequencies, and that at high beam powers and high magnetic field, a rather intense continuum begins to build up.

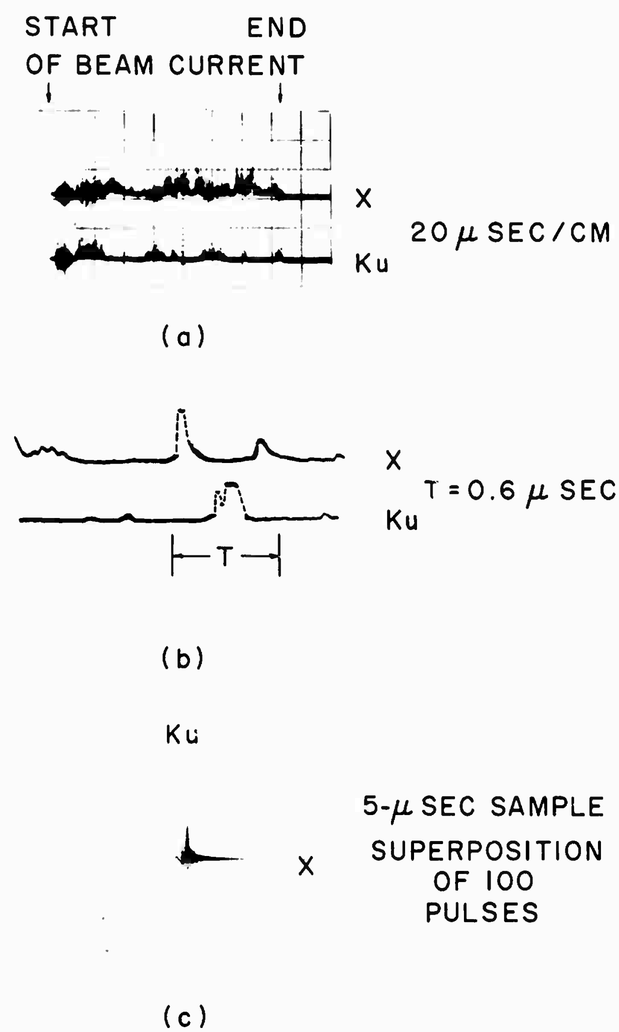

Fig. XVI-1. Oscillograms illustrating the general nature of the signals received by the Ku-band detector and the X-band detector. The experimental conditions for these three illustrations were not the same. (a) Groups of spikes received by the two detectors during the beam-plasma discharge. (b) Anti-coincidence of the two signals on an expanded time scale within a group.

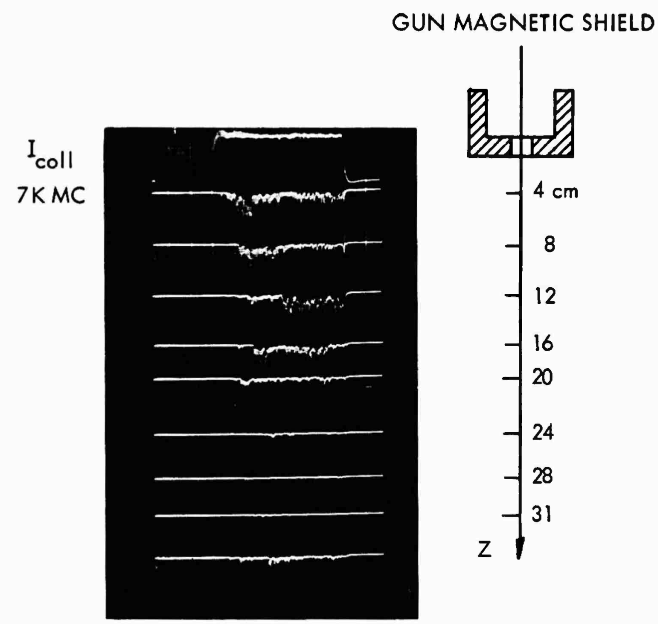

Fig. XVI-2. Oscillograms showing kmc oscillation amplitude as a function of axial position. The 7-kmc oscillation is picked up by a movable loop. The vertical calibrations are the same in the kmc oscillation traces except the last, which shows the 7-kmc signal at z = 31 cm when the vertical gain is increased by a factor of 10.

$P = 0.52\ \mu$ Hg	$B_o = 280$ gauss
$V_b = 5$ kv	$I_{coll} = 0.26$ amp
Time, 20 μsec/cm	Hydrogen

a. Oscillations in the Absence of Beam Current

Up to 15 μsec after the beam current ended, frequencies in the ranges 100-300 mc and 6-10 kmc were observed. The oscillations always occur during the time at which the collector current represents a net ion current, Fig. XVI-3. The intensity of the oscillations during this "afterglow" is usually smaller than, but sometimes comparable to, the intensity of the oscillations during the beam-plasma discharge. In system A, one of the necessary conditions for observing these afterglow oscillations is that the magnetic field must be above a certain critical value, which is ~600 gauss.

The oscillations always occur as spikes. The oscillations observed both with the broadband "video" detectors and with the spectrum analyzer occur as trains of spikes. The number of spikes in the train varies from two to six. The spikes in the train occur almost in regular intervals. The average period is approximately 2 μsec. The general tendency, not always true, is for the intervals within the train to decrease with time. The train correlates well with a regular oscillation (whose period also varies in the

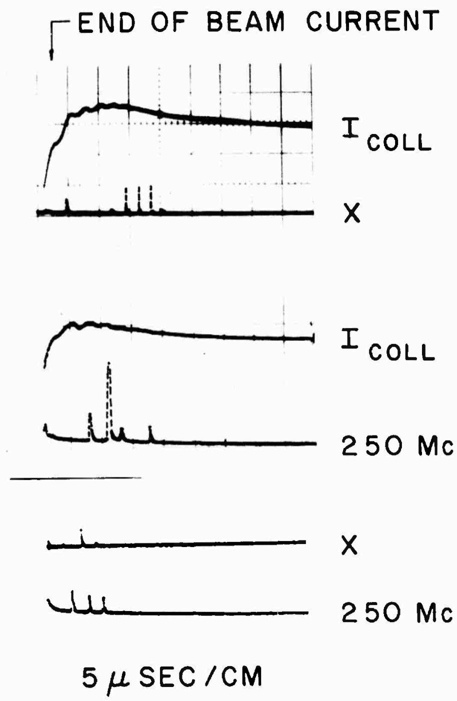

Fig. XVI-3. Oscillograms showing typical oscillations during the "afterglow."

$P = 0.55\ \mu$ Hg $\quad B_o = 630$ gauss

$V_b = 5$ kv $\quad I_{coll} = 0.24$ amp

Hydrogen

same way as the train's) observed on a magnetic probe. The train does not correlate well with the fluctuations seen on a Langmuir probe. The train often occurs during the time when the net ion current on I_{coll} is flat. At the moment, the ensemble of pictures collected does not show a correlation between the spikes and the fluctuations in the light output. The last rf spike usually occurs within 15 μsec after the end of the beam current.

The afterglow oscillations indicate the presence of a highly anisotropic electron velocity distribution, which persists for 10-15 μsec after the beam is turned off. The existence of microwave oscillations implies an electron density of the order of 10^{12} ions/cc during this time. The VHF oscillations (100-300 mc) lie in a range corresponding to the ion-plasma frequency. Presumably, they are both excited by an anisotropic velocity distribution of the electrons.[2]

H. Y. Hsieh

References

1. H. Y. Hsieh, Beam-plasma discharges. System A, Quarterly Progress Report No. 71, Research Laboratory of Electronics, M. I. T., October 15, 1963, pp. 114-115.

2. R. J. Briggs and A. Bers, Interaction of an electron beam with ions in a warm plasma of finite transverse dimensions, Quarterly Progress Report No. 71, Research Laboratory of Electronics, M. I. T., October 15, 1963, pp. 131-137.

2. SYSTEM B: ROTATIONAL INSTABILITY IN THE BEAM-PLASMA DISCHARGE

Space- and time-resolved light measurements indicate that a spoke of plasma rotates in a right-hand sense about the applied, axial magnetic field. The fields of view of the two telescopes[1] are shown in Fig. XVI-4. The oscillograms of the detected light output

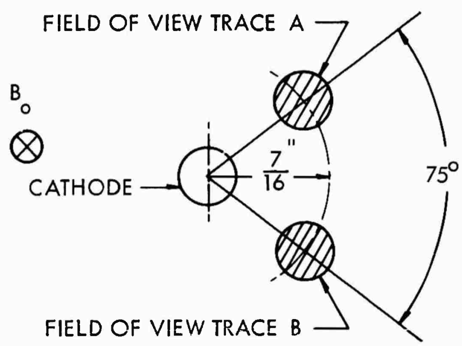

Fig. XVI-4. Fields of view of telescopes.

in Fig. XVI-5a show that trace A leads trace B by 0.2 period, which corresponds to the angular separation of the fields of view. The time lag between the two traces reverses with a reversal of the magnetic field. Oscillograms of probe current,[1] Fig. XVI-5b,

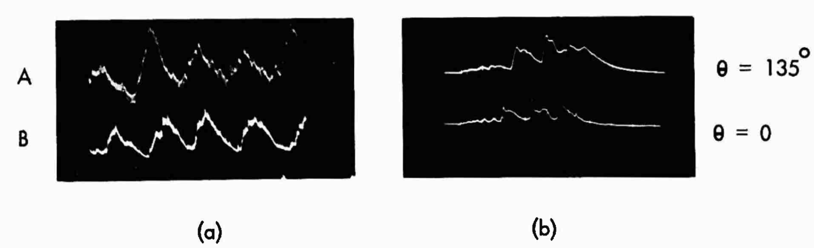

Fig. XVI-5. Rotational time lag.

(a) Light	(b) Probe currents
$p = 0.5\ \mu\ H_2$	$p = 0.5\ \mu\ H_2$
$B_o = 540$ gauss	$B_o = 350$ gauss
$V_o = 7.2$ kv	$V_o = 7.2$ kv
time, 10 μsec/cm	time, 20 μsec/cm

agree with the light measurements.

The instability begins above a critical magnetic field. Current to the beam collector for magnetic fields just below and above the critical field value is shown in Fig. XVI-6.

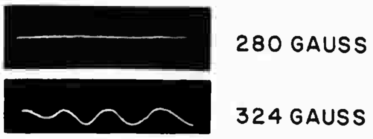

Fig. XVI-6. Beam collector current.

The critical magnetic field for onset of the instability is plotted in Fig. XVI-7.

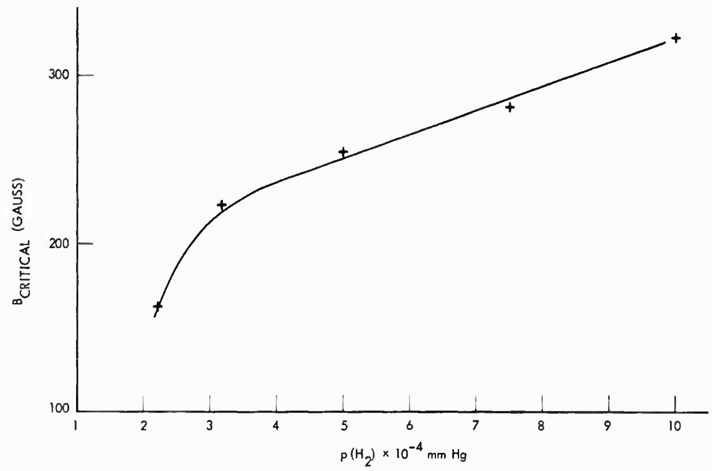

Fig. XVI-7. Critical magnetic induction for onset of instability.

Below approximately 550 gauss the oscillations on the beam collector are quite sinusoidal. Two electric probes at the same radial and azimuthal positions but at different axial positions indicate that the sinusoidal oscillations have no axial variation (Fig. XVI-7). The light and probe oscillograms of Fig. XVI-5 show that the variation must be $m = 1$ at low fields. Ion-current fluctuations on the beam-collector magnetic shield[2] occur 180° out of phase with ion-current fluctuations on the beam collector. This factor suggests an off-center rotation of a camlike plasma column about the beam collector, as shown in Fig. XVI-8.

Above approximately 550 gauss, probe signals at different axial positions are no longer well correlated (Fig. XVI-9). Coincident with the decrease in the crosscorrelation between probe signals, the plasma currents and light become irregular, which suggests that the plasma has become "turbulent." The period of rotation is plotted as a function of

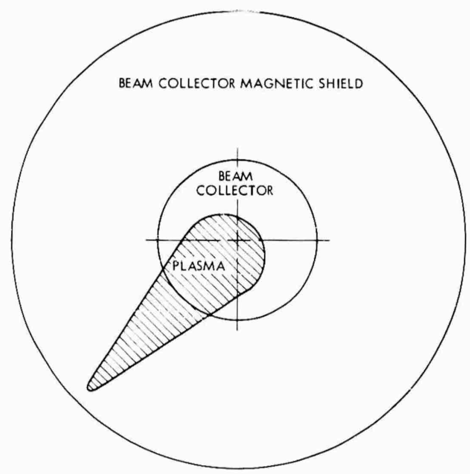

Fig. XVI-8. Plasma rotating off center.

magnetic field (at 0.5-μ pressure) in Fig. XVI-10. The abrupt decrease in rotational speed is associated with the onset of "turbulence." From measurements of light at various radii from the axis we have estimated the radial electron-density variation.

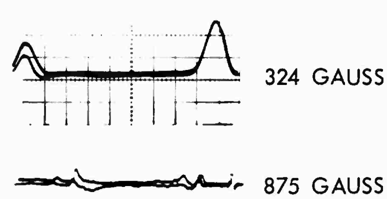

Fig. XVI-9. Axial variation in probe currents. Axial probe separation, 6.5 in.; $p = 0.4\ \mu\ H_2$; $V_o = 7.2$ kv. Upper: time, 5 μsec/cm. Lower: time, 20 μsec/cm.

The density e-folding length vs magnetic field at 0.5-μ pressure is plotted in Fig. XVI-10. The e-folding length decreases linearly with B when the plasma is stable. The magnetic field no longer squeezes the plasma in so well when the coherent rotation sets in, and the plasma actually expands when turbulence occurs.

The rotational instability is a mechanism by which plasma is transported across the magnetic field. After the beam breakup, current to the wall electrodes[2] increases very slowly with time. Coincident with the appearance of the rotation, the wall current

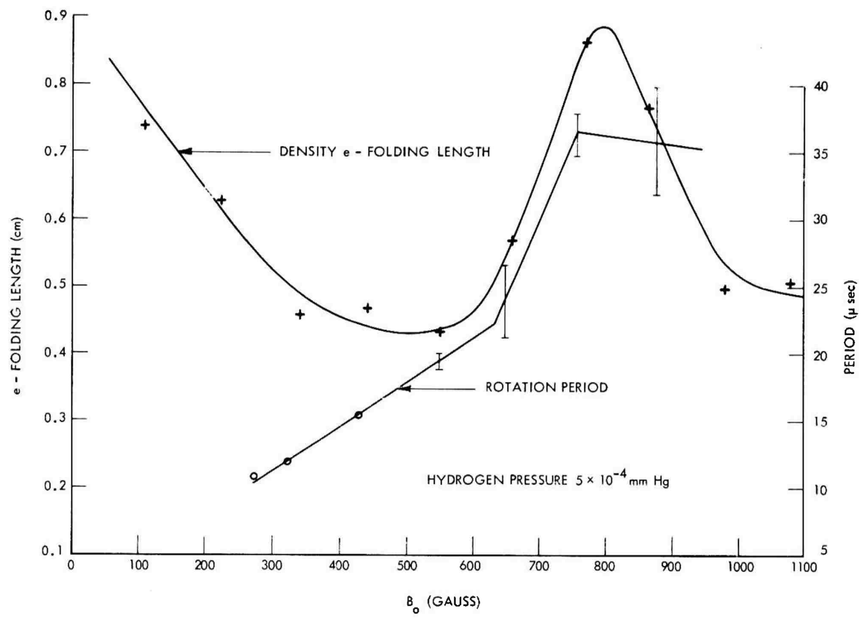

Fig. XVI-10. Density e-folding length and rotation period.

increases sharply. A decrease in net ion current to the wall electrodes at high fields is caused by a change in the potentials in the plasma, not by a decrease in particle flux. Above 1400 gauss the wall electrodes collect net electron current. Biased probes near the wall show that the ion density does not change much as the magnetic field is increased.

The existence of the rotation does not depend directly on the electron beam. After the beam is turned off, the plasma continues to rotate for several periods.

The transport of plasma across the magnetic field appears to be caused by an azimuthal electric field. Electric probe measurements show that the leading edge of the plasma spoke is negative with respect to the trailing edge. The resulting electric field is in such a direction that neutral plasma drifts radially outward. It is thought that the azimuthal electric field is caused by the difference between the electron and ion Hall mobilities. The inward electric field needed to drive the plasma in a right-handed rotation is thought to be caused by the trapping of a hot electron plasma in the magnetic mirror.

B. A. Hartenbaum

References

1. B. A. Hartenbaum, Beam-plasma discharges. System B: Rotational instability and quenching, Quarterly Progress Report No. 70, Research Laboratory of Electronics, M. I. T., July 15, 1963, pp. 111-113.

2. L. D. Smullin, W. D. Getty, B. A. Hartenbaum, and H. Y. Hsieh, Electron beam-plasma interaction experiments, Quarterly Progress Report No. 66, Research Laboratory of Electronics, M. I. T., July 15, 1962, p. 121.

B. ROTATING PLASMA INSTABILITIES

This study has been completed and the results are being prepared for submission to the Department of Electrical Engineering, M. I. T., as a doctoral thesis.

D. L. Morse

C. INSTABILITIES AND AMPLIFYING WAVES IN BEAM PLASMA SYSTEMS

This research has been completed and a doctoral thesis is being prepared for submission to the Department of Electrical Engineering, M. I. T.

R. J. Briggs

D. BEAM-EXCITED ION-PLASMA OSCILLATIONS

Recently, we have found theoretically that a beam of charged particles can interact with the ions of a plasma at the ion-plasma frequency, provided that the electron temperature of the plasma is sufficiently high. It is likely that such an interaction is the mechanism responsible for the VHF oscillations (100-800 mc) observed in the beam-plasma discharge.

We hope to get more direct experimental evidence of this interaction in the apparatus described here. A cyclotron discharge is excited by a 3-kmc power source in a multimode cavity placed in a magnetic mirror. The cavity is continuously pumped, and the gas pressure in the cavity can be regulated. Such a cyclotron discharge can produce a very hot electron gas. The temperature, however, is probably anisotropic with its largest components perpendicular to the magnetic field. Since the magnetic field is inhomogeneous, we may expect part of the transverse random energy to be transferred into the longitudinal direction.

An electron beam is launched into the cyclotron discharge along the axis of the magnetic bottle. The beam is provided by a tantalum cathode heated by electron bombardment from a second, directly heated, W cathdoe. The gun operates with perveance $I_o/V_o^{3/2} \approx 1\text{-}2 \times 10^6$.

Both the discharge and the beam have been operated, but in the early experiments we still have not found any evidence of interaction. The next steps are (i) to increase the microwave heating power from 50 watts to several hundred watts in order to provide a hotter and denser plasma; and (ii) to modulate the beam in the expected frequency band for the ion-plasma frequency (40-100 mc) in order to get a more sensitive test of interaction.

M. T. Vlaardingerbroek, M. A. Lieberman, L. D. Smullin

E. COUPLING OF EMPTY-WAVEGUIDE AND QUASI-STATIC MODES IN WAVEGUIDES LOADED WITH GYROTROPIC MEDIA

In a previous report we presented a new approach to the solution of wave propagation in gyrotropic waveguides.[1] We have since reformulated the coupled equations, so that the coupling between the various modes becomes more obvious. In this report we present the reformulated coupled equations, discuss the coupling between the various modes, and give the results of the numerical calculations for the example partially treated in our previous report, which was for a completely filled, circular, cold, plasma waveguide; the motion of ions is included.

1. Coupled-Mode Theory

We consider a gyrotropic medium characterized by dielectric and magnetic permittivity tensors given by Eqs. 1 and 2 of our previous report.[1] We analyze $\overline{E}$ and $\overline{H}$ in a rotational and an irrotational part according to Eqs. 3a and 3b given there.[1]

The orthogonality relations for electrostatic modes are

$$\int_A K_{\parallel}\Phi_{\ell}\Phi_m^* \, da = \delta_{\ell m} \tag{1a}$$

$$\int_A \nabla_T\Phi_m^* \cdot \overline{\overline{K}}_T \cdot \nabla_T\Phi_{\ell} \, da = \gamma_{\ell}^2\delta_{\ell m}. \tag{1b}$$

Here, the integration is taken over the cross section of the waveguide. In this report a double-bar superscript denotes a tensor, and [ ] denotes a matrix.

The orthogonality relations for magnetostatic modes are

$$\int_A L_{\parallel}\Psi_m\Psi_{\ell}^* \, da = \delta_{\ell m} \tag{2a}$$

$$\int_A \nabla_T\Psi_{\ell}^* \cdot \overline{\overline{L}}_T \cdot \nabla_T\Psi_m \, da = \gamma_m^2\delta_{\ell m}. \tag{2b}$$

We define

$$\hat{E}^r = \sum_i (V_i\hat{e}_{Ti}+I_iZ_i\hat{e}_{zi}) \tag{3a}$$

$$\hat{H}^r = \sum_i (I_i\hat{h}_{Ti}+V_iY_i\hat{h}_{zi}) \tag{3b}$$

$$\Phi = \sum_m F_\ell \Phi_\ell \tag{4}$$

$$\Psi = \sum_m M_m \Psi_m. \tag{5}$$

Substituting Eqs. 3-5 in Maxwell's equations and applying the orthogonality relations, we obtain

$$\gamma\overline{V} - [\Gamma_N][Z]\,\overline{I} = [a]\,\overline{I} + [b]\,\overline{M} \tag{6a}$$

$$\gamma\overline{I} - [\Gamma_N][Y]\,\overline{V} = [c]\,\overline{V} + [d]\,\overline{F} \tag{6b}$$

$$\left(\gamma^2-[\Gamma_L][\Gamma_L]\right)\overline{F} = \left(\frac{[d]}{j\omega\epsilon_o}\right)^{\dagger}\overline{V} - \gamma[e]\,\overline{I} \tag{7}$$

$$\left(\gamma^2-[\Gamma_M][\Gamma_M]\right)\overline{M} = -\gamma[f]\,\overline{V} + \left(\frac{[b]}{j\omega\mu_o}\right)^{\dagger}\overline{I}. \tag{8}$$

Here, the dagger indicates complex conjugate of the transpose of a matrix, and

$$a_{in} = j\omega\mu_o \int_A \hat{h}^*_{Ti}\cdot(\overline{\overline{L}}_T-\overline{\overline{I}}_T)\cdot\hat{h}_{Tn}\,da \tag{9a}$$

$$b_{im} = j\omega\mu_o \int_A \hat{h}^*_{Ti}\cdot\overline{\overline{L}}_T\cdot(-\nabla_T\Psi_m)\,da \tag{9b}$$

$$c_{in} = j\omega\epsilon_o \int_A \hat{e}^*_{Ti}\cdot(\overline{\overline{K}}_T-\overline{\overline{I}}_T)\cdot\hat{e}_{Tn}\,da \tag{9c}$$

$$d_{i\ell} = j\omega\epsilon_o \int_A \hat{e}^*_{Ti}\cdot\overline{\overline{K}}_T\cdot(-\nabla_T\Phi_\ell)\,da \tag{9d}$$

$$e_{\ell i} = \frac{p_{ei}^2}{j\omega\epsilon_o} \int_A K_{\parallel}\Phi_\ell^* \phi_i \, da \tag{9e}$$

$$f_{mi} = \frac{p_{hi}^2}{j\omega\mu_o} \int_A L_{\parallel}\Psi_m^* \psi_i \, da. \tag{9f}$$

Lower-case letters for potentials denote the empty-waveguide modes, and upper-case letters, the quasi-static modes. The symbol p denotes transverse wave numbers.

$[\Gamma_N]$ = diagonal matrix for the longitudinal wave numbers of empty-waveguide modes

$[\Gamma_L]$ = corresponding matrix for the electrostatic modes

$[\Gamma_M]$ = corresponding matrix for the magnetostatic modes.

2. Discussion

The dispersion equation of the coupled system may be derived easily from Eqs. 6-8. These equations show which modes have a dominant contribution in the coupling. The left-hand sides of these equations contain the differences $\gamma^2 - \gamma_i^2$. The right-hand sides contain the coupling coefficients. The coupling coefficients depend upon the interaction of the transverse fields of the coupled modes. When the transverse wave numbers of the coupled modes approach each other, the transverse fields of these modes tend to become similar, and therefore the corresponding coupling coefficient increases significantly.

Let us assume that the longitudinal wave numbers and the transverse wave numbers of several modes have large differences. Then the coupling coefficients are small and the difference $\gamma^2 - \gamma_i^2$ for the i^{th} mode is very large. Therefore we may factor $\gamma^2 - \gamma_i^2$ out of the dispersion relation, and this fact, of course, means that the i^{th} mode is not coupled to all of the other modes. If either the longitudinal wave numbers or the transverse wave numbers are close together, the differences $\gamma^2 - \gamma_i^2$ are of the same order or less than the coupling coefficients. In that case $\gamma^2 - \gamma_i^2$ cannot be factored out of the dispersion relation any longer and the i^{th} mode is coupled to the other modes.

3. Example

We consider a completely filled, circular, cylindrical, cold, plasma waveguide of radius a. The quasi-static mode QS_{10} has a transverse wave number $p = \frac{2.405}{a}$. Therefore there is a strong coupling between this quasi-static mode and the empty-waveguide mode TM_{10} which has the same transverse wave number. The mode QS_{10} is also coupled to the TE_{10} ($p = 3.83/a$) because their transverse wave numbers are close. For $\frac{\omega a}{c} > 4$ there is a strong coupling between the modes TE_{10} and QS_{10} because their <u>longitudinal</u> wave numbers are extremely close. The resulting dispersion diagram is

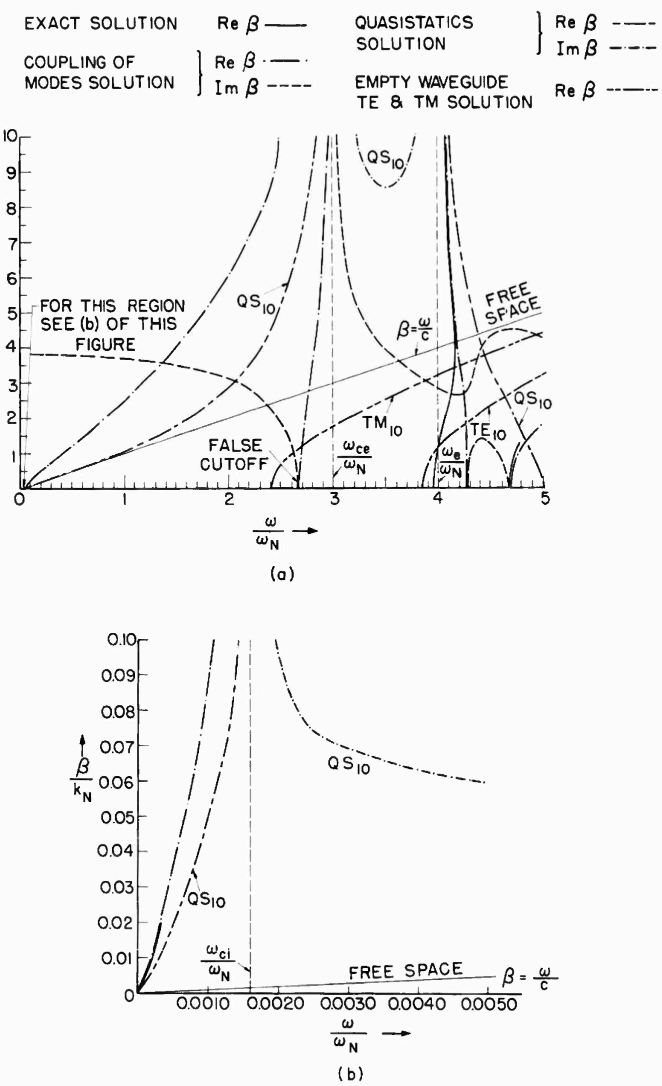

Fig. XVI-11. Dispersion diagrams for plasma-filled waveguide, $\omega_n = c/a$, $k_n = 1/a$, where a is the radius of the waveguide. For comparison, we show the solutions from quasi-static theory, exact theory, and coupling-of-modes theory, together with the uncoupled modes. (a) Frequency regime from the first cutoff above ω_{ci}. The second branch from coupling of modes is imaginary and similar to that of QS_{10} but with $(\beta/k_N)_{min} \approx 12.4$. (b) Low-frequency regime near and below ω_{ci}. The first branch from coupling of modes for $\omega > \omega_{ci}$ is imaginary, and it is out of the figure because $\beta/k_N > 10$ for $\omega_{ci}/\omega_N < \omega/\omega_N < 0.0050$. Its shape is similar to that of QS_{10}. The second root from coupling-of-modes theory is imaginary, and is given by $\approx +j3.83$ from $\omega/\omega_N = 0$ to $\omega/\omega_N = 0.1$. See (a).

shown in Fig. XVI-11. For comparison we have also shown in Fig. XVI-11 the known part of the exact dispersion diagram and the dispersion curve obtained under the quasi-static approximation.

A study of these dispersion curves shows that by use of the coupled-mode theory we significantly improve the quasi-static curve, and thus we obtain an extremely good approximation to the exact solution. We should notice that the couplings are due to the fact that the corresponding modes have longitudinal and/or transverse wave numbers very close to each other. Note that the coupling between the TM_{10} and QS_{10} modes produces strong effects on the dispersion diagram for all frequencies. This is due to the fact that the transverse wave numbers of these modes are identical for all frequencies, even though the longitudinal wave numbers are close only near plasma resonance.

The coupling of modes will, however, introduce extraneous solutions. These arise because (i) we have expanded the fields in a redundant (more than complete) set, and (ii) we use only a few of the modes that appear to be coupled strongest. Thus in our example, the approximate equation for the H-cutoffs[1] has a solution at $(\omega/\omega_n) = 2.63$. This is a false cutoff,[2] and hence the branch of β that starts from there must be disregarded. In general, the extraneous branches of β can be detected, since we have a means of obtaining the exact solutions at the cutoffs, near the resonances, and at very low frequencies.[2]

4. MHD Regime Approximation

Very good approximations to the exact solution have been given for cutoffs, resonances, and the very low frequency region (magnetohydrodynamic region).[2] In our previous report[1] we have shown that the coupled-mode theory provides results that are almost identical to the approximations given by Bers for resonances and cutoffs.[2] The same holds true for the magnetohydrodynamic region, as we show below.

By taking into consideration the fact that for very low frequencies $\omega^2 \to 0$ and $K_{\parallel} \to -\infty$ so that $\omega^2 K_{\parallel}$ is finite, the dispersion equation (13) of our previous report[1] yields

$$\gamma^2 = p_{h1}^2 - k_o^2 K_{\perp} \tag{10a}$$

$$\gamma^2 = \frac{K_{\perp}}{K_{\parallel}} p_{e1}^2 - k_o^2 K_{\perp}, \tag{10b}$$

which are identical to the approximate expressions for the magnetohydrodynamic region given by Bers.[2]

P. E. Serafim, A. Bers

References

1. P. E. Serafim and A. Bers, Coupling of empty-waveguide modes, electrostatic and magnetostatic modes in waveguides loaded with gyrotropic media, Quarterly Progress Report No. 69, Research Laboratory of Electronics, M.I.T., April 15, 1963, pp. 57-61.

2. W. P. Allis, S. J. Buchsbaum, and A. Bers, Waves in Anisotropic Plasmas (The M.I.T. Press, Cambridge, Mass., 1963), Chapter 9.

F. TURBULENT DIFFUSION ACROSS A MAGNETIC FIELD

1. Theory

It has been observed that the plasma columns generated by hollow-cathode arcs in our laboratory, and by other mechanisms elsewhere, exhibit large spatial and temporal fluctuations, and that the diffusion across the magnetic field often substantially exceeds that predicted by quiescent diffusion theory. Besides the well-known short-circuit end effect of "Simon" diffusion,[1] we must consider the effects of turbulent diffusion. In this report we consider an elementary model of the process, and the experimental evidence that supports it.

We presume that the plasma column has many unstable modes, whose origins we cannot properly determine, and that the resulting turbulence leads to an axial shredding of the plasma column, that is, density, potential, and so forth, are well correlated along magnetic-field lines, but are poorly correlated across field lines; this has been observed experimentally. These plasma strings move randomly at the stochastic $\mathbf{E} \times \mathbf{B}/B^2$ velocities across field lines.

A radial diffusion coefficient for these plasma strings can be conceptually defined as

$$D = \langle L_r V/3 \rangle. \tag{1}$$

Here, L_r is the radial distance that the string travels before a change in direction and is associated with the radial correlation length for plasma fluctuations. The speed V is

$$V = |E_\theta/B|. \tag{2}$$

From the magnitude of the fluctuating component ϕ of the plasma potential, we can obtain the random azimuthal electric field

$$|E_\phi| = |\phi/L_\theta|. \tag{3}$$

Here, L_θ is the distance over which it develops. Thus, apart from averaging coefficients of order one, we have

$$D \approx \left\langle L_r |\phi| / 3BL_\theta \right\rangle. \tag{4}$$

Equation 4 has the form of anomalous or "Bohm" diffusion.

We now argue heuristically that if there are many turbulent modes and none dominates, the correlation lengths will all be the same. The plasma strings are of radial size L_r; as they move and collide at random, they are polarized by their motion (or vice versa). Hence the radial correlation lengths for density and potential will be the same. The r versus θ correlation equalities are less clear. But we propose that even though the plasma rotates about the axis and may have a quasi-coherent rotating structure, the azimuthal motion does not of itself lead to radial diffusion. We presume (and evidence similar to that given below tends to bear us out) that within these organized motions, a θ-turbulence exists with approximately the same time and scale lengths. From these considerations, we have

$$D \approx \left\langle |\phi| / 3B \right\rangle, \tag{5}$$

a result that can be checked by measuring fluctuating potential amplitudes, radial flows, and radial mean-density gradients. Also, if correlations over a length L last a time t, we can write

$$L = Et/b, \tag{6}$$

and hence

$$L = \left\langle |\phi| t/B \right\rangle^{1/2}, \tag{7}$$

apart from factors of order one. Equation 5 can be expected to have validity in cases in which the turbulent diffusion greatly exceeds the classical rate.

2. The Experiment

The hollow-cathode arc described in detail by Alvarez de Toledo[2,3] was used. The plasma column, ≈1.5 m long, ran down the lines of magnetic induction, through a magnetic mirror (mirror ratio, 2.5). Other parameter ranges were: arc current, 15-35 amp; pressure, 10^{-4}-1.5×10^{-3} Torr; midplane induction, 0.025-0.11 weber/m^2. The plasma column was bounded axially by insulating end plates; thus the radial and azimuthal electric fields were not shorted out.

Plane and cylindrical Langmuir probes through ball joints, or on a sliding axial rail, were used to measure ion saturation current (to obtain ion density), and to measure floating potential. Occasional measurements of electron saturation current always correlated well with ion saturation current. Thus floating-potential fluctuations, which were found to be uncorrelated with density except when organized rotation was present, were assumed to indicate the fluctuating potential ϕ.

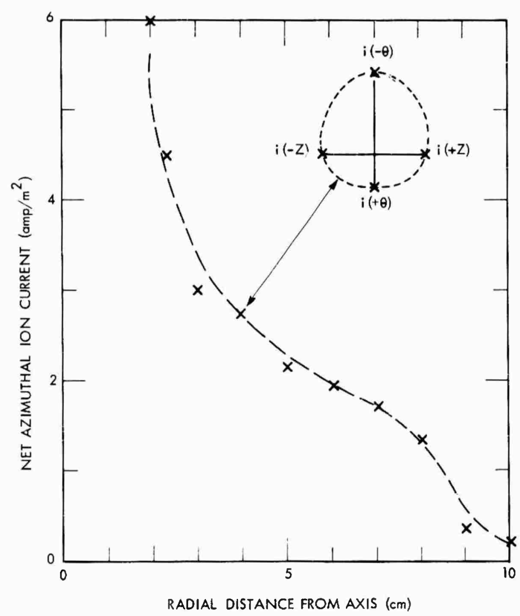

Fig. XVI-12. Net azimuthal ion current vs radial distance. Inset shows the current profile at r = 4 cm from directions normal to some radius. Thus i(±θ) are azimuthal currents and i(±z) are axial currents. Note the approximate axial symmetry. Arc current, 20 amp; B = 0.105 weber/m^2; p = 1.3 × 10^{-3} Torr.

To a first approximation, the mean azimuthal ion current can be measured with plane Langmuir probes sensitive to the arrival of particles from the ±θ directions. Then

$$eA\Gamma_\theta = i_{+s}(+\theta) - i_{+s}(-\theta). \tag{8}$$

Here, Γ_θ is net azimuthal current density, A is the probe area, and $i_{+s}(\pm\theta)$ are the ion saturation currents with the probe oriented in each direction. With the probes oriented, we observed an azimuthal flow comparable in magnitude to the radial current, whose value is estimated below. The flow is in the $\underset{\sim}{E} \times \underset{\sim}{B}$ direction, with $\underset{\sim}{E}$ pointing toward the arc axis. Figure XVI-12 shows the net current for a typical case.

In some instances, data taken with two midplane probes at different azimuths showed a spiral-like structure in the plasma, as in Fig. XVI-13. Simple turbulent diffusion theory did not fit these cases.

In principle, the net radial current could be measured by examining $i_{+s}(\pm r)$, but a probe with the required movements was not available. Thus the radial ion saturation current density was measured at the wall, radius r_w; the current density at radius r is

$$i_r(r) = i_r(r_w)(r_w/r), \tag{9}$$

if no sources or sinks are present.

The electron temperature was measured and was found to decrease with radius, being 1-3 ev near the core, and 0.25-0.5 ev at r = 10 cm. Figure XVI-14 shows a temperature

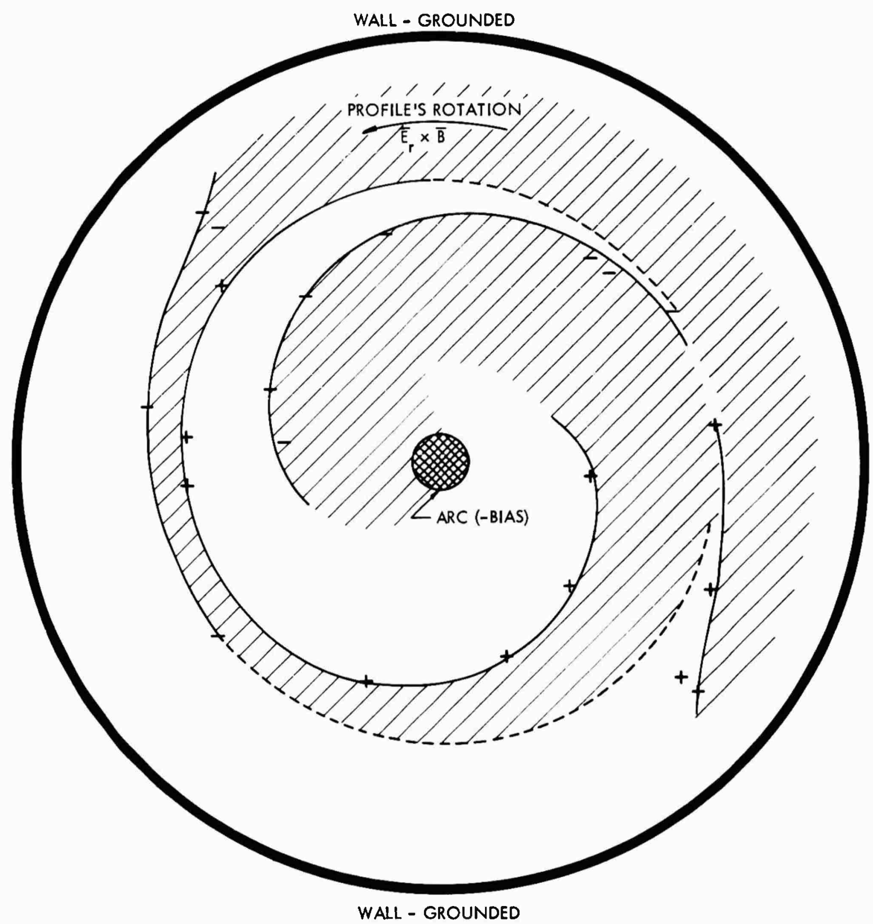

Fig. XVI-13. Plasma spiral structure with rotational instability. The negative space-charge front (−) and positive space-charge tail (+) are shown. Arc current, 35 amps; $B = 0.055$ weber/m^2; $p = 6 \times 10^{4}$ Torr.

profile similar to those obtained by Rothleder.[4] The profile remained similar for all of our runs, except for the absolute ordinate scale. Therefore the same profile, renormalized for each run at r = 4 cm, was used for the subsequent calculations.

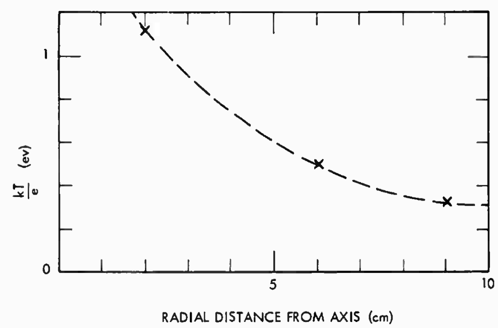

Fig. XVI-14.

Electron temperature as a function of radius. Arc current, 20 amps; B = 0.024 weber/m^2; p = 1 × 10^{-4} Torr.

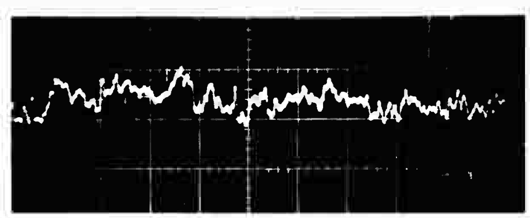

Fig. XVI-15.

Floating potential vs time. Vertical scale, 0.5 V/cm; horizontal scale, 200 μsec/cm. Probe at r = 6 cm. Arc current, 20 amps; B = 0.024 weber/m^2; p = 1 × 10^{-4} Torr; T_- = 0.5 ev.

The fluctuating potential ϕ, as a substitute for plasma potential, was photographed on an oscilloscope. Figure XVI-15 shows a typical trace.

3. Results

The diffusion current is

$$\Gamma = -\nabla(dn). \tag{10}$$

Then, for the turbulent diffusion, we have a radial ion current density

$$\Gamma_{+r} = -\frac{\partial}{\partial r}\left[\frac{\langle|\phi|\rangle n_+}{3B}\right]. \tag{11}$$

But

$$n_+ = j_{+s}\bigg/e\left[\frac{eT_-}{2.7m_+}\right]^{1/2}, \tag{12}$$

where j_{+s} is the saturation ion current density, m_+ is the ion (argon) mass, and T_- is the electron temperature. Thus the net radial ion current (in amperes) should be given by

$$i_{+r} = -\left(\frac{0.27m_+^{1/2}}{B}\right)\frac{\partial}{\partial r}\left[\frac{\langle|\phi|\rangle i_{+s}}{T_-^{1/2}}\right]. \tag{13}$$

Figure XVI-16 shows the two sides of Eq. 13 plotted against radial distance. The points are derived from the formula on the right-hand side of Eq. 13; all quantities are evaluated experimentally at each point. The shaded region is obtained from the wall current and

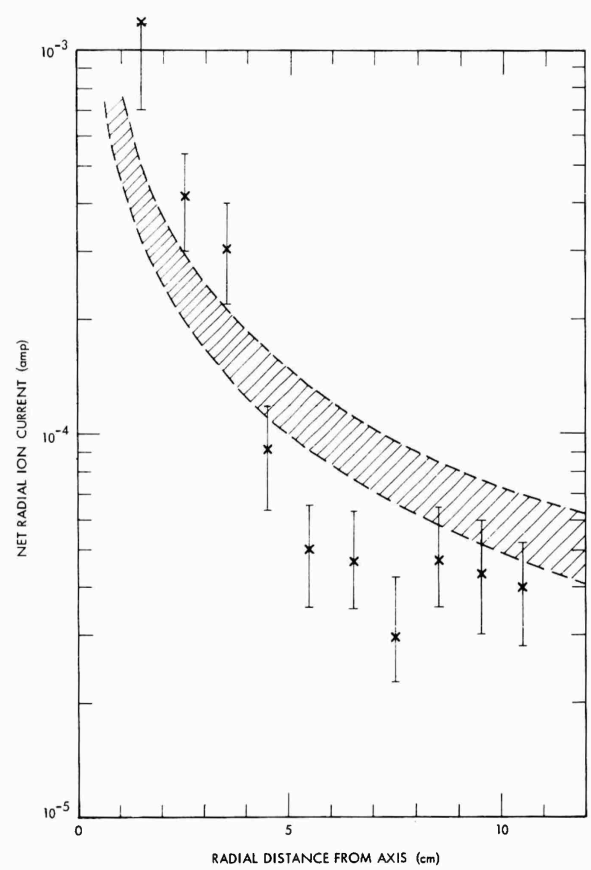

Fig. XVI-16. Net radial current vs radial position. Shaded area, evaluation of left-hand side of Eq. 13; points, evaluation of right-hand side of Eq. 13. Arc current, 20 amps; $B = 0.105$ weber/m^2; $p = 1.3 \times 10^{-3}$ Torr; probe area, ~4 mm^2.

Eq. 9, and includes an experimental error estimate. If we take into consideration the crudity of the theory and the experimental difficulty of measuring the various quantities (particularly the fluctuating potential and its average), the agreement is tolerable. Classical nonturbulent theory predicts radial currents approximately two orders of magnitude smaller.

We can make a few additional remarks pertaining to the applicability of a stochastic theory to the plasma motions. First, from visual inspection of simultaneous potential or density fluctuation on different $\underset{\sim}{B}$ lines, a rough estimate of the autocorrelation in distance and time can be made. Equation 7 was found to be accurate within a factor of ~2. Also, the theory of Yoshikawa and Rose,[5] for example, predicts that the density fluctuations should represent almost 100 per cent modulation in cases for which $\langle|\phi|\rangle$ is comparable to kT_-/e. Experimentally, this was observed to be the case.

F. Alvarez de Toledo, D. J. Rose

References

1. A. Simon, An Introduction to Thermonuclear Research (Pergamon Press, New York, 1959), pp. 150 ff.

2. F. Alvarez de Toledo, S. M. Thesis, Department of Nuclear Engineering, M. I. T., 1963.

3. F. Alvarez de Toledo, N. E. Report, Department of Nuclear Engineering, M. I. T., 1963.

4. S. D. Rothleder, Ph. D. Thesis, Department of Nuclear Engineering, M. I. T., 1962.

5. S. Yoshikawa and D. J. Rose, Anomalous diffusion of a plasma across a magnetic field, Phys. Fluids 5, 334-340 (1962).

XVII. PLASMA MAGNETOHYDRODYNAMICS AND ENERGY CONVERSION*

Prof. G. A. Brown
Prof. E. N. Carabateas
Prof. R. S. Cooper
Prof. S. I. Freedman
Prof. W. H. Heiser
Prof. M. A. Hoffman
Prof. W. D. Jackson
Prof. J. L. Kerrebrock
Prof. J. E. McCune
Prof. H. P. Meissner
Prof. J. R. Melcher
Prof. G. C. Oates
Prof. J. P. Penhune
Prof. J. M. Reynolds III
Prof. A. H. Shapiro
Prof. J. L. Smith, Jr.
Prof. R. E. Stickney
Prof. H. H. Woodson
Dr. A. T. Lewis
M. T. Badrawi
J. F. Carson
A. N. Chandra
J. M. Crowley
R. Dethlefsen
M. G. A. Drouet
D. A. East
R. K. Edwards
J. R. Ellis, Jr.
F. W. Fraim IV
J. W. Gadzuk
J. Gerstmann
J. B. Heywood
P. G. Katona
F. D. Ketterer
G. B. Kliman
A. G. F. Kniazzeh
M. F. Koskinen
K. S. Lee
R. F. Lercari
W. H. Levison
B. T. Lubin
S. A. Okereke
J. H. Olsen
E. S. Pierson
R. P. Porter
D. H. Pruslin
C. W. Rook, Jr.
A. W. Rowe
A. Shavit
A. Solbes
J. S. Weingrad
G. L. Wilson
J. C. Wissmiller

RESEARCH OBJECTIVES AND SUMMARY OF RESEARCH

1. Magnetohydrodynamics

Our work in magnetohydrodynamics is broadly concerned with the interactions between electromagnetic fields and electrically conducting fluids, particularly in those situations to which a continuum fluid description is applicable. Both plasmas and liquid metals are employed in the experimental aspects of our work and the development of measurement techniques receives particular attention. An important extension of this activity is the study of blood flow and related topics in biomedical engineering.

(a) Plasma Magnetohydrodynamics

The past year has been spent in improving the capabilities of the magnetic annular shock tube for producing clearly defined quantities of shock-heated gas and for measuring values of the physical quantities relevant to the experiments. These improvements are based upon experience with the original version of the shock tube. In particular, the following changes have been made:

(i) The duration and magnitude of the pre-ionization current have been increased to improve initial gas breakdown.

(ii) The sinusoidal drive current has been replaced by a square pulse to reduce time-variant effects.

(iii) All low-melting-point insulating materials have been removed, or covered with Pyrex, to reduce ablation from the surface of these insulators.

(iv) Eight magnetic field coils have been inserted around the annulus to measure the azimuthal distribution of drive current.

(v) A magnetic field coil has been provided to measure the variation of azimuthal magnetic field with time at a fixed axial position.

*This work was supported in part by the U. S. Air Force (Aeronautical Systems Division) under Contract AF33 (615)-1083 with the Air Force Aero Propulsion Laboratory, Wright-Patterson Air Force Base, Ohio; and in part by the National Science Foundation (Grant G-24073).

(vi) An electrostatic probe to complement the azimuthal magnetic field probe is being designed.

Experiments have begun and the results of these changes should soon be known. These experiments are particularly designed to test the azimuthal uniformity of the drive current. The long-range goals of these experiments are still the improvement of this type of shock tube and the careful investigation of magnetohydrodynamic shock waves.

A. H. Shapiro, W. H. Heiser, J. B. Heywood

(b) Mathematical Methods in Continuum Magnetohydrodynamics

This research is concerned with mathematical methods for the analysis of the interactions occurring in magnetohydrodynamics. The present work has grown out of the investigation of MHD channel flows; particularly out of the analytical and numerical techniques that were used to obtain solutions to the nonlinear differential equation governing the interaction of a traveling AC magnetic field with an MHD channel flow.

Our research concerns the application of techniques, such as perturbation expansions and iterational and variational methods, to a variety of nonlinear continuum MHD problems. The purpose of this effort is twofold: first, to produce solutions to specific problems that are of practical interest; second, to obtain a better understanding of the broad classes of problems to which these techniques are applicable. The analysis of the flow of an electrically conducting fluid around a sphere with a dipole magnetic field is at present being undertaken for the case in which the dipole axis is perpendicular to the direction of fluid flow.

J. P. Penhune

(c) Magnetohydrodynamic Wave Phenomena

One of our experiments is concerned with the excitation of Alfvén waves in a liquid metal (NaK alloy). Generation of these waves by using a current-sheet excitation has been verified, and shown to be markedly superior to the mechanical methods used in experiments reported previously. The systematic study of the excitation transmission, attenuation, and reflection of these waves in the hydromagnetic waveguide continues.

A second waveguide study is concerned with MHD wave propagation in nonuniform magnetic fields. NaK alloy again serves as the working fluid for the experimental part of this investigation.

A theoretical study of MHD surface waves on fluids of finite electrical conductivity is also being undertaken. An experimental study of some aspects of these waves has recently been initiated, and will also use NaK as the working fluid.

W. D. Jackson, J. P. Penhune

(d) Magnetohydrodynamic Channel Flow and Turbulence

The flow characteristics of electrically conducting fluids in channels or ducts are of interest in connection with many engineering applications of magnetohydrodynamics. While these include both liquid and ionized gas flows, the use of liquid metals has advantages for a considerable range of laboratory investigations.

A closed-loop flow facility has been constructed with NaK used as the working fluid. This loop is being used for study of pressure drop versus flow-rate relations (including those for MHD power-conversion devices), and the characteristics of turbulence in the presence of magnetic fields.

The character of MHD turbulence is modified when a pronounced Hall effect occurs in the flow. The characteristics of turbulence in this situation are being investigated, and work continues on the application of Norbert Wiener's "Calculus of Random Functionals" to the study of turbulent-flow situations.

W. D. Jackson

(e) Local Fluid-Velocity Measurement in an Incompressible Magnetohydrodynamic Flow

The behavior of different types of velocity probes is being investigated to develop devices capable of measuring the local fluid velocity in an MHD flow for the case in which the applied magnetic field is perpendicular to the fluid velocity. The development of such probes will be important for experimental investigation of MHD flows, particularly those associated with MHD power-generation schemes.

The behavior of a nonconducting Pitot tube is being investigated experimentally. Here the $\underline{J} \times \underline{B}$ forces increase the pressure measured at the stagnation point above the usual stagnation pressure. The velocity-pressure correlation has been determined experimentally as a function of applied magnetic field for a probe with a flat front end perpendicular to the axis of the tube. The effects of probe angle of attack and nose shape are now being studied.

A miniaturized electromagnetic flowmeter is also receiving attention.

A feasibility study is being made to determine whether a hot-wire anemometer can be constructed with sufficient sensitivity to be useful in the sodium-potassium eutectic liquid-metal flow loop described in (d) above.

A. H. Shapiro, W. D. Jackson, R. S. Cooper, D. A. East

(f) Ionization Waves in Weakly Ionized Plasmas

During the past year, some further studies have been made on the nature of certain macroscopic instabilities observed in the plasma of glow discharge tubes. The region of tube operation in which the instability is incipient has been defined for several gases, and the properties of shock-excited waves generated by external sources have been thoroughly examined in these regions.

Further work is being done toward the development of a theory to describe the behavior exhibited by the plasma in these experiments. Some new experiments are being performed to find additional methods of exciting the observed ionization waves. The interaction of the waves with internally generated sonic waves in the neutral gas is also being investigated both experimentally and theoretically.

R. S. Cooper

(g) Blood-Flow Studies*

Electrical methods are widely used in blood-flow measurement, and prominent among the devices used is the magnetohydrodynamic or electromagnetic flowmeter. Work reported under (e) above is being adapted for both mean and local blood-flow measurement and magnetohydrodynamic, thermal, and ultrasonic techniques are at present under investigation.

A second aspect of our blood-flow work is concerned with the application of engineering methods to the study of the cardiovascular system. We are engaged in this research jointly with Dr. Dexter and his associates at Peter Bent Brigham Hospital. A study of the pressoreceptor system has recently been completed as a step in the

*This work is supported in part by the National Institutes of Health (Grant No. 5 TI HE 5550-02).

identification and analysis of the mechanisms responsible for the regulation of cardiovascular functions.

G. O. Barnett,* W. D. Jackson

2. Energy Conversion

Our studies include both magnetohydrodynamic and thermionic methods of generating electrical power, and involve over-all system considerations, properties of working fluids, and operating characteristics of conversion devices.

(a) Magnetohydrodynamic Power Generation with Liquid Metals

The generation of electrical power in space vehicles offers a potential application for MHD generators to operate on a closed-cycle system in which a nuclear reactor is the thermal-energy source. An important feature of an MHD system is the absence of rotating parts, and, to utilize it, a working fluid is required with a sufficiently high electrical conductivity at the temperatures involved. A scheme in which a liquid metal is used as the working fluid in the MHD generator duct is under investigation. Kinetic energy is imparted to this flow by driving it with its own vapor in a condensing-ejector system.

A cycle analysis has been completed and has revealed efficiencies that are sufficiently attractive to warrant detailed investigation. During the coming year, the operation of condensing ejectors on alkali metals will be considered, the conductivity of two-phase flows in the presence of magnetic fields will be measured, the study of liquid-metal generator configurations will continue, and further cycle analysis will be performed.

W. D. Jackson, G. A. Brown

(b) Magnetohydrodynamic Induction Generator

The MHD induction machine utilizes the interaction between a traveling magnetic field (such as that produced by a polyphase winding) and a channeled, flowing fluid that may be either a plasma or a liquid metal.

The theoretical analysis of this machine has been extended to include such real machine effects as entry and exit conditions, finite core permeability, and velocity profile effects. This work has clearly demonstrated that the reactive power requirements of an induction generator are excessive when operated on a plasma flow but that satisfactory operation should be obtained with liquid metals.

A preliminary experimental investigation of a linear induction generator operating on an NaK flow with a two-phase, traveling-field coil system has demonstrated electrical power generation. This work will be extended and developed during the coming year.

W. D. Jackson

(c) Alkali-Metal Magnetohydrodynamic Generators

The over-all objective of this research is to investigate the feasibility of operating magnetohydrodynamic generators with alkali metals as working fluids. Our immediate objective is to establish the electrical properties of both superheated and wet alkali-metal vapor at temperatures up to 2000°K.

---

*Dr. G. O. Barnett is Established Investigator, American Heart Associate, Harvard Medical School, Boston, Massachusetts.

A small potassium loop, capable of a mass flow of 10 grams per second, has been constructed and is now being put into operation. Meanwhile, analytical studies of the wet vapor have been carried to the stage at which electrical conductivities can be computed, if the distribution in size of the droplets can be determined.

J. L. Kerrebrock

(d) Thermionic Energy Conversion

The research objectives of our group are oriented toward the evaluation of possible improvements of thermionic-converter performance based on the recent developments in the areas of surface and transport effects. The following studies are at present being conducted:

(i) Parametric evaluation of ideal converter performance as determined by the properties of cesium films on polycrystalline and single-crystal metallic surfaces.

(ii) Detailed study of the processes responsible for the creation of the highly conducting plasma in the interelectrode region of cesium thermionic converters, and interpretation of experimental current-voltage characteristics in the ignited mode.

(iii) Extension of previous measurements of the thermal conductivity of cesium vapor to higher temperatures and possibly to other alkali metals.

E. N. Carabateas

(e) A-C Properties of Superconductors

Recent intensive efforts to fabricate hard superconductors have opened up a wide range of possibilities for utilizing these materials in the production of high DC fields, particularly in situations for which these are required in large volume. The advantages associated with reducing field-power dissipation also apply to the production of AC fields, but there is an additional problem in that reactive power has to be circulated. This problem essentially implies zero-loss capacitive energy-storage elements, in addition to essentially infinite Q inductors. It is thus of interest to investigate the behavior of superconducting materials carrying AC currents in the presence of AC magnetic fields. As well as establishing the merits of superconducting materials in inductor and capacitor fabrication, such investigations provide an additional method of gaining insight into the mechanism of superconductivity.

Present investigations deal with superconducting materials in the form of wire or ribbon, and two experimental techniques are being pursued.

(i) The current-carrying capacities of short, straight lengths of superconducting wire or ribbon are being determined as a function of frequency in the range up to 10 kc.

(ii) A-C solenoids, fabricated to avoid electric eddy currents and insulated to accommodate electrical fields arising from $\partial B/\partial T$ effects, are being tested. In both cases, the AC current required for transition to normal conductivity has been obtained and, in the case of solenoids, the Q has been measured.

A third investigation is planned to obtain data on the behavior of superconductors in an externally applied AC field. These data will be derived either from a rotating magnet system or from a separate copper-conductor AC solenoid.

The work is, at present, experimental in character, but future theoretical studies are envisaged.

W. D. Jackson

A. WORK COMPLETED

1. LARGE-SIGNAL BEHAVIOR OF A PARAMETRIC MAGNETOGASDYNAMIC GENERATOR

This report summarizes an Sc. D. thesis with this title which was submitted to the Department of Electrical Engineering, M. I. T., September 20, 1963, and will appear as an RTD Technical Documentary Report

In this study the large-signal behavior of a parametric magnetogasdynamic generator, consisting of a cylindrical coil with batches of highly conducting plasma traveling along the coil axis, is considered. In this limit, the gas behavior is strongly affected by the magnetic forces. The purpose of this study was to determine (i) whether the requirements on the conductivity and velocity of the gas found for small-signal behavior are relaxed because of any enhancing mechanism during the interaction; (ii) what fraction of the gas power could be extracted as useful electrical power, that is, the over-all generator efficiency; (iii) how the interaction between the field and the gas leads to gas behavior that limits the growth of the parametric oscillations so that a stable operating point is reached; (iv) an estimate of the minimum size and power of a generator with present technology; and (v) the factors that control the scaling of the parametric generator.

To answer these questions, an analysis is presented for the small-signal behavior to establish the important parameters and provide a basis of comparison for the large-signal behavior. The large-signal electrical and gas behavior are treated separately as far as possible. A criterion is established for determining the steady-state operating point in terms of the electrical terminal behavior. The gas-flow interaction with the field is analyzed by using a quasi one-dimensional-flow model with the constraints for a strong interaction that the magnetic pressure balance the static gas pressure in the radial direction, and the power given up by the gas balance the gross electrical power generated.

A. T. Lewis

B. ALFVÉN WAVE STUDIES

1. SOME PROPERTIES OF MAGNETOHYDRODYNAMIC WAVEGUIDES

The dispersion equation for the MHD waveguide has been derived by a number of investigators.[1-7] Basically, the MHD waveguide consists of a hollow, rigid-wall cylinder of arbitrary, but constant, cross section immersed in a uniform, steady magnetic field aligned parallel to the cylinder axis as in Fig. XVII-1, and filled with a homogeneous electrically conducting fluid.

The total behavior of such a waveguide may be described in terms of transverse

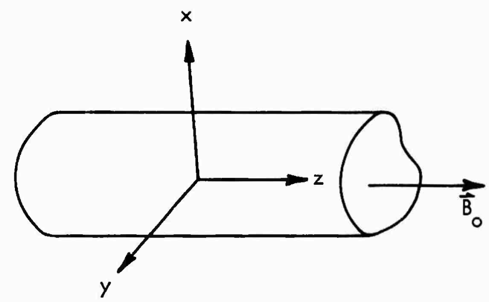

Fig. XVII-1. Coordinate system for the MHD waveguide.

magnetic (TM) and transverse electric (TE) modes. In general, any wave propagated consists of infinite sums of the two types of modes. In particular, if the fluid is inviscid and if the cross section and excitation are symmetric, single modes may be excited.[7]

In most magnetohydrodynamic waveguide problems, the critical fluid properties are the mass density and the electrical conductivity. Thus viscosity and displacement are neglected. Also, the modes of greatest interest are the TM modes and these do not compress the fluid, so that compressibility may also be neglected.

The resultant differential equation for the TM modes is

$$\nabla_t^2 e_z + T_{mn} e_z = 0, \tag{1}$$

where e_z is the longitudinal component of the electric field, and ∇_t^2 is the transverse Laplacian operator. Other symbols are defined as follows:

$$T_{mn}^2 = \frac{C^2 + i\omega\eta_t}{i\omega\eta_\ell}\left(\frac{\omega^2}{C^2 + i\omega\eta_t} - \beta_{mn}^2\right), \tag{2}$$

where the propagation has been taken as $e^{i(\omega t+\beta_{mn} z)}$;

$$C^2 = \frac{B_o^2}{\mu_o \rho} = \text{Alfvén velocity;}$$

$$\eta_\ell = \frac{1}{\mu_o \sigma_\ell} = \text{longitudinal magnetic diffusivity;}$$

$$\eta_t = \frac{1}{\mu_o \sigma_t} = \text{transverse magnetic diffusivity;}$$

with B_o, the magnitude of the applied magnetic field; ρ, the mass density of the fluid; σ_ℓ, the longitudinal electric conductivity; σ_t, the transverse electric conductivity; and μ_o, the permittivity of free space.

The solutions of (1) in rectangular coordinates are sinusoids and yield[8]

$$T_{mn}^2 = (2m+1)^2\left(\frac{\pi}{2a}\right)^2 + (2n+1)^2\left(\frac{\pi}{2b}\right)^2. \tag{3}$$

Here, a and b are the half-widths of a rectangular waveguide. In cylindrical coordinates the solutions of (1) are Bessel functions and yield

$$T_{mn}^2 = \left(\frac{\alpha_{mn}}{a}\right)^2. \tag{4}$$

Here, a is the radius of a cylindrical waveguide, and α_{mn} is the n^{th} root of the m^{th}-order Bessel function.

The propagation constant β is obtained from (2).

$$\beta_{mn}^2 = -\frac{\eta_\ell}{\eta_t} \frac{T_{mn}^2 + i\omega/\eta_\ell}{1 + C^2/i\omega\eta_t}. \tag{5}$$

At very low frequencies ($\omega \to 0$) (5) becomes

$$\beta_{mn} = \frac{T_{mn}}{c}\sqrt{\frac{\omega\eta_\ell}{2}}\,(1-i). \tag{6}$$

At very high frequencies ($\omega \to \infty$) (5) becomes

$$\beta_{mn} = \sqrt{\frac{\omega}{2\eta_t}}\,(1-i). \tag{7}$$

At intermediate frequencies such that

$$\eta_\ell T_{mn}^2 \ll \omega \ll C^2/\eta_t, \tag{8}$$

(5) becomes approximately

$$\beta_{mn} = \left(\frac{\omega}{c}\right)\left[1 - \frac{i}{2}\left(\frac{\omega\eta_t}{c^2} + \frac{T_{mn}^2}{\omega}\eta_\ell\right)\right]. \tag{9}$$

Equations 6 and 7 are characteristic of diffusion phenomena. At low frequencies the magnetic field diffuses through the fluid in a time short compared with the period of the excitation. Thus the field is not convected by the fluid. At high frequencies the field cannot penetrate the fluid. Thus the fluid is not convected by the field. But if ω satisfies (9), there is a region in which mutual convection of the fluid and the field gives rise to the Alfvén wave.

If the asymptotes of Re (β) and -Im (β) in (6), (7), and (9) are plotted in log-log coordinates, Fig. XVII-2 results. An exact evaluation of (5) for a shock-excited gas experiment is also plotted in Fig. XVII-2, and shows that the asymptotes are a very good approximation to the exact curves.

The intersections of the asymptotes are interesting points, two of which correspond to condition (8). Notice that the lower limit of the Alfvén region is controlled

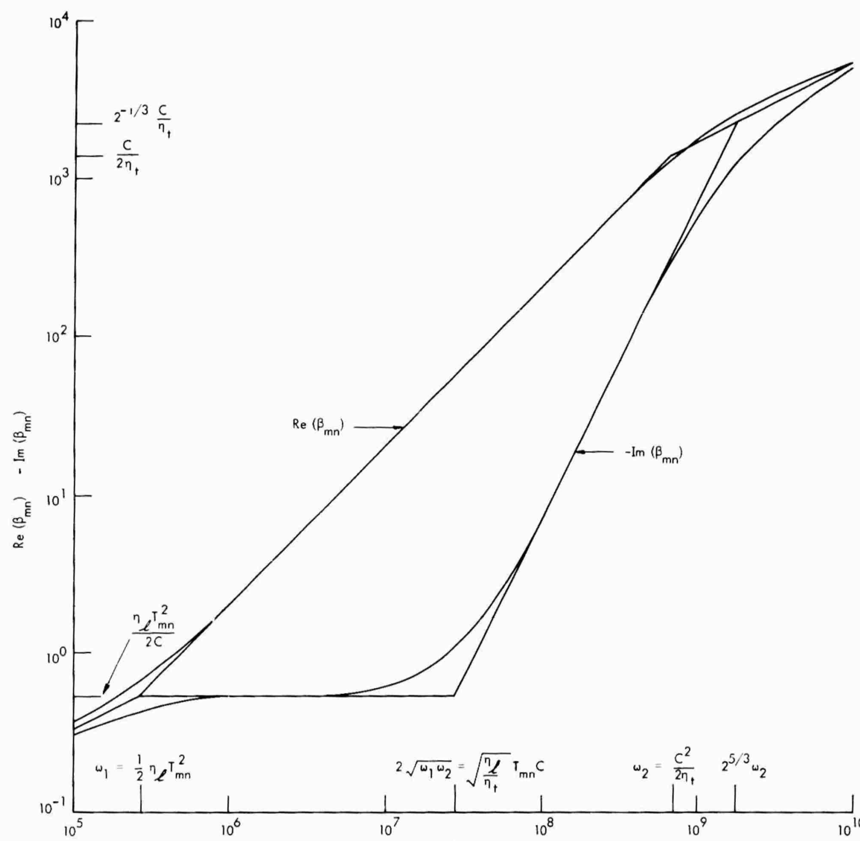

Fig. XVII-2. Typical shock-excited gas experiment.
$\sigma_\ell = \sigma_t = 4.5 \times 10^3$ v/m (Te = 3.5 ev); $\rho = 1.7 \times 10^{-5}$ kg/m^3 (n = 1.5×10^{15}/cc H^+); $B_o = 1.6$ w/m^2; b = 0.07 m; T_{01} = 3.8/b ($J_1(Tb) = 0$); Va = 5×10^5 m/sec; $\eta_\ell = \eta_t = 1.8 \times 10^2$ m^2/sec; $\omega_2/\omega_1 = 2.6 \times 10^3$.

by conductivity and geometry, while the upper limit is controlled by conductivity, density, and applied field. The frequency below which, under condition (8), the waveguide is distortionless is twice the geometric mean of the upper and lower

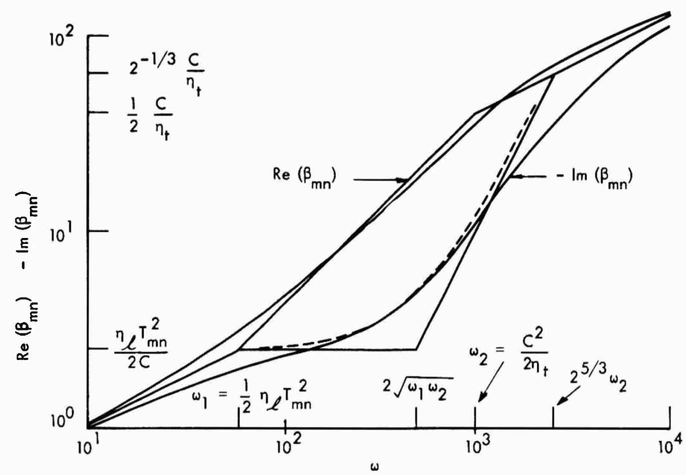

Fig. XVII-3. Typical liquid-metal experiment.
$\sigma_\ell = \sigma_t = 2.63 \times 10^6$ v/m; $\rho = 8.5 \times 10^2$ kg/m^3 (NaK);
$B_o = 0.8$ w/m^2; b = 0.19 m; $T_{01} = 3.8/b$ ($J_1(Tb) = 0$);
Va = 24.5 m/sec; $\eta_\ell = \eta_t = 0.3$ m^2/sec; $\omega_2/\omega_1 = 16$.

limits. In Fig. XVII-3 data are plotted for a typical liquid-metal experiment for comparison.

In view of these results, Eq. 5 should be rewritten

$$\beta_{mn}^2 = \left(\frac{\omega}{c}\right)^2 \frac{1 - 2i\frac{\omega_1}{\omega}}{1 + \frac{1}{2i}\frac{\omega}{\omega_2}}. \tag{10}$$

Now,

$$\frac{\omega}{2\omega_1} = \frac{\omega}{\eta_\ell T_{mn}^2} = \text{magnetic Reynolds number}$$

$$\frac{2\omega_2}{\omega} = \frac{C^2}{\omega\eta_t} = \text{Lundquist number.}$$

Thus, in order that an Alfvén wave exist, both the magnetic Reynolds and Lundquist numbers must be large compared with unity.

Listed below in tabular form is a comparison of a number of Alfvén wave experiments in terms of the critical frequencies.

	Experimenter	Medium	f_1	f_2
1.	Jephcott, Stocker, and Woods[4]	arc plasma	46.5 kc	51.3 mc
2.	Wilcox, da Silva, Cooper, and Boley[3]	shock plasma	41.4 kc	111.0 mc
3.	DeCourey and Bruce[9]	irradiated gas	57.2 mc	4.07 mc
4.	Gothard,[8] and Jackson and Carson*	NaK	9.75 cps	158 cps
5.	Lundquist[1]	Hg	159 cps	10.3 cps
6.	Lehnert[2]	Na	21.5 cps	770 cps

*See W. D. Jackson and J. F. Carson (Sec. XVII-B2).

G. B. Kliman

References

1. S. Lundquist, Phys. Rev. 83, 307 (1951).
2. B. Lehnert, Phys. Rev. 94, 815 (1954).
3. J. M. Wilcox, A. W. da Silva, W. S. Cooper, and F. I. Boley, Experiments on Alfvén Wave Propagation, in Radiation and Waves in Plasma, edited by M. Mitchner (Stanford University Press, 1961), p. 138.
4. D. F. Jephcott, P. M. Stocker, and L. C. Woods, IAEA Report CN-10/62, 1962.
5. R. W. Gould, STL Report TR-60-0000-09143, 1960.
6. J. Shmoys and E. Mishkin, Phys. Fluids 3, 473 (1960).
7. L. C. Woods, UKEA Research Group Report CLM-R5, 1961.
8. N. Gothard, S. M. Thesis, Department of Electrical Engineering, M. I. T., 1962.
9. D. J. DeCourey, Jr. and M. H. Bruce, Report AFCRL G2-550, 1962.

2. EXPERIMENTS WITH A LIQUID-METAL MAGNETOHYDRODYNAMIC WAVEGUIDE

The presence of hydromagnetic waves in conducting fluids was first established by Alfvén,[1] in 1942. Since that time, much progress has been made in the theoretical study of these waves, but experimental work has proceeded slowly. Lundquist,[2] in 1951, tried to excite waves in mercury, and Lehnert[3] repeated and improved the experiment, in 1954, using liquid sodium. Other experimental work has been done with shock-excited plasmas.[4,5] Most of the results thus far have been somewhat inconclusive, showing only partial agreement with theoretical predictions.

Many of the difficulties in experimental work have been caused by the need for a high-conductivity working fluid to avoid excessive attenuation. The Lundquist number, a reciprocal magnetic Reynolds number based on Alfvén velocity and wavelength, is defined as

$$\mathrm{Lu} = \frac{2\pi f}{B_o^2}\left(\frac{\rho}{\sigma}\right),$$

where f is the excitation frequency, B_o the applied magnetic field, ρ the fluid density, and σ the fluid electrical conductivity. It provides a convenient basis on which the suitability of a medium may be established and, to ensure propagation without undue attenuation, it must be much less than one, which in turn requires that the ratio of electrical conductivity to mass density be as large as possible. Lehnert was able to achieve improvement in the Lundquist number of over 100 by using sodium instead of mercury. Handling and instrumentation problems are always present in alkali-metal research, and the high temperature necessary to liquify sodium leads to additional complications. The use of sodium-potassium eutectic alloy as the working fluid affords an increase over mercury in the conductivity-density ratio about three times less than that of pure sodium. Sodium potassium affords the advantage of being liquid at room temperature, and accordingly has been chosen as the working fluid for this experiment.

Lundquist attempted to launch waves, using a vibrating disk with vanes attached. The device was intended to couple mechanically to the fluid and to cause torsional disturbances that would propagate along the axial magnetic-field lines, but the mechanism at work was really motional induction. Therefore Lehnert used a copper disk without vanes. The rotation of the disk in the magnetic field caused an induced electric field in the disk. Matching of tangential electric-field components across a boundary requires an induced current to flow in the fluid. This current in turn reacts with the magnetic field to form a $\overline{J} \times \overline{B}$ force that acts on the fluid to generate vorticity and, if conditions permit, the vorticity will propagate.

The search for an optimal means of excitation led to the use of a directly injected current sheet to launch the waves. A small disk, 5 cm in diameter, in the center of the waveguide shown in Fig. XVII-4 is fed with alternating current. A copper collecting ring soldered to the outside wall of the waveguide provides a return. The feed conductors leading from the ring to the source are designed to give equal resistance in all paths, and result in a reasonably symmetrical current-sheet excitation. Exciting currents are of the order of 100 amps.

The waveguide itself is constructed of stainless steel, and has an internal diameter

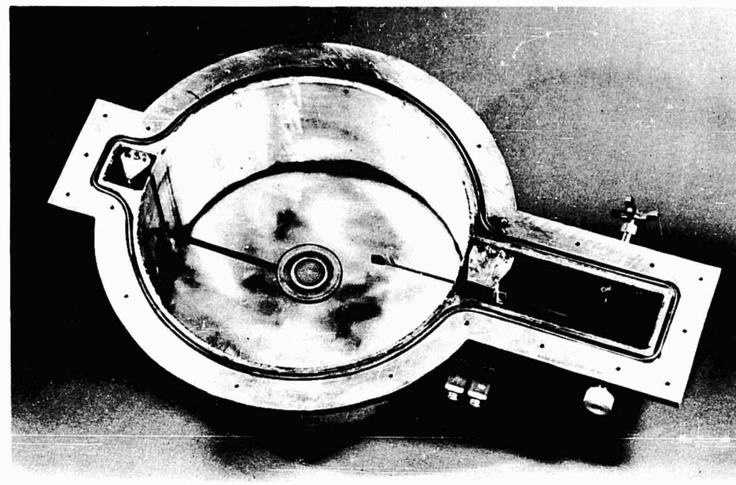

Fig. XVII-4. MHD waveguide showing excitation structure.

of 38 cm. The length of the waveguide is 18 cm, and is limited by the gap length of the magnet that was available. The applied magnetic field is 0.8 weber/meter^2. The rectangular chamber on the left of the waveguide contains the elevating mechanism for the exciter probe. With this arrangement it is possible to position the probe at any height within the waveguide. The chamber on the right contains the mechanism for both radial and axial movement of probes for local magnetic-field measurements. Counters attached to the shafts provide information about the location of the probes. The waveguide is filled and drained with the aid of a filling-station apparatus that contains the necessary valves and fittings for transferring the sodium potassium from storage cans to the waveguide.

If a sinusoidal drive and an $\exp(\overline{k}\cdot\overline{r})$ space dependence are assumed, the dispersion relation is obtained[6] from the pertinent hydrodynamic equations that yield values of the real and imaginary parts of the propagation vector as a function of frequency. The values of Alfvén speed v, wavelength λ, and attenuation α calculated for the conditions of the experimental apparatus are shown in Fig. XVII-5. The frequency dependence of v above ~200 cps indicates that this is a diffusion-controlled region and that waves should only be observed below this frequency. The method of excitation used in this experiment produced waves with magnetic-field components in the transverse plane only. The addition of a conducting center column would allow propagation of purely transverse electromagnetic waves.

Lundquist used a floating mirror to detect waves. Lehnert refined the measurement somewhat by measuring potential difference in the moving fluid with two probes. The approach taken in the present experiment was to look at the waveguide in as many ways

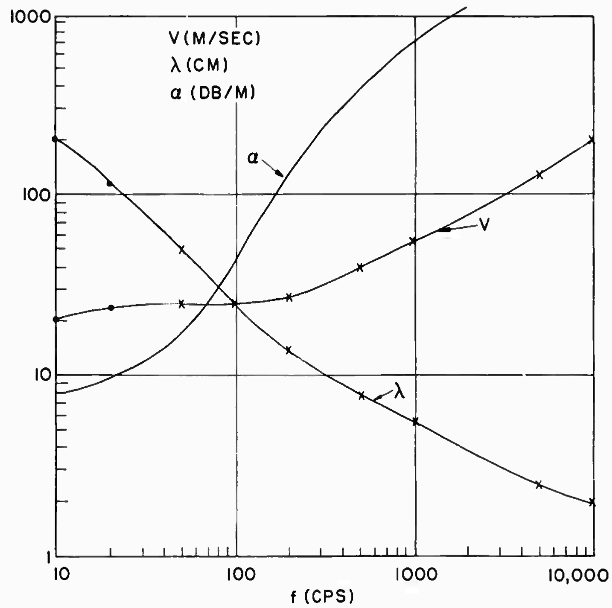

Fig. XVII-5. Wave properties as a function of frequency.

as possible. Two measurement schemes are possible when direct electric excitation is used. The relation of voltage and current at the driving terminals may be examined, and the internal fields of the waveguide may be measured. The field probe used for this experiment consisted of a solenoid, 3/8 in. in diameter, with 300 turns of number 37 wire. The coil was oriented so that the magnetic field induced in the ϕ direction was measured. The output of the probe was examined with an oscilloscope and voltmeter. A probe to measure local velocity in the fluid is under development, but was not available when the present experiment was performed.

Since the waveguide is of finite length, examination of the terminal impedance yields resonances. The results are shown in Fig. XVII-6 to be consistent with theoretical predictions based on calculated values of wavelength. The waveguide is essentially being run as a resonant cavity when operating at these points. The internal-field measurements were made at the resonances indicated on the impedance graph.

The measurements illustrated were taken with the exciter probe located at a height of 3 cm; this enabled the excitation of the $\lambda/2$ and $3\lambda/2$ resonances as indicated. Movement of the probe in the radial direction provided profiles of the type shown in Fig. XVII-7, while axial profiles obtained at a radius of 12 cm are given in Fig. XVII-8. To check that wave propagation was occurring, one set of data was obtained with a free surface at the top of the waveguide. Excitation without the applied field yielded a decay

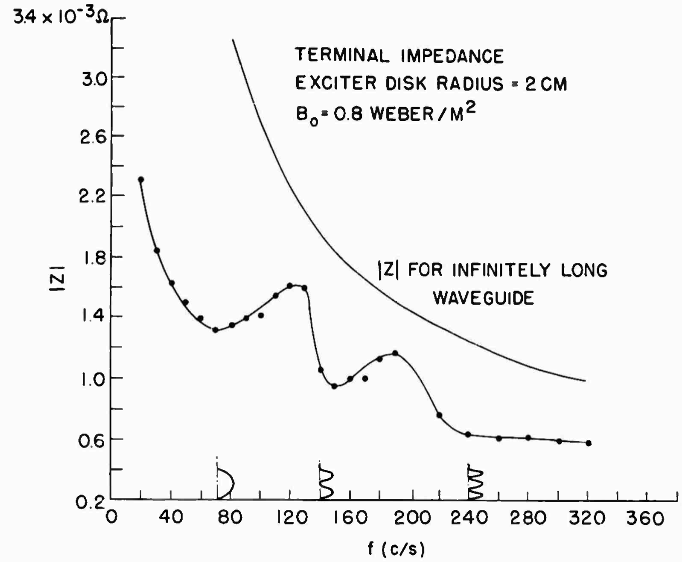

Fig. XVII-6. Resonance measurements.

of the induced field away from the exciter, while, with the field applied, an indication of free-surface motion was obtained as shown in Fig. XVII-8.

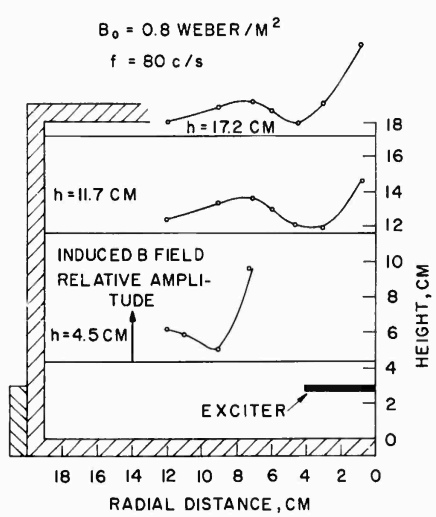

Fig. XVII-7. Induced B field — radial traverses.

The growth of the induced field along the axis is particularly evident in the case of the $3\lambda/2$ resonance, and is probably explained by the near-effects of the exciting-current sheet. The exciting disk was insulated on both top and bottom surfaces, and thus the fluid immediately above and below it is weakly coupled to the electromagnetic effects. The data of Fig. XVII-7 are consistent with the existence of a stationary volume of liquid above the exciter, but further experimental work is required to clarify the behavior in this region, and the waveguide is now being modified for this purpose.

The work reported here is of a preliminary nature, but it has served to indicate the feasibility of using a sodium-potassium alloy as the working fluid in the study of Alfvén waves, as an alternative to the transient conditions of a shock-excited plasma. Conduction-type direct electrical excitation has been shown to be greatly superior to the vibrating disks used by early

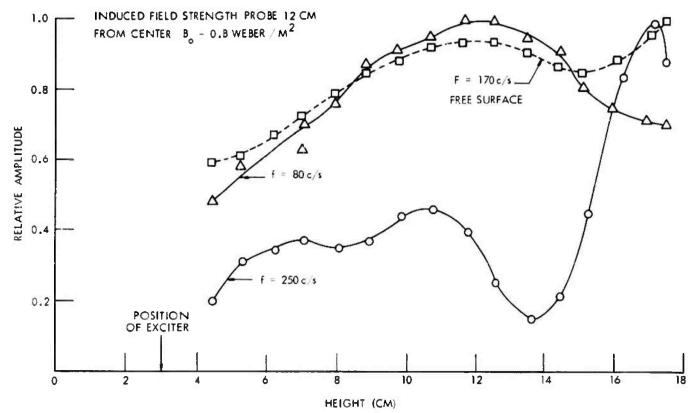

Fig. XVII-8. Induced B field — axial traverses.

experimenters, and magnetic field probes have proved to be satisfactory for the detection of wave conditions inside the waveguide. This study will continue, and will be concerned with both transverse magnetic and transverse electromagnetic modes, a different excitation, and different boundary conditions.

W. D. Jackson, J. F. Carson

References

1. H. Alfvén, Nature 150, 405 (1942).
2. S. Lundquist, Phys. Rev. 83, 307 (1951).
3. B. Lehnert, Phys. Rev. 94, 815 (1954).
4. J. M. Wilcox, A. W. da Silva, W. S. Cooper, and F. I. Boley, Experiments on Alfvén Wave Propagation, in Radiation and Waves in Plasma, edited by M. Mitchner (Stanford University Press, 1961), p. 138.
5. D. F. Jephcott, P. M. Stocker, and L. C. Woods, IAEA Report CN-10/62, 1962.
6. R. W. Gould, STL Report TR-60-0000-09143, 1960.
7. J. Shmoys and E. Mishkin, Phys. Fluids 3, 473 (1960).
8. L. C. Woods, UKEA Research Group Report CLM-R5, 1961.
9. N. Gothard, S.M. Thesis, Department of Electrical Engineering, M.I.T., 1962.
10. D. J. DeCourey, Jr. and M. H. Bruce, Report AFCRL G2-550, 1962.

C. MAGNETOHYDRODYNAMIC POWER GENERATION WITH LIQUID METALS

Preliminary studies on a liquid-metal MHD power system employing a condensing ejector have been completed. The objective was to determine the expected cycle efficiencies and specific weights by using available fluid-dynamic, thermodynamic, and

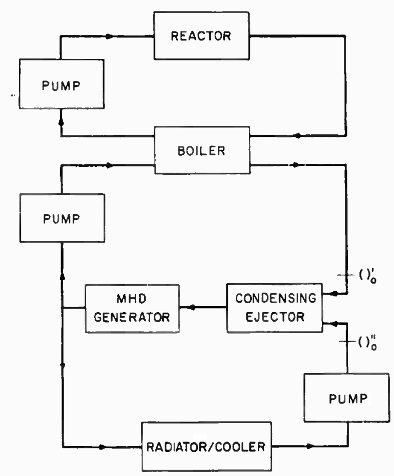

Fig. XVII-9. Liquid-metal MHD power system employing a condensing ejector.

heat-transfer information for the components and processes of the cycle. For the present, the liquid-metal MHD generator has been characterized as having a specified efficiency. Later studies will integrate the generator performance parameters with those of the components that are used to produce the liquid-metal stream in a complete system study.

The basic cycle is shown in Fig. XVII-9. Three loops are required for the conversion system. Energy from a nuclear reactor is transferred to a flowing liquid, perhaps lithium, which boils the primary working fluid, cesium, in the boiler section between the first and second loops. The cesium vapor then enters the condensing ejector at state $( )'_0$. The condensing ejector also receives "cool" liquid cesium, state $( )''_0$, which is returned from the radiator in the third loop. These two streams are mixed in the condensing ejector so as to produce a liquid-cesium stream having a high stagnation pressure. The liquid cesium stream is then split with a fraction being returned to the boiler and the remainder being returned to the radiator.

Available analytical and experimental data have been used to calculate the performance of the condensing ejector. Calculations have been made to establish the pressure drops and weights for the boiler and radiator, including state-of-the-art results for the two-phase flow, which occurs in the boiler under zero gravity conditions.

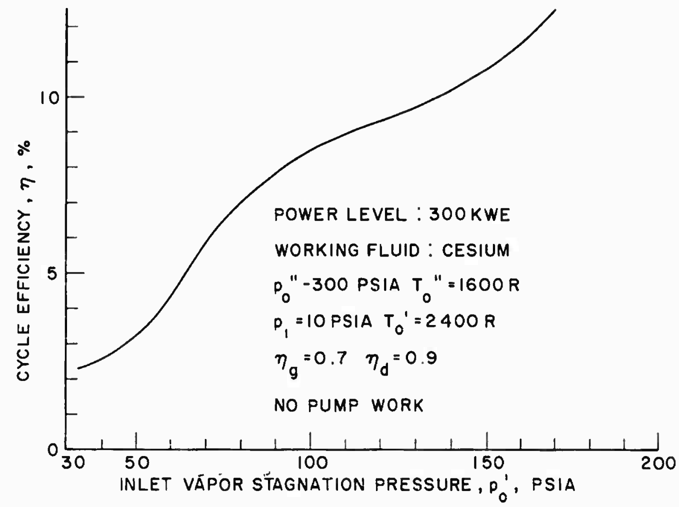

Fig. XVII-10. Effect of vapor stagnation pressure on cycle efficiency.

The cycle efficiency for the best conditions found thus far is shown in Fig. XVII-10. The conditions are for a space power system with a 300-kwe output. Cesium vapor is supplied to the condensing ejector at 2400 R and for the stagnation pressures shown in Fig. XVII-10. The cesium liquid enters at 1600 R and 300 psia. Both streams are then accelerated to a pressure of 10 psia in the condensing ejector. The liquid-cesium stream from the ejector is usually available at a high velocity, and can be diffused to any desired stagnation pressure before entry into the generator. A diffuser efficiency of 90 per cent has been used. A generator efficiency of 70 per cent has also been employed. The cycle efficiency is very low, approximately 2 per cent, when p_o'' is 30 psia, but increases steadily to approximately 12.5 per cent at 170 psia. The omission of the pump power for the reactor loop will drop the cycle efficiency by an increment of approximately 0.5 per cent.

Since the calculated cycle efficiencies and specific weights for the liquid-metal MHD power system are quite competitive with other systems now under consideration, further studies of it are planned.

G. A. Brown, W. D. Jackson, K. S. Lee

D. EXPERIMENTAL STUDY OF INDUCTION-COUPLED LIQUID-METAL MAGNETOHYDRODYNAMIC CHANNEL FLOW

The direct generation of electrical power from the kinetic power carried by an electrically conducting fluid may be achieved through the utilization of the inductive coupling between a traveling magnetic field and the moving fluid. It has been shown[1] that the operating characteristics of an MHD induction generator can be determined from the magnetic Reynolds number, based on wave speed and velocity and the velocity difference between the wave and the fluid. The conductivity and velocity attainable with ionized gas flows are too low to yield satisfactory operating conditions, but liquid metals yield more promising results as is indicated in Table XVII-1. Two methods of converting the thermal energy of a power-system heat source to the kinetic energy of a moving fluid have recently been proposed.[2,3]

Table XVII-1. Experimental results.

		Liquid Metal	Metal Vapor
velocity	v	10^2	10^3 m/sec
conductivity	σ	10^6	10^2 mhos/m
magnetic field	B	2	2 wb/m^2
power density	$\frac{1}{4}\sigma v^2 B^2$	10^{10}	10^8 W/m^3
wavelength	λ	50	50 cm
magnetic Reynolds number	$\frac{\mu\sigma v\lambda}{2\pi}$	10	10^{-2}

The magnetic Reynolds number criterion used in Table XVII-1 is attained from a one-dimensional analysis that ignores real machine effects, all of which may be expected to degrade performance. An induction-coupled liquid-metal MHD channel flow has been set up to investigate directly real machine effects such as end losses, fluid viscous losses, magnetic-field configuration, and edge effects. Eutectic sodium potassium alloy (NaK) was selected as the working fluid for a closed-loop flow facility driven by a positive displacement pump with a capacity of 20 gallons per minute at a head of 20 p.s.i. A 300 gallon per minute centrifugal pump will be obtained for future experiments. The entire flow loop is fabricated from stainless steel with neoprene connectors and O-rings. Figure XVII-11 shows the general layout of the flow facility, including the instrumentation used for the experimental study. Details of the design and construction of the loop have already been given.[4-6]

The traveling-field coil system is contained in the horizontal cylindrical tank on the table shown in Fig. XVII-11. It comprises 24 pairs of saddle coils assembled around a 4 1/4 inch diameter tube as shown in Fig. XVII-12. The coil pairs are spaced 6 inches

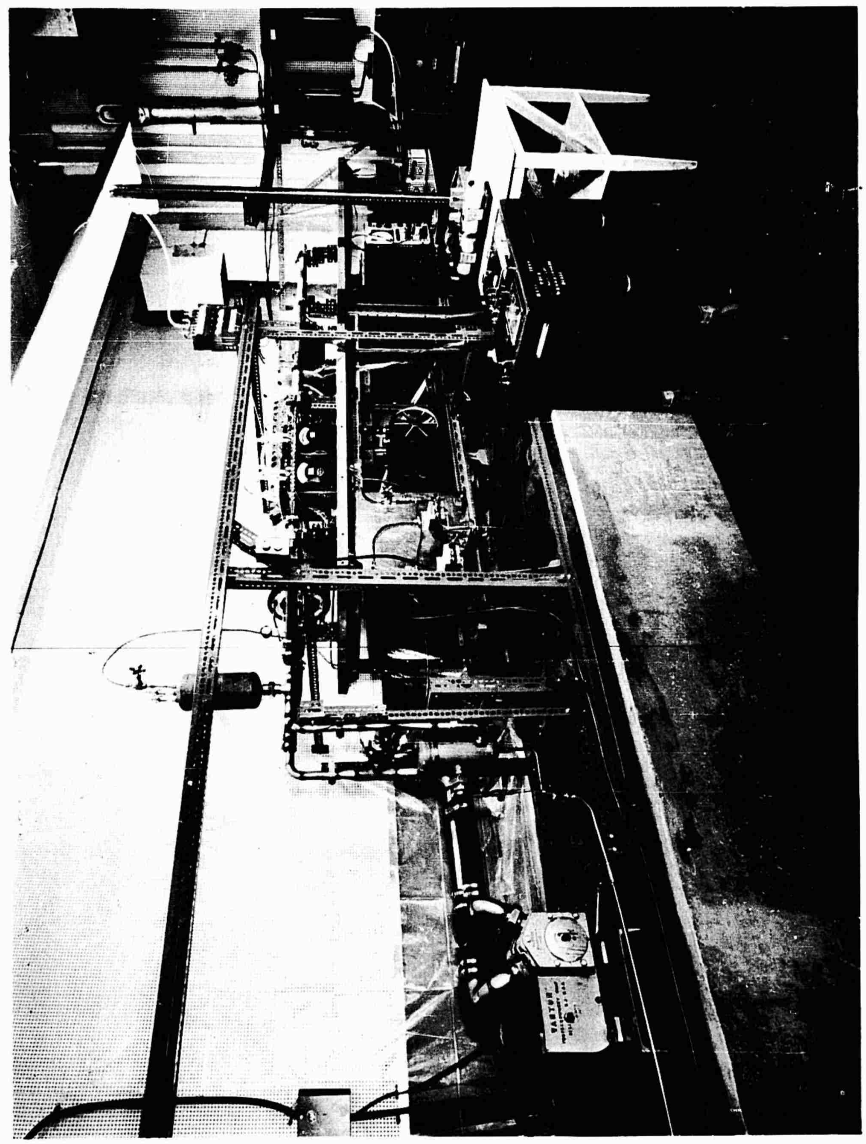

Fig. XVII-11. Liquid-metal flow facility.

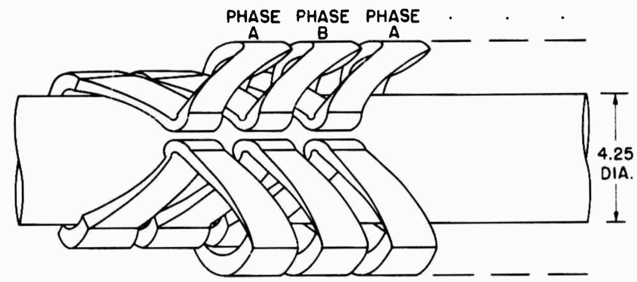

Fig. XVII-12. Traveling-field coil structure.

apart, and are connected to produce a two-phase system with a wavelength of 1 ft. The coil structure is kerosene-cooled, and powered from a 60-cps alternator rated at 44 kva at 230 volts. A variable-speed DC motor drive enables the alternator frequency to be varied.

A high aspect ratio rectangular channel was used in these experiments. The internal dimensions were 2 3/4 in. × 3/8 in. which yielded a velocity of approximately 10 ft per second at maximum capacity. The long sides of the channel were insulated with epoxy but, to minimize electrical losses in the chosen geometry, the remaining two sides of

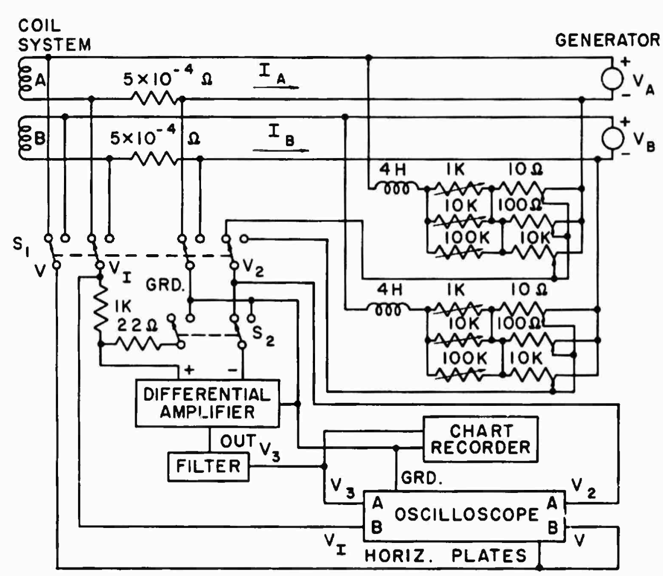

Fig. XVII-13. Power-flow measurement circuit details.

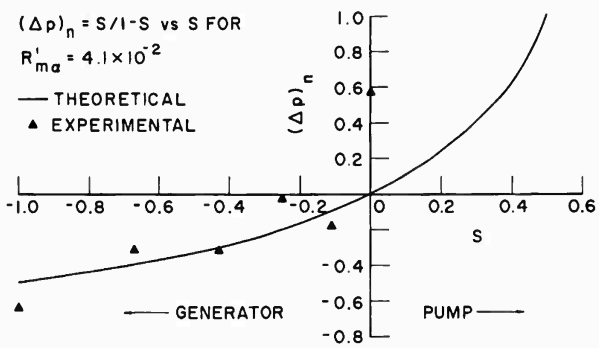

Fig. XVII-14. Normalized pressure vs slip.

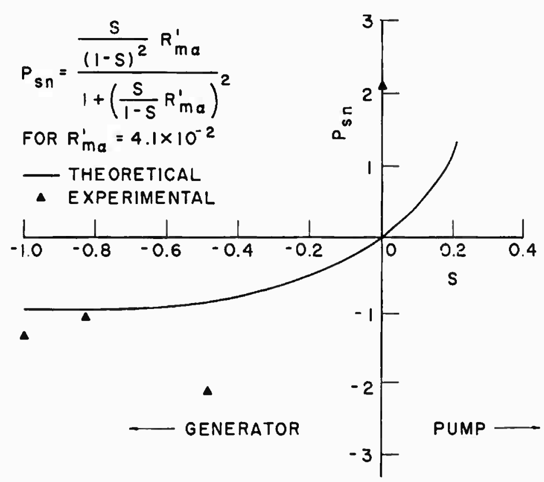

Fig. XVII-15. Normalized power vs slip.

the channel were of nickel-plated copper. Transition sections were provided at each end of the generator channel to connect to the 1.1 in. flow-loop tubing. Provision was made for fluid pressure to be measured at 6-inch intervals along the channel.

Measurements were made of fluid velocity, pressure drop along the MHD channel section, and power flow between the alternator and the coil system. The system was first filled with alcohol to check out operation and calibrate the venturi flowmeter. To minimize flow pulsations introduced by the positive displacement pump, the fluid velocity was kept at maximum value throughout runs with NaK, and the slip between the field and the fluid was varied by adjusting the speed of the alternator drive motor. Direct-reading NaK manometers did not function satisfactorily, and so a single mercury manometer was used. This was connected by a system of valves to the appropriate pressure measurement point.

Because of the small amount of electrical power flow involved in the MHD interaction, relative to the 1500 volts required to drive the field coils, direct measurement of power flow could not be made. Instead, the differential amplifier scheme shown in Fig. XVII-13 was used, and was calibrated directly by means of dummy loads connected across the coil terminals. Pressure-slip and power flow-slip data are given in Figs. XVII-14 and XVII-15, respectively, and a comparison with theoretical predictions is made.

The normalization of the experimental results and the theoretical curves are obtained in the following way. The power P_s delivered by the fluid to the coils[7] is given by

$$P_s = \frac{\mu_o c\lambda N^2 I^2}{K + \alpha} \frac{v_s s R_{m\alpha}}{1 + s^2 R_{m\alpha}^2}, \tag{1}$$

where μ_o is the fluid permeability, λ is the wavelength, v_s is the wave speed, NI is the magnetomotive force, c is the over-all width of the machine, and

$$s = 1 - v/v_s \tag{2a}$$

$$R_{m\alpha} = \frac{\mu_o \sigma_f a v_s}{K + \alpha} \tag{2b}$$

$$\alpha = ak \tag{2c}$$

$$K = \frac{\mu_o}{\mu_c}. \tag{2d}$$

In these definitions, s denotes the slip between v_s and the average fluid velocity v; $R_{m\alpha}$ is the relevant magnetic Reynolds number; σ_f, the fluid conductivity; a, the channel half-width; K, the ratio giving μ_o to the field-structure permeability μ_c; and α, the ratio that is a measure of the ratio of a to λ in terms of the wave number k.

As the experimental results are for a constant value of v, and the effect of changing $sR_{m\alpha}$ is of interest, it is convenient to define a constant value of magnetic Reynolds number $R'_{m\alpha}$ as

$$R'_{m\alpha} = R_{m\alpha} \frac{v}{v_s} = \frac{\mu_o \sigma_f a v}{K + \alpha}. \tag{3}$$

The normalized power P_{sn} is then obtained as

$$P_{sn} = \frac{P_s(K+\alpha)}{\mu_o c\lambda(NI)^2 v} = \frac{\frac{s}{(1-s)^2} R'_{m\alpha}}{1 + \left(\frac{s}{1-s}\right)^2 (R'_{m\alpha})}. \tag{4}$$

For the experimental conditions, $R'_{m\alpha} = 0.041$.

In a similar fashion, the pressure change along the channel,[7] Δp, is given by

$$\Delta p = \frac{\mu_o N^2 I^2 L}{2a(K+\alpha)} \frac{sR_{m\alpha}}{1 + s^2 R_{m\alpha}^2}, \tag{5}$$

and the normalized $(\Delta p)_n$ is

$$(\Delta p)_n = \Delta p \frac{2a(K+\alpha)}{L\mu_o(NI)^2} = \frac{\frac{s}{1-s} R'_{m\alpha}}{1 + \left(\frac{s}{1-s}\right)^2 (R'_{m\alpha})^2}. \tag{6}$$

For the region of experimental interest,

$$\left(\frac{sR'_{m\alpha}}{1-s}\right)^2 \ll 1 \tag{7}$$

and

$$(\Delta p)_n \approx \frac{s}{1-s}. \tag{8}$$

The correlation of theory with experiment in Figs. XVII-14 and XVII-15 is quite satisfactory when the difficulty of measuring values of P_s less than 0.5 watt is taken into account. It should be noted that the sign of both the pressure drop and power flow indicates generator action in the region of negative s, and shows that electrical losses resulting from end effects, etc., were not of sufficient magnitude to absorb the generated power. Because of the very low Hartmann number involved, fluid losses for the interaction region were estimated by using ordinary friction factor curves to the 21.31 watts for v = 10 ft per second. This is in good agreement with the measured value of 22.2 watts, and confirms the prediction that ordinary friction losses are the predominant effect in this experiment. The experimental apparatus is now being modified to obtain the stronger magnetohydrodynamic interactions that are evidently required for further study of induction-coupled flows.

W. D. Jackson, R. P. Porter

References

1. W. D. Jackson and E. S. Pierson, Operating Characteristics of the MPD Induction Generator, Magnetoplasmadynamic Electrical Power Generation, I.E.E. Conference Report Series No. 4, 1963.

2. W. D. Jackson, Review of MHD Power Generation, Proc. AMU-ANL Conference on Direct Energy Conversion, Argonne National Laboratory, Lemont, Illinois, November 1963.

3. D. G. Elliot, Two-fluid magnetohydrodynamic cycle for nuclear-electric power conversion, Am. Rocket Soc. J. 32, 924 (1962).

4. F. W. Fraim IV, Design and Construction of a Magnetohydrodynamic Channel Flow System, S. B. and S. M. Thesis, Department of Electrical Engineering, M. I. T., 1962.

5. J. F. Carson, Friction Factor Measurement for NaK Magnetohydrodynamic Channel Flow, S. B. Thesis, Department of Electrical Engineering, M. I. T., 1963.

6. M. H. Reid, Experimental Investigation of a Liquid Metal Induction Generator, S. M. Thesis, Department of Electrical Engineering, M. I. T., 1963.

7. E. S. Pierson, Power flow in the magnetohydrodynamic induction machine, Quarterly Progress Report No. 68, Research Laboratory of Electronics, M. I. T., January 15, 1963, pp. 113-119.

E. NEURAL PATTERNS IN BLOOD-PRESSURE REGULATION*

This study is concerned with the description of a part of the pressoreceptor reflex system, a biological control system involved in the regulation of blood pressure. The system consists of stretch-sensitive receptors located in the walls of certain arteries which transduce the pressure signal into related electrical activity on the nerve associated with the sensors; the nerve itself, which transmits the information to the brain; the vasomotor center of the brain, which processes the information; and the efferent nerves, which transmit the control signals to the heart and blood vessels, thereby closing the control loop.

The work reported on here deals with the transduction of the pressure signals into nerve firings on the nerve involved. Specifically, the relation between the firing frequency on the carotid sinus nerve and the pressure at the carotid sinus is considered. From the published data of single-fiber studies, it is possible to construct a model that qualitatively at least reproduces the behavior of the biological system.

The static behavior of the system is characterized by no neural activity below a threshold level of pressure, a firing rate proportional to pressure above the threshold value, and an asymptotic approach to a maximum firing frequency as the static pressure is raised to a sufficiently high level.

The dynamic response of the system, as determined by the system response to step-like variations in pressure, exhibits a rapid increase of firing rate upon application of a positive step which is followed by a decay to a final value that is higher than the value of

*This work was supported in part by the National Institutes of Health (Grant No. 5 TI HE 5550-02.

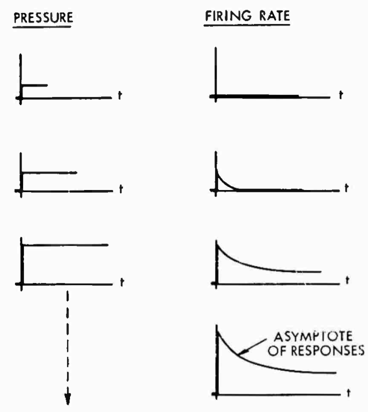

Fig. XVII-16. Step responses on a single fiber.

firing rate before application of the step. A negative step produces an initial cessation of firing, after which the firing rate grows back to a steady value lower than its initial value.

If the pressure steps are started at 0 mm Hg and their amplitude is increased, the (idealized) responses are observed as shown in Fig. XVII-16. These observations, as well as observations of ramp responses, suggest that the system may be modeled in the manner of Fig. XVII-17. The first nonlinear section results in the successive step responses approaching an asymptotic response. The use of the linear filter corresponds to approximating the step response by the sum of a step and a single decaying exponential. The effect of the second nonlinear section corresponds to that of the static threshold and accounts for the nature of the responses to negative steps.

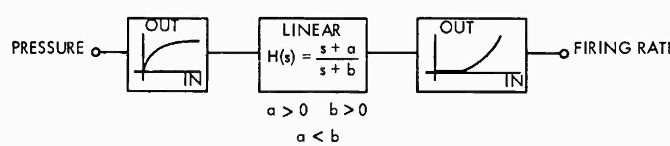

Fig. XVII-17. Model whose response approximates the response of a single fiber.

The complexity of this model can be increased by adding more poles and zeros (approximating the step response by sums of decaying exponentials).

The experimental part of this study consisted of the application of (almost) sinusoidal pressure variations imposed upon static levels of pressure, and the recording of the resultant activity on the carotid sinus nerve. The recordings were obtained from multifiber preparations. The activity corresponding to 10 cycles of each stimulus frequency at each static level was recorded, so that some averaging could be performed to reduce the effects of noise (noncorrelated) components in the outputs.

The data-reduction scheme consists of thresholding the outputs to obtain a clean base line, and counting the number of firings in a window whose position with respect to the stimulus is controllable, as indicated in Fig. XVII-18. Using this scheme, we obtained curves of firing rate vs time corresponding to the stimulation; a typical example appears

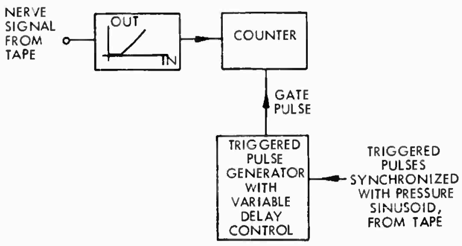

Fig. XVII-18. Block diagram of data reduction scheme.

in Fig. XVII-19. Qualitatively, the peaks of these curves tend to occur in the region in which the corresponding pressure is near its peak. Since these curves are not sinusoidal, their first harmonics are being calculated, and the amplitude and phase of the first harmonics with respect to the amplitude and phase of the pressure are being examined. Preliminary results indicate that the angle of the system function (angle of first harmonic of averaged firing rate vs time minus angle of pressure) is positive. This agrees with the fact that the coefficients of the decaying exponentials used to approximate the step response are positive, that is, that the residues in the poles of H(S) are positive, which implies that

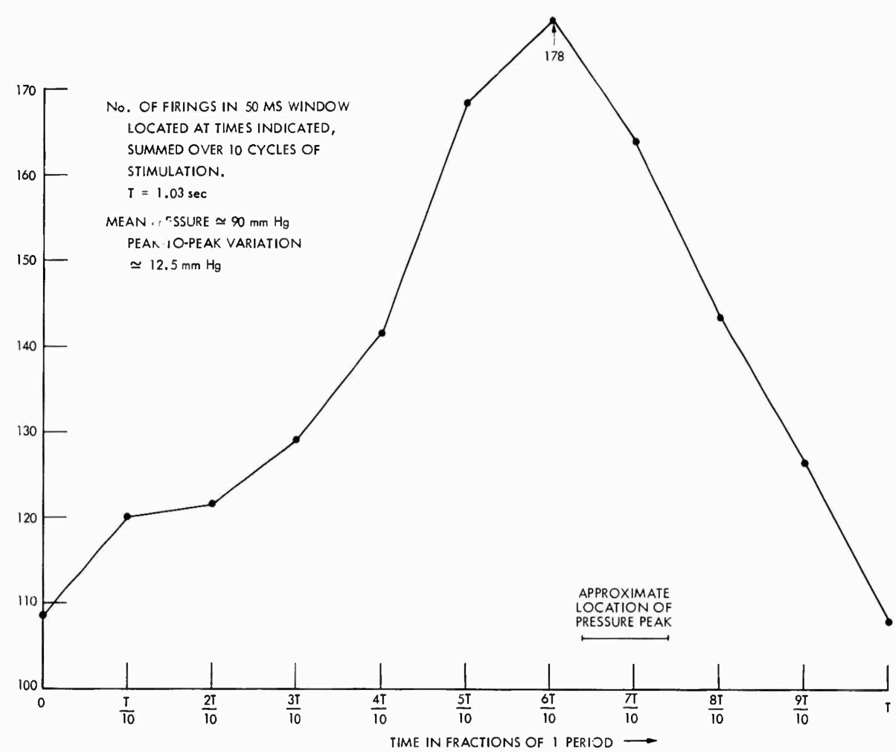

Fig. XVII-19. Typical experimental curve of firing rate vs time obtained from gross recordings.

the negative real poles and zeros of H(S) alternate, with a zero nearest the origin. Requiring the critical frequency nearest the origin to be a zero, together with requiring the number of poles to equal the number of zeros, implies positive phase shift.

These preliminary results also indicate that the system gain (amplitude of first harmonic of the averaged firing rate versus time divided by amplitude of the pressure sinusoid) is an increasing function of frequency. This trend agrees with the amplitude vs frequency behavior of the system function $H(S) = \frac{s+a}{s+b}$, $0 < a < b$.

D. H. Pruslin

F. PENETRATION OF AN ION THROUGH AN IONIC DIPOLE LAYER AT AN ELECTRODE SURFACE

When cesium is adsorbed on a metallic surface in the form of ions, these ions and their images form a dipole layer.[1,2] If an ion is introduced to the surface, it travels through a fraction f of the potential difference caused by this dipole layer from the image plane to a point at infinity,[2] as shown in Fig. XVII-20. Values of the penetration

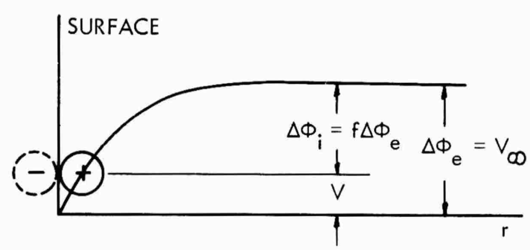

Fig. XVII-20. Potential of an ion with respect to the potential of a substrate surface as a function of distance from the surface.

coefficient have been computed by Rasor and Warner[3] and by Kennedy.[4] In this report it is shown that the penetration coefficient can be evaluated as a function of coverage in two different ways, one for an immobile film, and the other for a completely mobile film. Subsequently, values of the penetration coefficient can be obtained from the Langmuir-Taylor data for cesium on tungsten in two different ways. Both methods give values for the penetration coefficient which agree closely with each other over the entire range of the coverage, and these values fall between the theoretical expressions for f obtained for the cases of immobile and mobile films.

1. Penetration Coefficient for an Immobile Film

For an immobile film the cesium ions occupy fixed lattice sites, as shown in Fig. XVII-21a. A cross-section view of the surface is shown in Fig. XVII-21b. The following nomenclature is used.

Symbol	Definition
d	lattice constant of the crystal
λ	distance of the center of charge of an adsorbed ion from the image plane, taken to be equal to the hard-core ionic radius of cesium
r	distance of an ion from the image plane
r_{ij+}	distance between an ion at r and any adsorbed ion at i,j
r_{ij-}	distance between an ion at r and an image of any adsorbed ion at i,j
r_{ij}	distance between an adsorption site and any other site at i,j
$\theta_i = \frac{\sigma_i}{\sigma_1}$	ionic coverage
$\sigma_1 = \frac{1}{4d^2}$	surface density of adsorbates at full coverage

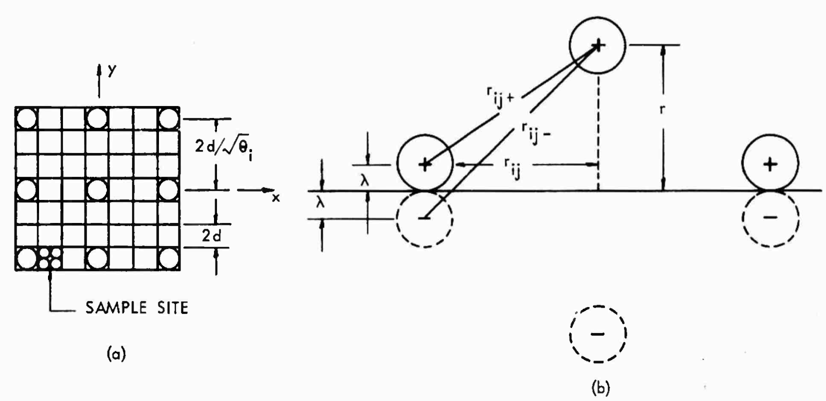

Fig. XVII-21. (a) Immobile adsorbate-substrate system. (b) Cross section of adsorbate-substrate system.

The potential on an ion at any r as a result of being in the field of the remaining adsorbed ions and their images can be expressed as

$$V(r) = q \sum \left(\frac{1}{r_{ij+}} - \frac{1}{r_{ij-}}\right), \tag{1}$$

in which the summation is performed over every adsorbate, and each adsorbate corresponds to a distinct distance r_{ij}. For the square lattice model with perfect arrangement of adsorbates,

$$r_{ij+}^2 = (r-\lambda) + r_{ij}^2 \tag{2a}$$

$$r_{ij-}^2 = (r+\lambda) + r_{ij}^2 \tag{2b}$$

with

$$r_{ij}^2 = \frac{4d^2}{\theta_i}(i^2+j^2). \tag{2c}$$

Equation 1 is rewritten

$$V(r) = q \sum \frac{r_{ij-} - r_{ij+}}{r_{ij+}r_{ij-}} \frac{(r_{ij-}+r_{ij+})}{(r_{ij-}+r_{ij+})}$$

or

$$V(r) = q \sum \frac{r_{ij-}^2 - r_{ij+}^2}{r_{ij+}r_{ij-}^2 + r_{ij+}^2 r_{ij-}}. \tag{3}$$

Substituting Eq. 2 in Eq. 3, for $r = \lambda$, yields

$$V(r=\lambda) = 4q\lambda^2 \sum_{-\infty}^{\infty}\sum \frac{1}{\left[4\lambda^2 + \frac{4d^2}{\theta_i}(i^2+j^2)\right]\left[\frac{4d^2}{\theta_i}(i^2+j^2)\right]^{1/2} + \left[4\lambda^2 + \frac{4d^2}{\theta_i}(i^2+j^2)\right]^{1/2}\left[\frac{4d^2}{\theta_i}(i^2+j^2)\right]} \tag{4}$$

in which i,j take on all values except $i = j = 0$.

Since $\lambda^2 \ll \frac{d^2}{\theta_i}(i^2+j^2)$, we neglect λ^2 in the denominator of Eq. 4 to obtain

$$V(r=\lambda) = \frac{q\lambda^2\theta_i^{3/2}}{4d^3} \sum_{-\infty}^{\infty}\sum \frac{1}{(i^2+j^2)^{3/2}}. \tag{5}$$

Evaluating the sum[5] then gives the potential of an adsorbed ion resulting from the other adsorbed ions, in other words, the value of V in Fig. XVII-21b, which is equal to

$$V(r=\lambda) = \frac{2.21q\lambda^2}{d^3}\theta_i^{3/2}. \tag{6}$$

The potential at infinity with respect to the image surface is identified as V in Fig. XVII-20. For large r, the potential felt by an ion from the discrete dipoles is approximately the same as that which would be felt from a continuously distributed dipole layer. This value has been stated[1,6] to be

$$\lim_{r\to\infty} V = V_\infty = 2\pi M\sigma_1\theta_i \qquad \text{for } M = 2q\lambda. \tag{7}$$

2. Mobile Films

For mobile films the cesium ions can move freely from one lattice site to another, and hence each lattice site has the same probability of being occupied by a cesium ion that is simply the coverage. Hence

$$p(\theta) = \theta. \tag{8}$$

The potential, then, of an ion at distance r is obtained by summing over each lattice site and multiplying this potential by the probability of occupation. For the mobile film, $r_{ij}^2 = 4d^2(i^2+j^2)$, so that

$$V(r=\lambda) = \frac{q\lambda^2}{4d^3} \sum_{-\infty}^{\infty}\sum \frac{P(\theta)}{(i^2+j^2)^{3/2}}. \tag{9}$$

Evaluating the sum gives

$$V(r=\lambda) = \frac{2.21q\lambda^2\theta_i}{d^3}. \tag{10}$$

3. Determination of f

The penetration coefficient is determined by the relation $f = \frac{\Delta\phi_i}{\Delta\phi_e}$, where $\Delta\phi_i$ is the change of ionic work function, and $\Delta\phi_e$ is the change of electron work function. The increase in ionic work function occurs because the ion penetrates through the potential $V_\infty - V$ of Fig. XVII-20. Thus $\Delta\phi_i = V_\infty - V$. The electron work function decreases as a result of the accelerating potential V_∞, so that $\Delta\phi_e = V_\infty$. Thus we obtain the relation

$$f = 1 - \frac{V}{V_\infty}. \tag{11}$$

Substituting the calculated values for V and V_∞, we obtain for the immobile film

$$f_{im} = 1 - \frac{2.21\lambda^\infty}{\pi d}\,\theta_i^{1/2} = 1 - 0.362\theta_i^{1/2}. \tag{12}$$

For the completely mobile film independent of coverage,

$$f_m = 1 - \frac{2.21\lambda}{\pi d} = 0.632. \tag{13}$$

4. Ionic Coverage

The ionic coverage is related to the total coverage by Fermi-Dirac statistics, and the following relation has been derived.[7]

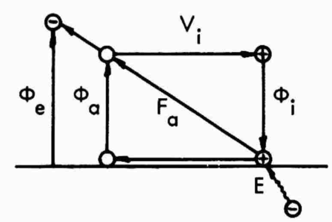

Fig. XVII-22. Born-Haber cycle.

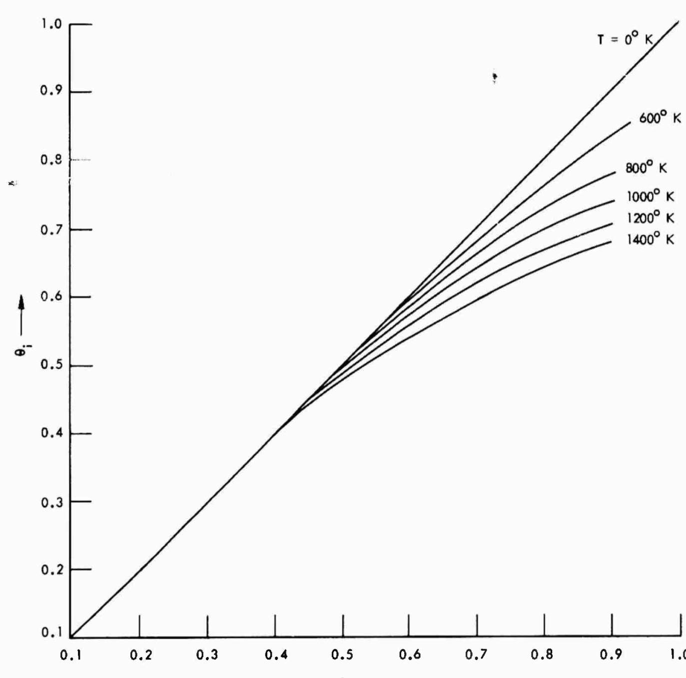

Fig. XVII-23. Ionic coverage vs total coverage for various surface temperatures.

$$\theta_i = \frac{\theta}{1 + \exp(-E/kT)}, \tag{14}$$

where E is the difference in energy between a bound 6S electron of a surface adsorbate atom and the Fermi level of the substrate. This quantity is determined from experiment in the following manner. Consider the Born-Haber cycle of Fig. XVII-22. Two energy balances result from this cycle:

$$f_a = \phi_e - V_i + \phi_i \tag{15}$$

and

$$f_a = \phi_a + E. \tag{16}$$

Equation 15 can be solved for f_a by using the atomic heat of adsorptions data of Taylor and Langmuir.[2] If it is assumed that ϕ_a does not change with coverage — which is reasonable since the atom is not acted upon by the electric forces of the dipole layer — and if f_a for various materials tends towards the same value at higher coverages, then knowing $f_a = f_a(\theta)$ and ϕ_a, we can calculate the value of $E = E(\theta)$ and substitute it in Eq. 13; this procedure yields $\theta_i = \theta_i(\theta)$. This is plotted for various temperatures in Fig. XVII-23 for cesium tungsten.

5. Correlation of Experimental Results

Theoretical values for f from Eqs. 11 and 12, for the two limiting cases of mobile and immobile films, are plotted against θ in Fig. XVII-24. Curves are also drawn on the same coordinates by computing $f = \frac{\Delta\phi_i}{\Delta\phi_e}$ from previous experimental data.[2,8] The values of f computed from Taylor-Langmuir data fall between the theoretical values obtained for the two limiting cases considered. Furthermore, values of f calculated in two different ways from the Taylor-Langmuir measurements agree within experimental uncertainties. Curve 4 is calculated from direct measurement of ϕ_i. By using the cycle of Fig. XVII-22, together with the relations

$$\phi_i(\theta) = \phi_{io} + \Delta\phi_i, \tag{17}$$

$$-\Delta\phi_e = \phi_e - \phi_{eo}, \tag{18}$$

$$\Delta\phi_i = f\Delta\phi_e, \tag{19}$$

so that

$$\phi_i(\theta) = \phi_{io} + f(\phi_{eo} - \phi_e) \tag{20}$$

(where the zero subscripts denote values at zero coverages), the expression for f is obtained.

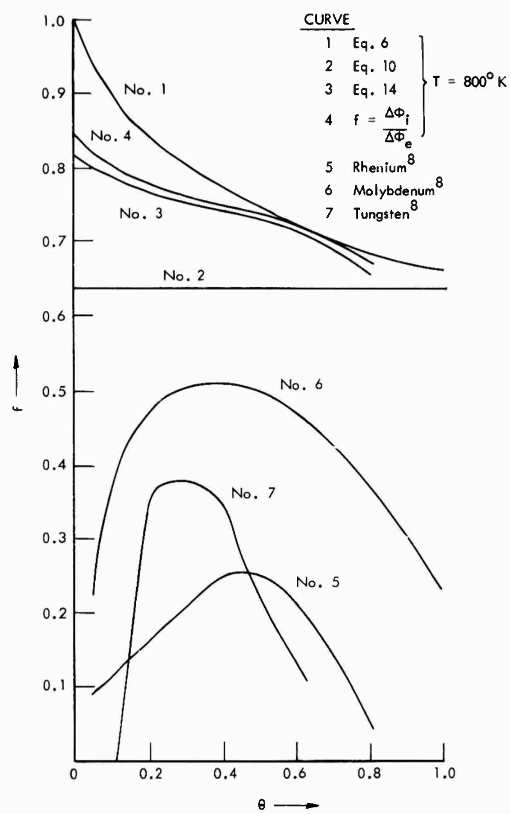

Fig. XVII-24. Penetration coefficient vs coverage.

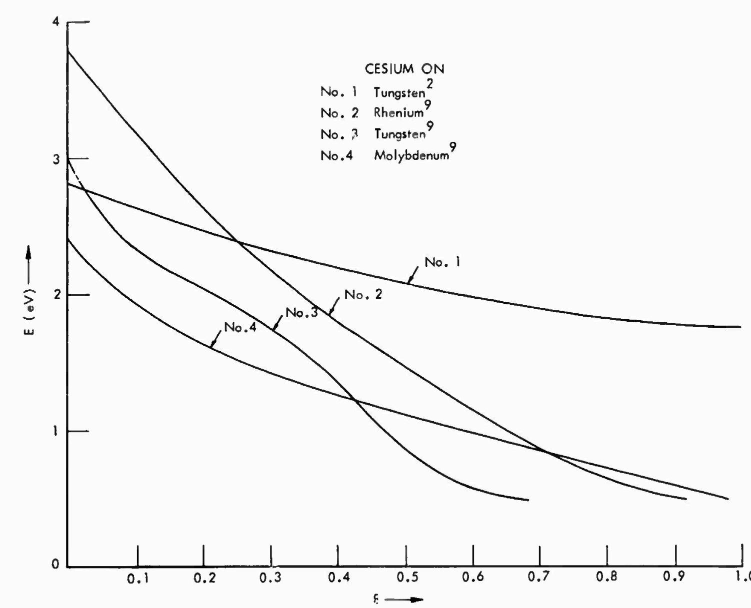

Fig. XVII-25. Atomic heater adsorption vs coverage.

Table XVII-2. Experimental values of relevant potentials and penetration coefficients.

θ	$E(0)$eV	ϕ_e(eV) (measured)	$\Delta\phi_e$(eV)	ϕ_i(eV) (measured)	ϕ_i(eV)	f_a(eV) (measured)	Curve 3 f (computed)	Curve 4 f (computed)
0	1.1	4.62	0	2.05	0	2.82		
.05	.99	4.12	.5	2.46	.41	2.72	.80	.82
.1	.90	3.75	.87	2.76	.71	2.63	.782	.817
.2	.73	3.10	1.52	3.22	1.17	2.47	.77	.77
.3	.58	2.62	2.0	3.58	1.53	2.32	.75	.765
.4	.45	2.20	2.42	3.87	1.82	2.19	.739	.751
.5	.34	1.89	2.73	4.06	2.01	2.09	.733	.737
.6	.26	1.74	2.88	4.13	2.08	1.98	.704	.723
.7	.205	1.70	2.92	4.07	2.02	1.90	.685	.693
.8	.165	1.78	2.84	3.96	1.91	1.84	.655	.673

$$f = \frac{f_a + V_i - \phi_{io} - \phi_e}{\phi_{eo} - \phi_e}. \tag{21}$$

Equation 17 is used with the Taylor-Langmuir measurements of $f_a = f_a(\theta)$ to calculate curve 3. This double agreement increases the confidence placed in the Taylor-Langmuir data. Table XVII-2 lists the numerical values used in the calculations.

The results of Charbonnier and others[8] for the variation of the energy of adsorption with coverage are shown in Fig. XVII-25. From this figure it is seen that there is a much stronger variation of the energy of desorption with coverage; this result is in disagreement with the Taylor-Langmuir data. In Fig. XVII-24, the penetration coefficient as obtained from Eq. 17, with data of Charbonnier, Swanson, Cooper, and Strayer[8] used, is also shown. The values obtained for f versus coverage do not fall between the two limiting cases of mobile and immobile films, as do the values obtained from Taylor-Langmuir data.

J. W. Gadzuk

References

1. I. Langmuir, J. Am. Chem. Soc. 54, 2798 (1932).

2. J. B. Taylor and I. Langmuir, Phys. Rev. 44, 423 (1933).

3. N. S. Rasor and C. Warner III, Correlation of Electron, Ion and Atom Emission Energies, Atomics International Report AI-6799, November 1961.

4. A. J. Kennedy, Adv. Energy Conv. 3, 207-222 (1963).

5. J. Topping, Proc. Roy. Soc. (London) A114, 67 (1927).

6. J. H. de Boer and C. F. Veenemans, Physica 1, 953-965 (October-November 1934).

7. E. N. Carabateas, Analytical Description of Cesium Films on Metal, Report to the National Science Foundation, "Basic Studies of Cesium Thermionic Converters," June 1963.

8. F. M. Charbonnier, L. W. Swanson, E. C. Cooper, and R. P. Strayer, Investigations of the Migration, Desorption, and Voltage Breakdown Properties of Cesium Films on Refractory Electrodes, Field Emission Corporation Report Log. No. 63020, April 1963.

COMMUNICATION SCIENCES

AND

ENGINEERING

XVIII. STATISTICAL COMMUNICATION THEORY*

Prof. Y. W. Lee	J. D. Bruce	D. E. Nelsen
Prof. A. G. Bose	A. M. Bush	A. V. Oppenheim
Prof. M. Schetzen	M. Chessman	R. E. Parente
Prof. H. L. Van Trees	G. Crimi	M. A. Rich
Prof. V. R. Algazi	S. Greenblatt	P. M. Rogo
R. Alter	T. G. Kincaid	M. J. Schaffer
R. F. Bauer	D. C. Kurtz	D. W. Steele
C. J. Boardman		C. I. M. Uchoa

RESEARCH OBJECTIVES

This group is interested in a variety of problems in statistical communication theory. Our current research is concerned primarily with the following problems:

1. Work continues on the analysis and application of the "Two-State Modulation System" that was first described in Quarterly Progress Report No. 66 (pages 187-189). A static analysis of the system has been made, and work now in progress on the dynamic analysis is directed toward both control and power-amplification applications.

2. During the past year algorithms have been developed whereby optimum nonuniform quantizers can be designed when the quantizer input is either a signal or a signal contaminated by noise. This study will continue with emphasis placed upon the evaluation of these optimum quantizers. The effects of linear pre-emphasis and post-emphasis on the optimum quantizer will be investigated. Also, attempts will be made to apply algorithms similar to these quantizer algorithms to other forms of nonlinear filtering.

3. The use of Linear Algebra in the analysis and characterization of nonlinear systems is being investigated. This study has led to a generalization of the principle of superposition and a canonical form for systems satisfying this generalized principle.

4. Theoretical work predicts that the threshold level in multidimensional demodulation schemes can be reduced by use of more sophisticated demodulators. Experimental work is being conducted to verify these predictions.

5. The study of the performance of optimum and nonoptimum filters with emphasis on qualitative aspects of their behavior has continued. An investigation is being made of the limits on the performance of nonlinear filters when some of the message characteristics, such as average power, peak power, power spectrum, and so forth, are known.

6. Many physical processes can be phenomenologically described in terms of a large number of interacting oscillators. A theoretical and experimental investigation is being made.

7. A nonlinear system can be characterized by a set of kernels. The synthesis of a nonlinear system involves the synthesis of these kernels. A study of efficient methods for synthesizing these kernels continues.

8. A method for the construction of function generators was reported in Quarterly Progress Report No. 71 (pages 176-178). Work on the method, both theoretical and experimental, is in progress.

9. The central idea in the Wiener theory of nonlinear systems is to represent the output of a system by a series of orthogonal functionals with the input of the system being a white Gaussian process. An attempt is being made to extend the orthogonal representation to other types of inputs that may have advantages in the practical application of the theory.

*This work was supported in part by the National Science Foundation (Grant G-16526), the National Institutes of Health (Grant MH-04737-03), and in part by the National Aeronautics and Space Administration (Grant NsG-496).

10. A study is being made to relate the random variations in the composition of magnetic recording tape to the noise introduced into a signal recorded on the tape. This will involve an experimental study of the variations in the packing density, orientation, and magnetic properties of the Fe_2O_3 particles making up the magnetic coating, in order to verify a theoretical relation between these properties and the noise.

Y. W. Lee

A. GENERALIZED SUPERPOSITION

1. Introduction

The ease of analysis and characterization of linear systems stems primarily from the fact that they satisfy the principle of superposition. Through the use of this principle, the response of a linear system to inputs that are representable as linear combinations of a set of building blocks can be described by its response to each of the building blocks. When the building blocks are impulses, for example, the system is described through the superposition integral; when the building blocks are complex exponentials and the system is time invariant, it is described through its system function.

The principle of superposition in its usual form is a statement of the definition of linearity and hence, by definition, cannot be satisfied by a nonlinear system. It can be generalized, however, in such a way that it encompasses a wide class of nonlinear systems. This report is concerned with a generalization of the principle of superposition, and an investigation of the class of nonlinear systems which obeys this generalized principle. The investigation has been carried out within the framework of linear algebra. Rather than bury the discussion under the formalism of linear algebra, however, we shall give only a general discussion of the approach used and the results obtained. In future reports, details in the analysis will be considered.

2. Homomorphic Systems

Linear algebra deals with linear transformations between vector spaces. The operations of vector addition and scalar multiplication, which impose an algebraic structure on the vector spaces, satisfy the algebraic postulates that we normally associate with addition of time functions and multiplication of time functions by scalars. There are, however, many other operations, which satisfy these same postulates, that can be performed on time functions. Multiplication of time functions, for example, is commutative and associative. Similarly, convolution is a commutative and associative binary operation. Transformations between such vector spaces, although linear in an algebraic sense, may be nonlinear in a more conventional interpretation.

Systems that are characterized by such transformations satisfy a generalized principle of superposition. Specifically, if "o" denotes the binary operation on the inputs and "□" denotes the binary operation on the outputs, then

$$T[v_1(t) \circ v_2(t)] = w_1(t) \;\square\; w_2(t) \tag{1}$$

where

$$T[v_1(t)] = w_1(t),$$

$$T[v_2(t)] = w_2(t),$$

and T is the system transformation. Also, if the combination of an input v(t) with a scalar λ is denoted by $[\lambda_{>} v(t)]$ and the combination of an output w(t) with a scalar λ is denoted by $[\lambda/w(t)]$, then

$$T[\lambda_{>} v(t)] = \lambda/w(t) \tag{2}$$

where

$$T[v(t)] = w(t).$$

If, for example,

$$T[v(t)] = e^{v(t)}, \tag{3}$$

then

$$T[v_1(t)+v_2(t)] = w_1(t)\, w_2(t)$$

and

$$T[\lambda v_1(t)] = [w_1(t)]^{\lambda}$$

for all inputs $v_1(t)$ and $v_2(t)$ and all scalars λ.

Because of the algebraic interconnection between addition and scalar multiplication, scalar multiplication can be interpreted in terms of the addition operation when the scalar is rational. Multiplication by irrational scalars can be taken to be a continuous extension of the definition for rational scalars. Similarly, the operation ">" can be

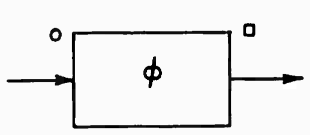

Fig. XVIII-1. Representation of a general homomorphic system.

interpreted in terms of the operation "○". Hence, the operations under which a system satisfies the generalized principle of superposition can usually be summarized by the operations "○" and "□". A system obeying the generalized principle of superposition will be referred to as a homomorphic system. The operation "$\circ$" will be referred to as the input operation and the operation "$\square$" will be referred to as the output operation. A homomorphic system with system transformation ϕ will be denoted as shown in Fig. XVIII-1. For example, a system with transformation

$$T[x] = y = x^k \tag{4}$$

is homomorphic with multiplication as the input and output operation and, hence, would be denoted in the manner shown in Fig. XVIII-2.

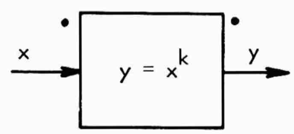

Fig. XVIII-2. Example of a homomorphic system with multiplication as both the input operation and the output operation.

Although the few examples of homomorphic systems which have been given are memoryless, that is, operate only on instantaneous values of the input, this is not a restriction on homomorphic systems in general. The entire class of linear systems, many of which have memory, is homomorphic with addition as both the input and output operation. When the canonical form for homomorphic systems is discussed, it will be clear that many homomorphic systems with memory exist.

The class of homomorphic systems is a very general class and, in fact, can be shown to include any invertible system. To see this, consider a system with an invertible system transformation ϕ. Let $\circ$ denote any input operation consistent with the algebraic restrictions stated previously. Let $\square$, the output operation, be defined as

$$w_1(t) \;\square\; w_2(t) = \phi\left[\phi^{-1}(w_1) \circ \phi^{-1}(w_2)\right], \tag{5}$$

and let

$$\lambda / w(t) = \phi\left[\lambda_{>} \phi^{-1}(w)\right]. \tag{6}$$

It is easily verified that with this choice of output operations the system is homomorphic. Thus any invertible system is homomorphic under any choice of input operation. It can further be shown that for any homomorphic system, the output operation is specified uniquely by the input operation, together with the system transformation. Hence, we are assured that the output operation defined by Eqs. 5 and 6 is the only output operation under which the system is homomorphic, when the input operations have been specified. The construction of the output operation by means of Eqs. 5 and 6 does not necessarily aid in the analysis of homomorphic systems, for it requires a precise characterization of the system transformation. It does, however, allow the construction of examples of homomorphic systems as an aid to developing the theory, and by virtue of the uniqueness of the output operation, examples constructed in this way will not rely on a trivial choice for the output operation.

In summary, then, the class of homomorphic systems includes a wide variety of nonlinear systems. In particular, it includes all invertible systems, as well as many systems that are not invertible.

3. Canonical Representation of Homomorphic Systems

For any choice of input operation o, there exists an invertible homomorphic system with addition as the output operation. This system is determined entirely by the operation o. This fact leads to a convenient and useful representation of homomorphic systems.

Consider a general homomorphic system as shown in Fig. XVIII-1. By virtue of the existence of an invertible homomorphic system with o as the input operation and

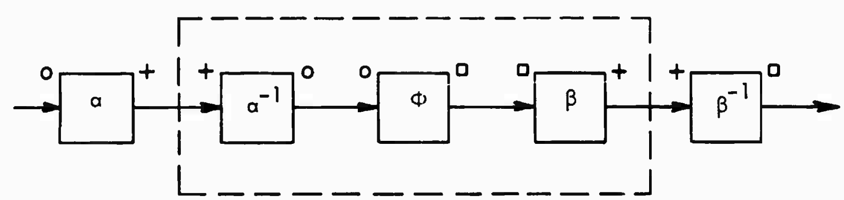

Fig. XVIII-3. Equivalent representation of a general homomorphic system.

addition as the output operation, and an invertible homomorphic system with □ as the input operation and addition as the output operation, the system of Fig. XVIII-1 can be represented in the form of Fig. XVIII-3. The system enclosed in the dotted line, however,

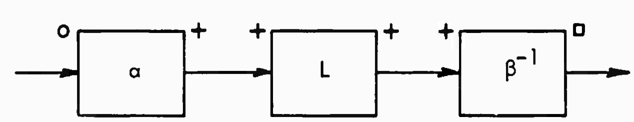

Fig. XVIII-4. Canonical representation of a general homomorphic system.

is a linear system, and thus the system of Fig. XVIII-1 can be represented by the system shown in Fig. XVIII-4. Hence, any homomorphic system can be represented as the cascade of three systems, in which the first and last are dependent only on the input and output operations, respectively, and the second system is a linear system. Furthermore, it is easily verified that for any choice of the linear system the cascade will be a homomorphic system with input operation o and output operation □. Hence, to generate the entire class of homomorphic systems having specified input and output operations, we determine the systems α and β from knowledge of the input and output operations and then consider all choices for the linear system L.

As an example, let us return to the homomorphic system of Fig. XVIII-2. The system defined by Eq. 3 is an invertible homomorphic system with addition as the input operation and multiplication as the output operation. Hence, its inverse, the natural logarithm, is an invertible homomorphic system with multiplication and addition as the input and output operations, respectively. It should be clear that the system of Fig. XVIII-2 can be represented as shown in Fig. XVIII-5. The entire class

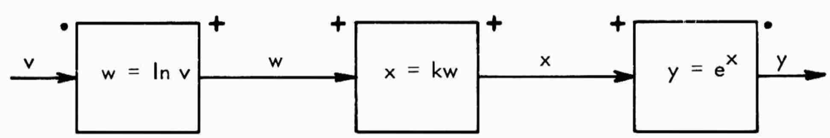

Fig. XVIII-5. Representation of the system of Fig. XVIII-2 in the canonical form of Fig. XVIII-4.

of homomorphic systems with multiplication as both the input and output operation can be generated by replacing the amplifier of gain K by other linear systems.

The canonical representation of Fig. XVIII-4 is effectively a substitution of variables which reduces a homomorphic system to a linear system. The substitution of variables is dependent only on the input and output operations of the homomorphic system. It can be shown that if the system α is memoryless, then the operation o is memoryless, that is, it is an operation on the instantaneous values of the inputs. Similarly, if β is memoryless, then the output operation □ must also be memoryless. Furthermore, it can be shown that if o and □ are memoryless operations, then all of the memory in the homomorphic system can be concentrated in the linear portion.

4. Systems with Nonadditive Feedback

Consider a feedback system in which the forward and reverse paths contain homomorphic systems and the signal fed back is combined with the input according to some binary operation o, as shown in Fig. XVIII-6. The output operation of ϕ_1 and the input operation of ϕ_2 are identical. Also, the input operation of ϕ_1 and the output operation of ϕ_2 are taken to be the same as o. If ϕ_1 and ϕ_2 are replaced by their canonical representations, the system of Fig. XVIII-7 results. Because α and α^{-1} are homomorphic, some elementary block diagram manipulations permit the system of Fig. XVIII-7 to be

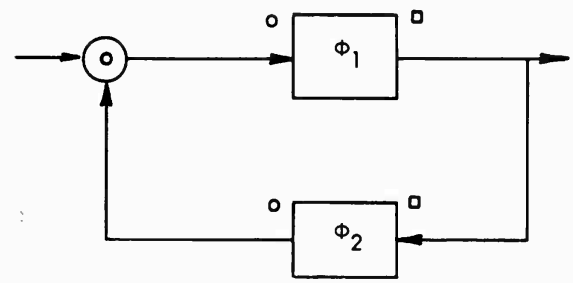

Fig. XVIII-6. Homomorphic feedback system with nonadditive feedback.

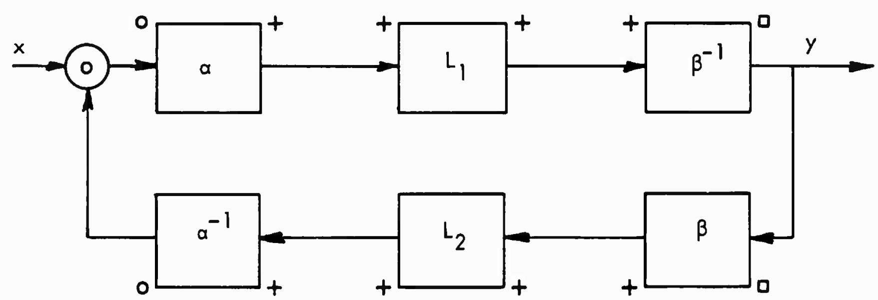

Fig. XVIII-7. Equivalent representation of a feedback system having the form shown in Fig. XVIII-6.

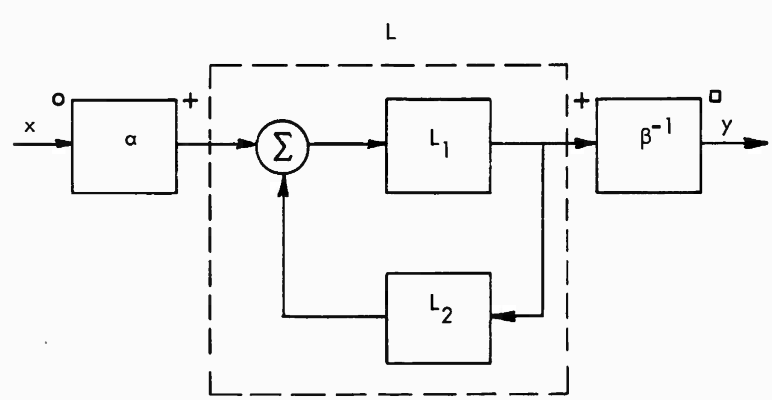

Fig. XVIII-8. Canonical representation of a homomorphic feedback system with nonadditive feedback.

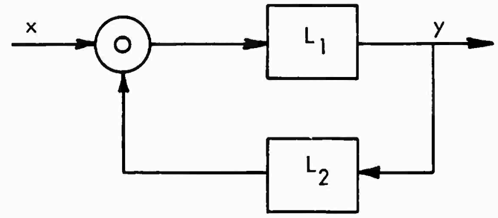

Fig. XVIII-9. General feedback system with linear elements and nonadditive feedback.

redrawn as shown in Fig. XVIII-8. Hence, the system of Fig. XVIII-6 is homomorphic with the same input and output operations as ϕ_1. Furthermore, the linear system L in its canonical representation is an additive feedback system with the linear portion of ϕ_1 in the forward path and the linear portion of ϕ_2 in the feedback path.

If the systems in the forward and feedback paths are linear systems but the feedback operation is not addition, then the nonlinearity in the system cannot be removed from the feedback loop as it could in the system of Fig. XVIII-6. The notion of homomorphic feedback systems, however, does permit representation of this type of feedback system as an additive feedback system with nonlinearities in the forward path. Specifically, consider the feedback system of Fig. XVIII-9. It was stated previously that there will always exist an invertible homomorphic system with "o" as the input operation and addition as the output operation. If we denote this system by γ, then the system of

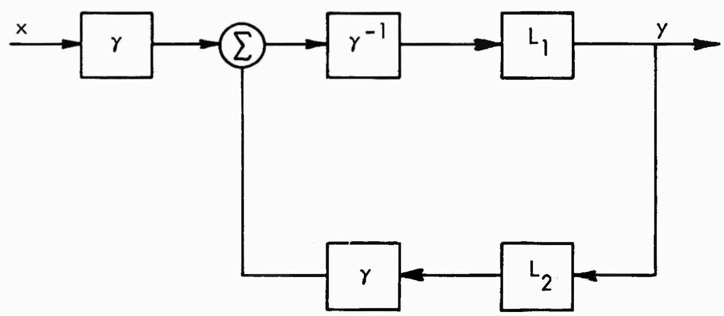

Fig. XVIII-10. Equivalent representation of the feedback system of Fig. XVIII-9.

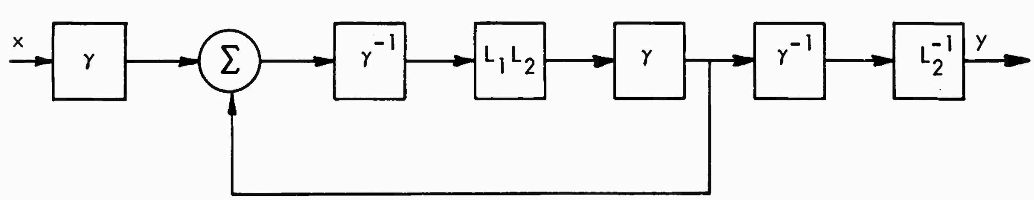

Fig. XVIII-11. Representation of a feedback system having the form shown in Fig. XVIII-9.

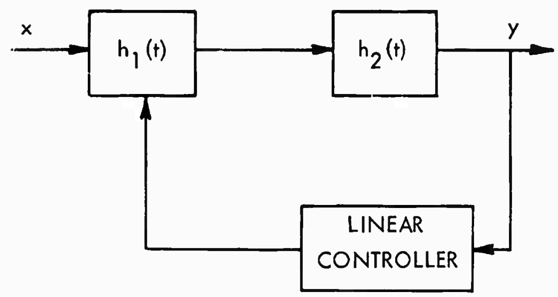

Fig. XVIII-12.
Example of a feedback system of the form shown in Fig. XVIII-9.

Fig. XVIII-9 can be represented in the form of Fig. XVIII-10. If the linear system L_2 is invertible, then the block diagram of Fig. XVIII-10 can be manipulated into the form of Fig. XVIII-11. The essential feature in the representation of Fig. XVIII-11 is that a system with nonadditive feedback has been represented in a more conventional form.

As an example, we might consider the system shown in Fig. XVIII-12. The systems $h_1(t)$ and $h_2(t)$ are linear systems. The impulse response $h_1(t)$ is linearly dependent on the output $y(t)$. This represents a feedback system in which convolution is the binary feedback operation. Hence, this system can be represented in the form of Fig. XVIII-9, with $\circ$ taken to be convolution.

5. Conclusions

The results obtained to date concerning homomorphic systems seem to indicate that this is a useful means of classifying many nonlinear systems. The canonical representation of these systems permits their investigation in terms of linear systems, for which many analytical tools are available. It is difficult to predict the areas in which homomorphic systems will assume practical significance. It is hoped that as the theory progresses its engineering applications will become clear.

A. V. Oppenheim

B. ENERGY DISTRIBUTION IN TRANSIENT FUNCTIONS

In this report, we shall present some results that have been obtained concerning the distribution of energy in transient functions, $f(t)$, which are zero for $t < 0$. The Laplace transform, $F_1(s)$, of the transient function $f_1(t)$ is

$$F_1(s) = \int_0^\infty f_1(t)\, e^{-st}\, dt, \tag{1}$$

in which $s = \sigma + j\omega$. Also, the partial energy, which is the energy in the first τ seconds of $f_1(t)$, is

$$E_1(\tau) = \int_0^\tau |f_1(t)|^2 \, dt. \tag{2}$$

We assume that $F_1(s)$ contains a zero at $s = p_1$ so that it can be written as

$$F_1(s) = [s-p_1] \, G(s). \tag{3}$$

If the zero in the s-plane is moved to a new position at $s = p_2$, the transient function $f_2(t)$ results for which

$$F_2(s) = [s-p_2] \, G(s). \tag{4}$$

The results that we shall present in this report concern the difference between the partial energies of $f_1(t)$ and $f_2(t)$ for the case in which the zero in the s-plane is moved parallel to the σ axis. For our derivations, we shall consider only those transient functions for which

$$f_1(0+) = \lim_{s\to\infty} sF_1(s) < \infty \tag{5a}$$

and

$$f_1(\infty) = \lim_{s\to 0} sF_1(s) = 0. \tag{5b}$$

To obtain an expression for the difference of the partial energies, we let $g(t)$ be the inverse transform of $G(s)$. Equation 3 then can be expressed in the time domain as

$$f_1(t) = \frac{d}{dt} g(t) - p_1 g(t). \tag{6}$$

Thus the square of the magnitude of $f_1(t)$ is

$$|f_1(t)|^2 = f_1(t)\,\overline{f_1(t)} = |g'(t)|^2 + |p_1 g(t)|^2 - p_1 g(t)\,\overline{g'(t)} - \overline{p}_1 \overline{g(t)}\, g'(t), \tag{7}$$

in which the prime indicates the derivative and the bar indicates the complex conjugate of the function. In a similar manner, the square of the magnitude of $f_2(t)$ from Eq. 4 is

$$|f_2(t)|^2 = |g'(t)|^2 + |p_2 g(t)|^2 - p_2 g(t)\,\overline{g'(t)} - \overline{p_2}\,\overline{g(t)}\, g'(t). \tag{8}$$

Consequently,

$$|f_1(t)|^2 - |f_2(t)|^2 = \left[|p_1|^2 - |p_2|^2\right] |g(t)|^2 + 2\,\mathrm{Re}\left\{[p_2-p_1]\, g(t)\,\overline{g'(t)}\right\}, \tag{9}$$

in which Re means the real part of the quantity within the braces. Since the zero is moved parallel to the σ axis, we have $p_2 - p_1 = \sigma_2 - \sigma_1$ and $|p_1|^2 - |p_2|^2 = \sigma_1^2 - \sigma_2^2$, so that Eq. 9 can be written

$$|f_1(t)|^2 - |f_2(t)|^2 = \left[\sigma_1^2 - \sigma_2^2\right] |g(t)|^2 + 2(\sigma_2 - \sigma_1) \operatorname{Re} \{g(t) \overline{g'(t)}\}$$

$$= \left[\sigma_1^2 - \sigma_2^2\right] |g(t)|^2 + (\sigma_2 - \sigma_1) \frac{d}{dt} |g(t)|^2. \tag{10}$$

The difference between the partial energies of $f_1(t)$ and $f_2(t)$ is

$$E_1(\tau) - E_2(\tau) = \left(\sigma_1^2 - \sigma_2^2\right) \int_0^\tau |g(t)|^2 \, dt + (\sigma_2 - \sigma_1) \int_0^\tau \frac{d}{dt} |g(t)|^2 \, dt$$

$$= \left(\sigma_1^2 - \sigma_2^2\right) A + (\sigma_2 - \sigma_1) B, \tag{11}$$

in which the partial energy of $g(t)$, A, is

$$A = \int_0^\tau |g(t)|^2 \, dt > 0 \tag{12a}$$

and

$$B = |g(\tau)|^2 \geqslant 0. \tag{12b}$$

As a function of σ_2, Eq. 11 is the equation of a parabola that crosses the σ_2 axis at the points $\sigma_2 = \sigma_1$ and $\sigma_2 = \frac{B}{A} - \sigma_1$. The parabola has a maximum at $\sigma_2 = \frac{B}{2A}$, at which point $E_1(\tau) - E_2(\tau) = A\left[\frac{B}{2A} - \sigma_1\right]^2$. Figure XVIII-13 is a plot of $E_1(\tau) - E_2(\tau)$ vs σ_2 for

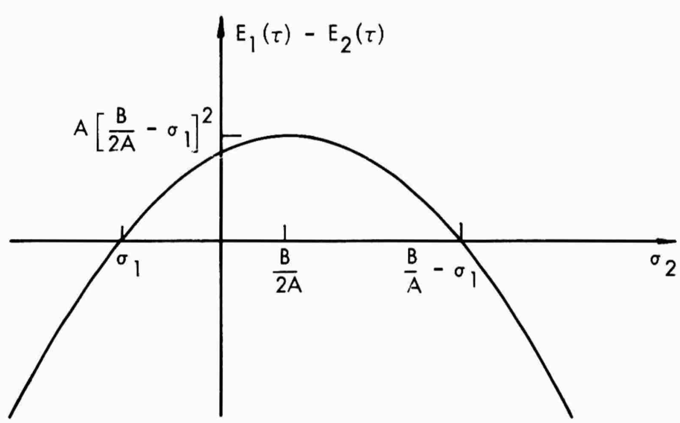

Fig. XVIII-13. Difference of the partial energies versus σ_2.

$\sigma_1 < 0$. We observe from Fig. XVIII-13 that $E_2(\tau) < E_1(\tau)$ for σ_2 in the range $\sigma_1 < \sigma_2 < \frac{B}{A} - \sigma_1$, and that $E_2(\tau)$ is a minimum for $\sigma_2 = \frac{B}{2A} \geqslant 0$. Thus for $p_1 \neq 0$ the total energy of $f_2(t)$ which is $E_2(\infty)$ is a minimum for $\sigma_2 = 0$ because $B = 0$ at $\tau = \infty$. We show that it is a minimum from (3), (5b), and (12b) and the fact that $p_1 \neq 0$, for which we have

$$\lim_{\tau \to \infty} g(\tau) = \lim_{s \to 0} sG(s) = \lim_{s \to 0} \frac{s}{s - p_1} F_1(s)$$

$$= -\frac{1}{p_1} \lim_{s \to 0} sF_1(s) = 0.$$

This result implies that if the s-plane zeros of a transform, F(s), are moved parallel to the σ axis, then, of all the corresponding transient functions, the transform of the one with the minimum total energy has every one of its zeros on the $j\omega$ axis.

Let us now consider the special case for which $\sigma_2 = -\sigma_1 > 0$. For this case, $|F_1(\omega)| = |F_2(\omega)|$ and, consequently, the energy-density spectrum of $f_1(t)$ is identical with that of $f_2(t)$. Then, from Eq. 11, the difference of their partial energies is

$$E_1(\tau) - E_2(\tau) = -2\sigma_1 B$$

$$= -2\sigma_1 |g(\tau)|^2 \geq 0, \tag{13}$$

since we have assumed that $\sigma_1 < 0$. We thus note that of all transient functions with the same energy-density spectrum, the transform of the one with the greatest partial energy has all its zeros in the left half of the s-plane and the transform of the one with the smallest partial energy has all its zeros in the right half of the s-plane.

As another application of this last result, let $F_2(s) = F(s) \dfrac{s - p_1}{s + p_1}$ and $F_1(s) = F(s) \dfrac{s + p_1}{s + p_1} = F(s)$. Then $E_2(\tau) \leq E_1(\tau)$. Thus, in general, the partial energy of the transient input of an all-pass system is greater than that of the output. For example, the partial energy of the Laguerre functions, $l_n(t)$, is a monotonically decreasing function of n, since the Laplace transform of $l_n(t)$ is

$$L_n(s) = \sqrt{2p} \frac{(p-s)^n}{(p+s)^{n+1}} = \frac{p - s}{p + s} L_{n-1}(s).$$

Since the total energy of each Laguerre function is one, this result means that the energy of successive Laguerre functions is delayed, and this delay is a monotonically increasing function of n.

M. Schetzen

XIX. PROCESS ANALYSIS AND SYNTHESIS*

Dr. M. V. Cerrillo
Prof. H. J. Zimmermann
J. S. MacDonald
Rita K. Toebes

RESEARCH OBJECTIVES

For the past several years the aim of this research has been to seek theoretical descriptions of some of the subjective aspects of communication. Experimental verification of the plausibility of theoretical results is also being pursued.

The theory of groups and the generalized concepts of symmetry are being used in an attempt to describe certain aspects of perception and recognition. It is assumed that the structure of such processes can be described by a set of elements and by a set of rules that operate on these elements.

The processes now being investigated include perception of brightness, color, depth, and form. Handwriting is also being studied by methods aimed at extending the work of Dernier van der Gon. A rudimentary simulator of the handwriting process has been constructed, and an improved version is being completed. Work in the immediate future will comprise the use of this simulator to test the validity of the principles of simulation and to attempt to describe some of the principles involved in the recognition of handwriting. Work is also being done on the subjective structure of music.

Mathematical work includes the investigation of the complete subgroup structure of the symmetric group of degree five, the theory of uniformization of curves and the theory of moments in connection with the algebraic domain.

A tabulation of the extended Lommel functions is being prepared, together with graphical representations. These results are not directly related to the investigations cited above, but are based on previous research.

M. V. Cerrillo

A. HANDWRITING SIMULATION

This project has its origin in a paper published by Dernier van der Gon and others,[1] in which a very simple system for the simulation of fast cursive handwriting was discussed. The present research seeks to extend the results reported by van der Gon. The van der Gon system is based on four postulates that are assumed to hold for fast cursive handwriting. (i) Fast handwriting is done without instantaneous position feedback. (ii) Writing movements are caused by two independent groups of muscles. Each group governs movements to and fro in one direction. The directions of these two groups are more or less perpendicular. (iii) These two pairs of antagonistic groups of muscles alternately apply forces to hand and pencil. The hand-pencil combination can be considered as a mass with viscous friction. (iv) After its onset, the force rises to a certain fixed value and remains more or less constant. The duration of application of this force is related to the magnitude of the writing movement. Thus different lengths of

*This work was supported in part by the National Science Foundation (Grant G-16526), the National Institutes of Health (Grant MH-04737-03), and the National Aeronautics and Space Administration (Grant NsG-496).

strokes in uninterrupted handwritten characters are caused by a different time of application, and not by a different magnitude of force. Van der Gon reported that an

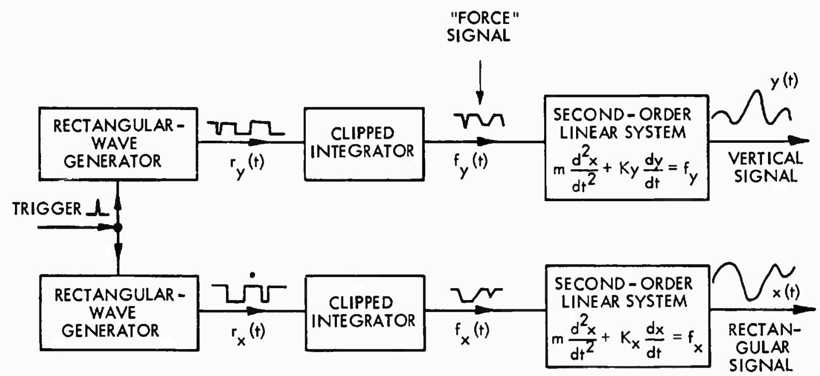

Fig. XIX-1. Block diagram of simulator.

electromechanical device based upon these principles gave an oscillographic output that could be adjusted to match a given signature quite closely.

Figure XIX-1 is a block diagram of van der Gon's simulator. The rectangular wave generators simulate the force waveforms in accordance with postulate (iv). They share a common trigger, but are otherwise independent. They have provision for adjustment of the position in time of all transitions of the wave. Each rectangular wave generator is followed by a clipped integrator which simulates the nonzero rise-time of the muscles. The positive and negative clipping levels on the integrator can be adjusted independently, but there is no provision for providing different amplitudes of the segments of the wave. These in turn are followed by second-order linear systems in accordance with postulate (iii). This second-order system is represented by the differential equation

$$m_x \frac{d^2x}{dt^2} + k_x \frac{dx}{dt} = f_x(t), \tag{1}$$

where x is the displacement in one of the independent directions, f_x is the force acting in this direction, and m_x and k_x are the associated mass and friction constants, respectively. There is a similar equation that is assumed for y-displacement. The output of the entire system is displayed on an oscilloscope with one of the independent channels controlling vertical deflection, and the other channel controlling horizontal deflection.

The first step in the present investigation was to build an all-electronic simulator having essentially the same block diagram as Fig. XIX-1. The only change in our system is that the clipped integrator is replaced by a first-order lag network, giving the "force" an exponential rather than linear rise.

This device was used to generate simulated handwriting. A typical example is shown in Fig. XIX-2b. Figure XIX-2a is the original handwriting that the simulated output of

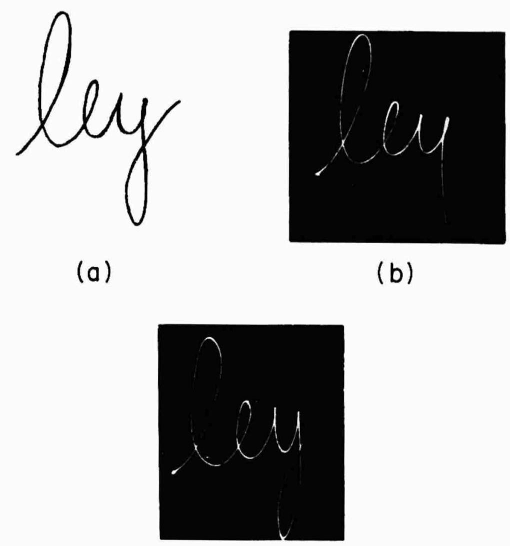

(a) (b)

(c)

Fig. XIX-2. (a) Original sample.
(b) Simulated sample.
(c) Simulated sample with tail of "y" completed.

Fig. XIX-2b is supposed to match. It should be emphasized here that the matching procedure as it now stands is simply one of trial and error; the transitions in the rectangular waves are adjusted to give the best possible match between the output of the simulator and the sample.

The simulation is quite successful except for the tail of the "y". It was found that the last stroke on the tail of the "y" could not be made to have the same shape as the sample without changing the rest of the work so that it did not agree with the sample. Figure XIX-2c presents an attempt to compromise between matching the "y" and matching the "le". It is easy to see that this sample fails quite badly, particularly on the tail of the "y". Figure XIX-3 shows the rectangular waves and the linear-system outputs pertinent to the sample of Fig. XIX-2b.

The example shown in Fig. XIX-3 indicates that the principles of the simulator, though compatible with the production of handwritinglike outputs, are not completely compatible with an arbitrary sample of cursive script. By constructing a system that provides for independent variation of the amplitude of the segments of the "force" waveform, as well as for their duration (violates postulate (iv)), it was found that the "y"

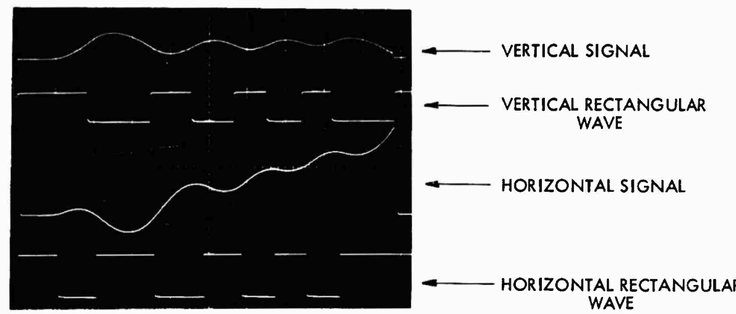

Fig. XIX-3. System outputs for the sample in Fig. XIX-2b.

in the example above could be matched quite well. The result appears in Fig. XIX-4. Only the "y" appears because the new rectangular wave generator as it existed when the sample shown in Fig. XIX-4 was made had only enough sections to generate approximately one letter at a time. A complete rectangular wave generator permitting variable amplitude and duration of individual "force" segments has been designed and is under construction at the present time.

Fig. XIX-4. Improved simulation of "y" in Fig. XIX-2a.

The simulation of errors commonly made in handwriting is interesting. Examples using the word "in" appear in Fig. XIX-5. In these two samples, the only difference between them is the positions of the transitions of the rectangular waves. The linear systems are the same in both samples.

The discussion above opens the question of modifying van der Gon's postulate (iv). Upon completion of the above-mentioned rectangular wave generator, simulations will be carried out to explore this question further. Also, there does not seem to be any reason to assume that the independent directions of the force are perpendicular, that they are constant over a sequence of several words or that the angle between them and the writing-line remains constant. Equipment is now being designed for a system to allow simulation of these cases.

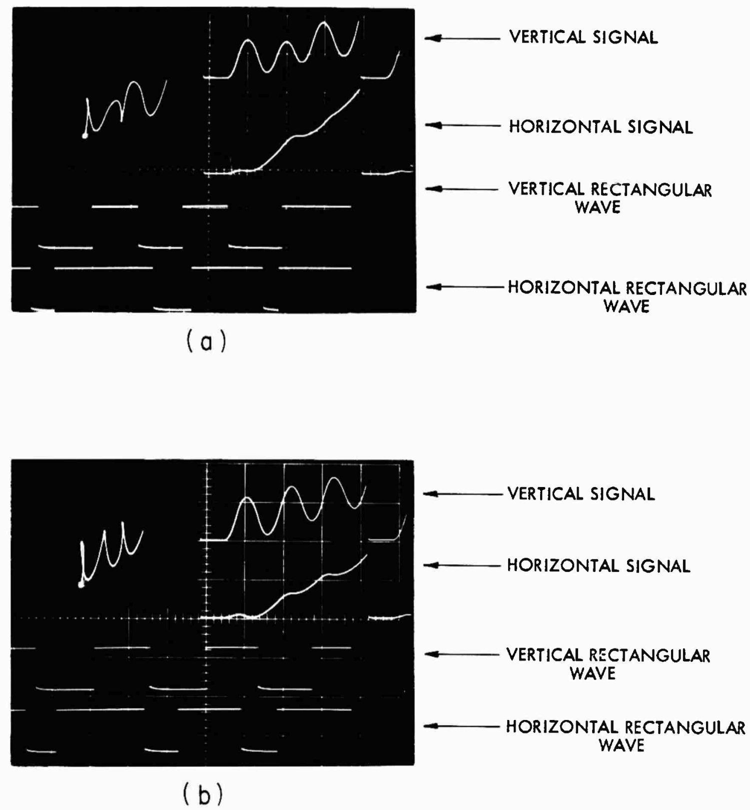

Fig. XIX-5. Two simulations of the word "in" obtained by varying only the transitions in the rectangular waves. Time scales for vertical and horizontal signals differ from those for the rectangular waves.

Work is also progressing on a system to analyze actual handwriting in terms of the model assumed in this simulation.

J. S. MacDonald

References

1. J. J. Dernier van der Gon, J. Ph. Thuring, and J. Strackee, A Handwriting Simulator, Phys. Med. Biol. 6, 407-414 (January 1962).

XX. PROCESSING AND TRANSMISSION OF INFORMATION*

Prof. R. M. Fano
Prof. R. G. Gallager
Prof. F. C. Hennie III
Prof. T. S. Huang
Prof. I. M. Jacobs
Prof. C. L. Liu
Prof. A. M. Manders
Prof. B. Reiffen
Prof. W. F. Schreiber
Prof. C. E. Shannon
Prof. I. C. Stiglitz
Prof. O. J. Tretiak
Prof. J. M. Wozencraft
E. R. Berlekamp
D. G. Botha
J. E. Cunningham
S. M. Diamond
J. R. Disbrow
H. Dym
P. M. Ebert
D. D. Falconer
E. F. Ferretti
G. D. Forney, Jr.
R. E. Grabowski
D. N. Graham
N. Gramenopoulos
U. F. Gronemann
G. S. Harlem
J. L. Holsinger
K. Ikushima
Y. Iwadare
C. W. Niessen
R. Pilc
E. A. Prange
J. E. Savage
J. R. Sklar
K. D. Snow
W. R. Sutherland
M. G. Taylor
H. L. Yudkin

RESEARCH OBJECTIVES

1. Picture Processing

Work is continuing on the processing of pictures by means of computers. The broad objective of this work is to elucidate the fundamental properties of vision as they apply to image transmission and reproduction. Among the more specific objectives are the design of efficient image-transmission systems, and the development of devices capable of performing some "human" operations, such as noise reduction, image detection, and quality improvement.

Progress during the past year toward reaching these objectives has been made in studies pertaining to the visibility of noise of known spectral content, the improvement of image quality through linear filtering, and the synthesis of motion-picture sequences from a small portion of the information of each frame. Studies are continuing on two-dimensional image synthesis techniques for improving transmission efficiency.

W. F. Schreiber

2. Communications

Preliminary work on the transmission of vocoded speech has emphasized the need for an experimental vocoder suitable for use in conjunction with various modulation and coding schemes. Such a vocoder must be flexible in its configuration. Accordingly, the IBM 7090 is being programmed, through use of the BTL BLD-DI compiler, to provide a general-purpose speech-processing facility. Various techniques for the reduction of redundancy will be used, together with error-correcting codes, in an effort to improve voice communication over noisy channels.

Adequate analytical treatment of the performance of encoding and decoding schemes over noisy time-variant channels is very difficult. Theoretical investigations of this work continue, but it is certain that experimental evaluation of the ideas generated by such studies will be necessary. To this end, a channel characterized by acoustic reflection from air bubbles in water has been constructed in the laboratory, and is now being evaluated. It appears that most of the communication difficulties inherent in channels with a time-bandwidth product greater than unity are exhibited by this acoustic channel.

---

*This research was supported in part by the National Science Foundation (Grant G-16526), the National Institutes of Health (Grant MH-04737-03), the National Aeronautics and Space Administration (Grant NsG-496); and in part by Purchase Order DDL BB-107 with Lincoln Laboratory, a center for research operated by Massachusetts Institute of Technology, with the support of the U.S. Air Force under Contract AF 19(628)-500.

In order to complete the laboratory facilities needed to support experimental communication study, a flexible encoder-decoder is required. Special-purpose adjuncts, added to a general-purpose digital computer, would provide an efficient compromise between speed and flexibility. The conceptual design of these ancillary devices, and the evaluation of the over-all performance resulting from their use, is under way.

In addition to the experimental program outlined above, fundamental theoretical work in the processing and transmission of information continues on a broad front. Significant progress has been made recently on the bounding of the error performance achievable by means of coding. One of the most important results is new insight into the interrelation of coding and modulation, and the solution of certain related problems has already been forthcoming. A considerable amount of further work in this direction is now in progress.

J. M. Wozencraft

3. Digital Machines and Automata

Work continues on the basic capabilities of digital machines and automata. Two primary objectives of this work are: to gain a better understanding of the relationship between a given processing problem and the amounts of equipment and computation time that it requires; and to achieve description and synthesis of digital processors in the form of arrays of identical building blocks.

F. C. Hennie III

A. PICTURE PROCESSING

1. THE SUBJECTIVE EFFECTS OF PICTORIAL NOISE

A study has been made of the subjective effects of the class of independent additive rectangular lowpass Gaussian noises.[1] Three original pictures, varying in the amount of detail, were used. The general shapes of the isopreference surfaces in σ-k_1-k_2 space, where σ is the rms value, and k_1 and k_2 are the bandwidths of the noise in the horizontal and vertical directions, respectively, were found to be similar for all three pictures. In particular: (a) If we keep σ constant and go radially outward from the origin in the k_1-k_2 plane, the objectionable noise will increase, reach a maximum, then fall off. (b) Noises with vertical streaks are more objectionable than those with horizontal streaks.

The details of the isopreference surfaces, however, depend very much on the original picture. Generally speaking, noises that contain frequencies similar to those of the picture are less annoying.

The agreement among the observers was rather good. They were more in agreement as to the effect of changes in noise power than in noise bandwidths.

If objectionable noise is additive, then we may deduce that for the class of noises whose power density spectra are symmetrical with respect to both horizontal and vertical frequencies, the weighting function in the integral representing objectionable noise is similar in shape to the isopreference surface mentioned above.

T. S. Huang

References

1. T. S. Huang, Pictorial Noise, Sc.D. Thesis, Department of Electrical Engineering, M.I.T., August 30, 1963.

2. CODING COLOR PICTURES

A computer-simulation study of efficient coding for color pictures has been undertaken.[1] Two typical color transparencies were resolved into three primaries, sampled in a square array and recorded digitally on magnetic tape. The computer program transformed these data into luminance and chrominance quantities, performed certain parameter modifications, reconverted them into primary-color quantities and wrote them on an output tape. The parameters that were modified were the effective number of samples per picture and the number of quantum values each for the luminance and for the chrominance. The output tape was played back through the recorder-reproducer to produce images of the coded pictures on the face of the cathode-ray tube, which were photographed through appropriate filters on color film. The resultant transparencies were later viewed and compared by a number of observers to determine the absolute and relative quality achievable with the various codes (as affected by the variously modified parameters). Also, a test was run with a large number of observers to determine the relative recognizability of objects in one of the pictures when variously coded in color or monochromatically.

The results show that while the best monochromatic reproduction achievable in the experimental system requires a transmission rate of 5 bits per sample (with logarithmic quantization used), the best color reproduction in the same system (with the same luminance sample density) requires an average of 5.55 bits per sample. This is achieved by quantizing chrominance to approximately 1000 values and reducing the spatial density of chrominance samples to 1/18 of that of luminance. The results also indicate that the luminance sample density of a color picture can be reduced by a factor of from 1.5 to 18, or more, and still be equal in quality to the monochromatic reproduction, the amount depending on the subject matter and on the criterion used for comparison.

Two major conclusions were drawn from this study. (i) A normal monochromatic picture can be converted into a full color picture of the same apparent sharpness by transmitting additionally only a fraction of a bit per sample. (ii) For many purposes, inclusion of color may result in an over-all lower transmission rate requirement than would the same picture coded monochromatically; for some purposes, such as recognizing objects, this reduction can be substantial.

U. F. Gronemann

References

1. U. F. Gronemann, Coding Color Pictures, Ph.D. Thesis, Department of Electrical Engineering, M.I.T., January 13, 1964.

B. EXPERIMENTAL FACILITY FOR SEQUENTIAL DECODING

This report presents progress on a study concerning the advisability of constructing special-purpose digital equipment to work in conjunction with an IBM 7094 computer for the purpose of aiding the investigation of sequential decoding processes. We hope that suitable equipment can be developed which will be adaptable to a large class of channels and modulation processes and will increase the speed with which information bits may be decoded by a factor of 10, or more, over that possible with computer-simulation programs.

1. Motivation

The need for an experimental facility for the study of sequential decoding is quite obvious. For any but the simplest channel, analytic results are hard to obtain because of the mathematical difficulties that arise. Experimental results can be used to great advantage in combination with the analytic results that are now available to extend our understanding of sequential decoding processes to the more complicated channels found in the real world.

Questions of interest at present are: What and how much information should be saved at the receiver for each use of the channel? For example, if one of M orthogonal signals is sent each time that the channel is used, then there will be M signal values (from the M matched filters) available at the receiver. If all of these values were saved for use later in the tree-search algorithm, an excessive amount of storage would be required, and computations involving this many numbers would be complicated. Various alternatives suggest themselves: (a) Save only the information as to which of the M signals was largest. (b) Save an ordered list of the ℓ largest signals (which one was largest, which was second largest, and so forth). (c) Save an ordered list as in (b), but also include the values of the signals. (d) Save the largest signal, plus the sum of the squares of all of the other signal values. Clearly, the less information retained about each use of the channel, the lower will be the effective $R_{\text{comp.}}$. Experimental results would determine just how much $R_{\text{comp.}}$ is lowered by each of the suggested decoding procedures.

2. Machine Organization

From consideration of the sequential decoding process as described by Fano,[1] we can break up the proposed special-purpose machine into several parts. (See Fig. XX-1.)

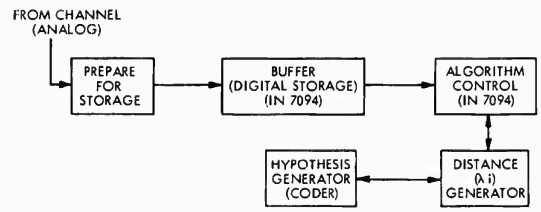

Fig. XX-1. Block diagram of sequential decoder.

Assume that the machine is to be working with a real channel, or at least that input information is in analog form. One section of the machine must abstract from the analog input signal a certain amount of digital information about each use of the channel (that is, for each baud). The proposed machine (as the design is now formulated) would prepare an ordered list of the 16 largest of the M channel symbols, together with the values of these 16 signals and the sum of the squares of all M signals. (Remember that the larger the output of the matched filter, the greater the probability that symbol was sent, for orthogonal signals on a memoryless channel.) Any part of the prepared list could be saved in the buffer memory for use later in the tree-search algorithm. A list of the type just described would allow all of the previously suggested decoding methods to be tested. We would place a limit of 256 on M.

The next question is the required size of the buffer memory, which would be part of the memory of the IBM 7094 computer. If the decoder is to work with a channel that produces bauds "on call," then it need only be large enough to store the information associated with a number of bauds corresponding to approximately 3 constraint lengths (in information bits), so as to allow the machine to search back that far. The experimental facility would normally run with an "on call" channel, since this would result in the fastest decoding rate. Waiting-line behavior could be simulated very easily with such a channel.

The execution of a search algorithm like Fano's requires two quantities that we may think of as being supplied by two different sections of the machine.

First is the hypothesis generator, which is a replica of the convolutional encoder; constraint lengths of up to 100 bits could be handled. The hypothesis generator would generate the signals corresponding to all of the branches stemming from a node in the tree. It would be able to handle up to 4 information bits/baud (corresponding to 16 branches/node) and be able to put out up to 16 check bits/node. Information bits plus check bits then specify one of the M channel symbols, or a series of channel symbols.

The second piece of equipment must generate a number (for each hypothesis signal at a node) which is the "distance" between the received signal and that particular hypothesis signal. This "distance" (λ_i in Fano's notation) is related to Pr $(\rho|X)$, where ρ is the information saved about this baud and X is the particular hypothesis signal. This equipment must return to the search algorithm control the λ of the n^{th} most likely hypothesis, where n is a parameter specified by the search algorithm.

The last section of the sequential decoder is the search-algorithm control. This section is concerned with the decision making and bookeeping required for the execution of the algorithm. We have left this part of the machine as a program in the IBM 7094 computer to anticipate changes in the algorithm, changes to make use of two-way strategies, and changes to allow various amounts of information to be printed out concerning the behavior of the decoder, the amount depending on the particular experiment being run.

The sequential decoding system described briefly above has been designed in detail, and it has been estimated that it would be able to decode approximately 3500 nodes per second. This speed is calculated for the case of an "on call" channel and a tree structure of one baud per branch. It is almost independent of alphabet size and number of branches per node. This speed is in excess of 10 times the speed of an entirely programmed decoder working with the same input channel.

3. Channel Simulation

For the equipment that has been designed, the channel is required to deliver one baud in M microseconds (M is the number of channel symbols). The outputs of the matched filters are converted to 7-bit binary numbers. Thus, in effect, the channel delivers 7 megabits/second to the decoder. This rate is substantually larger than IBM tape machines can handle, so we must eliminate the possibility of generating a channel output at some distant location, recording it on tape, and then at a later time playing it back into the decoder. We are lead to the necessity of designing "on-line" channel simulators. Investigations are being made into the equipment necessary to simulate channels of interest. Designs for coherent and incoherent detection of orthogonal signals in white Gaussian noise on constant and Rayleigh-fading channels have been completed thus far.

C. W. Niessen

References

1. R. M. Fano, A heuristic discussion of probabilistic decoding, IEEE Trans., Vol. IT-9, No. 2, pp. 64-74, April 1963.

C. AN ERROR BOUND FOR FIXED TIME-CONTINUOUS CHANNELS WITH MEMORY

The author has previously demonstrated[1] that the channel in Fig. XX-2 can be represented by the vector equation

$$\underline{y} = [\sqrt{\lambda}]\,\underline{x} + \underline{n}, \tag{1}$$

where $\underline{x}$, $\underline{y}$, and $\underline{n}$ are column vectors representing the channel input, output, and additive noise, respectively, the matrix $[\sqrt{\lambda}]$ is diagonal, and the components of $\underline{n}$ are statistically independent and identically distributed Gaussian random variables. This report

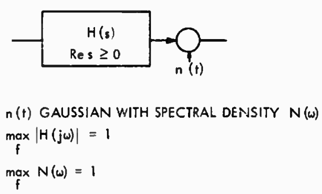

Fig. XX-2. Gaussian channel with memory.

presents an upper bound to the probability of error for this channel based on the representation of Eq. 1 and a slight generalization of a bound derived previously by Gallager.[2]

1. Vector Dimensionality Problem

Before proceeding with the derivation of the error bound, it is necessary to consider in detail the dimensionality of the vectors involved. In deriving the representation of Eq. 1 it was shown[1] that the basis functions used in defining $\underline{x}$ are complete in the space of all $\mathscr{L}_2(0,T)$ signals, that is, in the space of all finite-energy signals defined on the interval $[0,T]$. Since it is well known that this space is infinite-dimensional,[3] it follows that, in general, the vectors, as well as the matrix, of Eq. 1 must be infinite-dimensional. In many cases this infinite dimensionality is of no concern and mathematical operations can be performed in the usual manner. An attempt to define a "density function" for an infinite-dimensional random vector, however, leads to conceptual, as well as mathematical, difficulties. Consequently, problems in which this situation arises are usually approached[4] by assuming initially that all vectors are finite-dimensional. The analysis is then performed and an attempt is made to show that a limiting form of the answer is obtained as the dimensionality becomes infinite. (If such a limiting result exists, it is asserted to be the desired solution.) This approach is used in the following derivations in which all vectors are initially assumed to be d-dimensional. If desired, the number d can be considered to be arbitrarily large but finite. For this case, however, it will be shown that for minimum probability of error, the vectors will be constrained to be finite-dimensional. This constraint arises because the λ_i approach zero for large "i", and it gives an indication of the useful dimensionality of the channel.

2. Random-Coding Bound

Let $\underline{x}_1, \ldots, \underline{x}_M$ be a set of M d-dimensional code words (that is, $\underline{x}_1 \ldots \underline{x}_M$ are the vector representations, with respect to the set of basis functions defined by the channel and noise, of a set of M signals of T-sec duration) for use with the channel of Fig. XX-2. Let the a priori probability of each code word be 1/M and assume that maximum-likelihood detection[4] is used. Then, given that $\underline{x}_j$ is transmitted, the probability of error is given by

$$P_j(e) = \int_{\underline{Y}} P(\underline{y}|\underline{x}_j)\, C(\underline{y},\underline{x}_j)\, d\underline{y}, \tag{2}$$

where

$$C(\underline{y},\underline{x}_j) = \begin{cases} 0 & \{\underline{y}:\ P(\underline{y}|\underline{x}_j) > P(\underline{y}|\underline{x}_i) \quad \text{all } i \neq j\} \\ 1 & \{\underline{y}:\ P(\underline{y}|\underline{x}_j) \leq P(\underline{y}|\underline{x}_i) \quad \text{some } i \neq j\}. \end{cases}$$

Equation 2 as given is mathematically intractable. A useful upper bound to Eq. 2 is obtained by first upper-bounding $C(\underline{y},\underline{x}_j)$, and then averaging the result over a suitable ensemble of code words.

An obvious inequality is

$$C(\underline{y},\underline{x}_j) \leq \left\{\sum_{\substack{k=1\\k\neq j}}^{M} \left[\frac{P(\underline{y}|\underline{x}_k)}{P(\underline{y}|\underline{x}_j)}\right]^{\alpha}\right\}^{\rho} \qquad \alpha,\ \rho \geq 0,$$

since the right-hand side is always greater than zero, and is not less than 1 when $P(\underline{y}|\underline{x}_j) \leq P(\underline{y}|\underline{x}_i)$ for some $i \neq j$. Thus

$$P_j(e) \leq \int_{\underline{Y}} P(\underline{y}|\underline{x}_j)^{1-\alpha\rho} \left\{\sum_{\substack{k=1\\k\neq j}}^{M} P(\underline{y}|\underline{x}_k)^{\alpha}\right\}^{\rho} d\underline{y}. \tag{3}$$

Let each code word be chosen according to a probability measure $P(\underline{x})$ and average both sides of Eq. 3 over this ensemble of codes. Now, let

$$\overline{P_j(e)} = \overline{P}_e \leq \int_{\underline{Y}} \overline{P(\underline{y}|\underline{x}_j)^{1-\alpha\rho}}\ \overline{\left\{\sum_{\substack{k=1\\k\neq j}}^{M} P(\underline{y}|\underline{x}_k)^{\alpha}\right\}^{\rho}}\ d\underline{y}. \tag{4}$$

Here, the bar denotes averaging with respect to the ensemble of codes. Equation 4 can be further upper-bounded by noting that $\overline{z^{\rho}} \leq \overline{z}^{\rho}$ for $0 \leq \rho \leq 1$.[5] Introducing this inequality into Eq. 4, and recalling that the average of a sum of random variables equals the sum of the individual averages, gives

$$\overline{P}_e < M^{\rho} \int_{\underline{Y}} \overline{P(\underline{y}|\underline{x})^{1-\alpha\rho}}\ \overline{P(\underline{y}|\underline{x})^{\alpha}}^{\rho}\ d\underline{y} \qquad 0 \leq \rho \leq 1. \tag{5}$$

By straightforward but tedious differentiation, it can be shown that with ρ fixed the right-hand side of Eq. 5 has an absolute minimum for variation of α when $\alpha = 1/(1+\rho)$. Thus

$$\overline{P}_e < e^{-TE(R,\rho)} \qquad 0 \leq \rho \leq 1, \tag{6}$$

where

$$E(R,\rho) = E_o(\rho) - \rho R$$

$$E_o(\rho) = -\frac{1}{T} \ln \int_{\underline{Y}} \left[\int_{\underline{X}} P(\underline{y}|\underline{x})^{1/(1+\rho)} P(\underline{x})\, d\underline{x} \right]^{1+\rho} d\underline{y}$$

$$R = \frac{\ln M}{T}.$$

This bound will now be applied to the channel of Fig. XX-2. For convenience, let the noise variance in Eq. 1 be normalized to unity. Then

$$P(\underline{y}|\underline{x}) = \prod_{i \in I} \frac{1}{\sqrt{2\pi}} \exp\left[-\frac{1}{2} (y_i - \sqrt{\lambda_i}\, x_i)^2 \right], \tag{7}$$

where the set I is, at this point, an arbitrary collection of d non-negative integers. Furthermore, let $P(\underline{x})$ be chosen to be

$$P(\underline{x}) = \prod_{i \in I} \frac{1}{\sqrt{2\pi\sigma_i^2}} \exp\left[-\frac{1}{2} \left(x_i^2 / \sigma_i^2 \right) \right]. \tag{8}$$

The reasons for this choice of $P(\underline{x})$ are several.

(a) This form of $P(\underline{x})$ results in a mathematically tractable expression for the error exponent of Eq. 6.

(b) It is known[6] that this choice for $P(\underline{x})$ leads to maximum average mutual information between the $\underline{x}$ and $\underline{y}$ vectors when the values of $\overline{x_i^2}$ are specified. Furthermore, maximization of the resulting mutual information with respect to the $\overline{x_i^2}$ yields a meaningful definition of capacity for this channel.

(c) When the resulting exponent is specialized to the case considered by Shannon,[7] it is within a few per cent of his exponent, which is the best known.

Finally, assume an average power constraint on the ensemble of codes of the form

$$\sum_{i \in I} \sigma_i^2 = ST. \tag{9}$$

Substituting Eqs. 7 and 8 in Eq. 6 gives, after evaluation of the integrals,

$$E(R, \rho, \underline{\sigma}) = \frac{\rho}{2T} \sum_{i \in I} \ln \left(1 + \frac{\lambda_i \sigma_i^2}{1+\rho}\right) - \rho R, \tag{10}$$

where

$$\underline{\sigma} = \left(\sigma_1^2, \sigma_i^2, \ldots \sigma_k^2, \ldots\right).$$

For fixed R, maximization of Eq. 10 over ρ, $\underline{\sigma}$, and the set I gives the desired random-coding error exponent. For convenience, let this maximization be performed in the order I, $\underline{\sigma}$, ρ.

Maximization over the set I is easily accomplished by recalling[1] that the λ_i are by assumption ordered so that $\lambda_0 \geq \lambda_1 \geq \lambda_2 \ldots$. Thus, the monotonic property of $\ln x$ for $x \geq 1$ implies that $E(R, \rho, \underline{\sigma})$ is maximized over the set I by choosing $I = \{0, 1, \ldots, d-1\}$.

The maximization over $\underline{\sigma}$ is most readily accomplished by using the properties of convex functions[8] defined on a vector space. For this purpose, the following definitions and a theorem of Kuhn and Tucker[9] (in present notation) are presented.

DEFINITION 1: A region of vector space is defined as convex if for any two vectors $\underline{\alpha}$ and $\underline{\beta}$ in the region and for any λ, $0 \leq \lambda \leq 1$, the vector $\lambda\underline{\alpha} + (1-\lambda)\underline{\beta}$ is also in the region.

DEFINITION 2: A function $f(\underline{\alpha})$ whose domain is a convex region of vector space is defined as concave if, for any two vectors $\underline{\alpha}$ and $\underline{\beta}$ in the domain of f and for any λ, $0 < \lambda < 1$,

$$\lambda f(\underline{\alpha}) + (1-\lambda) f(\underline{\beta}) \leq f[\lambda\underline{\alpha} + (1-\lambda)\underline{\beta}].$$

From these definitions is follows that the region of Euclidean d-space defined by the vector $\underline{\sigma}$, with

$$\sigma_i^2 \geq 0, \text{ and } \sum_{i=0}^{d-1} \sigma_i^2 = TS,$$

is a convex region of vector space, that ln x is a concave function for $x \geq 1$, that a sum of concave functions is concave, and thus that $E(R, \rho, \underline{\sigma})$ is a concave function of $\underline{\sigma}$.

THEOREM 1 (Kuhn and Tucker): Let $f(\underline{\sigma})$ be a continuous differentiable concave function in the region in which $\underline{\sigma}$ satisfies $\sum_{i=0}^{d-1} \sigma_i^2 = TS$ and $\sigma_i^2 \geq 0$, $i = 0, 1, \ldots, d-1$. Then a necessary and sufficient condition for $\underline{\alpha}$ to minimize f is

$$\left.\frac{\partial f(\underline{\sigma})}{\partial \sigma_i^2}\right|_{\underline{\sigma}=\underline{\alpha}} \leq A \qquad \text{for all } i \text{ with equality if and only if } \sigma_i^2 \neq 0.$$

Here, A is a constant independent of i whose value is adjusted to satisfy the constraint $\sum_{i=0}^{d-1} \sigma_i^2 = TS$. It follows that the $\underline{\sigma}$ maximizing Eq. 10 must satisfy

$$\frac{\partial E(R,\rho,\underline{\sigma})}{\partial \sigma_i^2} = \frac{\rho}{2T} \frac{(-\lambda_i)/(1+\rho)^2}{1+\left(\lambda_i\sigma_i^2\right)/(1+\rho)} \leqslant A \qquad \text{all } i = 0, \ldots, d-1$$

with equality if and only if $\sigma_i^2 > 0$.

Thus

$$\sigma_i^2 = \begin{cases} (1+\rho)\left\{\dfrac{1}{B_T(\rho)} - \dfrac{1}{\lambda_i}\right\} & i = 0, 1, \ldots, N-1 \\ 0 & i = N \ldots d-1 \end{cases} \tag{11}$$

where N is defined by

$$\lambda_{N-1} > B_T(\rho) \geqslant \lambda_N$$

and

$$\frac{1}{B_T(\rho)} \triangleq \frac{-\rho}{2TA(1+\rho)^2}.$$

The value of $B_T(\rho)$, and thus N, is chosen to satisfy the constraint

$$\sum_{i=0}^{N-1} \sigma_i^2 = TS,$$

which yields

$$\frac{1}{B_T(\rho)} = \frac{\dfrac{ST}{1+\rho} + \displaystyle\sum_{i=0}^{N-1} \lambda_i^{-1}}{N}. \tag{12}$$

Substituting Eqs. 11 and 12 in Eq. 10 gives

$$E(R,\rho) = \frac{\rho}{2T} \sum_{i=0}^{N-1} \ln \frac{\lambda_i}{B_T(\rho)} - \rho R. \tag{13}$$

Maximization over ρ is accomplished by using standard techniques of differential calculus. Since N is an implicit function of ρ in Eq. 13, there is a possibility that $E'(R,\rho)$ might not exist for values of ρ and N, such that $B_T(\rho) = \lambda_N$. It can be shown, however, that $E'(R,\rho^-) = E'(R,\rho^+)$ for all ρ. Thus the final result is

$$E_T(\rho) = \left(\frac{\rho}{1+\rho}\right)^2 \frac{S}{2} B_T(\rho) \qquad R(1) \leqslant R \leqslant R(0) = C_T \tag{14}$$

where

$$R(\rho) = \frac{1}{2T} \sum_{i=0}^{N-1} \ln \frac{\lambda_i}{B_T(\rho)} - \frac{\rho}{(1+\rho)^2} \frac{S}{2} B_T(\rho) \qquad 0 \leq \rho \leq 1 \tag{15}$$

and

$$E_T(R) = \frac{1}{2T} \sum_{i=0}^{N-1} \ln \frac{\lambda_i}{B_T(1)} - R \qquad 0 \leq R \leq R(1). \tag{16}$$

A bound that is in some cases more useful, and in all cases more readily evaluated, can be derived by considering Eqs. 14-16 for $T \to \infty$. It can be shown by a generalization of a result derived by Jordan,[10] and other arguments too long to be presented here, that the resulting form for the exponent is

$$E(\rho) = \left(\frac{\rho}{1+\rho}\right)^2 \frac{S}{2} B(\rho) \qquad R_c \leq R \leq C \tag{17}$$

$$R(\rho) = \int_W \ln \frac{|H(j\omega)|^2}{N(\omega)\, B(\rho)}\, df - \frac{\rho}{(1+\rho)^2} \frac{S}{2} B(\rho) \qquad 0 \leq \rho \leq 1 \tag{18}$$

$$E(R) = \int_W \ln \frac{|H(j\omega)|^2}{N(\omega)\, B(1)}\, df - R \qquad 0 \leq R \leq R_c, \tag{19}$$

where

$$C = R(0)$$

$$R_c = R(1)$$

$$\frac{1}{B(\rho)} = \frac{\dfrac{S}{2(1+\rho)} + \displaystyle\int_W \frac{N(\omega)}{|H(j\omega)|^2}\, df}{W}$$

$$W = \left\{ + f\colon \frac{|H(j\omega)|^2}{N(\omega)} \geq B(\rho) \right\}.$$

A convenient method for interpreting the significance of $B(\rho)$ and W is illustrated in Fig. XX-3. This is the well-known "water-pouring" interpretation discussed by Fano[6] and others for the special case of channel capacity. Pertinent properties of the exponents of Eqs. 14-16 and that of Eqs. 17-19 are presented in Fig. XX-4 in which the notation of the latter exponent is used.

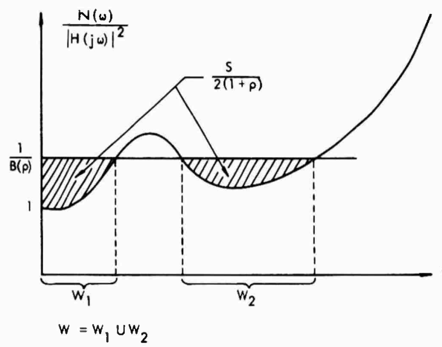

Fig. XX-3. Concerning the interpretation of B(ρ) and w.

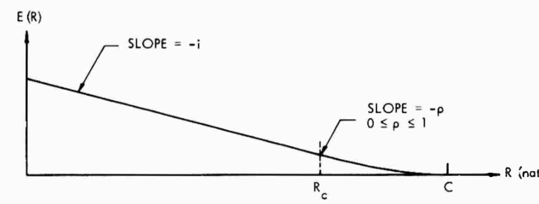

Fig. XX-4. Error exponent for channel of Fig. XX-2.

3. Random-Coding Bound for $S \ll 1$

In this section an asymptotic form for the bound of Eqs. 17-19 is determined for the condition $S \to 0$. For convenience, it is assumed that $K(f) \stackrel{\Delta}{=} |H(j\omega)|^2/N(\omega)$ has a lowpass characteristic. It will be clear from the derivation, however, that an identical result holds for the general case. Consider the bound for $0 \leq \rho \leq 1$. By expanding Eq. 17 in a Taylor series about $S = 0$, it follows that $E(\rho)$ becomes approximately

$$E(\rho) \cong E(\rho)\Big|_{S=0} + \frac{dE(\rho)}{dS}\Big|_{S=0} S = \left(\frac{\rho}{1+\rho}\right)^2 \frac{S}{2}. \tag{20}$$

Likewise,

$$R(\rho) \cong R(\rho)\Big|_{S=0} + \frac{dR(\rho)}{dS}\Big|_{S=0} S.$$

Using the lowpass assumption for $K(f)$ and also assuming that $K(0) = 1$, $K(f) < 1$ for $|f| > 0$, gives

$$\frac{dR(\rho)}{dS}\Big|_{S=0} = -W\frac{K'(W)}{K(W)}\frac{dW}{dS}\Big|_{S=0} - \frac{\rho/2}{(1+\rho)^2}. \tag{21}$$

The assumptions on $K(f)$ imply, however, that for $S \to 0$

$$B(\rho) = K(W)$$

and

$$\frac{S}{2(1+\rho)} = \int_0^W \left[\frac{1}{B(\rho)} - \frac{1}{K(f)}\right] df,$$

which leads to

$$\frac{dW}{dS} = -\frac{1}{2(1+\rho)} \frac{B^2(\rho)}{WK'(W)}.$$

Combining this with Eq. 21 gives

$$R(\rho) \cong \frac{1}{2(1+\rho)} S. \tag{22}$$

Finally, solving for ρ from Eq. 22 and substituting in Eq. 20 gives the desired exponent

$$E(R) = C\left[1 - \sqrt{\frac{R}{C}}\right]^{1/2} \qquad R_c \leq R \leq C \tag{23}$$

where

$$C = S/2$$

$$R_c = S/8.$$

A similar analysis gives

$$E(R) = C\left[\frac{1}{2} - \frac{R}{C}\right] \qquad 0 \leq R \leq R_c. \tag{24}$$

This exponent is presented in Fig. XX-5 and has several noteworthy features.

(i) It is independent of both the channel filter characteristics and the shape of the

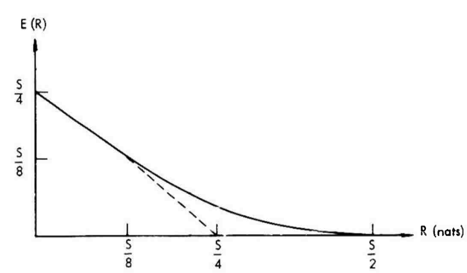

Fig. XX-5. Error exponent for $S \ll 1$.

noise spectrum. This fact may be interpreted physically in terms of Fig. XX-3 in the following manner. When S is "sufficiently small," the water-pouring interpretation shows that the ratio $|H(j\omega)|^2/[B(\rho)N(\omega)]$ is "almost" unity and, furthermore, that $|H(j\omega)|^2/N(\omega)$ is "almost" constant for $f \in W$. Thus to a first-order approximation Eqs. 17 and 18 become

$$E(\rho) \cong \left(\frac{\rho}{1+\rho}\right)^2 \frac{S}{2} \qquad R_c \leq R \leq C$$

and

$$R(\rho) \cong \int_W \left[\frac{|H(j\omega)|^2}{N(\omega)\ B(\rho)} - 1\right] df - \frac{\rho}{(1+\rho)^2}\frac{S}{2} = \frac{S}{2(1+\rho)^2} \qquad 0 \leqslant 1 \leqslant \rho$$

which, when combined, yield Eq. 24.

(ii) It agrees precisely with that found by Shannon[7] for the analogous case in his problem, and is also identical to a bound found by Gallager[11] for "very noisy" discrete memoryless channels. Thus this bound could in some sense be considered to be a universal bound for "very noisy" channels.

The application of Theorem 1 and the theory of convex functions to this problem was brought to the author's attention by Professor R. G. Gallager.

J. L. Holsinger

References

1. J. L. Holsinger, Vector representation of time-continuous channels with memory, Quarterly Progress Report No. 71, Research Laboratory of Electronics, M.I.T., October 15, 1963, pp. 193-202.

2. R. G. Gallager, A simple derivation of the coding theorem, Quarterly Progress Report No. 69, Research Laboratory of Electronics, M.I.T., April 15, 1963, pp. 154-157.

3. R. Courant and D. Hilbert, Methods of Mathematical Physics (Interscience Publishers, Inc., New York, 1953).

4. C. W. Helstrom, Statistical Theory of Signal Detection (Pergamon Press, New York, 1960).

5. G. H. Hardy, J. E. Littlewood, and G. Polyá, Inequalities (Cambridge University Press, London, 1959), Theorem 190.

6. R. M. Fano, Transmission of Information (The M.I.T. Press, Cambridge, Mass., and John Wiley and Sons, Inc., New York, 1961), Chapter 5.

7. C. E. Shannon, Probability of error for optimal codes in a Gaussian channel, Bell System Tech. J. 38, 611-656 (1959).

8. H. G. Eggleston, Convexity, Cambridge Tracts in Mathematics and Mathematical Physics No. 47 (Cambridge University Press, London, 1958).

9. H. W. Kuhn and A. W. Tucker, Nonlinear Programming, Second Berkeley Symposium on Mathematical Statistics and Probability (University of California Press, Berkeley, 1951), p. 486, Theorem 3.

10. K. L. Jordan, Jr., Discrete Representation of Random Signals, Technical Report 378, Research Laboratory of Electronics, M.I.T., July 14, 1961, Appendix B.

11. R. G. Gallager, Examples of Upper Bound to Pe (unpublished notes).

XXI. ARTIFICIAL INTELLIGENCE*†

Prof. M. L. Minsky
Prof. H. Putnam
Prof. A. L. Samuel
Prof. C. E. Shannon
Dr. S. Papert
D. G. Bobrow
D. J. Edwards
T. P. Hart
M. I. Levin
D. C. Luckham
J. Moses
L. Norton

RESEARCH OBJECTIVES

The purpose of our work is to investigate ways of making machines solve problems that are usually considered to require intelligence. Our procedure is to attack the problems by programming a computer to deal directly with the necessary abstractions, rather than by simulating hypothetical physiological structures. When a method for solving a problem is not known, searches over spaces of potential solutions of the problem, or of parts of the problem, are necessary. The space of potential solutions of interesting problems is ordinarily so enormous that it is necessary to devise heuristic methods[1-3] to replace the searching of this space by a hierarchy of searches over simpler spaces. The major difficulty, at present, is the excessive length of time required for building machinery or even for writing programs to test heuristic procedures. For this reason, a major part of our effort is going into the development of ways of communicating with a computer more effectively than we can now communicate. This work has two aspects: development of a system for instructing the computer in declarative, as well as imperative, sentences, called the advice-taker,[4] and development of a programming language called LISP[5-8] for manipulating symbolic expressions that will be used for programming the advice-taker system and will also be of more general use.[9] We are embarking on a major effort to integrate this work into the new M. I. T. time-shared real-time computer system.

Maintenance and further development of LISP will be continued by Professor J. McCarthy, who is now at Stanford University. We plan to continue close association with his group.

It is our belief that the field of artificial intelligence is limited only by the amount of qualified effort that can be put into it, and by the machine limitations that still prohibit more ambitious experiments.

M. L. Minsky

References

1. M. L. Minsky, Some Methods of Artificial Intelligence and Heuristic Programming, Proc. Symposium on the Mechanisation of Thought Processes, National Physical Laboratory, Teddington, England, November 24-27, 1958 (H. M. Stationery Office, London, 1959).

2. M. L. Minsky, Steps toward artificial intelligence, Proc. IRE 49, 8-30 (1961).

3. M. L. Minsky, A selected, descriptor-indexed bibliography to the literature on artificial intelligence, Trans. IRE, Vol. HFE-2, No. 1, pp. 39-55, March 1961.

*This work is supported in part by the National Science Foundation (Grant G-16526); in part by the National Institutes of Health (Grant MH-04737-03); and in part by the National Aeronautics and Space Administration (Grant NsG-496).

†Several members of this group, working at the Computation Center, are not members of the Research Laboratory of Electronics: Prof. J. Weizenbaum (Visiting Associate Professor of Electrical Engineering, M. I. T.), Dr. O. G. Selfridge (Lincoln Laboratory, M. I. T.), and the following graduate students: W. A. Martin and B. Raphael.

4. J. McCarthy, Programs with Common Sense, Proc. Symposium on the Mechanisation of Thought Processes, National Physical Laboratory, Teddington, England, November 24-27, 1958 (H. M. Stationery Office, London, 1959).

5. J. McCarthy, Recursive functions of symbolic expressions in computation by machine, Part I, Commun. Assoc. Computing Machinery 3, 184-195 (April 1960).

6. J. McCarthy, A Basis for a Mathematical Theory of Communication, Proc. Western Joint Computer Conference, Los Angeles, California, May 1961.

7. J. McCarthy, Computer Programs for Checking Mathematical Proofs, a paper presented at the Symposium on Recursive Function Theory, New York, April 1961.

8. The Computation Center and Research Laboratory of Electronics, LISP 1.5 Programmer's Manual, August 17, 1962 (reprinted by The M. I. T. Press, Cambridge, Mass.).

9. J. McCarthy, Time-Sharing Computer Systems (lecture, M.I.T., May 1961); Management and the Computer of the Future (The M. I. T. Press, Cambridge, Mass., and John Wiley and Sons, Inc., New York, 1962).

XXII. SPEECH COMMUNICATION*

Prof. K. N. Stevens	Dr. A. W. F. Huggins	V. V. Nadezhkin
Prof. M. Halle	Dr. B. E. F. Lindblom†	A. P. Paul
Prof. J. B. Dennis	Dr. S. E. G. Öhman†	J. Rome
Prof. J. M. Heinz	Jane B. Arnold	R. Tomlinson
Dr. A. S. House	W. L. Henke	E. C. Whitman

RESEARCH OBJECTIVES

The objectives of our work are to further our understanding: (a) of the process whereby human listeners decode an acoustic speech signal into a sequence of discrete linguistic symbols such as phonemes; and (b) of the process whereby human talkers encode a sequence of discrete linguistic symbols into an acoustic signal.

Present activities related to these objectives include the development of procedures for the analysis and synthesis of speech, and the use of these procedures in the study of human speech processes. Improved techniques of the automatic extraction of vocal-tract resonances from the speech signal are under development, and work is continuing on speech analysis methods that provide a description of the speech signal in terms of parameters specifying the activity of an articulatory model that could generate that signal. A new dynamic analog of the vocal tract is under development, and programs that will enable this synthesizer to be controlled from a digital computer are being evolved. Data on the acoustic characteristics of utterances corresponding to phonemes in various linguistic contexts and with various durational characteristics are being accumulated, and this study is being combined with and related to studies of articulatory motions during speech production through cineradiographic techniques, direct cinephotography, and palatography. Attempts are being made to formulate models for the speech production process that will account for the various coarticulation effects observed in human speech production. Studies of the process of speech perception continue and are now centered on examination of the perception of spoken sentences subject to dichotic switching and other types of processing, and on investigations of the perception of synthetic utterances characterized by time-variant formant patterns.

K. N. Stevens, A. S. House, M. Halle

*This research is supported in part by the U.S. Air Force (Electronic Systems Division) under Contract AF 19(628)-3325; in part by the National Science Foundation (Grant G-16526); in part by the National Institutes of Health (Grant MH-04737-03 and Grant NB-04332-01); and in part by the National Aeronautics and Space Administration (Grant NsG-496).

†On leave from the Speech Transmission Laboratory, Royal Institute of Technology, Stockholm, Sweden.

XXIII. MECHANICAL TRANSLATION*

V. H. Yngve
Carol M. Bosche
Elinor K. Charney
Ann Congleton
J. L. Darlington
Muriel S. Kannel
E. S. Klima
B. S. Knobe
Meri Lehtinen
J. D. McCawley
T. More, Jr.
W. K. Percival
G. Rondeau
A. C. Satterthwait
J. M. Winett
J. S. Wright

RESEARCH OBJECTIVES

The primary objective of our research program is to find out how languages can be meaningfully manipulated and translated by machine, and to evaluate the quality that can be achieved with different approaches, the usefulness of the results and their costs. A further objective is to achieve a basic understanding of human communication and language use, and to add to the general knowledge of noncomputational uses of digital computing machinery.

We have always stressed a basic, long-range approach to the problems of mechanical translation. We are placing emphasis on completeness, when completeness is possible, and on finding out how to do a complete job if one is not now possible. This emphasis has led us into the study of many of the fundamental questions of language and translation. We are not looking for short-cut methods that might yield partially adequate translations at an early date — an important goal that is being pursued by other groups. We are seeking definitive solutions that will be permanent advances in the field, rather than ad hoc or temporary solutions that may eventually have to be discarded because they are not compatible with improved systems.

A broad and basic program of research is being carried out. In linguistic theory, a computer model of linguistic behavior is being studied which has already provided insight into the reasons why human languages are complex. Work has been progressing on linguistic descriptions for English, German, French, Arabic, Finnish, and Chinese. An experimental Arabic to English translation program has been completed. In the area of semantics, work is proceeding along several avenues in an attempt to program a machine to understand English. Language is also being studied from a logical point of view to clarify the semantic significance of certain difficult and crucial words. The nature of the translation relation is being given special emphasis. Computer programming languages are being studied. The group has developed and is improving COMIT, a convenient large-scale computer programming system which greatly reduces the effort required to write programs related to the research.

V. H. Yngve

*This work is supported in part by the National Science Foundation (Grant G-24047).

XXIV. LINGUISTICS*

Prof. R. Jakobson	Dr. M. E. Jones	R. P. V. Kiparsky
Prof. A. N. Chomsky	Dr. Paula Menyuk	S.-Y. Kuroda
Prof. M. Halle	Dr. W. Weksel	D. T. Langendoen
Prof. J. A. Fodor	Dr. K. Wu	T. M. Lightner
Prof. J. J. Katz	T. G. Bever	P. S. Peters, Jr.
Prof. G. H. Matthews	M. J. Chayen	C. B. Qualls
Prof. P. M. Postal	S. K. Ghosh	J. J. Viertel
Dr. L. K. Bendall	Barbara C. Hall	A. M. Zwicky, Jr.
	Y. Isami	

RESEARCH OBJECTIVES

This group sees as its central task the development of a general theory of language. The theory will attempt to integrate all that is known about language and to reveal the lawful interrelations among the structural properties of different languages as well as of the separate aspects of a given language, such as its syntax, morphology, and phonology. The search for linguistic universals and the development of a comprehensive typology of languages are primary research objectives.

Work now in progress deals with specific problems in phonology, morphology, syntax, language learning and language disturbances, linguistic change, semantics, as well as with the logical foundations of the general theory of language. The development of the theory influences the various special studies and, at the same time, is influenced by the results of these studies. Several of the studies are parts of complete linguistic descriptions of particular languages (English, Russian, Siouan) that are now in preparation.

Since many of the problems of language lie in the area in which several disciplines overlap, an adequate and exhaustive treatment of language demands close cooperation of linguistics with other sciences. The inquiry into the structural principles of human language suggests a comparison of these principles with those of other sign systems, which, in turn, leads naturally to the elaboration of a general theory of signs, semiotics. Here linguistics touches upon problems that have been studied by modern logic. Other problems of interest to logicians – and also to mathematicians – are touched upon in the studies devoted to the formal features of a general theory of language. The study of language in its poetic function brings linguistics into contact with the theory and history of literature. The social function of language cannot be properly illuminated without the help of anthropologists and sociologists. The problems that are common to linguistics and the theory of communication, the psychology of language, the acoustics and physiology of speech, and the study of language disturbances are too well known to need further comment here. The exploration of these interdisciplinary problems, a major objective of this group, will be of benefit not only to linguistics; it is certain to provide workers in the other fields with stimulating insight and new methods of attack, as well as to suggest to them new problems for investigation and fruitful reformulations of questions that have been asked for a long time.

R. Jakobson, A. N. Chomsky, M. Halle

*This work was supported in part by the National Science Foundation (Grant G-16526); in part by the National Institutes of Health (Grant MH-04737-03); in part by the U.S. Air Force (Electronic Systems Division) under Contract AF19(628)-2487; and in part by the National Aeronautics and Space Administration (Grant NsG-496).

A. THE PROSODIC QUESTIONS OF SLAVIC HISTORICAL PHONOLOGY RESTATED

1. Pattern

"Before the gradual dissolution of Common Slavic, its phonemic vowel system contained two prosodic features: 1) long (marked) vs. short, 2) high-pitched (marked) vs. low-pitched, and two inherent features: 1) diffuse vs. compact, 2) acute vs. grave.*** Any long syllable of the word and any final short syllable could carry a phonemic high pitch. Before a high-pitched syllable, any syllable of the same word apparently displayed a redundant high pitch. The rest of the syllables were low-pitched. There were two prosodic types of words: high-pitched words with one (and never more than one) phonemically high-pitched syllable, and low-pitched words without any high-pitched syllable."[1]

This statement requires a more precise formulation with respect to the interrelationship of the two prosodic features – the quantitative and the tonic one – and to their distribution within the word boundaries.

In regard to the treatment of prosodic features, three kinds of word syllables – initial, internal, final – and correspondingly three dichotomies are to be considered: 1) initial-noninitial (internal and final); 2) final-nonfinal (initial and internal); 3) internal-marginal (initial and final).

Since the last or only high pitch within a word was phonemic, and no word contained more than one phonemic high pitch, the latter jointly functioned as a distinctive and culminative feature.[2] Under such conditions, the minimal pairs do not involve commutation but permutation – a choice between words carrying the same feature on different syllables; cf. Russian words distinguished from each other by the place of their stress: /kúpala/ 'cupola' (gen.)-/kupála/ 'bathed' (fem.)-/kupalá/ 'cupolas.'

In Common Slavic, words, all other things being equal, could differ by the place of high pitch. The high pitch, capable of falling on any word syllable, was phonemic in every position. Only the initial syllable, however, actually involves commutation; there is a free choice between both phonemic opposites; e.g., a high-pitch dipthong in the Common Slavic prototype of Serbocroat. vȑana, Rus. voróna 'crow' vs. the low-pitch dipthong in the prototype of Serbocroat. vrāna, Rus. vórona 'raven' (gen.).

Phonemic features are not, while redundant features are, predictable from the phonemic environment. The initial long syllable could carry either the high or the low pitch; this was the only position where the low pitch could not be predicted from the pitch distribution in the other syllables of the same word unit. Any noninitial syllable carried a nonphonemic low pitch when one of the preceding syllables was high-pitched or when the initial syllable was low-pitched. Thus the opposition of high and low pitch was phonemic only in the initial syllable.

The low pitch of a short initial syllable is predictable: any short initial syllable carried a nonphonemic low pitch, when none of the noninitial syllables was high-pitched. The long low-pitched initial syllable participated in two phonemic oppositions: the length distinguished this syllable from short initial syllables, while the low pitch opposed it to the high-pitched syllables.

The length of a nonfinal syllable under a phonemic high pitch is predictable, since among the nonfinal syllables only the long ones may carry a phonemic high pitch. Except for nonfinal syllables under a phonemic high pitch, any syllable offers a free choice between phonemic length and shortness.

2. Evolution

Toward the end of the last millennium the diffuse short vowels (ŭ, ĭ) of the word end lost the capacity of carrying a high pitch, so that the previously redundant high pitch of the penults became phonemic. Originally this shift was confined to the allegro variety of language. The final high pitch on short diffuse vowels and the prefinal high pitch in the same words were but stylistic variants. Within the allegro subcode of the late Common Slavic, the prefinal high pitch, caused by the shift from the short final diffuse vowels and labelled 'neoacute', was a stylistic alternant of the traditional high pitch on the final diffuse shorts, and at the same time it was a contextual variant with respect to the pretonic penults followed by long and/or compact vowels. The new prefinal high pitch fell on both longs and shorts and was in complementary distribution with longs and shorts in pretonic penults.

The long and short varieties of the neoacute presented an imminent complication for the prosodic pattern of dissyllabic words, in which one and the same syllable simultaneously shared the initial and prefinal status. The adjustment to this challenge required significant changes in vocalic quantity, and in spite of considerable dialectal differences in these modifications, for the whole Slavic area they inaugurated a new system of long-short oppositions and transformed the traditional quantitative distinctions into qualitative differences.

In the Serbo-Slovenian type of prosodic evolution the phonemic length was preserved, while the nonphonemic, redundant length was abolished. Thus the longs remained intact both under the low pitch and under the neoacute, while the old high-pitched vowels were shortened.

In the Western Slavic prosodic type, the quantitative opposition supplanted the tonic one. In particular, the following treatment is shown by the first vowel of dissyllables: The pretonic length remained intact; likewise, the combination of the quantitative and tonic marks, namely, the phonemic length under high pitch (neoacute), was maintained; but the low-pitched length, i.e., the marked term of the quantitative opposition, combined with the unmarked term of the tonic opposition, was shortened.

The high-pitched shorts, which arose with the neoacute, are treated differently in the Lekhitic and Slovak varieties of the Western Slavic type. Lekhitic solved the conflict between the tonic mark and the unmarked quantity in the latter's favor, whereas Slovak substituted the quantitative mark for the tonic mark: length for high pitch.

While Lekhitic and Slovak have shortened the nonphonemic, redundant length tied to the old high pitch, in the Czecho-Lusatian variety of the same type any high-pitched syllable was kept long.

Thus a comparative inquiry into the Lekhitic, Slovak, and Czecho-Lusatian prosodic treatment of the initial penult discloses that the Western Slavic type has eliminated the tonic feature by substituting shortness for low pitch and, on a varied scale, length for high pitch.

In Common Slavic, the last or the only high-pitched syllable, and in absence of high pitch, the initial syllable carried the word accent. With the annulment of high pitch in the Western type, the word accent became automatically attached to the initial syllable.

The Eastern (East Slavic and Bulgarian) type abolished the distinction between the phonemic low and high pitch in favor of the latter; hence high pitch coalesced with word accent, and the vocalic length became a concomitant redundant attribute of the accent.

R. Jakobson

References

1. R. Jakobson, A Phonemic Approach to the Structure and Evolution of the Common Slavic Prosodic Pattern, American Contributions to the V International Congress of Slavists (1963). Cf. J. Kurylowicz, L'accentuation des langues indo-européennes (1958), Chap. III.

2. R. Jakobson, Selected Writings, I (Mouton and Company, The Hague, 1962), pp. 268f., 288ff., and 469.

B. DESCRIPTION OF DEVIANT LANGUAGE PRODUCTION

1. Problem

Those concerned with language disorders have become increasingly aware of their need to gain a greater understanding of the processes of development (both physiological and psychological) of language production and perception.[1] The general conclusion has been that it is necessary to describe adequately language production in any instance rather than just disorder production. Furthermore, in order to determine in what way, and eventually why, some language productions deviate strikingly from the norm, it has been concluded that there has to be an adequate description of the norm. Those who conduct research in this field feel that these processes have to be described adequately so that there is some model against which diagnostic distinctions can be clarified and diagnostic measures devised, so that future growth can be predicted, and therapeutic decisions have some basis in the facts of the properties of language and of language development.

Workers in this field have turned to linguists and psycholinguists to provide procedures and terminology for these descriptions. There have been detailed and careful studies of the phonological[2] and syntactic[3] components of language which convince us of the fact that the process of grammatical development is rapid and largely resistant to distortion. Many questions remain as to how this process occurs and certainly as to how distortions, which have no known physiological basis, occur. Attempts have been made to formulate diagnostic techniques to isolate and then relate functions that are intuitively felt to be related in the processes of acquisition and development of language such as patterning of visual, auditory, and motor skills.[4] Many questions remain about the nature of these functions, the relation of these functions, and certainly about methods for eliciting information about them.

In this study a generative model of grammar was used to compare the grammar of children diagnosed as using a deviant language production (infantile speech) with that of children using normal speech in an attempt to describe more adequately a language production simply characterized as infantile.

2. Procedure

Language was elicited and recorded in various stimulus situations from 10 children using "infantile" speech and 10 children with normal speech who were matched in age, sex, socio-economic status, and I.Q. The groups ranged in age from 3 years to 5 years, 10 months. The language of one child was sampled periodically from age 2 to age 3. The language sample of each child was analyzed, and the syntactic structures used were postulated. A number of children in each group were asked to repeat a list of sentences containing syntactic structures found in children's grammar.

Comparisons were made of i) the number of children in each group who used various transformations and the number who used forms that deviated from complete grammaticalness, ii) the frequency of usage by the two groups of forms that deviated, and iii) the number of children in each group who repeated and did not repeat all of the sentences presented and the number who corrected deviant structures. The correlation between age and increase in usage of transformations and decrease in usage of deviant forms and the correlation between sentence length and nonrepetition for both groups were also tested. A comparison was made of the grammar of the 2 to 3 year old child with normal speech and the grammatical usage of children throughout the age range of the "infantile" speech group.

3. Results

It was found that more children with normal speech used the various transformations and more of the children with "infantile" speech used the deviant forms (primarily those of omission of rules) and used them with significantly greater frequency. Essentially the same results were obtained when the 5 youngest members of the normal speech group were compared with the 5 oldest members of the "infantile" speech group. Also, age was significantly correlated with decrease in usage of deviant forms for the normal but not the "infantile" speech group. Significantly, more of the children in the "infantile" speech group repeated sentences with omissions or with just the last phrase, word or words of a sentence. Sentence length was significantly correlated with nonrepetition for the "infantile" but not the normal speech group. At age 2 the child with normal speech did not use some of the syntactic structures found throughout the age range in the grammar of the "infantile" speech group, but by age 3 he exceeded even the oldest child in the group in grammatical production (by using more transformations and fewer deviant forms).

4. Discussion

By using a generative model of grammar to describe these children's language production, the following trends and differences were observed. The term "infantile" seems to be a misnomer, since at no age level did the grammatical production of a child with deviant speech match or closely match the grammatical production of a child with normal speech. The children with deviant speech, in terms of the model of grammar used for description, formulated their sentences with the most general rules, whereas children with normal speech, as they matured, used structures that require increasingly differentiating rules for their formulation. This also seemed to be the case with the articulation difficulties found in this group. The most frequent sound errors were omission and substitution. The initial <u>s</u> and final <u>t</u> were omitted by more than 50 per cent of the children with deviant speech, and the following substitutions were also used by more than 50 per cent of the children: the sound <u>w</u> was used for <u>w</u>, <u>r</u>, and <u>l</u>; the sound <u>t</u> was used for <u>t</u>, <u>k</u>, and the unvoiced <u>th</u>; the sound <u>d</u> was used for <u>d</u>, <u>g</u>, and the voiced <u>th</u>.

It is hypothesized that the differences found in the use and repetition of syntactic structures between the groups may be due to differences in how the coding processes for perception and production of language are used. The results indicate that the most significant factor may be the difference in the children's ability to determine the complete sets of rules that are used to generate and differentiate structures at any level of the grammar.

Since the population was small, none of the trends observed were considered conclusive differentiating factors in the description of the two groups. However, it was felt that using a generative model to describe language production provided a much more adequate and discriminating description of the differences in language production of the two groups than had previously been obtained.

Paula Menyuk

References

1. Research Needs in Speech Pathology and Audiology, J. Speech and Hearing Disorders, Monog. Suppl. 5, September 1959.

2. O. C. Irwin, Some factors related to the speech development of the young child, J. Speech and Hearing Disorders 17, 269-279 (1952).

3. M. C. Templin, Certain Language Skills in Children (University of Minnesota Press, Minneapolis, 1957).

4. G. Arnold, The Illinois test of psycholinguistic abilities and severe articulation problems (Abstract) ASHA 5, 789 (1963).

XXV. COMMUNICATIONS BIOPHYSICS*

Prof. M. Eden
Prof. J. L. Hall II
Prof. W. T. Peake†
Prof. R. R. Pfeiffer†
Prof. W. A. Rosenblith
Prof. W. M. Siebert
Prof. T. F. Weiss
Dr. J. S. Barlow‡
Dr. E. Giberman**
Dr. R. D. Hall
Dr. N. Y-S. Kiang†
Dr. G. P. Moore
Dr. R. H. Wendt
R. M. Brown
S. K. Burns
R. R. Capranica
R. J. Clayton
A. H. Crist
N. I. Durlach
J. L. Elliot
P. R. Gray
J. J. Guinan, Jr.
F. N. Jordan
Patricia Kirkpatrick
K. C. Koerber†
D. Langbein
R. G. Mark
P. Mermelstein
M. J. Murray
Ann M. O'Rourke
R. F. Otte
Cynthia M. Pyle
M. B. Sachs
N. D. Strahm
I. H. Thomae
J. R. Welch
M. L. Wiederhold

RESEARCH OBJECTIVES AND SUMMARY OF RESEARCH

The major efforts of this group continue to be directed toward an understanding of the communication senses — particularly hearing. Activity is concentrated in the four major areas of neuroelectric studies, psychophysical and behavioral studies, investigations of mathematical models, and research on problems in instrumentation and data processing. Typical examples of recent or current studies are:

1. Studies of hearing in the frog.
   a. Single-unit responses in the green frog.
   b. Calling behavior and variations in heart rate of bullfrogs evoked by various auditory stimuli.
2. Electrophysiological studies of discrimination behavior in the rat.
3. Investigation of the modifications in the responses of the cochlea and the auditory nerve resulting from stimulation of the olivocochlear bundle of cats.
4. Study of single-unit responses in the superior olivary complex of cats to binarual stimulation.
5. Study of membrane properties related to excitation processes and of the functional interaction of nerve cells.
6. Psychophysical investigations of sound localization, discrimination, masking, and adaptation.
7. Exploration of various mathematical models related to auditory nerve activity and auditory psychophysics.
8. Development of a compact digital correlator for on-line use.

Close cooperation continues with the Eaton-Peabody Laboratory at the Massachusetts Eye and Ear Infirmary, Boston. In particular, we are working together on activity of

---

*This work was supported in part by the National Science Foundation (Grant G-16526); in part by the National Institutes of Health (Grant MH-04737-03); and in part by the National Aeronautics and Sapce Administration under Grant NsG-496.

†Also at Massachusetts Eye and Ear Infirmary, Boston, Massachusetts.

‡Research Associate in Communication Sciences from the Neurophysiological Laboratory of the Neurology Service of the Massachusetts General Hospital, Boston, Massachusetts.

**From the Department of Physics, Weizmann Institute of Science, Israel.

single units in the cochlear nucleus of cats and on the measurement of motion in the cat's middle ear.

W. M. Siebert, W. A. Rosenblith

Selected References

1. J. A. Aldrich, Interaural time difference thresholds for band-limited noise, S. M. Thesis, Department of Electrical Engineering, M. I. T., June 1963.

2. M. A. B. Brazier, The problem of periodicity in the electroencephalogram: Studies in the cat, EEG Clin. Neurophysiol. 15, 287-298 (April 1963).

3. G. L. Gerstein and B. Mandelbrot, Random-walk models for the spike activity of a single neuron (to be published in Biophys. J.)

4. P. R. Gray, A Design Philosophy for Psychophysical Experiments, S. M. Thesis, Department of Electrical Engineering, M. I. T., January 1963.

5. J. L. Hall II, Binaural Interaction in the Accessory Superior Olivary Nucleus of the Cat — An Electrophysiological Study of Single Neurons, Ph. D. Thesis, Department of Electrical Engineering, M. I. T., September 1963. (This thesis will be published as Technical Report 416 of the Research Laboratory of Electronics, M. I. T.)

6. F. T. Hambrecht, A Multi-channel Electroencephalographic Telemetry System, S. M. Thesis, Department of Electrical Engineering, M. I. T., May 1963. (A report based on this thesis has appeared as Technical Report 413, Research Laboratory of Electronics, M. I. T., September 30, 1963.)

7. F. T. Hambrecht, P. D. Donahue, and R. Melzack, A multiple-channel EEG telemetering system, EEG Clin. Neurophysiol. 15, 323-326 (1963).

8. R. R. Pfeiffer, Electrophysiological Response Characteristics of Single Units in the Cochlear Nucleus of the Cat, Ph. D. Thesis, Department of Electrical Engineering, M. I. T., June 1963.

9. W. A. Rosenblith, Computers and brains: Competition and/or coexistence, Proc. Seventy-fifth Anniversary Symposium on Engineering for Major Scientific Programs, Georgia Institute of Technology, Atlanta, Georgia, 1963, pp. 117-128.

10. D. M. Snodderly, Activity of Single Neurons in the Lateral Geniculate of the Rat, S. B., S. M. Thesis, Department of Electrical Engineering, M. I. T., June 1963.

11. T. F. Weiss, A Model for Firing Patterns of Auditory Nerve Fibers, Ph. D. Thesis, Department of Electrical Engineering, M. I. T., June 1963. (This thesis will be published as Technical Report 418, Research Laboratory of Electronics, M. I. T.)

12. M. L. Wiederhold, Effects of Efferent Pathways on Acoustic Evoked Responses in the Auditory Nervous System, S. M. Thesis, Department of Electrical Engineering, M. I. T., June 1963.

13. G. R. Wilde, An On-line Digital Electronic Correlator, S. M. Thesis, Department of Electrical Engineering, M. I. T., June 1963.

14. L. S. Frishkopf and M. H. Goldstein, Jr., Responses to acoustic stimuli from single units in the eighth nerve of the bullfrog, J. Appl. Phys. 35, 1219-1228 (1963).

A. FURTHER OBSERVATIONS OF RESPONSE CHARACTERISTICS OF SINGLE UNITS IN THE COCHLEAR NUCLEUS TO TONE-BURST STIMULATION

A previous report[1] described a type of response pattern that was common to a large number of units in the cochlear nuclei of cats. Since that report many more units have been studied and at least two more types of response patterns have been found. Systematic investigations have been restricted to the characteristic frequency, CF, of each unit (that frequency for which the threshold is lowest). From visual observations, however, it has been found that the type of response pattern of any one unit is more dependent on the stimulus intensity than on having the stimulus frequency at the CF.

Figure XXV-1 shows data for typical units representing each of the three common types. In each case, a sample from the spike-train data, and the corresponding post-stimulus time (PST) and interval (INT) histograms[2] are shown. The first unit, P27-7, is of the type previously reported.[1] An examination of the spike train shows that the interspike intervals appear relatively uniform, the INT histogram is unimodal and symmetric, and the PST histogram shows several peaks. All of these observations indicate that the firings are regular and time-locked to the onset of the stimulus. For the second unit, P25-8, an initial firing is followed by an interval of greatly diminished activity (approximately 10-12 msec in duration), which in turn is followed by one or two firings during the latter portion of the tone burst. The INT histogram for these data is bimodal – the later peak representing the interspike time intervals between the initial and second firings, and the earlier peak representing the intervals between multiple firings occurring during the latter portions of the tone bursts. The PST histogram clearly indicates the presence of the initial firing, the interval of diminished activity, and the resumption of activity. For the third representative unit, P29-5, the spike train shows that the interspike intervals are not uniform (as they were for unit P27-7), and that a fixed interval of reduced activity does not occur (as it did for unit P25-8). The INT histogram shows that the interspike time intervals range in length from approximately 1 msec to 11 msec (for this unit and this stimulus intensity) with shorter intervals occurring most frequently. The PST histogram has a relatively smooth envelope lacking the several distinct peaks, as in unit P27-7, and the region of inactivity, as in unit P25-8.

These three types of response activity are most clearly described and most easily identified by the shape of the PST histograms. Almost all of the units for which detailed tone-burst data are available have responses that are easily identified as belonging to one of these three types (80, 60, and 22 units, respectively, from a total of approximately 200). Many others have been identified by visual observations of responses as seen on an oscilloscope. Thus far, the units that do not fall into one of these categories are (i) units with low CF's, which have spikes that are phase-locked to the stimulus, (ii) units that seldom respond to the stimulus so that the number of responses is insufficient to determine to which of the three types, if any, they belong, and (iii) units that are similar to the second type described above except that they do not produce any spikes at high intensities of stimulation (only two units).

To illustrate the dependence of this activity on stimulus intensity, three typical

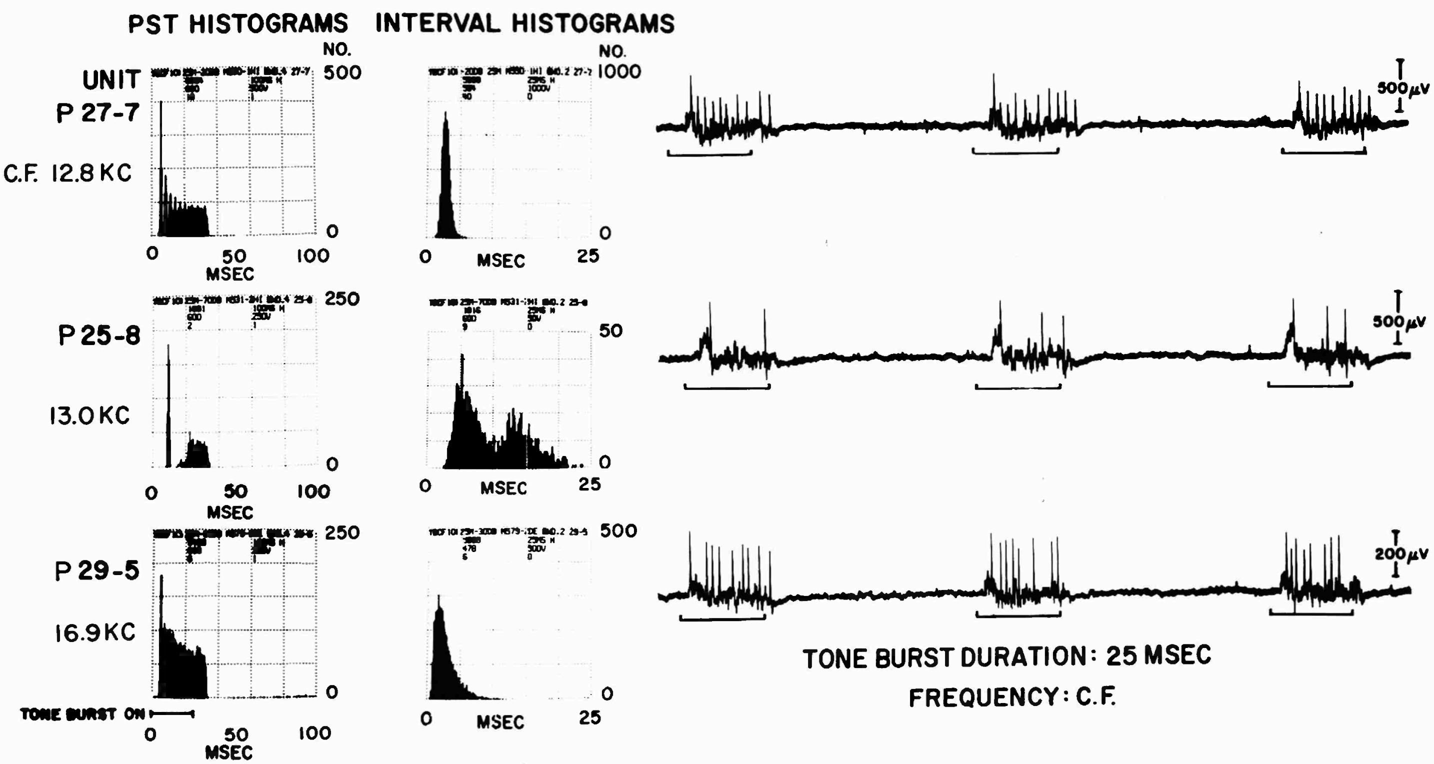

Fig. XXV-1. Poststimulus time and interval histograms of responses to tone-burst stimuli for 3 different units. Individual responses to 3 tone bursts are shown on the right for each unit. All tone bursts had 2.5-msec rise and fall times, 25-msec durations, and 10/sec repetition rates. The stimulus intensity with respect to threshold for visual detection of synchronized responses on an oscilloscope (UVDL — unit visual detection level) was 73, 28, and 55 db from top to bottom. Each PST histogram represents responses to 600 stimuli. The INT histograms represent 584, 600, and 478 stimuli. Locations of the units were posterior ventral cochlear nucleus, dorsal cochlear nucleus, and ventral cochlear nucleus, respectively.

examples of variations in the PST histograms with changes in stimulus intensity are shown in Figs. XXV-2, XXV-3, and XXV-4.

Figure XXV-2 shows an intensity series for unit P28-9, another representative of the first type of unit discussed. The top PST histogram is obtained from the spontaneous activity of this unit. As expected, there is no locking in time of the spikes and the artificial stimulus marker. The second histogram (-65 db) shows the presence of responses to the stimulus. At -60 db, the responses are seen clearly, but the histogram does not have several distinct peaks. The peaks for this unit emerge at higher intensities (between -60 and -50 db). Most often, for these units, the peaks emerge at threshold, but always within 10 db of threshold.

Figure XXV-3 shows an intensity series for a unit of the second type. Responses are seen to be present at -80 db. At -70 db three distinct, regularly spaced peaks are present. At higher intensities, however, the region of greatly diminished activity, characteristic of the second type of unit, appears. Thus far in this study, all of the units of this type required signal intensities between 20 db and 25 db above their thresholds to produce this zone of reduced activity.

Figure XXV-4 shows an intensity series for a unit of the third type. The presence of a response is just noticeable at -80 db. As the intensity increases, the histograms show neither several distinct peaks nor a region of inactivity within the response portion.

Thus it can be seen that these three types of activity are distinct over a wide range of intensity, although it is difficult in some cases to make judgments of type near threshold. Whereas no discrimination can be made between the first two types for intensities within 25 db of unit thresholds, unambiguous determinations for all three types are always possible at intensities above the 25-db level.

All three types of activity are usually observed in the same animal, for example, units P27-6, P27-7, and P27-13 are different types, but are all from cat 27. Furthermore, these types do not appear to depend on depth of anesthesia because they all can be found both at the beginning and at the end of an experiment (usually approximately 12-18 hours in duration). These types of activity, however, do seem to depend on the location of the electrode tip. The gross anatomical location of the electrode tip can be determined on the basis of results obtained by Rose et al.[3] and Rose[4] which pertain to the "tonotopic" organization of the single units in the cochlear nucleus. Their results showed that successive units encountered in a given electrode pass exhibited CF's that changed in an orderly sequence except for distinct discontinuities correlated with the boundaries of gross anatomical structures. On the basis of the location of a unit with respect to the distinct discontinuities in the sequences of the CF's one is thus able to determine if a unit is in the dorsal cochlear nucleus (DCN), ventral cochlear nucleus (VCN), or one of the latter's subdivisions – the posterior ventral or anterior ventral

Fig. XXV-2

Poststimulus time histograms of responses to repeated tone bursts as a function of stimulus intensity. The first PST histogram is of 1 minute of spontaneous activity of this unit. Intensity increases from top to bottom. Each histogram represents responses to 600 stimuli (1 minute of data). The UVDL of this unit was -63 db. Stimulus-locked responses can be seen at intensities below UVDL, that is, below -65 db. This unit was located in the posterior ventral cochlear nucleus. The abscissa scale has a 0.4-msec quantization interval. All tone bursts had 2.5-msec rise and fall times.

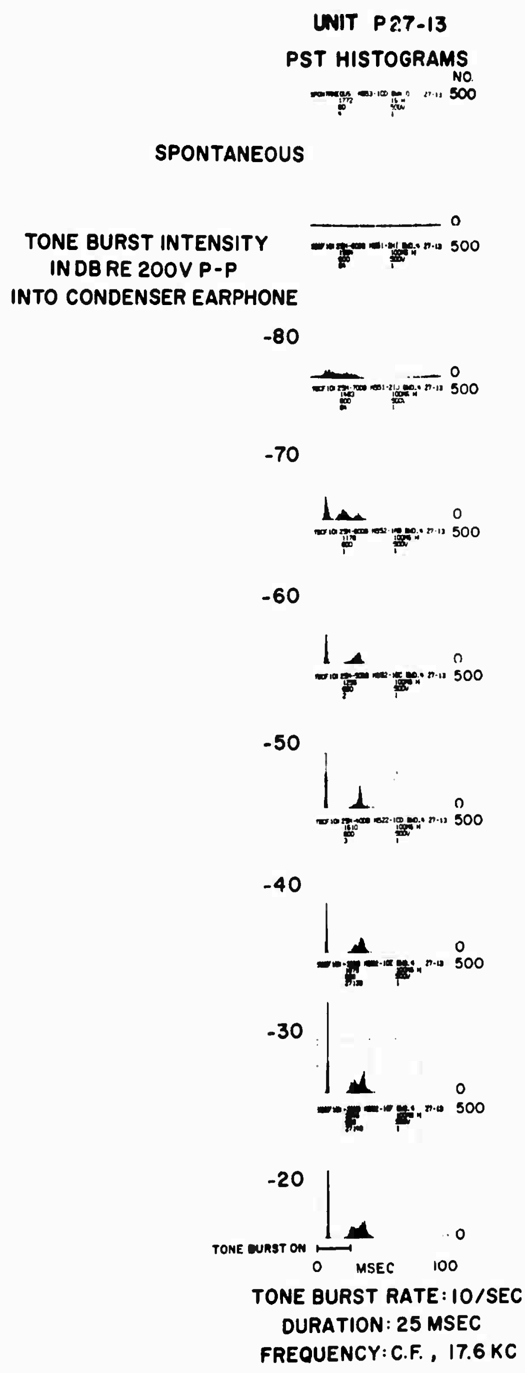

Fig. XXV-3.

Poststimulus time histograms of responses to repeated tone bursts as a function of stimulus intensity. The first PST histogram is of 1 minute of spontaneous activity of this unit. Intensity increases from top to bottom. Each histogram represents responses to 600 stimuli (1 minute of data). The UVDL of this unit was -85 db. This unit was located in the dorsal ccchlear nucleus. The abscissa scale has a 0.4-msec quantization interval. All tone bursts had 2.5-msec rise and fall times.

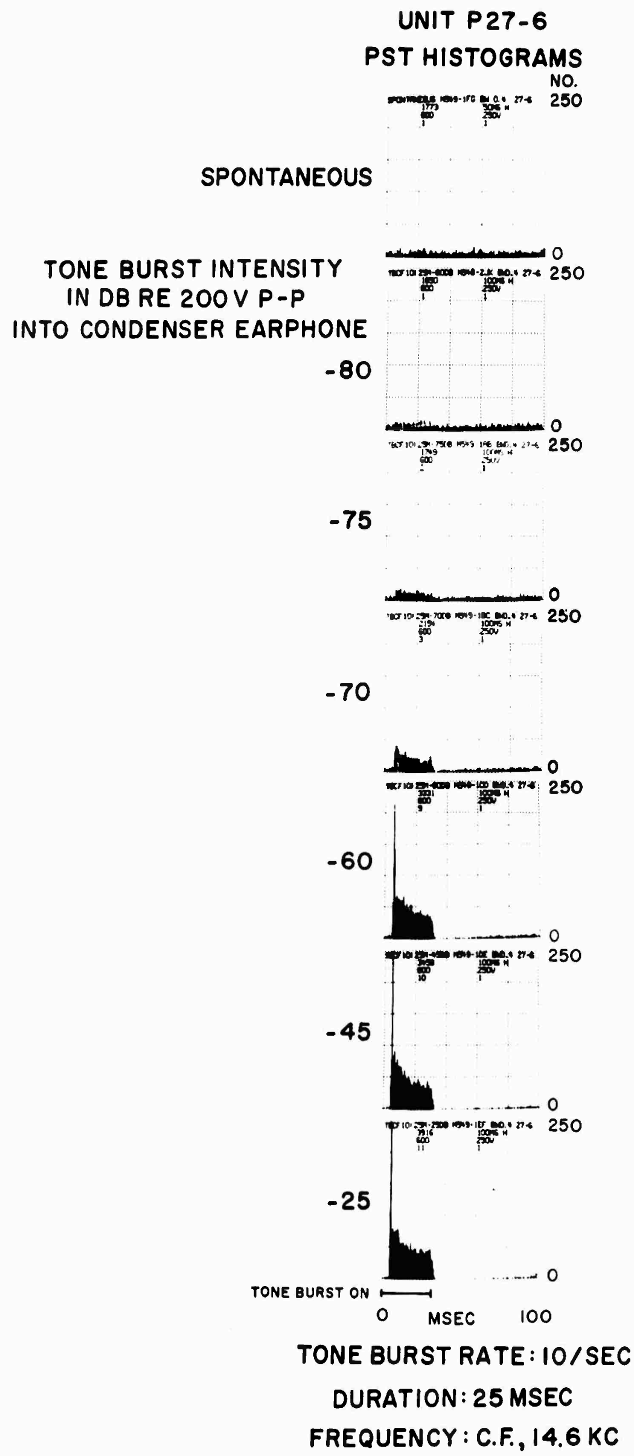

Fig. XXV-4.

Poststimulus time histograms of responses to repeated tone bursts as a function of stimulus intensity. The first PST histogram is of 1 minute of spontaneous activity for this unit. Intensity increases from top to bottom. Each histogram represents responses to 600 stimuli (1 minute of data). The UVDL of this unit was -75 db. Stimulus-locked responses can be seen at intensities below the UVDL, that is, below -80 db. This unit was located in the posterior ventral cochlear nucleus. The abscissa scale has a 0.4-msec quantization interval. All tone bursts had 2.5-msec rise and fall times.

cochlear nucleus, PVCN and AVCN, respectively. By using this method, units of the first type described, for example, P27-7 and P28-9, have been found almost exclusively in the VCN, with a few (6) in the DCN. The second type, for example, P25-8 and P27-13, has only been found in the DCN (or extremely close to the DCN-PVCN border on the PVCN side). The last type described above, for example, P29-5 and P27-6, has only been found in the VCN, and, when finer location was possible, it has always been found in the PVCN.

We also found,[5] and will report elsewhere, that correlations exist between these types of response activity and other properties of the units, such as their spontaneous activity and their response patterns to other types of stimuli.

R. R. Pfeiffer

References

1. R. R. Pfeiffer, Some response characteristics of single units in the cochlear nucleus to tone-burst stimulation, Quarterly Progress Report No. 66, Research Laboratory of Electronics, M.I.T., July 15, 1962, pp. 306-315.

2. G. L. Gerstein, Analysis of firing patterns in single neurons, Science 131, 1811-1812 (1960).

3. J. E. Rose, R. Galambos, and J. R. Hughes, Microelectrode studies of the cochlear nuclei of the cat. Bull. Johns Hopkins Hospital 104, 211-251 (1959).

4. J. E. Rose, Organization of frequency sensitive neurons in the cochlear nuclear complex of the cat, Neural Mechanisms of the Auditory and Vestibular Systems, edited by G. L. Rasmussen and W. F. Windle (Charles C. Thomas, Springfield, Illinois, 1960).

5. R. R. Pfeiffer, Electro-physiological Response Characteristics of Single Units in in the Cochlear Nucleus of the Cat, Ph.D. Thesis, Department of Electrical Engineering, M.I.T., May 1963.

XXVI. NEUROPHYSIOLOGY*

W. S. McCulloch
F. S. Axelrod
H. A. Baldwin
P. O. Bishop
M. Blum
J. E. Brown
S. Frenk
R. C. Gesteland
M. C. Goodall
B. H. Howland
W. L. Kilmer
K. Kornacker
W. J. Lennon
J. Y. Lettvin
Diane Major
L. M. Mendell
W. F. Pickard
W. H. Pitts
Helga Schiff
A. Taub
P. D. Wall

RESEARCH OBJECTIVES

1. Basic Theory

The general problem of reliable computation in vertebrate central nervous systems has been solved in principle.[1] Also, neurophysiologists are making rapid progress on the functional organization of specialized regions in such systems. But no one has yet reported a way for thinking effectively about how the brain stem reticular system performs its task of committing an entire organism to either one mode of behavior or another.

Our problem is to construct a theory for the reticular system[2-4] which is compatible with known neuroanatomy and neurophysiology, and which will lead to testable hypotheses concerning its operation.

Our first approach was through the theory of ordinary one-dimensional iterative logic nets.[5-7] But all of the crucial questions in this theory turned out to be recursively unsolvable when considered generally, and combinatorially intractable when particularized with the required degrees of dependency among the variables.

Our second approach was through the theory of coupled nonlinear oscillators, but we soon found that there is not nearly enough of the right kind of mathematics to be of much help in our problem.

All we can report at the moment is that we are embarked on a kind of iterative net statistical decision theory which is comprehensive, versatile, and penetrating enough to stand a reasonable chance of success.

W. L. Kilmer, W. S. McCulloch

References

1. Cf. W. S. McCulloch, Biological Computers, IRE Trans., Vol. EC-4, No. 3, pp. 190-192, 1957; M. A. Arbib, Brains, Machines and Mathematics (McGraw-Hill Publishing Company, New York, in press); S. Winograd and J. D. Cowan, Reliable Computation in the Presence of Noise (The M.I.T. Press, Cambridge, Mass., 1963).

2. M. Scheibel and A. Scheibel, Biological models for command automata, Mitre Report 55-3, First Congress on the Information System Sciences, November 1962.

3. H. Jasper and others (eds.), The Reticular Formation of the Brain, Proc. Henry Ford Hospital International Symposium (Little, Brown and Company, Boston, 1958).

---

*This work was supported in part by the Bell Telephone Laboratories, Inc.; The Teagle Foundation, Inc.; the National Science Foundation (Grant G-16526); the National Institutes of Health (Grants MH-04737-03 and NB-04897-01); the U.S. Air Force (Aeronautical Systems Division) under Contract AF33 (616)-7783; and the National Aeronautics and Space Administration (Grant NsG-496).

4. E. R. Ramey and D. S. O'Doherty (eds.), Electrical Studies on the Unanesthetized Brain (Harper and Row, New York, 1960).

5. F. C. Hennie III, Iterative Arrays of Logical Circuits (The M.I.T. Press, Cambridge, Mass., 1961).

6. W. L. Kilmer, On dynamic switching in one-dimensional logic networks (Information and Control, in press).

7. W. L. Kilmer, Topics in the theory of one-dimensional iterative networks (to be published in Information and Control).

2. Project Plans

(a) The Nature of Biological Membrane. For some time we have felt that the performance of cell membrane could be understood in terms of the logical consequences of two or three extremely simple and reasonable assumptions. We are now hopeful about the outcome of this work. But it appears that there are several elementary, but lengthy, experiments to be done with tracers on semipermeable membranes, and these must be finished before we are willing to commit ourselves. The development is only distantly related to, and is also more transparent than, the current theories based on irreversible thermodynamics.

W. F. Pickard, J. Y. Lettvin

(b) The Nature of Form-Function Relations in Neurons. After Lettvin and Maturana proposed certain anatomical features as underlying the operation of retinal ganglion cells in the frog, the question arose as to whether it would be possible to test the notion. During this past year we discovered that the use of time constants of adaptation suggested the combinatorials that were proposed. This finding has done much to hearten us to make a more exact statement of connectivity, and we are now engaged in setting up a quantitative study.

S. Frenk, J. Y. Lettvin

(c) The Character of Certain Receptor Processes. It was suggested by Lettvin, in his analysis of color vision, that some receptors may have to be characterized by two variables at their outputs. For example, imagine a receptor like a rod that has a photosensitive pigment attached to the membrane. Let every patch of membrane with pigment on it have an equal effect at the output. Let a pigment molecule, on receipt of a quantum, first change in such a way as to open a channel for ions not at equilibrium with the membrane potential, thus causing a current flow. Thereafter the pigment further changes and either moves away from the membrane or becomes attached in a different way so as to open a channel only for ionic species at equilibrium with the membrane potential. In this way, the signal imposed by light at any instant is attenuated by a weighted integral of the amount of light shining in the immediate past (there is also a restoration process) and this process yields a total signal current which is logarithmically, or quasilogarithmically, related to the average intensity of light. Such a receptor process has two degrees of freedom. The idea that certain stimuli increase signal current while others attenuate that current by division is useful when one suspects combinatorials of stimuli to be taken at the very input. Some of the results of Gesteland on the olfactory mucosa suggest that such a process occurs there. We expect to examine this in some detail. A preliminary report has been prepared.

R. C. Gesteland, W. H. Pitts, J. Y. Lettvin

(d) Properties of Cerebellar Cells. The writer reported in Quarterly Progress Report No. 69 (pages 241-246) on the curious combinatorials of stimuli necessary to excite cells in the cerebellum of the frog. This research has continued and the results will be presented as a doctoral dissertation in 1964.

F. S. Axelrod

(e) Properties of Second-Order Vestibular Neurons in Frogs. The ganglion cells of the three major vestibular nuclei are related to the firing pattern of the different vestibular branches in definite ways that are still difficult to define. We intend to try to define these functions.

Helga Schiff, J. Y. Lettvin

(f) Properties of Second-Order Olfactory Neurons in Frogs. There seems to be an indication that the transients recorded on the surface of the olfactory lobe are not only related to the firing of mitral and other cells but also to glomerular activity. At any rate, the slower transients look suspiciously as if they arise from primary processes. This is only a hint thus far, but will be pursued, since the difficulty of interpreting primary receptor processes may be eased by getting some notion of how the information appears aggregated at the junctions in olfactory lobe.

H. A. Baldwin, J. Y. Lettvin

(g) Is the Rapid Water Movement in Some Plants Attributable to an Ion Pump? The current explanation of the very quick changes in turgor of some cells in Mimosa is that the osmotic pressure changes are brought about by the breaking up of starch. We suspect that an alternative is the movement of water by something like a potassium pump. This idea will be subjected to test during the early part of 1964 by Barbara Pickard.

J. Y. Lettvin

(h) Color Vision. The views reported in part in Quarterly Progress Report No. 70 (pages 327-337) will be carried farther by psychological studies, rather than by physiological experiments on monkeys.

J. Y. Lettvin

(i) Instrumentation Projects. Divers instruments will be built as the occasion arises, if the research demands them and industry is incapable of furnishing them. (Barbara Pickard will be connected with this project.)

H. A. Baldwin, J. Y. Lettvin

(j) Models of Electrochemical Processes. There is some reason to hope that some of the theory of weak interactions may be useful in a general theory of strong electrolytes. This idea will be pursued to test for adequacy.

W. H. Pitts

(k) Physical Optics. There are enough tricks of design left in physical optics that one can say the field is far from exhausted. This is particularly true when one wants to deal with the dioptrics of living eyes. Some of our results have appeared in Quarterly Progress Reports No. 67 (pages 197-204) and No. 71 (pages 267-273), and we intend to look for still more.

B. H. Howland

3. Problems of Sensory Projection Pathways

During the past year, we have concentrated on two major lines of approach to the problems of cutaneous sensory mechanisms. The first has dealt with the control system situated about the first central synapse where nerve fibers from the skin converge on cells in the dorsal part of the spinal cord. We have shown that the very small cells scattered throughout the region of these synapses and which make up the substantia gelatinosa are involved in modulating the transmission of impulses across this first junction. This censorship of arriving nerve impulses is affected by previous activity in the same pathway, by activity in neighboring areas of skin, by intense activity in distant areas, particularly in paws and face, and by stimulation of the cerebellum, mid-brain, pons, and medulla. The censorship mechanism seems to be in continuous action, and we believe that it is best studied by steady stimuli, rather than by sudden brief changes in the environment. The mechanisms that we have seen in the cat would predict interactions between various types of skin stimuli, and we have carried out concomitant experiments on man to examine these hypotheses. These psychological experiments have shown that there is a most interesting interaction in man between light-pressure stimuli and electrical stimulation. We have published some of this work in Brain and in the Journal of Physiology, and two other papers will appear in the latter journal in 1964. In the coming year, we shall pursue the study of the censorship mechanism in an attempt to find something of its role in the normal functioning of the animal.

Our second line of approach is an attempt to discover the language used by the skin in telling the brain about the location of the stimulus. We are studying two reflexes that require the motor mechanisms to know the exact location of the stimulus. The first is the scratch or swipe reflex, and the second is the eye blink. We are studying the pathways over which the information is carried both in normal animals and in frogs and salamanders who have been operated on in their youth. If dorsal and ventral skin are reversed in the tadpole, the scratch reflex of the adult frog is aimed at the embryological position of the skin, and not at its actual position, so that it is evident that some message is going from skin to central nervous system which tells the nature of the skin rather than its position. We hope to discover the nature of this message by microelectrode studies of the cord. Similar work is being done on amphibia in which an additional eye is implanted on the head. The extra eye will generate a blink reflex in the normal eye if it is touched, and so we know that nerves are somehow capable of telling the brain that they are in cornea and not in ordinary skin. This problem has been studied in normal frogs; a paper based on Karl Kornacker's doctoral dissertation has appeared in Experimental Neurology, and this work will continue.

A. Taub, K. Kornacker, Diane Major, P. D. Wall

A. ALGORITHMIC THEORIES OF GROWTH AND DIFFERENTIATION

This report is a summary of a paper that has been submitted for the Biophysical Society Annual Meeting to be held in Chicago, February 26-28, 1964.

The analogy of growth and differentiation to the unfolding of a computer program is obvious. No programs yet devised, however, satisfy the essential requirement of a biological model, which is functional stability in the face of a fluctuating environment. This poses a certain antithesis: on the one hand, analog systems possess only a local stability; on the other, digital systems can, by functional redundancy,[1] achieve stability in the large.

A model combining these features closely reflects what is known about cellular differentiation and morphogenesis. That is, each cell contains the basic genetic code represented by the substitution rules R of Thue[2] associative system, together with current word S_i, and address A_i (for next application of R). S_i determines the rate constants of the cell metabolism regarded as a nonlinear system.[3] Finally, the concentrations of metabolites operate a threshold control system CS which determines A_i and the next application of R. This model is computable, but its main value at present would appear to be as a conceptual framework in which to discuss problems of epigenesis.

M. C. Goodall

References

1. W. S. McCulloch, The Stability of Biological Systems, Brookhaven Symp. 10, 207 (1957).

2. M. Davis, Computability and Unsolvability (McGraw-Hill Book Company, New York, 1958).

3. B. Goodwin, Temporal Organization in Cells (Academic Press, Inc., New York, 1963).

B. MEASURES ON THE COMPUTATION SPEED OF PARTIAL RECURSIVE FUNCTIONS

Given sufficient time, a man can perform all of the operations of a modern digital computer. The value of the computer, therefore, lies in the speed with which it operates, not in the particular operations that it performs. The intent of this report is to define precisely this concept of speed of computation, and to derive some theorems that characterize it.

1. The Measure Function Φ

It is natural to associate with a computer program P_i both the function ϕ_i that it computes and a measure function Φ_i that might indicate the speed of the program. For example, $\Phi_i(x)$ might be the number of symbols printed or erased during the computation of $\phi_i(x)$ (by means of P_i), or the number of times that the computer changes state, or the number of seconds that elapse from the moment that the computer starts until the time at which it stops, or even the amount of tape used in the computation. From another point of view, the computation of $\phi_i(x)$ could be interpreted as a proof of the appropriate statement $\phi_i(x) = y$. $\Phi_i(x)$ would then be the length of a proof terminating in a string of the form $\phi_i(x) = y$.

2. Applications of the Measure Function Φ

It is evident that the measure function is useful in comparing the speed of two programs for the same function. If programs P_i and P_j serve to compute the same function

$\phi_i = \phi_j$ and if $\Phi_i(x) < \Phi_j(x)$ for all x, then P_i is a "quicker" program than P_j.

This measure is also linked with the difficulty of computation. For example, the function 2^{2^x} naturally takes more time to compute than the function 2x, since the answer takes so much longer to print, but a function with values 0 and 1 which takes as long to compute as 2^{2^x} must have difficulties inherent in its computation.

Fermat, ca. 1650, conjectured that $2^{2^x}+1$ is prime for all non-negative integers x. This he verified for x = 0 through x = 4, and, without further evidence, he challenged his comtemporaries to disprove it. Euler accepted the challenge, and, with characteristic cunning, proved that $2^{2^5}+1 = 641 \times 6,700,417$ is not a prime. Since his time, a number of persons have investigated this conjecture for x larger than 5. In all cases tried, they have found that $2^{2^x}+1$ has proper factors. Fermat's conjecture can be reformulated in terms of the function

$$f(x) = \begin{cases} 1 & \text{if } 2^{2^x}+1 \text{ is prime} \\ 0 & \text{otherwise.} \end{cases}$$

The evidence suggests the hypothesis: $f(x) = 0$ for $x \geq 5$, and if true, a quick program for the computation of f muxt exist. Such a program simply sees to it that an output 1 is printed for inputs x less than 5 and that a 0 is printed for inputs x greater than 5. If, on the other hand, it can be shown that every program that computes f is slower than the quick program suggested above, the hypothesis must be false. Hence the measure provides important information about this function. Unfortunately, the results of this report do not suffice to provide this information, but we take a step in the right direction by defining the measure function and deriving some of its properties.

3. M-Computers

For clarity, it is essential to distinguish between computers and their mathematical models, which we call M-Computers. There are to be thought of as ideal devices that can be programmed to compute any partial recursive function. We pick one such device here as standard: The standard M-Computer is a device equipped with a container for cards, a tape scanner, and a tape that is infinite in both directions. The tape is divided into squares along its length and the scanner can look at one square at a time. The device is equipped to print one of the symbols B(blank), 0, 1, ..., 9 on the square that it is examining and shift the tape to right or left by one square. The container can hold an arbitrarily large but finite number of cards, called the program. On each card is printed a single 5-tuple $\langle q_i, S_i, S_j, D, q_j \rangle$. The symbols q_i, $i = 0, 1, 2, \ldots$ are internal states, S_i is one of the symbols B, 0, 1, ... 9, and D is a direction R(right) or L(left). When the device is in state q_i and scans the symbol S_i, it prints the symbol S_j, shifts the tape to right or left as dictated by D, and changes its internal state to q_j. If the device is in state q_k and scans the symbol S_k, and if no card in the container has printed on it a 5-tuple of the form $\langle q_k, S_k, \ldots \rangle$, then the device stops. Any program is allowed, subject to the condition that any two cards must differ at either the first internal state q_i or the first symbol S_i.

We can associate with each program a partial recursive function ϕ as follows: The program is placed in the container, an input integer x is written in radix 10 on the tape, the scanner is placed over the rightmost digit of x, and the device is put in state q. The device then operates in accordance with the instructions printed in the program. If it never stops, we say that the function $\phi(x)$, which it computes, diverges. If it does stop, we let $\phi(x)$ be the integer that remains on the tape after all B's are cancelled.

We can effectively list the programs P_o, P_1, ... for a standard M-Computer, their associated partial recursive functions ϕ_o, ϕ_1, ... (ϕ_i is computed by P_i), and their measure functions Φ_o, Φ_1, ... defined by the statement: $\Phi_i(x)$ diverges if $\phi_i(x)$ diverges, and $\Phi_i(x)$ is the number of seconds required to compute $\phi_i(x)$ if $\phi_i(x)$ converges.

The standard M-Computer with a program in its container is a Turing machine.

A basic result of recursive function theory states that for a large class of idealized computers, a function that is computable by one such device is computable by all others. Hence it is unnecessary for most authors to distinguish among them. It is essential for us to make this distinction, however, since we are concerned with measure functions, and since the particular measure function associated with a program must depend on our choice of computer. In fact, we shall define an M-Computer abstractly in terms of the measure functions associated with its programs.

DEFINITION: <u>An M-Computer ${}^{\xi}C$</u> is a list of pairs of partial recursive functions $(\phi_o, {}^{\xi}\Phi_o)$, $(\phi_1, {}^{\xi}\Phi_1)$, $(\phi_2, {}^{\xi}\Phi_2)$... where $\phi_o, \phi_1, \phi_2, \ldots$ is the enumeration of all partial recursive functions as determined by the standard M-Computer,[1] and ${}^{\xi}\Phi_o, {}^{\xi}\Phi_1, {}^{\xi}\Phi_2, \ldots$, is an enumeration of partial recursive functions called <u>measure functions</u>, with the properties:

(i) For all i and x, $\phi_i(x)$ converges iff ${}^{\xi}\Phi_i(x)$ converges.

(ii) There exists a total recursive function α such that for all i and x

$$\alpha(i, x, y) = \begin{cases} 1 & \text{if } {}^{\xi}\Phi_i(x) = y \\ 0 & \text{otherwise.} \end{cases}$$

NOTATION: We use f, g, and h to denote arbitrary partial recursive functions, and the symbol ϕ_i to denote the i^{th} partial recursive function in our standard listing. To every partial recursive function f there corresponds infinitely many different i's for which $\phi_i = f$. Given such an i, we may sometimes write f_i for ϕ_i and ${}^{\xi}F_i$ for ${}^{\xi}\Phi_i$ in order to emphasize that ϕ_i equals f.

We now give some examples to indicate how the measure function may be interpreted.

EXAMPLE 1: We have defined $\Phi_i(x)$ to be the number of seconds required to compute $\phi_i(x)$ on the standard M-Computer. Property (i) of the measure functions states that $\phi_i(x)$ converges iff its computation takes a finite time $(\Phi_i(x))$. Similarly, property (ii) states that it is effectively possible to determine whether or not $\phi_i(x)$ converges in y seconds. One begins the computation of $\phi_i(x)$ with stop watch in hand; if the computation takes exactly y seconds, we let $a(i,x,y) = 1$; otherwise, we let $a(i,x,y) = 0$.

EXAMPLE 2: The measure function might measure the number of squares of tape used in the computation. Take the standard M-Computer and let

$$ {}^{\xi}\Phi_i(x) = \begin{cases} y & \text{if } \phi_i(x) \text{ converges and } y \text{ squares of tape are used in the computation} \\ \text{divergent} & \text{if } \phi_i(x) \text{ diverges.} \end{cases} $$

Clearly, $\phi_i(x)$ converges if and only if ${}^{\xi}\Phi_i(x)$ converges. A simple argument based on the number of possible machine tape configurations that involve a fixed finite amount of tape proves that a is total recursive. Hence ${}^{\xi}C$ is an M-Computer.

EXAMPLE 3: Begin the computation of $\phi_i(x)$ with the standard M-Computer. Let ${}^{\xi}\Phi_i(x)$ be the number of symbols required to write the program P_i, plus the number of state changes during the computation of $\phi_i(x)$, plus the number of squares of tape used. Then ${}^{\xi}C$ is an M-Computer.

EXAMPLE 4: Let C' be some characterization other than the standard M-Computer. Denote the programs and corresponding partial recursive functions of C' by

$$P'_o, P'_1, P'_2, \ldots$$

$$\phi'_o, \phi'_1, \phi'_2, \ldots .$$

Under what conditions may we assume that $\phi_o = \phi'_o$, $\phi_1 = \phi'_1$, ... ? If the enumeration theorem and the s-m-n theorem[2] are to hold true for C', it can easily be shown that there must exist total recursive functions g and h such that $\phi'_{g(i)} = \phi_i$ and $\phi'_i = \phi_{h(i)}$ for all i. If, in addition, there exists a total recursive function k such that $\phi_{k(i)} = \phi_i$ and $k(i) > i$ for all i, then g and h can be taken to be 1-1 recursive functions. By means of a Schröder-Bernstein type of proof, it can then be shown that there exists a 1-1 onto total recursive function f such that $\phi'_{f(i)} = \phi_i$ for all i. Without loss of generality, we may then assume that f is the identity function. It follows, we hope, that the choice of a standard M-Computer in the definition given above is not too demanding.

In order to compute ${}^{\xi}\Phi_i(x)$, we must first find a partial recursive function $\phi_j = {}^{\xi}\Phi_i$, since we have a program for computing ϕ_j but none for computing ${}^{\xi}\Phi_i$. Our first theorem asserts that there is an effective procedure for going from an index i for a measure function to an index j for the equivalent partial recursive function in our standard listing.

THEOREM 1: To each M-Computer ${}^{\xi}C$ there corresponds a total recursive function β such that ${}^{\xi}\Phi_i = \phi_{\beta(i)}$ for all i.

PROOF: We begin by defining a function $f(i, x) = {}^{\xi}\Phi_i(x)$. Formally,

$$f(i, x) = \begin{cases} y & \text{if } \alpha(i, x, y) = 1 \\ \text{divergent} & \text{otherwise.} \end{cases}$$

Since α is a total recursive function, it is effectively possible to compute f, hence by Church's thesis, f is a partial recursive function. The s-m-n theorem ensures the existence of a total recursive function β such that $\phi_{\beta(i)}(x) = f(i, x)$ for all i and x. Therefore $\phi_{\beta(i)} = {}^{\xi}\Phi_i$ for all i, and β is the desired total recursive function. Q.E.D. Since the recursive functions are countable, it follows immediately that the class of M-Computers is also countable.

4. A Theorem by Rabin

Suppose that you want to find a function f such that no matter what program you choose to compute it, the calculation of f(x) always takes more that 2^x seconds. All that you need to do is to pick a function f with values so large that it takes 2^x seconds just to print the answer. A similar method can be used to find a function that takes more than g(x) seconds to compute, g being any total recursive function. A nontrivial problem, however, would be to find a function f with values 0 and 1 such that every program for f necessarily takes more than g(x) seconds to compute for almost all x (for all x greater than some integer x_o). (Question: Why for almost all x?) By means of an interesting diagonalization process, M. O. Rabin proved the existence of such 0-1 valued functions.[3] His theorem, with a somewhat different proof, is reproduced here. The process involved is an essential feature of most of the proofs in this report.

THEOREM 2 (Rabin): Let C be an M-Computer and let g be any total recursive function. Then there exists a total recursive function f with values 0 and 1 such that for every index i for f, ${}^{\xi}F_i(x)$ exceeds g(x) for almost all x.

PROOF: We construct f: First, a Gödel table is made which contains the symbol $\phi_r(c)$ in the intersection of row r and column c.

	0	1	2	3	4
0	$\phi_o(0)$	$\phi_o(1)$	$\phi_o(2)$	$\phi_o(3)$	$\cancel{\phi_o(4)}$
1	$\phi_1(0)$	$\phi_1(1)$	$\cancel{\phi_1(2)}$	$\cancel{\phi_1(3)}$	$\cancel{\phi_1(4)}$
2	$\phi_2(0)$	$\phi_2(1)$	$\phi_2(2)$	$\phi_2(3)$	$\phi_2(4)$
3	$\phi_3(0)$	$\phi_3(1)$	$\phi_3(2)$	$\phi_3(3)$	$\phi_3(4)$
4	$\phi_4(0)$	$\phi_4(1)$	$\phi_4(2)$	$\phi_4(3)$	$\phi_4(4)$

Then all entries $\phi_i(x)$ that converge in g(x) seconds at most are circled, that is, $\phi_i(x)$ is circled if ${}^{\xi}\Phi_i(x) \leq g(x)$. This circling can be done effectively, since ${}^{\xi}\Phi_i(x) \leq g(x) \leftrightarrow$ $\alpha(i, x, y) = 1$ for some y less than or equal to g(x), and g is total recursive.

The next stop is to go to column 0: If $\phi_o(0)$ is circled, check it, cancel the remaining part of row 0, and go to column 1. If $\phi_o(0)$ is not circled, go directly to column 1. In general, when you reach any column, x, check the first circled uncancelled entry in that column, $\phi_i(x)$, such that $i \leq x$. Then cancel all entries to the right of $\phi_i(x)$. If no such entry exists, do nothing to column x. Go to column x+1. This check procedure is clearly effective. Moreover, a row with infinitely many circled entries must have 1 and only 1 checked entry.

To compute f(x), first determine if one of the entries $\phi_o(x), \phi_1(x), \ldots, \phi_x(x)$ is checked (by the procedure above, one of these entries at most can be checked). If, say, $\phi_i(x)$ is checked, it must converge (since $\phi_i(x)$ converges iff ${}^{\xi}\Phi_i(x)$ converges, and ${}^{\xi}\Phi_i(x) \leq$ g(x)). Compute $\phi_i(x)$ and let

$$f(x) = \begin{cases} 1 & \text{if } \phi_i(x) = 0 \\ 0 & \text{otherwise.} \end{cases}$$

If none of the entries is checked, let f(x) = 1. Clearly, f is a total recursive function. To see that it is the desired function, suppose that i is an index for f and that, to the contrary, there exist infinitely many x such that ${}^{\xi}F_i(x) \leq g(x)$. Then, according to the procedure given above, row i must have a single checked entry $\phi_i(y)$. But, by definition of f, $f(y) \neq \phi_i(y)$, hence i cannot be an index for f, which is a contradiction. Therefore f must be the desired function. Q.E.D.

The next theorem and its proof is an immediate generalization of Rabin's theorem to all partial recursive functions. The statement of this theorem will be needed as a lemma subsequently in this report.

THEOREM 3: Let ${}^{\xi}C$ be an M-Computer and let g be a partial recursive function. Then there corresponds to g a 0-1 valued partial recursive function f such that f(x) converges iff g(x) converges; if j is any index for f, then for almost all x ${}^{\xi}F_j(x) > g(x)$ whenever g(x) converges. Moreover, there is a total recursive function, γ, which takes any index i for g into an index $\gamma(i)$ for f.

PROOF: Fix an integer i and construct a list of pairs of integers according to the following procedure (these pairs correspond to the checked entries in the proof of Rabin's theorem)[4]:

Stage 0: If ${}^{\xi}G_i(0) = 0$ (i.e., $\alpha(i, 0, 0) = 1$) and ${}^{\xi}\Phi_o(0) \leq g(0)$ (${}^{\xi}G_i(0) = 0 \rightarrow g_i(0)$ converges), put (0, 0) in the list; otherwise, do nothing. Go to stage 1.

Stage n = (p, q): Determine whether or not ${}^{\xi}G_i(p) = q$. If not, go to stage n+1. If so, then $g_i(p)$ converges. See if any of the function values ${}^{\xi}\Phi_o(p), {}^{\xi}\Phi_1(p), \ldots {}^{\xi}\Phi_p(p)$

are less than or equal to $g_i(p)$. (This can be done with the α-function.) If not, go to stage n+1. If so, then ${}^{\xi}\Phi_{s_1}(p), \ldots, {}^{\xi}\Phi_{s_t}(p)$ $(s_1 < \ldots < s_t \leq p)$ will be less than or equal to $g_i(p)$. If all of the pairs $(s_1, z_1), \ldots, (s_t, z_t)$ appear in the list thus far constructed for some values of $z_1, \ldots, z_t$, go to stage n+1. If not, pick the smallest integer s_k such that (s_k, z_k) does not appear in the list thus far constructed for any value of z_k. (This integer s_k can be chosen effectively, since the list thus far constructed is finite.) Put (s_k, p) in the list. Go to stage n+1.

The list of pairs obtained in this way is obviously recursively enumerable. Note that for all s, s', p, p', if (s, p) appears in the list, then (s, p') and (s', p) do not appear in the list: (s, p') cannot appear for obvious reasons; (s', p) cannot appear since to do so, it must appear in stage $n = \langle p, q\rangle$ where ${}^{\xi}G_i(p) = q$, but this is precisely the stage in which (s, p) must be placed in the list, and at each stage at most one pair of integers can be placed in the list.

We now give an effective procedure for computing a partial recursive function h of two variables i and x from which we shall obtain the function f by an application of the s-m-n theorem. To compute h(i, p): First, compute $g_i(p)$. If it diverges, let h(i, p) diverge. If $g_i(p)$ converges, then ${}^{\xi}G_i(p) = q$ for some integer q. In this case, generate the list and see if (s, p) appears in it for some integer s. (If it does appear, then it must do so in stage $n = \langle p, q\rangle$; hence it is effectively possible to determine if (s, p) is in the list for some s.) If (s, p) does <u>not</u> appear in the list for some s, let h(i, p) = 1. If it does appear, then $\phi_s(p)$ converges and ${}^{\xi}\Phi_s(p) < g_i(p)$ (by construction of the list) and s is unique (for if $t \neq s$, then (t, p) does not appear in the list). Let

$$h(i,p) = \begin{cases} 0 & \text{if } \phi_s(p) \neq 0 \\ 1 & \text{if } \phi_s(p) = 0. \end{cases}$$

Clearly, h is a partial recursive function, so that, by the s-m-n theorem, there exists a total recursive function γ such that $f_{\gamma(i)}(x) = h(i, x)$ for all i and x.

We assert that γ is the desired total recursive function of the theorem: If i is an index for a partial recursive function g, then $\gamma(i)$ is an index for a partial recursive function f such that, for all x, f(x) converges iff g(x) converges and f(x) = 0 or 1 if it converges, by definition of h. We want to prove that if j is any index for f, then ${}^{\xi}F_j(x) >$ g(x) for almost all x whenever g(x) converges. Suppose on the contrary that for infinitely many x, g(x) converges and ${}^{\xi}F_j(x) \leq g(x)$. Let $x_1, x_2, \ldots$ be the subset of these x that satisfy $x_k > j$. Then (j, x_k) does not appear in the list for any integer x_k, for otherwise $h(i, x_k) \neq f_j(x_k)$ (by definition of h and the fact that $g_i(x_k)$ converges), which is a contradiction; thus, as we said, (j, x_k) does not appear in the list. But at stage $n = \langle x_k, {}^{\xi}G_i(x_k)\rangle$, (j, x_k) is a candidate for the list, since ${}^{\xi}F_j(x_k) \leq g(x_k)$. Hence there exists an integer s less than j such that ${}^{\xi}\Phi_s(x_k) \leq g(x_k)$ and (s, z) does not appear in the list up to that point for any integer z; this must be true for $x = x_1, x_2, \ldots$. But there can be at most j such integers s, namely $s = 0, \ldots, s = j - 1$. But there are an infinite number of integers x_k and thus eventually the integers s must be exhausted, which is a contradiction. Q.E.D.

5. Bounds on the Measure Function

Suppose that f(x) is defined in terms of p(x), q(x), ... Then one might expect that the time that it takes to compute f with a "reasonable" program (one that does not do complicated and unnecessary intermediate calculations) is bounded by a function of the time that it takes to compute p(x), q(x), ... For example, the enumeration theorem[2] asserts the existence of a partial recursive function f defined by $f(<i,x>) = \phi_i(x)$.[4] Can we bound the time that it takes for a reasonable program to compute f by some function of the time that it takes to compute each of the ϕ_i? We show that this is possible on the standard M-Computer with a particular program that computes f(n) in the following way.

1. Decode n to the form $n = <i,x>$.

2. Enumerate the list of machine programs until the i^{th} machine program P_i is reached and erase everything on the tape except the integer x and the instructions P_i.

3. Begin the computation of $\phi_i(x)$ by operating on x more or less as P_i would. Naturally, this requires that occasional reference be made to the instructions P_i that are printed on the tape.

4. When the solution $\phi_i(x)$ is reached, erase the symbols representing the machine program P_i and leave only the symbols representing this output.

Suppose that P_j is this program for f. Then the contributions to $F_j(n)$ made by the four steps outlined above are:

1. $g'(n)$ = time required to decode n as $<i,x>$.

2. $g''(i)$ = time required to enumerate the programs up to P_i.

3. $g'''(\Phi_i(x))$ = time required to compute $\phi_i(x)$ with occasional glances at P_i. (g''' is total, although $g'''(\Phi_i(x))$ will diverge if $\phi_i(x)$ diverges.)

4. $g''''(i)$ = time required to erase P_i.

Hence $F_j(<i,x>) = g'(<i,x>) + g''(i) + g'''(\Phi_i(x)) + g''''(i)$, where $g', \ldots, g''''$ are total recursive functions. More accurately,

$$F_j(\ i,x\ ) = \begin{cases} g'(<i,x>) + g''(i) + g'''(\Phi_i(x)) + g''''(i) & \text{if } \phi_i(x) \text{ converges} \\ \text{divergent} & \text{otherwise.} \end{cases}$$

Our next theorem deals with an arbitrary M-Computer ${}^{\xi}C$; it proves that if j is any index for the function f, then there exists a total recursive function g determined by the index j such that ${}^{\xi}F_j(<i,x>) \leq g(i) + g(x) + g\left({}^{\xi}\Phi_i(x)\right)$ for all i and x. An unexpected feature of this theorem is that it holds even when the program for f is "unreasonable."

LEMMA: Let h be a total recursive function of n variables. Then there exists a monotonically increasing total recursive function g of one variable such that $h(x_1, \ldots, x_n) \leq g(x_1) + \ldots + g(x_n)$ for all non-negative integers $x_1, \ldots, x_n$.

PROOF: Trivial. Q.E.D.

THEOREM 4: Let ${}^{\xi}C$ be an M-Computer. Let j be an index for the function f defined by $f(\langle i, x \rangle) = \phi_i(x)$ for all i and x. Then there exists a total recursive function g such that, for all i and x, ${}^{\xi}F_j(\langle i, x \rangle) \leq g(i) + g(x) + g\left({}^{\xi}\Phi_i(x)\right)$ whenever $\phi_i(x)$ converges.

PROOF: We shall prove the existence of a total recursive function h such that for all i and x, if $\phi_i(x)$ converges, then ${}^{\xi}F_j(\langle i, x \rangle) = h\left(i, x, {}^{\xi}\Phi_i(x)\right)$. The existence of the desired g then follows from the lemma. To compute h(i, x, z), first, determine, by means of the a-function, whether or not ${}^{\xi}\phi_i(x) = z$. If not, let h(i, x, z) = 0. Otherwise, compute ${}^{\xi}F_j(\langle i, x \rangle)$ (it must converge, since ${}^{\xi}\Phi_i(x)$ convergent $\rightarrow \phi_i(x)$ convergent $\rightarrow f_j(\langle i, x \rangle)$ convergent $\rightarrow {}^{\xi}F_j(\langle i, x \rangle)$ convergent), and let $h(i, x, z) = {}^{\xi}F_j(\langle i, x \rangle)$. This h is clearly the desired total recursive function. Q.E.D.

We shall now give three other theorems that are very much like the one above. Our purpose is to provide a method, although the statements are interesting in themselves. All theorems are proved for an arbitrary M-Computer ${}^{\xi}C$.

THEOREM 5: Let x_o be a non-negative integer. Let s be a total recursive function such that for all i, j and x

$$f_{s(i,j)}(x) = \begin{cases} \phi_i(x) & \text{if } x \leq x_o \\ \phi_j(x) & \text{if } x > x_o. \end{cases}$$

Then there exists a total recursive function g such that for almost all x greater than x_o, ${}^{\xi}F_{s(i,j)}(x) \leq g(x) + g(j) + g\left({}^{\xi}\Phi_j(x)\right)$ whenever $\phi_j(x)$ converges.

PROOF: Note that the existence of a total recursive function s follows from an application of the s-m-n theorem to the function

$$r(i, j, x) = \begin{cases} \phi_i(x) & \text{if } x \leq x_o \\ \phi_j(x) & \text{if } x > x_o. \end{cases}$$

We first prove the existence of a total recursive function h such that for almost all x ${}^{\xi}F_{s(i,j)}(x) \leq h\left(x, j, {}^{\xi}\Phi_j(x)\right)$ whenever $\phi_j(x)$ converges. To compute h(x, j, z), proceed as follows: If $x \leq x_o$, let h(x, j, z) = 0. If $x > x_o$, determine whether or not ${}^{\xi}\Phi_j(x) = z$. If not, let h(x, j, z) = 0. Otherwise, it follows that $\phi_j(x)$ converges and, by definition of s, $f_{s(i,j)}(x)$ converges for all i. Let

$$h(x, j, z) = \text{maximum}\left[{}^{\xi}F_{s(o,j)}(x), {}^{\xi}F_{s(i,j)}(x), \ldots {}^{\xi}F_{s(x,j)}(x)\right].$$

Clearly, h is a total recursive function, and, if $x \geq \max[i, x_o]$, then $h\left(x, j, {}^{\xi}\Phi_j(x)\right) \geq {}^{\xi}F_{s(i,j)}(x)$ whenever $\phi_j(x)$ converges. The existence of the desired function g follows from the existence of h by the lemma. Q.E.D.

THEOREM 6: Let s be a total recursive function such that $\phi_{s(i)}(x) = \phi_{\phi_i(x)}(x)$ for all i and x. Then there exists a monotonically increasing total recursive function g such that for all i and x

$$ {}^{\xi}\Phi_{s(i)}(x) \leq g(x) + g(i) + g\left({}^{\xi}\Phi_i(x)\right) + g\left({}^{\xi}\Phi_{\phi_i(x)}(x)\right) $$

wherever $\phi_{s(i)}(x)$ converges.

PROOF: The existence of the total recursive function s follows from a single application of the s-m-n theorem. First, we prove the existence of a total recursive function h such that for all i and x ${}^{\xi}\Phi_{s(i)}(x) = h\left(x, i, {}^{\xi}\Phi_i(x), {}^{\xi}\Phi_{\phi_i(x)}(x)\right)$ whenever $\phi_{s(i)}(x)$ converges. To compute $h(x, i, y, z)$, determine whether or not ${}^{\xi}\Phi_i(x) = y$. If not, let $h(x, i, y, z) = 0$. Otherwise, determine whether or not ${}^{\xi}\Phi_y(x) = z$. If not, let $h(x, i, y, z) = 0$. Otherwise, compute ${}^{\xi}\Phi_{s(i)}(x)$, which must converge because ${}^{\xi}\Phi_{\phi_i(x)}(x)$ converges to z. Let $h(x, i, y, z) = {}^{\xi}\Phi_{s(i)}(x)$. Obviously, h is a total recursive function and the existence of the desired total recursive function g follows. Q.E.D.

THEOREM 7: Let γ be the function defined in Theorem 3. Then there exists a monotonically increasing total recursive function g such that for all i and x

$$ {}^{\xi}\Phi_{\gamma(i)}(x) \leq g(x) + g(i) + g\left({}^{\xi}\Phi_i(x)\right) $$

whenever $\phi_i(x)$ converges.

PROOF: Let

$$ h(x, i, z) = \begin{cases} 0 & \text{if } {}^{\xi}\Phi_i(x) \neq z \\ {}^{\xi}\Phi_{\gamma(i)}(x) & \text{if } {}^{\xi}\Phi_i(x) = z. \end{cases} $$

h is total recursive and ${}^{\xi}\Phi_{\gamma(i)}(x) = h\left(x, i, {}^{\xi}\Phi_i(x)\right)$ whenever $\phi_i(x)$ converges. The existence of g follows immediately. Q.E.D.

6. Existence Theorems

The complexity of a function f often increases with x, so that a reasonable program for f computes f(x) more slowly than f(x-1) for all x. For example, the function $f(x) = 2^{2^x}$ seems to be of this type. If f is 0-1 valued, however, the time that it takes a program to compute it can often be drastically cut by a second program for infinitely many choices of x, and for these x the second program often computes f(x) more quickly than

$f(x-1)$. For example, it seems that a reasonable program for the function

$$f(x) = \begin{cases} 1 & \text{if } 2^x+1 \text{ is prime} \\ 0 & \text{otherwise} \end{cases}$$

must require more time to compute $f(x)$ than $f(x-1)$, since the time required to compute 2^x+1 exceeds the time required to compute $2^{x-1}+1$. A theorem in number theory, however, states that 2^x+1 can be an odd prime only if $x = 2^y$ for some y; hence $f(x) = 0$ if $x \neq 2^y$. Clearly, this theorem speeds the computation of $f(x)$ for $x \neq 2^y$, so that, for infinitely many x, $f(x)$ can be computed more quickly than $f(x-1)$. Nevertheless, it does not seem that every 0-1 valued total recursive function f can be simplified in this way. Intuition tells us that there exist 0-1 valued functions f with the property that every reasonable program for f must compute $f(x)$ more slowly than $f(x-1)$. We now confirm our suspicions.

THEOREM 8: To each total recursive function h there corresponds a total recursive function r with $r(x) > h(x)$ for all x, and a 0-1 valued total recursive function f so that

i. If i is any index for f, then ${}^{\xi}F_i(x) > r(x)$ for almost all x.

ii. There exists an index k for f so that $r(x+1) > {}^{\xi}F_k(x) > r(x)$ for almost all x.

PROOF: Let g be the total recursive function of Theorem 7. First, we prove the existence of a total recursive function ϕ_j such that $\phi_j(x) > \max\left[h(x), g(x-1)+g(j)+g\left({}^{\xi}\Phi_j(x-1)\right)\right]$ for all x. Then we define p as follows:

$$p(i,x) = \begin{cases} h(0)+1 & \text{if } x = 0 \\ 1+\max\left[h(x), g(x-1)+g(i)+g\left({}^{\xi}\Phi_i(x-1)\right)\right] & \text{if } x > 0 \text{ and } \phi_i(x-1) \text{ converges} \\ \text{divergent} & \text{otherwise.} \end{cases}$$

Here, p is partial recursive, since h and g are total recursive, and the convergence of $\phi_i(x-1)$ implies the convergence of ${}^{\xi}\Phi_i(x-1)$. By the s-m-n theorem, there exists a total recursive function s such that $\phi_{s(i)}(x) = p(i,x)$ for all i and x. The recursion theorem[5,6] asserts the existence of an integer j such that $\phi_j = \phi_{s(j)}$; hence, $\phi_j(x) = p(j,x)$ for all x. To see that ϕ_j is the desired total recursive function, first note that $\phi_j(0) = h(0)+1$. Assume that $\phi_j(y)$ converges for all $y < x$. Then by definition of p and the fact that ${}^{\xi}\Phi_j(x-1)$ converges, $\phi_j(x) = 1+\max\left[h(x), g(x-1)+g(j)+g\left({}^{\xi}\Phi_j(x-1)\right)\right]$ must converge. Hence the existence of ϕ_j is proved.

Let $r = \phi_j$. Then r is total recursive and $r(x) > h(x)$ for all x (by definition of ϕ_j) as desired. Let $\gamma(j)$ be the index of a function f. Then by Theorem 3 and the fact that r is total, $f(x) = 0$ or 1 for all x, and if i is any index for f, then ${}^{\xi}F_i(x) > r(x)$ for almost all x. This proves property (i). $\phi_j(x) > g(x-1) + g(j) + g\left({}^{\xi}\Phi_j(x-1)\right)$ (by definition of p) $\geq {}^{\xi}\Phi_{\gamma(j)}(x-1)$ (by Theorem 7) $= {}^{\xi}F_{\gamma(j)}(x-1)$ (by definition of f). Let $k = \gamma(j)$. Then since $\phi_j = r$, $r(x) > {}^{\xi}F_k(x-1) > r(x-1)$ for all positive integers x. This proves property (ii) and completes the proof of this theorem. Q.E.D.

Note: The recursion theorem can be tricky and must be applied with care. In particular, the statement $\phi_j = \phi_{s(j)}$ does not imply that ${}^{\xi}\Phi_j = {}^{\xi}\Phi_{s(j)}$, since s(j) may be different from j.

A function rarely enjoys a unique quickest program for its computation. If the function is reasonably complex, no matter what program is chosen to compute it, another can be found which cuts the computation time in half for infinitely many x. Thus a program for f which takes x seconds to compute for infinitely many x could be replaced by another program that takes only x/2 seconds, and then again by another program that takes only x/4 seconds, and so on. As a simple example, suppose that we wish to know if an integer written in radix 10 is a palindrome. To solve this problem we write a program for the standard M-Computer which computes the function

$$f(x) = \begin{cases} 1 & \text{if } x \text{ is a palindrome} \\ 0 & \text{otherwise.} \end{cases}$$

The program is such that when the input integer is x = 3726854586273, the computer scans the rightmost digit 3 and goes down the tape to compare it with the leftmost digit 3, then back up to rightmost digit 7, and down to leftmost digit 7, and so on. After opposing digits have been compared, the computer prints an output 1. With a quicker program, the computer scans the rightmost digits 7 and 3 simultaneously, then goes down the tape to leftmost digits 3 and 7, then back up to digits 6 and 2, and so on, comparing the digits two at a time rather than one at a time. This program takes approximately one-half the time of the slower one for all palindromes. It can be shown, in fact, that no matter which program is chosen to compute this f, another can be given which computes f in one-half the time for almost all palindromes. One can further prove the existence of a total recursive function g with the property that to every program P_i for g there corresponds a quicker program P_j for which $G_i(x) > 2G_j(x)$ for almost all x. Can a stronger theorem be proved? In particular, can we find a function with the property that to every program P_i for f there corresponds a program P_j so much quicker that $F_i(x) > 2^{F_j(x)}$ for almost all x?

THEOREM 9: Let r be a total recursive function of two variables. Then there exists a total recursive function f with values 0 and 1 such that to every index i for f, there corresponds another index j for f such that ${}^{\xi}F_i(x) > r\left(x, {}^{\xi}F_j(x)\right)$ for almost all x.

PROOF: (1) The d and s functions.

Construct a Gödel table that contains the symbol $\phi_r(c)$ at the intersection of row r and column c. To compute d(i, x): First, compute $\phi_i(0)$, $\phi_i(1)$, ..., $\phi_i(x)$. If any of these diverge, let d(i, x) diverge. Otherwise, use the α-function to circle all entries

$\phi_j(x)$ in column x with $j \leqslant x$ and ${}^{\xi}\Phi_j(x) \leqslant \phi_i(x-j)$. Then check the first circled entry $\phi_k(x)$, if any, with the property that $\phi_k(y)$ has not been checked for $y < x$ (it is possible to determine if $\phi_k(y)$ has been checked for $y < x$, since $\phi_i(0), \ldots, \phi_i(x)$ converge). If none of the entries $\phi_o(x), \ldots, \phi_x(x)$ in column x are checked, let $d(i,x) = 0$. Otherwise (a single entry $\phi_k(x)$ is checked), let $d(i,x) = 0$ if $\phi_k(x) \neq 0$ and let $d(i,x) = 1$ if $\phi_k(x) = 0$. Clearly, d is partial recursive and if ϕ_i is total then d is total. Let s be a total recursive function which satisfies the equation $d(i,x) = \phi_{s(i)}(x)$ for all i and x (the existence of s is ensured by the s-m-n theorem). Note that if ϕ_i is total and if j is any index such that $\phi_j = \phi_{s(i)}$, then ${}^{\xi}\Phi_j(x) > \phi_i(x-j)$ for almost all x (for otherwise ${}^{\xi}\Phi_j(x) \leqslant \phi_i(x-j)$ for infinitely many $x = x_1, x_2, \ldots$; then in the computation of d, an entry $\phi_j(x_k)$ is checked and thus, $d(i,x_k) \neq \phi_j(x_k)$, which implies that $\phi_j \neq \phi_{s(i)}$ which is a contradiction).

(2) The e and t functions.

Define a function e of four variables x, u, v, i as follows:

CASE I $v \leqslant u$: Let $e(x,u,v,i) = e(x,u,u+1,i)$.

CASE II $v > u$: Construct a Gödel table and box row u and column v.

				$v = 3$	
	$\phi_o(0)$	$\phi_o(1)$	$\phi_o(2)$	$\phi_o(3)$	$\phi_o(4)$
$u = 1$	$\phi_1(0)$	$\phi_1(1)$	$\phi_1(2)$	$\phi_1(3)$	$\phi_1(4)$
	$\phi_2(0)$	$\phi_2(1)$	$\phi_2(2)$	$\phi_2(3)$	$\phi_2(4)$
	$\phi_3(0)$	$\phi_3(1)$	$\phi_3(2)$	$\phi_3(3)$	$\phi_3(4)$
	$\phi_4(0)$	$\phi_4(1)$	$\phi_4(2)$	$\phi_4(3)$	$\phi_4(4)$

If $x < v$, let $e(x,u,v,i) = d(i,x)$. If $x \geqslant v$, compute $\phi_i(0), \phi_i(1), \ldots, \phi_i(x-u)$ and, if any of these diverge, let $e(x,u,v,i)$ diverge. Otherwise, circle all entries $\phi_j(x)$ in column x with $j \geqslant u$ and $j \leqslant x$ and ${}^{\xi}\Phi_j(x) \leqslant \phi_i(x-j)$. Then check the first circled entry $\phi_k(x)$, if any, with the property that $\phi_k(y)$ has not been checked for $v \leqslant y < x$ during the computation of $e(y,u,v,i)$ or for $y < v$ during the computation of $d(i,y)$. If none of the entries $\phi_u(x), \ldots, \phi_x(x)$ is checked, let $e(x,u,v,i) = 0$. Otherwise (a single entry $\phi_k(x)$ is checked), let $e(x,u,v,i) = 0$ if $\phi_k(x) \neq 0$, and let $e(x,u,v,i) = 1$ if $\phi_k(x) = 0$. Clearly, e is partial recursive, and, if ϕ_i is total, then e is total. Let t be a total recursive function such that $e(x,u,v,i) = \phi_{t(u,v,i)}(x)$ for all x, u, v, and i. Note that

$$\phi_{t(o,o,i)}(x) = e(x,o,o,i) = d(i,x) = d_{s(i)}(x) \qquad \text{for all } i \text{ and } x.$$

(3) Choose a total recursive 1-1 map of the integers onto the set of all 1-tuples, 2-tuples, 3-tuples, ... of integers. Let $\langle\langle a_o, \ldots, a_n \rangle\rangle$ denote the integer that

maps into $(a_o, \dots, a_n)$. <u>We now prove the existence of a total recursive function g such</u> that for all x, u, v, and i

$$^{\xi}\Phi_{t(u,v,i)}(x) = \begin{cases} g\left(x,u,v,i,\langle\langle {}^{\xi}\Phi_i(0),\dots,{}^{\xi}\Phi_i(x-u)\rangle\rangle\right) & \text{if } \phi_i(0), \dots, \phi_i(x-u) \text{ converge} \\ \text{diverges} & \text{otherwise.} \end{cases}$$

To compute $g(x,u,v,i,z)$, first, expand z according to the above-given coding as $z = \langle\langle a_o, \dots, a_{x-u}\rangle\rangle$. Then, determine, by means of the α-function, whether or not ${}^{\xi}\Phi_i(0) = a_o, \dots, {}^{\xi}\Phi_i(x-u) = a_{x-u}$. If not, let $g(x,u,v,i,z) = 0$. Otherwise, $\phi_{t(u,v,i)}(x)$ converges; thus let $g(x,u,v,i,z) = {}^{\xi}\Phi_{t(u,v,i)}(x)$.

(4) Let r be the function in the statement of the theorem and let g be the function of part (3). <u>We now prove the existence of a total recursive function</u> ϕ_{i_o} such that for all u and v and for almost all x

$$r\left[x, g\left(x,u,v,i_o, \langle\langle {}^{\xi}\Phi_{i_o}(0), \dots, {}^{\xi}\Phi_{i_o}(x-u)\rangle\rangle\right)\right] \le \phi_{i_o}(x-u+1).$$

Define h as follows:

$$h(i,o) = 0$$

$$h(i,z+1) = \begin{cases} \max\limits_{\substack{0\le v\le z\\ 0\le w\le z}} r\left[z+w, g\left(z+w,w,v,i,\langle\langle {}^{\xi}\Phi_i(0),\dots {}^{\xi}\Phi_i(z)\rangle\rangle\right)\right] & \text{if } \phi_i(0), \dots, \phi_i(z) \text{ converge} \\ \text{divergent} & \text{otherwise} \end{cases}$$

By the s-m-n theorem, there exists a total recursive function ρ such that $h(i,z) = \phi_{\rho(i)}(z)$ for all i and z. By the recursion theorem,[5] there exists an index i_o such that $\phi_{\rho(i_o)}(z) = \phi_{i_o}(z)$ for all z. Then $\phi_{i_o}(0) = 0$. Assume that $\phi_{i_o}(x)$ converges for $x \le z$. Then $\phi_{i_o}(z+1)$ converges, since g and r are total recursive, and convergence of ϕ_{i_o} for $x \le z$ implies convergence of ${}^{\xi}\Phi_{i_o}(x)$ for $x \le z$. Therefore ϕ_{i_o} is total recursive. Fix the values of u and v; then, for $x > \max[2u, u+v]$, $\phi_{i_o}(x-u+1) \ge r\left[x, g\left(x,u,v,i_o, \langle\langle {}^{\xi}\Phi_{i_o}(0), \dots, {}^{\xi}\Phi_{i_o}(x-u)\rangle\rangle\right)\right]$.

(5) We now show that for all u there exists a v such that $\phi_{t(u,v,i_o)} = \phi_{t(o,o,i_o)}$. Since ϕ_{i_o} is total recursive, so is $\phi_{t(o,o,i_o)}$. Recall that the computation of $\phi_{t(o,o,i_o)}(x)$ proceeds in two stages.

<u>Stage 1:</u> With respect to the Gödel table, certain entries in column x are circled and then one of these entries may be checked.

<u>Stage 2:</u> $\phi_{t(o,o,i_o)}(x)$ is made equal to zero if no entry in column x is checked;

otherwise, its value is made to depend on that of the checked entry.

If, in the Gödel table, row u is boxed, the number of entries above this row which are checked in the computation of $\phi_{t(o,o,i_o)}$ must be finite, since a row may contain at most one checked entry. Box the column v that lies to the right of the last checked entry above row u. Then by definition of t,

$$\phi_{t(o,o,i_o)}(x) = \phi_{t(u,v,i_o)}(x) \qquad \text{for all } x.$$

(6) We now define the function f in the statement of the theorem as $f(x) = \phi_{t(o,o,i_o)}(x)$ for all x. The function f is total recursive, since ϕ_{i_o}, and therefore $\phi_{t(o,o,i_o)}$, is total recursive. To prove the theorem, let i be any index for f. Let v be chosen according to part (5), so that $\phi_{t(i+1,v,i_o)} = \phi_{t(o,o,i_o)} = f$. Then

$$r\left[x, {}^{\xi}\Phi_{t(i+1,v,i_o)}(x)\right] = r\left[x, g\left(x, i+1, v, i_o, \langle\langle {}^{\xi}\Phi_{i_o}(0), \ldots, {}^{\xi}\Phi_{i_o}(x-i-1)\rangle\rangle\right)\right]$$

(according to part (3), since ϕ_{i_o} is total)

$$\leq \phi_{i_o}(x-i)$$

(according to part (4))

$$< {}^{\xi}F_i(x)$$

(since $f(x) = \phi_{t(o,o,i_o)}(x) = \phi_{s(i_o)}(x)$ as pointed out in the last sentence of (2), and for reasons stated in the last sentence of (1)).

for almost all x. Let $j = t(i+1, v, i_o)$. Then for almost all x, $r\left[x, {}^{\xi}F_j(x)\right] < {}^{\xi}F_i(x)$ as desired. Q.E.D.

7. Implications of Theorem 9

The implications of Theorem 9 are stated for the standard M-Computer, although they are true for any other M-Computer.

1. Let $r(x,y) = 2^y$. Then Theorem 9 asserts the existence of a total recursive function f such that to every index i for f there corresponds another index j such that $F_i(x) > 2^{F_j(x)}$ for almost all x. Hence it also asserts that to index j there corresponds an index k such that $F_i(x) > 2^{2^{F_k(x)}}$ and to k an index l such that $F_i(x) > 2^{2^{2^{F_l(x)}}}$, and so on. Hence there exists an infinite sequence of programs for f, starting with any program that one chooses so that each program in the sequence is followed by a much quicker one. Unfortunately, Theorem 9 does not provide an effective procedure for going from one program in the sequence to the next.

2. Let $r(x,y) = 2^x + 2^y$ and let f be the corresponding function of Theorem 9. Let g(x) be a lower bound on the time that it takes to compute f(x), that is, $g(x) < F_i(x)$ for every index i for f and for almost all x. The function g(x) can be taken to be at least as large as 2^x, since there corresponds to every index i for f an index j such that $F_i(x) > 2^x + 2^{F_j(x)}$, and therefore $F_i(x) > 2^x$ for almost all x. Given any such lower bound g(x), we know that $2^{2^{g(x)}}$ is also a lower bound, since there corresponds to the index j for f which is given above another index k such that $F_j(x) > 2^x + 2^{F_k(x)}$ and $F_k(x) > g(x)$ so that $F_i(x) > 2^x + 2^{2^x + 2^{F_k(x)}} > 2^{2^{F_k(x)}} > 2^{2^{g(x)}}$ for almost all x. In this way we can obtain an increasing sequence of lower bounds on the computation time of f, starting with any lower bound that we choose. Note in particular that there can be no such thing as a greatest lower bound on the computation time of f.

3. Theorem 9 exhibits a function f, and in fact infinitely many distinct functions, so that the time required to compute f with any program can be halved for almost all x by some other program, that is, there corresponds to every index i for f another index j such that $F_i(x) > 2F_j(x)$ for almost all x. This suggests a possible way of dealing with the function

$$f(x) = \begin{cases} 1 & \text{if } 2^{2^x}+1 \text{ is prime} \\ 0 & \text{otherwise,} \end{cases}$$

which was introduced in section 2. The hypothesis there asserts that f = g, where

$$g(x) = \begin{cases} 1 & \text{if } x < 5 \\ 0 & \text{if } x \geq 5. \end{cases}$$

On the standard M-Computer, one can give a program for g whose computation time cannot be reduced by any other program. If one can show, therefore, that the computation time of every program for f can be halved for almost all x, or even for infinitely many x, then the hypothesis must be false.

4. Rabin has defined a partial ordering on the set of partial recursive functions in terms of the time required to compute these functions. Essentially, f is said to be more difficult to compute than g, written $f \succ g$, if there exists a program P_i for g such that $F_j(x) > G_i(x)$ for all programs P_j for f and for almost all x. Rabin's theorem, then, asserts that to every total recursive function g there corresponds a 0-1 valued total recursive function f such that $f \succ g$. We can now obtain another interesting fact. Let $r(x,y) = 2^y$ and let f be the corresponding total recursive function of Theorem 9. Let h and g be total recursive functions such that $h \succ f \succ g$. Then there exists a program P_i for g such that $F_j(x) > G_i(x)$ for all programs P_j for f and for almost all x. Theorem 9

asserts that there exists a program P_k for f such that $F_j(x) > 2^{F_k(x)}$ and, since $F_k(x) > G_i(x)$, it follows that $F_j(x) > 2^{G_i(x)}$ for almost all x. Similarly, one can show that $F_j(x) > 2^{2^{G_j(x)}}$ for almost all x, and so on. On the other hand, since $h \succ f$, there exists a program P_k for f such that $H_\ell(x) > F_k(x)$ for every program P_1 for h. Since $H_\ell(x) > F_j(x) > 2^{F_k(x)}$, it follows that $H_\ell(x) > 2^{2^{F_k(x)}}$ for almost all x. This argument can be continued. Hence h is much more difficult than f and f is much more difficult than g, and since h and g are arbitrary total recursive functions satisfying $h \succ f \succ g$, it follows that no function comparable to f comes even close to being equal in difficulty to f.

M. Blum

References

1. Any effective list of all partial recursive functions is equivalent to the list ϕ_o, ϕ_1, ... determined by the standard M-Computer, as we show in Example 4.

2. The enumeration theorem asserts the existence of a partial recursive function f of two variables i and x such that

$$f(i,x) = \begin{cases} \phi_i(x) & \text{if } \phi_i(x) \text{ converges} \\ \text{divergent} & \text{otherwise.} \end{cases}$$

The s-m-n theorem, in a weak form that we require, asserts the existence of a total recursive function s such that $\phi_i(<x,y>) = \phi_{s(i,x)}(y)$ for all i, x, and y.

3. M. O. Rabin, Degree of Difficulty of Computing a Function and a Partial Ordering of Recursive Sets, Hebrew University, Jerusalem, Israel, April, 1960.

4. The symbol <> denotes the standard coding of N × N into N: $<0,0> = 0$, $<0,1> = 1$, $<1,0> = 2$, $<0,2> = 3$, $<1,1> = 4$, $<2,0> = 5$, ...

5. A simplified form of Kleene's recursion theorem asserts that to every total recursive function s there corresponds an integer j such that $\phi_{s(j)} = \phi_j$.

6. H. Rogers, Jr., Recursive Functions and Effective Computability (McGraw-Hill Book Company, Inc., New York, in press).

C. OLFACTION

The slow potential of the frog's olfactory mucosa (the electro-olfactogram or EOG), which is recorded by a surface electrode when an odor reaches the nose, is a complex waveform. This has become apparent from a series of experiments in which a wide variety of odorous stimuli[1] was used. In addition to the large negative potential described by Ottoson,[2] there are at least two phenomena that occur before the negative swing and are generated at a different location from that of the negative potential. The early events are seen in different combinations with different stimuli and consist either of an initial positive swing (thought by Ottoson to be an artefact resulting from charged water-vapor molecules) or an initial small negative wave, or both. Figure XXVI-1 illustrates the

Fig. XXVI-1. The EOG recorded from the olfactory mucosa of the frog. Calibration marks in all figures indicate 1 mv (positive upward) and 1 sec. Short puffs of anisole vapor were delivered just before the sharp upward deflection. The response was recorded with a gelatin salt bridge electrode, 30 μ in diameter, touching the mucosa surface.

initial positive-going potential. It shows the response to 6 successive short puffs of anisole vapor on a single sweep 20 seconds in duration. The first puff elicits a small positive (upward) deflection followed by a large negative deflection. The next puff of odor appears to interrupt the negative process and return the potential very nearly to the resting value for a very short time before the large negative potential occurs again.

Following a notion recently advanced by Lettvin to account for membrane and receptor phenomena,[4] we suggest this explanation of the phenomena shown in Fig. XXVI-1: The odor molecules can have two effects on the membrane or receptor sites. Those stimuli to which a receptor or part of a receptor is sensitive in one way (that is, which cause an action potential to be generated) cause the receptor to depolarize there, which in these experiments shows up as a small initial negative potential. Other receptors that are sensitive in another way to the odor are actively clamped to membrane potential by a mechanism that causes a low impedance across the membrane without changing its potential. It is not unreasonable to connect the depolarization with sodium ion permeability, and the impedance shunt with potassium ion or chloride ion permeability. The tendency to return to resting potential independently of the magnitude of the large negative wave (shown in Fig. XXVI-1) is reminiscent of the crayfish stretch receptor.[5] There is no reason, in principle, why a stimulus, particularly a chemical one, cannot be inhibitory in the same sense as the postulated chemical transmitters. For a given stimulus there are many more nonresponding cells than there are responding units; hence the initial negative event is seen only under special conditions related to a highly sensitive

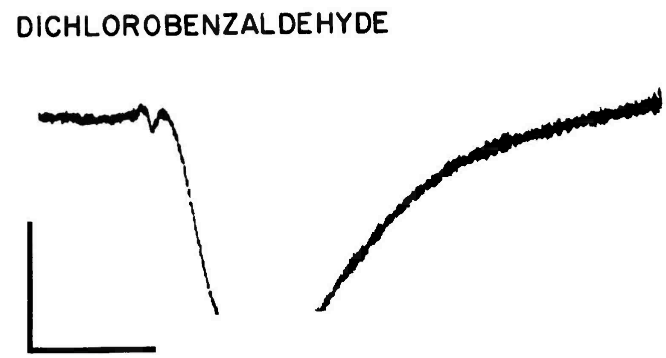

Fig. XXVI-2. Response to 2, 4-dichlorobenzaldehyde.

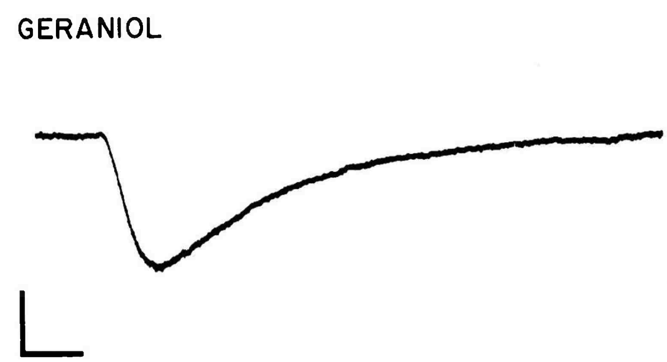

Fig. XXVI-3. Response to geraniol.

Fig. XXVI-4. Response to methanol.

depolarization effect and a rather insensitive shunt effect. This is shown in Fig. XXVI-2. Stimuli that can diffuse quickly and reach the receptor with very little spread in arrival time will show the initial events more clearly than slower-moving molecules. In the latter case, the action-potential response will mask most of the early events, as shown in Fig. XXVI-3. Methanol, which is odorless to the experimenters, produces the EOG shown in Fig. XXVI-4. It is positive only, with no sign of an initial depolarization and little or no sign of the action-potential negative wave.

R. C. Gesteland, J. Y. Lettvin, W. H. Pitts

References

1. R. C. Gesteland, Some Positive Aspects of Smell, Proc. Conferences on Recent Advances in Odor, New York Academy of Sciences, 1963 (in press).

2. D. Ottoson, Acta Physiol. Scand. (Stockholm) 35, Suppl. 122, 1956.

3. D. Ottoson, Acta Physiol. Scand. (Stockholm) 47, Suppl. 149, 1959.

4. J. Y. Lettvin, Quarterly Progress Report No. 70, Research Laboratory of Electronics, M.I.T., July 15, 1963, page 327.

5. C. Eyzaguirre and S. W. Kuffler, J. Gen. Physiol. 39, 87 (1955).

XXVII. NEUROLOGY*

L. Stark
J. F. Dickson III
C. Benet
T. Cheek
H. Horibe
Anne Horrocks
G. A. Masek
E. G. Merrill
J. A. Michael
D. Miller
Yvette Mintzberg
J. Moore
N. Orloff
O. Sanchez-Felipe
A. A. Sandberg
L. Seligman
J. I. Simpson
D. Slosberg
A. Smith
A. Troelstra
E. C. Van Horn, Jr.
G. H. Whipple
L. R. Young
B. L. Zuber

RESEARCH OBJECTIVES

Physiology has had, first, biochemistry and, more recently, biophysics separated from it; these new disciplines deal with chemical and physical mechanisms within the biological organism. "Systems biology," the study of the organizational and control properties of these mechanisms, now constitutes the core of physiology. Our group, composed of medical scientists, engineers, and physiologists, is applying concepts and methods of communication and control theory to the analysis of neurological and biological systems.

Examples of design properties in biological systems that have been investigated here are the discontinuous or sampled-data characteristics of the human hand- and eye-tracking servomechanisms. Nonlinear scale-compression operators in the pupil and lens systems permit them to exhibit stability in one domain, and instability with complex limit cycles in another. Even-error signals have been found to be employed in the accommodation control system. The relationship of system behavior to underlying mechanisms has been explored by means of neurophysiological experiments on cats and crayfish, mechanical analysis of iris kinematics, pharmacological dissection, and by evaluating disease syndromes as naturally occurring interferences. Interaction between systems has been studied, in particular in the multiple-control system for eye movement. Certain inputs add algebraically; for others complete control shifts from one input to another. The ability to inject several different inputs may permit dissection and analysis of a system into component transfer functions.

As in any field of science, techniques must be developed pari passu with scientific advances. Our on-line digital computer provides function generation, real-time analysis, executive control of experiments, data editing, and display of results. It has further been used as part of a hybrid digital-analog simulation system. We have also established remote laboratories in three Boston hospitals, Massachusetts General Hospital, Massachusetts Eye and Ear Infirmary, and Boston University Medical Center where on-line digital-computer experiments are carried out with telephone lines for analog-data transmission. An adaptive-filter pattern-recognition scheme for electrocardiographic diagnosis is being reformulated as an on-line system in which we utilize both our own G.E. 225 computer and the IBM 7094 computer of the Computation Center, M.I.T.

L. Stark

---

*This research is supported in part by the National Science Foundation (Grant G-16526) and the National Institutes of Health (Grant MH-04737-03). Major support is provided by the U.S. Public Health Service (B-3055-3, B-3090-3, MH-06175-01A1), the Office of Naval Research (Nonr-1841(70)), the Air Force (AFOSR 155-63), and the Army Chemical Corps (DA-18-108-405-CML-942), administered by the Electronic Systems Laboratory, M.I.T.

A. NONLINEAR OPERATOR IN THE PUPIL SYSTEM

"Biological adaptation" may be considered the acceptance of a new steady-state input level as the desired reference and the subsequent rearrangement of the feedback loop. This should be distinguished from both "input adaptation" and "task adaptation." The precognitive input predictor, which enables the hand- and eye-tracking systems to anticipate repetitive input signals and thus to eliminate delays in response, is an example of input adaptation. The hand's possessing an adaptive controller with the ability to compensate for a wide variety of loads and still perform skilled movements is a prime example of task adaptation.

An outstanding example of biological adaptation is found in the retina, which responds similarly, as seen by measurement of pupillary constriction to a step increase of 10 per cent in light intensity over a 6 $\log_{10}$ change in initial baseline light intensity. In Fig. XXVII-1 the left-hand block represents this division by the average light intensity, $\bar{I}$. The middle block represents a general operator for the remainder of the

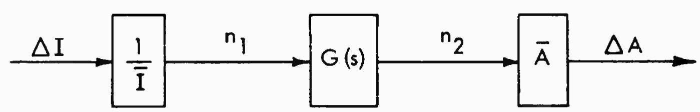

Fig. XXVII-1. Block diagram of the $\bar{A}$-multiplier.

pupil system except for the right-hand block. This is the $\bar{A}$-multiplier and indicates multiplication of the penultimate signal by average area, $\bar{A}$, to yield the actual output, A or area.

In early linearization of the pupil signal the incremental dimensionless open-loop gain was defined as

$$G(s) = \frac{F_i}{F_e} = \frac{\Delta A \cdot \bar{I}}{\Delta I \cdot \bar{A}} = \frac{\Delta A/\bar{A}}{\Delta I/\bar{I}} \tag{1}$$

$$g(s) = \frac{\Delta A}{\Delta I} = \frac{1}{\bar{I}} \cdot G(s) \cdot \bar{A}. \tag{2}$$

Here, F_i is flux change controlled by iris response, F_e is flux change controlled by external intensity control, ΔI and ΔA are incremental changes in light intensity and in area, respectively, G(s) is incremental gain, and g(s) is incremental gain with the DC levels $\bar{A}$ and $\bar{I}$ ignored. As studies of nonlinear behavior of the pupil progressed, it was noted that the incremental gain definition was a good predictor, even in domains in which the underlying assumptions were no longer valid. It then became apparent that two nonlinearities in the pupil system compensated for range changes to normalize input and response. The first of these, the division by $\overline{I}$ and its impressive resultant scale compression, has been known experimentally for a long time.

The $\overline{A}$-multiplier does not seem to have been noted by previous workers. Although it first came to our attention when DC changes in $\overline{A}$ occurred secondarily to large changes in range of $\overline{I}$, this, of course, provides only a somewhat circular argument.

A more direct experimental approach is to change $\overline{A}$ by using another stimulus such as the near response; the pupil constricts synkinetically with lens accommodation to focus on a near object. Figure XXVII-2 shows the results of such an experiment, in which it is possible to see the constriction of the pupil with voluntary accommodation

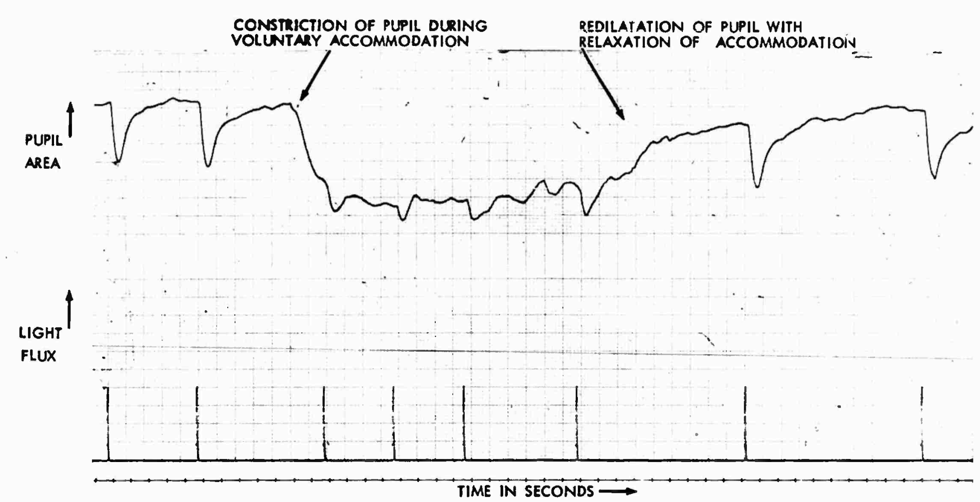

Fig. XXVII-2. Constriction and redilatation of the pupil during accommodation.

and the redilatation of the pupil with relaxation of accommodation. It is clear that identical light inputs (the pupil is receiving open-loop stimulation) cause area changes of very different sizes which are directly proportional to the actual DC level of area. Figure XXVII-3, a graph of ΔA as a function of $\overline{A}$ for several such responses, bears this out.

The locus of this $\overline{A}$-multiplier is of interest. We know that changes of $\overline{A}$ that are secondary to light-intensity, accommodation or noise changes produce the same effect. This application of the "multi-input analysis" method suggests that only those portions of the pupil system that are common to all three inputs can serve as the location of the $\overline{A}$-multiplier, that is, either the Edinger-Westphal nucleus or the motor nerve and

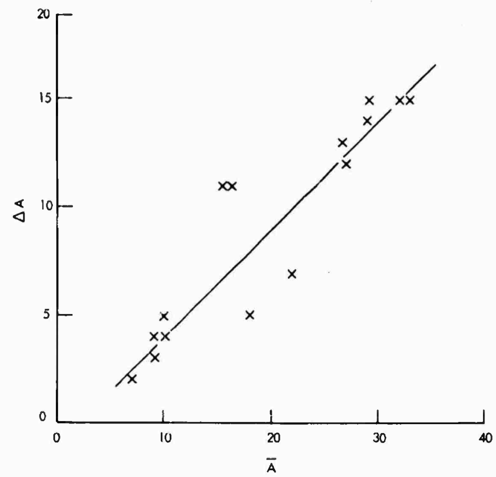

Fig. XXVII-3. Change in area as a function of $\bar{A}$.

neuromuscular apparatus elements.

We have used pharmacological methods to further dissect the system in preliminary experiments. If local drugs are placed on the cornea to change pupil area, then the $\bar{A}$-multiplier continues to have the same action. Under these conditions, since the iris has no proprioceptive feedback mechanisms and visual feedback is eliminated with the optical open-loop technique, the central nervous system and the motor neuron and motor nerves cannot be involved. We are left with the neuromuscular apparatus as the locus of the $\bar{A}$-multiplier. It may be that the sphincter muscle is more excitable when stretched, or that the active contractile components contract more vigorously when stretched, or that series elasticity (with a hard-spring nonlinearity) permits more of the contractile force to express itself as dimension change when stretched.

A latent nonlinearity that acts to "linearize" the pupil system over a wide range of output levels has been defined and discussed. By using the multi-input analysis technique, together with open-loop and pharmacological "dissection" of the pupil system, this nonlinearity has been localized to the effector organ, the iris muscle.

L. Stark

B. DOUBLE OSCILLATIONS IN THE PUPIL SERVOMECHANISM

The interesting phenomenon of two simultaneous pupil oscillations, each with its own gain, phase lag, and frequency, is shown in Fig. XXVII-4. Such oscillations were first noticed during environmental clamping of the pupil servomechanism.[1] The pupil-area curve of Fig. XXVII-4 can be approximated by Eq. 1. The phase-plane plot of Eq. 1 is shown in Fig. XXVII-5.

$$p(t) = 3.5 \sin 2\pi(0.183)\, t + \sin 2\pi(1.28)\, t \qquad (1)$$

The oscillations of Fig. XXVII-4 were achieved by inserting a "clamping box" in the pupil servomechanism loop. The "clamping box" provided adjustment of gain and phase delay. The phase delay of the "clamping box," however, is a nonlinear function of frequency.

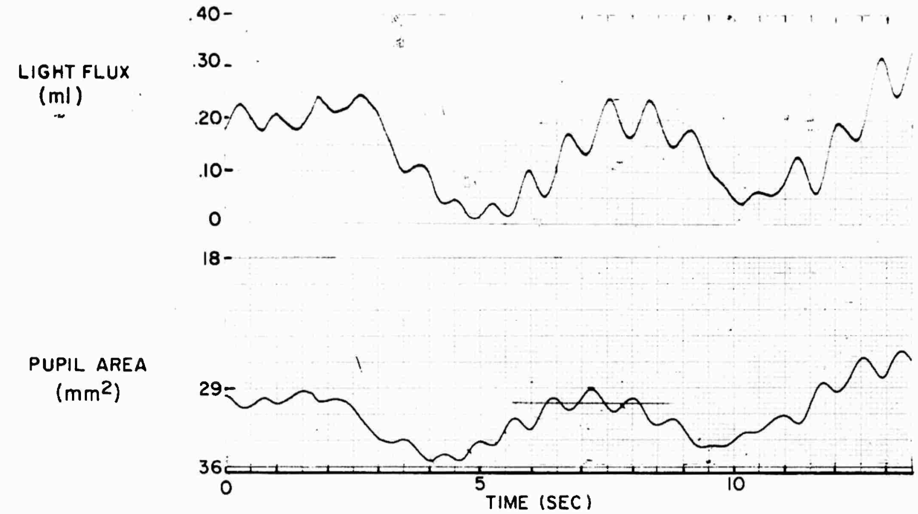

Fig. XXVII-4. Double oscillations of the pupil servomechanism.

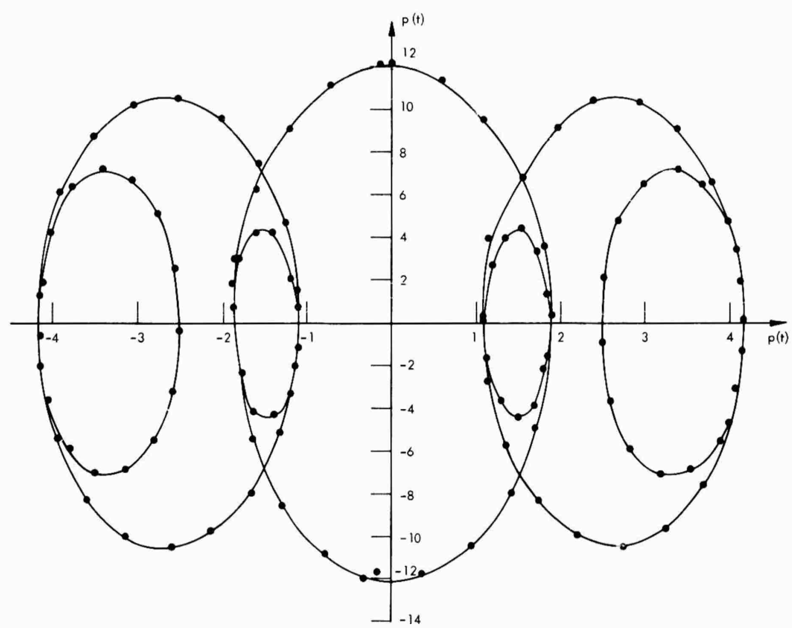

Fig. XXVII-5. Phase-plane plot of Eq. 1.

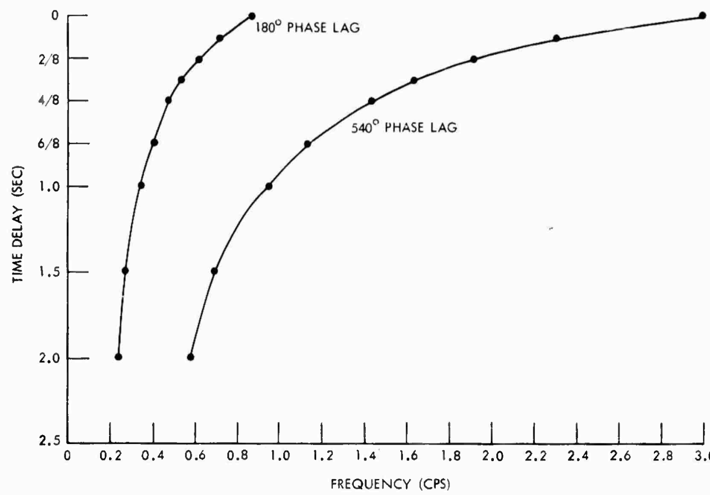

Fig. XXVII-6. Predicted frequencies of double oscillations.

When the "clamping box" is composed of an amplifier and a delay line, arbitrary gain and phase as a linear function of frequency can be induced.[2] By using the phase response of the pupil servomechanism, the additional phase delay required to produce a total delay of 180° and 540° can be calculated. Thus the frequencies of oscillation as a function of time delay can be predicted. These predictions are shown in Fig. XXVII-6 for 180° and 540°.

Experiments are under way to see whether or not sustained double oscillations occur at frequencies that are comparable with those predicted in Fig. XXVII-6. One difficulty still remaining in the experimental procedure is the lack of control over mean pupil area. Once the pupil drifts into saturation, either fully opened or fully closed, the oscillations cease.

D. U. Wilde, L. Stark

References

1. L. Stark, Environmental clamping of biological systems: Pupil servomechanism, J. Opt. Soc. Am. 52, 925-930 (1962).

2. The G.E. 225 computer, programmed and operated by Allen A. Sandberg, is used as the delay line of variable delays.

C. ACCOMMODATION TRACKING

In a previous report[1] experiments were described which were designed to elucidate the nature of the error signal on which the accommodative system operates.

We have found that control of extraneous clues is the one most important factor in determining an experimental situation in which the accommodative system makes approximately 50 per cent errors.

An attempt was made to eliminate all clues in the following manner: Horizontal target movement was minimized by use of a horizontal line target and a variable diaphragm. Vertical target movement was minimized by control of head position, precise initial alignment of the target by means of a plastic reference grid, and matching the symmetry of blur in extreme positions. At times difference in size of blur at the near and far positions could be eliminated by symmetrically enlarging the step. The subject wore a set of headphones that produced a relatively loud sound at 360 cps to mask any auditory clues made by the movement of the target.

1. Results

A series of experiments was run in which the target remained in position until focus was accomplished. Subject A showed initial tracking errors of 41 per cent and 50 per cent in two trials of approximately 100 stimuli under white-light illumination. In Fig. XXVII-7 the percentage of initial errors in successive sets of 10 trials is shown. It can be seen that the average error is approximately 50 per cent, and that no trends or learning occurred.

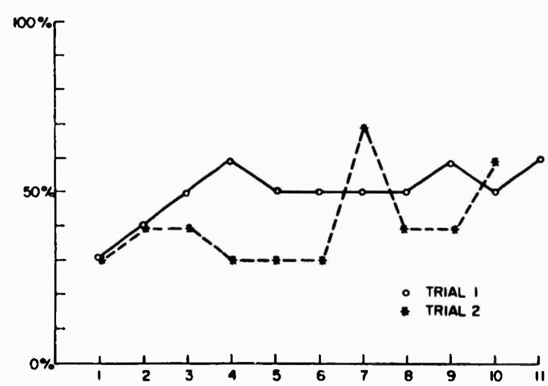

Fig. XXVII-7.
Percentage of erroneous initial tracking attempts (ordinate) in successive 10 trials vs sequence of sets of 10 trials (abscissa).

To confirm the randomness of the response system, the number of intervals between successive failures was analyzed. Figure XXVII-8 shows these intervals as a distribution function with a logarithmic ordinate scale. By assuming that the occurrence of correct initial response is random, the probability of getting n successive correct initial responses is given by

$$P_n = \left(\frac{1}{2}\right)^n. \tag{1}$$

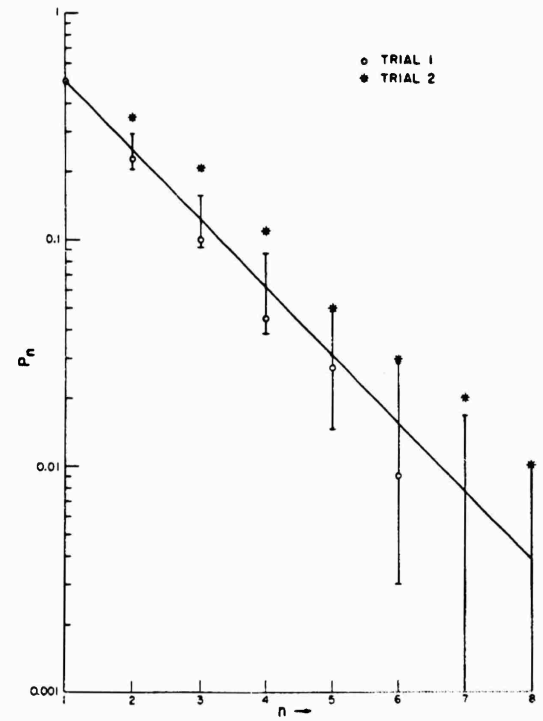

Fig. XXVII-8. Probability of getting n successive correct responses (P_n) versus n. Straight line is predicted from the theoretical equation (1).

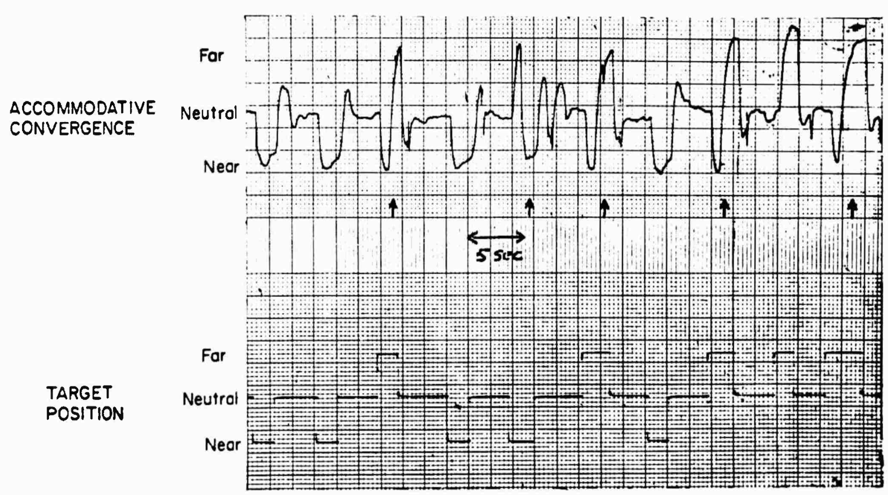

Fig. XXVII-9. Ten responses with 5 initial errors from a typical experiment.

Therefore, if n = 1, $P_n = \frac{1}{2}$ or 50 per cent. If n = 4, $P_n = \frac{1}{16}$ or 6.25 per cent. This means that the chances of getting 4 successive correct initial responses are 16 to 1. Figure XXVII-8 illustrates the theoretical straight line resulting from Eq. 1. The vertical bars represent a standard deviation of ±1. The experimental data closely follow the theoretical line, further illustrating that the errors of initial tracking follow a chance or random pattern. Figure XXVII-9 shows 10 responses with 5 mistakes taken from a typical experiment. The subject was aware of all erroneous responses, as well as of oscillations.

When the target was illuminated with red light, subject A showed a similar frequency of initial errors. Although two other subjects showed clear responses to all stimuli, they made no initial errors, thereby indicating their inability to eliminate all perceptual clues.

Many trials on each subject emphasized and re-emphasized the difficulty involved in eliminating all perceptual clues. Of three subjects, subject A was the only one for which it was possible to eliminate all perceptual clues, and even for him it was not possible in all experiments.

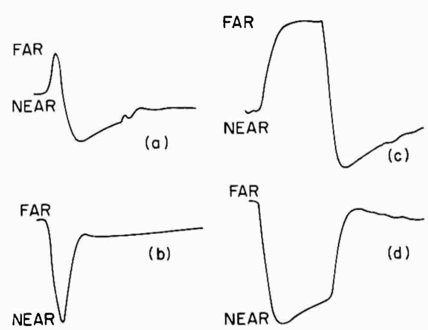

Fig. XXVII-10.

(a) and (b) Averaged responses to pulse stimuli. (c) and (d) Step stimuli. Note the difference in response shape and delay time depending on direction. Near-to-far delay time, 0.34 sec; far-to-near delay time, 0.21 sec.

The delay time or latent period between change in target position and vergence movement was studied by averaging 20 responses by means of a digital computer. Subject A was presented with 20 step stimuli (target allowed to come into focus) and 20 pulse stimuli (200-msec presentation). Figure XXVII-10 illustrates these average responses, including the delay times.

2. Discussion

If one were to consider the accommodative system as an automatic control system, the crux of this study would seem to revolve around the characteristics of the information flow between retinal blur on the one hand and brain, ciliary muscle, and medial recti on the other hand. It is assumed that the brain, in some manner, compares the characteristics of a given retinal image with those of a well-focused retinal image, and any discrepancy is registered as an error signal. The question that this study poses is whether the signal flow of the accommodative system, stripped of its connections with other clue systems, contains information about the magnitude and direction of the error (an odd-error signal) or only about the magnitude of the error (an even-error signal).

In studying accommodation, it was assumed that fluctuations in accommodation were faithfully reflected by changes in vergence. Experimental and clinical studies regarding the linearity and constancy of this AC-to-A ratio (accommodative convergence to accommodation ratio) would appear to support this assumption.[2-5] Nonaccommodative vergence movements such as fusional vergence were eliminated by use of a monocular viewing system.

The results of the study stress the importance of eliminating all extraneous clues by controlling the following factors:

(a) learning (by use of random-target presentation);

(b) horizontal and vertical target movement;

(c) auditory clues;

(d) blur symmetry and size in both near and far positions; and

(e) illumination uniformity and size clues.

If these conditions are met, the initial-tracking-direction component of the accommodative system seems to operate on a trial-and-error basis and thus produces approximately 50 per cent errors in initial judgment.

From reanalyzing published data, as well as from our own experiments, we conclude that it is easy to attain 100 per cent correct accommodative responses. It is only through painstaking attention to every detail of the stimulus that all clues may be eliminated and the randomness of the system appreciated. Here, too, the experience and skill of the subject are essential in isolating and eliminating each extraneous clue.

A. Troelstra, B. L. Zuber, D. Miller, L. Stark

References

1. A. Troelstra, B. L. Zuber, D. Miller, and L. Stark, Accommodation tracking, Quarterly Progress Report No. 71, Research Laboratory of Electronics, M.I.T., October 15, 1963, pp. 293-294.

2. E. F. Fincham and J. Walton, The reciprocal action of accommodation and convergence, J. Physiol. 137, 488-508 (1957).

3. M. Alpern and P. Ellen, A quantitative analysis of the horizontal movements of the eye in the experiment of Johannes Muller. I. Method and results, Am. J. Ophthalmol., Vol. 42, No. 4, Part 2, pp. 289-296 (1956).

4. M. W. Morgan, Jr., The clinical aspects of accommodation and convergence, Am. J. Opt. 21, 301-313 (1944).

5. K. N. Ogle and T. G. Marten, On the accommodative convergence and proximal convergence, Am. Arch. Ophthalmol. 57, 702-715 (1957).

D. EXPERIMENTS ON ERROR AS A FUNCTION OF RESPONSE TIME IN HORIZONTAL EYE MOVEMENTS

Previous studies of eye movements have suggested that further investigation be carried out regarding the error related to response time in tracking a horizontally moving target.[1-3] In the present experiments we used square-wave frequencies, primarily of 0.4 cps and 0.5 cps, since these were found to give optimum prediction, as well as delayed responses.[1] The target moved through a constant angle of ±5 degrees. Prediction of a target's movement usually results in error, as shown in Fig. XXVII-11a; a delay of 80 msec or more usually produces little, if any, error. Figure XXVII-11b

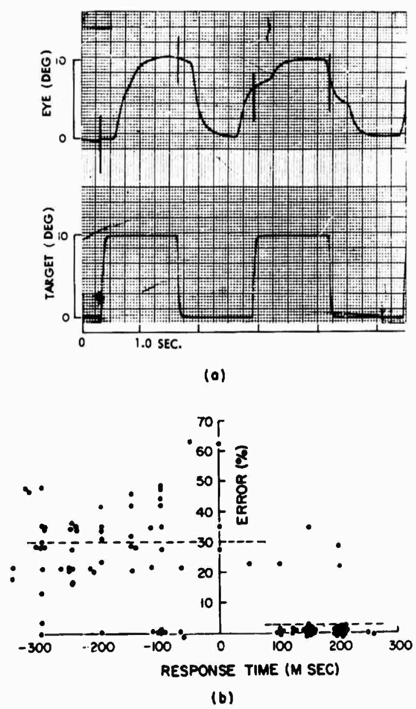

Fig. XXVII-11.
(a) Typical responses to target movement showing both delay and prediction.
(b) Plot of percentage error as a function of response time for a typical experiment (square wave, 0.4 cps).

shows the error plotted as a function of response time for a typical experiment. A χ^2 analysis showed that the frequency of the occurrence of error greater than 5 per cent is significantly higher in prediction than in delay, $\chi^2 = 40.08$, $p < 0.001$. This corroborates earlier results,[3] for which $\chi^2 = 21.9$, $p < 0.001$.

In order to determine the time at which the subject no longer depends on remembered target position (with resultant error) and is able to apply information obtained after the target's movement to correct his responses, we were led to study the delayed responses between 0 msec and 130 msec, the minimum response time. Thus, we employed a new method, one that yielded fewer predictive and more delayed responses than the previous technique.[1-3] This second method, used in a study of motor coordination,[4] presented a predictable target for a short period of time which alternated with an unpredictable target (a summation of three square waves) for a short period of time. With this method, more time delays were observed.

The results showed that median error of 15-25 per cent falls off to zero error after an 80-msec delay, indicating that information is unable to be correctly assimilated in a shorter period of time. Figure XXVII-12 shows the median and interquartile range of four experiments. (At 180 msec of response time very few points were available for

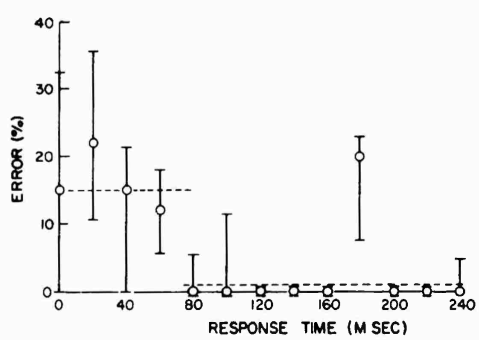

Fig. XXVII-12. Median and interquartile range of percentage error as a function of response time for 4 experiments. Only delayed responses are shown (square waves, 0.4 cps and 0.5 cps).

determining the mean and interquartile range, which may account for the fact that it is not in agreement with the rest of the data.) A χ^2 analysis showed that the frequency of error greater than 5 per cent between 0 msec and 80 msec after the movement of the target was higher than after an 80-msec delay ($\chi^2 = 17.1$, $p < 0.001$). This is a shorter time delay than found earlier[3] in which χ^2 analysis of the difference of responses greater than 5 per cent error between those occurring earlier than 130 msec and after that time was equal to 7.08, $p < 0.001$. The present experiment with this same time delay showed $\chi^2 = 5.2$, $p < 0.05$ but >0.02. Thus there is a suggestion that some modification of responses may take place within the earlier proposed minimum response time.

We noted that even with this second method, relatively few responses occurred between 0 msec and 100 msec (Fig. XXVII-13). This seems to be in agreement with an

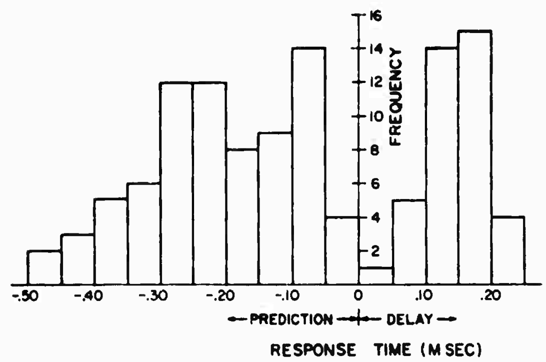

Fig. XXVII-13. Histogram of the frequency of occurrence of eye-movement response times for target motions (square wave, 0.4 cps).

earlier eye-movement experiment[1] for which histograms of response times at similar frequencies also show fewer responses in that time span. This phenomenon may indicate an inhibition of response in that period of time for possible correction; for those responses that do occur, error usually results. Further investigation of these findings is planned.

Anne Horrocks, L. Stark

References

1. L. Stark, G. Vossius, and L. R. Young, Predictive control of eye movements, IRE Trans., Vol. HFE-3, pp. 52-57, September 1962.

2. L. R. Young, A Sampled Data Model for Eye Tracking Movements, Technical Report, Joint Automatic Control Conference, 1963, pp. 606-607.

3. L. R. Young and L. Stark, Dependence of accuracy of eye movement on prediction, Quarterly Progress Report No. 67, Research Laboratory of Electronics, M.I.T., October 15, 1962, pp. 212-214.

4. J. W. Billheimer, A Markov Analysis of Adaptive Tracking Behavior, E.E. Thesis, Department of Electrical Engineering, M.I.T., September 1963.

E. OPTOKINETIC NYSTAGMUS IN MAN: THE STEP EXPERIMENT

This experiment is a continuation of work reported in Quarterly Progress Reports No. 70 (pages 357-359) and No. 71 (pages 286-290). The apparatus used in this experiment is shown in Fig. XXVII-14. The subject looks through a telescope at a visual field reflected from a galvanometer mirror. Eye-movement recordings are made from the left eye, which is also used for calibration. The experimenter controls the angle of the mirror so that the subject sees either stimulus A or stimulus B through the lenses

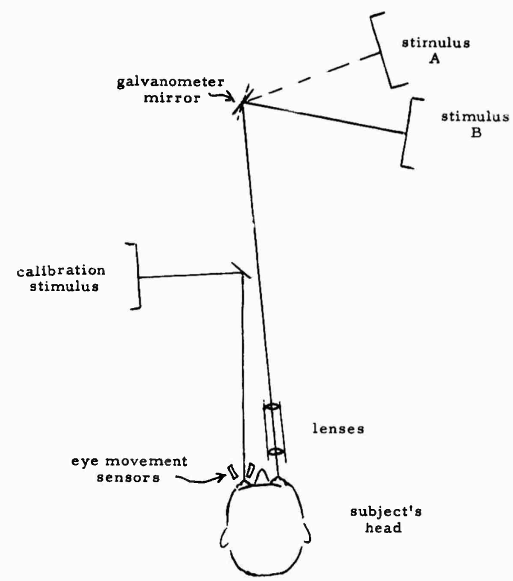

Fig. XXVII-14. Experimental apparatus.

forming the telescope. This apparatus can also be used for velocity feedback experiments, in which the eye position drives the galvanometer. In this case, the slow phase velocity will add a velocity component to the field movement.

In the step experiment, stimulus A consisted of a uniformly moving, vertically striped field. This field, as seen by the subject through the lenses, is 30° in diameter. Stimulus B was a dark, featureless space. The experiment consisted of applying a DC step to the galvanometer, which resulted in rapidly switching from stimulus B to A, or stimulus A to B. From unpublished experiments performed in this laboratory we have found that the optokinetic nystagmus response is binocular and identical in each eye, whether the stimulus is uniocular or binocular. Monitoring the left eye, which during the course of the experiment sees nothing except a dark blank field, is equivalent to monitoring the right eye, which sees the striped field. Figure XXVII-15 shows some responses to variable-width pulses applied to the galvanometer. The vertical line on the records shows the appearance of the stripes. A few responses are shown to the stripes that are being turned off (off step). Both on and off steps are random in time. In this experiment, there is no fixation point. The subject is directed to maintain a forward gaze on the center of the field. In this situation, the slight drift seen in the beginning of the record is normal.

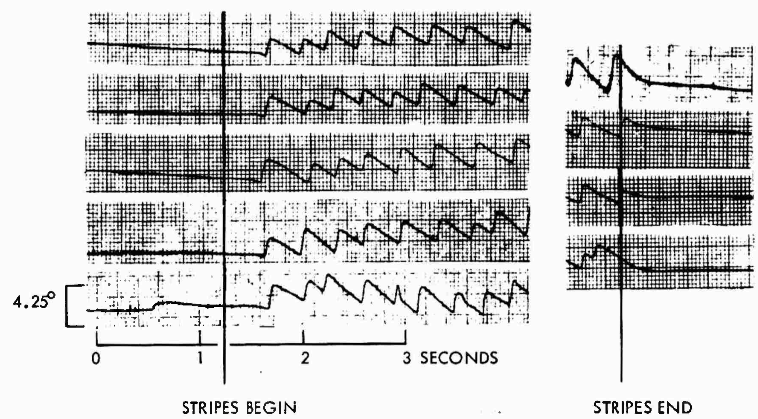

Fig. XXVII-15. Responses to variable-width pulses.

Four features of the on-step responses have been noted:

(i) The response begins with a fast phase.

(ii) This fast phase moves the eye away from the position of forward gaze toward the direction from which the stripes appear.

(iii) The response time, measured to the beginning of the fast phase, is approximately 300 msec.

(iv) A suggestive slow phase lasting only approximately 80 msec seems to precede the first fast phase.

Three features of the off-step responses have been noted:

(i) The last phase is a slow phase.

(ii) The response time, measured to a point of approximately zero velocity, is again approximately 300 msec.

(iii) There does not seem to be any "afternystagmus" persisting beyond a normal response time after the stimulus ceases.

From this experiment we conclude that optokinetic nystagmus is a reflex response with two components, a fast phase and a slow phase. This finding is in agreement with the magnitude correlations, published in Quarterly Progress Report No. 71 (pages 286-290), in which the lack of correlation between the fast phase and the preceding slow phase was shown. This suggests that the fast phase is not a positional servo correction to forward gaze error caused by the slow phase. The present experiment contains further evidence against the interpretation that the function of the fast phase is a positional correction for the error introduced by the preceding slow phase. The first response is a fast phase, which itself throws the eye into positional error.

Thus it seems that optokinetic nystagmus is a curious sort of double response. The fast phase, saccadic in nature because of its high velocity, is not a positional correction in the same sense as the saccade in normal eye tracking. The slow phase is not functionally the same as smooth tracking, as evidenced by the quantitative addition of the slow phase with a smooth tracking response (Quarterly Progress Report No. 71, pages 286-290).

E. G. Merrill, L. Stark

F. REMOTE ON-LINE COMPUTER DIAGNOSIS OF THE CLINICAL ELECTROCARDIOGRAM: SMOOTHING OF THE ELECTROCARDIOGRAM

Rapid advances in digital-computation techniques now make it possible to approach the problem of automatic diagnosis of clinical electrocardiograms with confidence that a solution will be found. This problem is being explored by a cooperating group from the Neurology Section of the Electronic Systems Laboratory and the Department of Biology, M.I.T., and the Division of Medicine of the Boston University School of Medicine. The objective of these studies is to develop a program for automatic on-line digital-computer interpretation of the electrocardiogram by using pattern-recognition techniques. Achievement of this goal has profound implications for improved clinical practice and efficiency, for improved reproducibility of interpretation, and for the development of new methods of investigation and validation of results of current interpretation problem areas.

In this on-line diagnostic system the electrocardiogram is relayed instantaneously from Boston University Medical Center over DC paired telephone lines to our laboratory at M.I.T. where it enters a G.E. 225-IBM 7094 computer complex through the analog-to-digital converter of the G.E. 225 computer. The electrocardiographic signals originating at the Medical Center, however, are obscured by noise, and smoothing of these tracings is necessary to facilitate the computer pattern-recognition analysis by adaptive matched-filter techniques.

In an electrocardiogram, the frequency components of the information signal are relatively low, approximately 0.2-100 cps.[1] The general standard for a clinical electrocardiograph is that the frequency response at 40 cps does not fall below 4 db of the DC response.[2] Unfortunately, the majority of clinical electrocardiographs do not meet this standard,[3] having a poor upper limit of frequency response. Langner and others[4-6] and Kerwin,[7] however, have emphasized the clinical importance of high-frequency components in the electrocardiogram, particularly for myocardial infarction. According to the present standard, set by the American Medical Association, frequency components in the electrocardiogram higher than 100 cps can be presumed to be non-informational noise and may be removed if necessary. If the high-frequency components do not interfere with the analysis of the electrocardiogram, they may be retained, since they may reveal factors of clinical significance that are still not well recognized.

As we reported[8] the logic for our point-recognition technique needs the first and/or second derivative of the original signal to detect the QRS complex that corresponds to the electrical activation of the cardiac ventricle. This means that the discrimination of the QRS complex from the other components is most certain by using these derivative functions, particularly if the electrocardiographic record is free from the higher frequency noise that originates in analog tape-recorder systems.

Two methods for eliminating high-frequency noise – curve fitting by the least-squares method, and the moving-average method – have been adapted for the electrocardiogram. The smoothing effect and the signal degradation produced by these procedures is a fundamental, controversial problem. It is clear that the problem is related to the length of segment to be fitted and with the functions assumed for the least-squares method, and with the weighting function, as well as the length of the segment, for the moving-average method. The measure of signal degradation largely depends on how one subsequently analyzes the signal for diagnostic purposes.

Figures XXVII-16, XXVII-17, and XXVII-18, show the effect of the length of the segment to be fitted or averaged. The function used for the least-squares method is a quadratic curve (parabola), and the weighting function for the moving-average method is a straight line, that is, no weighting on any points. Before and after the smoothing procedure these electrocardiograms were plotted on the auxiliary oscilloscope of the IBM 7094 computer. The amplitude of the QRS complex gradually decreased, as shown in Fig. XXVII-19, as the segment to be fitted or averaged became longer. This was particularly prominent in the moving-average method. The longer the segment, the wider the duration of the P, QRS, and QT complexes. This is more apparent in the moving-average method than in the least-squares method. If some weighting were put on the value of the center point in the segment, this greater degradation of the signal would be lessened in the moving-average method. In order to have the same smoothing effect as that provided by the 15 points (0.025 sec) used for the least-squares parabola method, the length of segment to be averaged was found to be approximately 6 points (0.01 sec) for the moving-average method. The derivatives of the electrocardiographic signal were most efficient in discriminating the QRS complex from the other components, as the amplitude of QRS complex could be smaller than the T wave. As shown in Fig. XXVII-18, however, the discrimination of the QRS component by the derivative was very poor before the smoothing procedure, but after smoothing by moving-average method the discrimination was nearly perfect. Figure XXVII-20 shows the result of Fourier analysis of an electrocardiogram before and after the smoothing procedure by the moving-average method in which the length of segment was 0.0015 sec (9 data points). The sampling rate was 600 points per second in these experiments, that is, 6 points per 10 msec. The computation time was less than 12 sec for

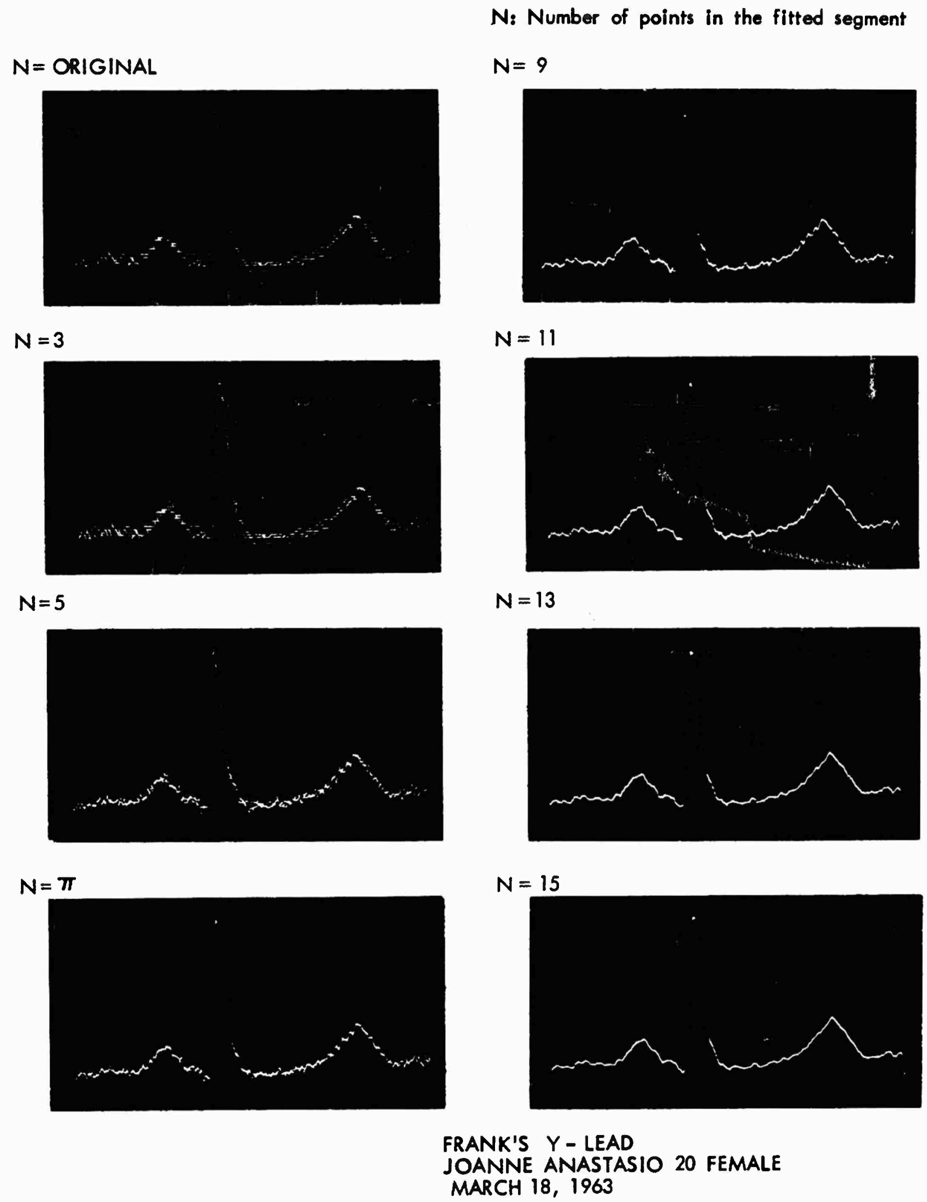

Fig. XXVII-16. Smoothing of electrocardiogram, least-squares parabolic method.

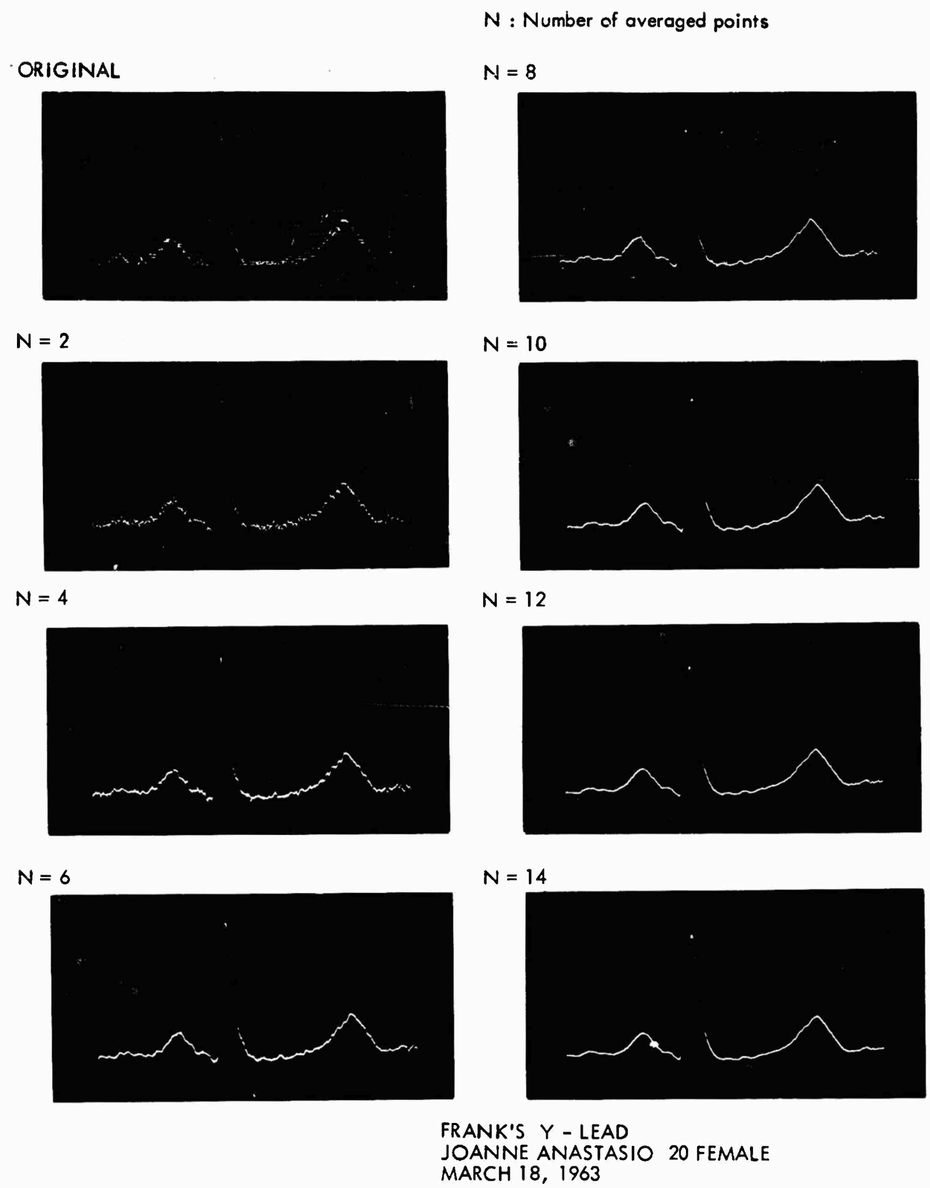

Fig. XXVII-17. Smoothing of electrocardiogram, moving-average method.

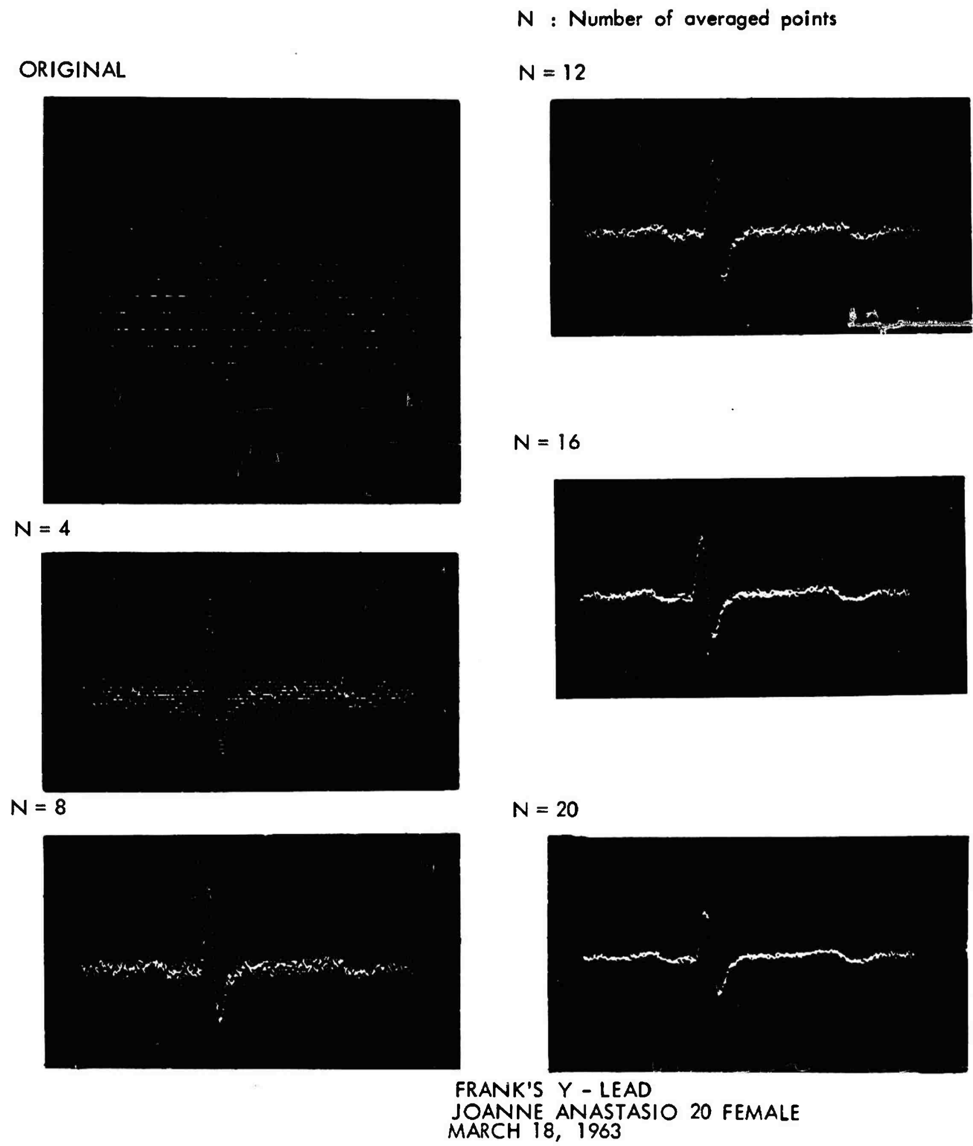

Fig. XXVII-18. Effect of smoothing by moving-average method on first derivative of electrocardiogram.

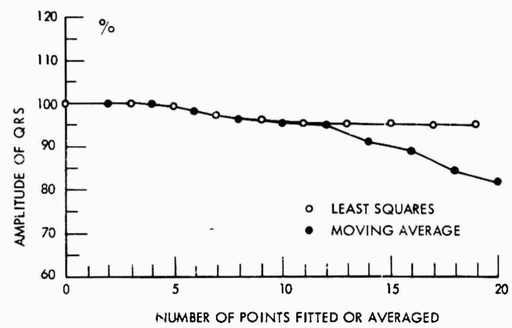

Fig. XXVII-19. Relation of amplitude of QRS complex to segment length.

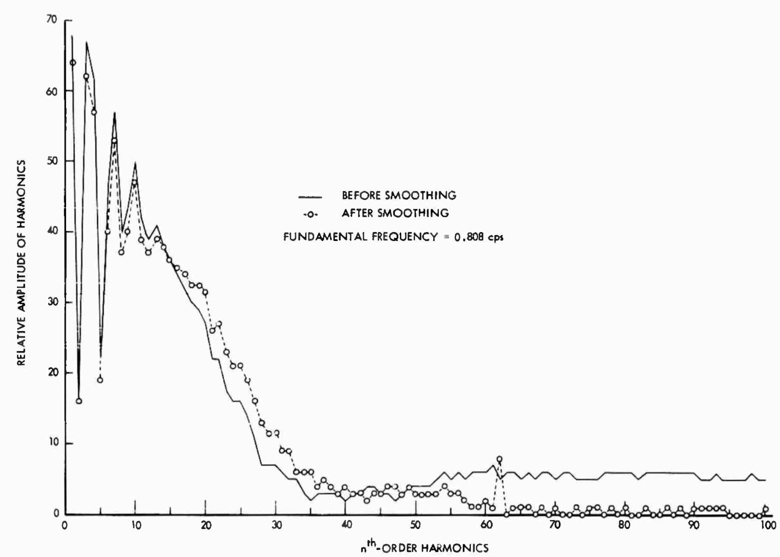

Fig. XXVII-20. Fourier analysis of electrocardiogram before and after smoothing (moving-average method).

the smoothing procedure for the X, Y, and Z components of a vectorcardiogram 2 sec long. At present, we are unable to recognize any significant difference between the smoothing effects of several high-order curve fittings as far as the electrocardiogram is concerned.

We found that either the method of the moving average or the least-squares parabola was quite satisfactory for the analysis of the electrocardiogram if the characteristics of each smoothing procedure were well understood. When these techniques were used properly, there was no preference found for one method over the other. The length of the segment to be smoothed, the weighting factor, and the degree of the curve to be used should all be considered in achieving the best results.

H. Horibe, G. H. Whipple, J. F. Dickson III, L. Stark

References

1. A. M. Scher and A. C. Young, Frequency analysis of the electrocardiogram, Circulation Res. 8, 344 (1960).

2. Council on Physical Medicine, Minimum requirement for acceptable electrocardiographs (revision), JAMA 143, 654 (1950).

3. G. E. Dower, A. D. Moore, W. G. Ziegler, and J. A. Osborne, On QRS amplitude and other errors produced by direct writing electrocardiographs, Am. Heart J. 65, 307 (1963).

4. D. B. Geselowitz, P. H. Langner, and F. T. Mansure, Further studies on the first derivative of the electrocardiogram, including instruments available for clinical use, Am. Heart J. 64, 805 (1962).

5. P. H. Langner, Further studies in high fidelity electrocardiography: Myocardial infarction, Circulation 8, 905 (1953).

6. P. H. Langner, D. B. Geselowitz, and F. T. Mansure, High fidelity components in the electrocardiograms of normal subjects and of patients with coronary heart disease, Am. Heart J. 62, 746 (1961).

7. A. J. Kerwin, The effect of the frequency response of electrocardiographs on the form of electrocardiograms and vectorcardiograms, Circulation 8, 98 (1953).

8. M. Okajima, L. Stark, G. H. Whipple, and S. Yasui, Computer pattern recognition techniques: Some results with real electrocardiographic data, IEEE Trans., Vol. BME-10, p. 106, 1963.

XXVIII. SENSORY AIDS RESEARCH*

Prof. S. J. Mason
Prof. D. E. Troxel
J. K. Dupress
W. L. Black
J. K. Clemens
R. W. Donaldson
E. Landsman

RESEARCH OBJECTIVES

The long-range objective of our work is to contribute to the development of useful technological aids for blind and blind-deaf people. Most of our present work is concerned with studies of the acquisition and processing of visual information for presentation to the nonvisual senses. Our projects include mobility-aid simulation, reading-machine problems, tactile and kinesthetic displays, multimodality sensory communication, and real-time computer-facility development.

S. J. Mason

*This work is supported in part by the National Science Foundation (Grant G-16526), the National Institutes of Health (Grant MH-04737-03), and the National Aeronautics and Space Administration (Grant NsG-496).

XXIX. CIRCUIT THEORY AND DESIGN

Prof. P. Penfield, Jr.
Prof. R. P. Rafuse
Prof. C. L. Searle
Prof. R. D. Thornton

RESEARCH OBJECTIVES

We wish to investigate circuits containing devices that are nonlinear and/or time-variant and/or active, including transistors, tunnel diodes, and varactor diodes. Such investigations include (a) theoretical and experimental behavior of parametric amplifiers, frequency multipliers, mixers, transistor and tunnel-diode circuits; and (b) theoretical study of those properties that are invariant under certain types of imbeddings, in part by means of a general voltage-current conservation theorem.

P. Penfield, Jr., R. P. Rafuse, C. L. Searle, R. D. Thornton

A. RECENT DEVELOPMENTS IN PARAMETRIC MULTIPLIERS*

1. Introduction

This report is a compendium of some of the theoretical and experimental work carried out here and at Lincoln Laboratory, M.I.T., since the summer of 1962 on varactor multipliers. Diamond[1,2] has carried out analyses on the effects of "extra" (larger number than necessary) idlers on quadruplers and octuplers with somewhat surprising results. An analysis has also been made on overdriven doublers using both abrupt- and graded-junction diodes[3] with very simple models assumed for the forward characteristics. The results of the overdriven doublers lead to simple analysis techniques for doublers using diodes with radical nonlinear capacitances. Some experimental circuits have been developed which yield stable, high-efficiency, low spurious-content operation.

The use of more idlers than necessary yields higher efficiency and power handling than does the use of just the necessary number. When overdriven, the graded junction shows higher efficiency than the abrupt-junction in the doubler circuit. Care in circuit design can result in stable, clean operation of frequency multipliers.

2. Extra Idlers

As is now well known, nonoverdriven abrupt-junction multipliers of order greater than X2 require currents flowing at some of the lower harmonics in order that nonzero output be achieved. The necessary "idler" frequencies can easily be identified by realizing that the junction voltage is proportional to the square of the junction charge. As shown by Penfield and Rafuse,[4] the necessary idler configurations for some of the

*This work was supported in part by the National Aeronautics and Space Administration (Grant NsG-419).

low-order multipliers become

(a) Tripler: 1-2-3

(b) Quadrupler: 1-2-4

(c) Quintupler: 1-2-3-5, 1-2-4-5

(d) Sextupler: 1-2-3-6, 1-2-4-6

(e) Septupler: 1-2-3-6-7, 1-2-4-6-7,
1-2-3-5-7, 1-2-3-4-7, 1-2-4-5-7, 1-2-4-8-7*

(f) Octupler: 1-2-4-8.

Note that these idler schemes contain the minimum necessary number of idlers. The septupler marked with the asterisk is unusual in that an idler at a frequency higher than the output frequency is necessary for output at $7\omega_o$.

The question that now arises concerns the effect of "unnecessary" or "extra" idlers. For example, although the 1-2-4 quadrupler configuration will operate efficiently, what would be the effect of adding an extra idler to form a 1-2-3-4 quadrupler? Similarly, what would be the effects produced in a 1-2-3-4-5 quintupler or a 1-2-4-6-8 octupler?

The problem is very complex and can, in general, only be solved by detailed computation, with the aid of a digital computer, on each multiplier. Two solutions for extra-idler multipliers have been obtained by Diamond,[1,2] namely, the 1-2-3-4 and 1-2-4-6-8. The results are of extreme interest.

First, we compare the two quadrupler configurations in the notation of Penfield and Rafuse.[4] The symbols used in the tables that follow are:

$\omega_c = S_{max}/R_s$, the varactor cutoff frequency (at breakdown)
ω_o = drive frequency
ω_{out} = output frequency
R_s = varactor series-loss resistance
$C_{min} = S_{max}^{-1}$ = minimum junction capacitance (at V_B)
V_B = breakdown voltage
ϕ = contact potential
V_o = average bias voltage.

The others are self-explanatory. The formulation for low-frequency efficiency is due to Uhlir.[5]

We note in Table XXIX-1 that the 1-2-3-4 configuration has not only higher efficiency, but higher power handling (without overdriving) as well. Perhaps the lossless idler approximation masks some disabilities of the 1-2-3-4 quadrupler. If we assume an idler-loss resistance equal in value to the varactor series-loss resistance R_s (external idler circuit Q = diode Q) and again compare the two circuits $\alpha(1\text{-}2\text{-}4) = 25$ and $\alpha(1\text{-}2\text{-}3\text{-}4) = 16$, $\beta(1\text{-}2\text{-}4) = 0.020$ and $\beta(1\text{-}2\text{-}3\text{-}4) = 0.023$. It is obvious that the presence of idler loss only serves to accentuate the better efficiency of the 1-2-3-4 circuit over the 1-2-4. The power levels are relatively unchanged.

Table XXIX-1. Comparison of 1-2-4 and 1-2-3-4 quadruplers. In each case, the idler circuit loss is assumed to be zero (only diode loss present). Values are useful for $\omega_{out} < 0.1\,\omega_c$.

PARAMETER	1 - 2 - 4	1 - 2 - 3 - 4
EFFICIENCY $\epsilon \simeq e^{-\alpha(\omega_{out}/\omega_c)}$	$\alpha = 15.6$	$\alpha = 11.4$
POWER INPUT $P_{in} \simeq \beta(V_B+\phi)^2 C_{min}\omega_o$	$\beta = 0.0196$	$\beta = 0.0226$
INPUT RESISTANCE $R_{in} \simeq A\, S_{max}/\omega_o$	$A = 0.150$	$A = 0.096$
LOAD RESISTANCE $R_4 \simeq B\, S_{max}/\omega_o$	$B = 0.0513$	$B = 0.0625$
BIAS VOLTAGE $\hat{V} = \frac{V_0+\phi}{V_B+\phi}$	$\hat{V} = 0.334$	$\hat{V} = 0.330$

A similar comparison is made between the 1-2-4-8 and 1-2-4-6-8 octuplers in Table XXIX-2. It is again obvious that the 1-2-4-6-8 configuration exceeds in both efficiency and power handling the 1-2-4-8 octupler. As before, a comparison with equal external idler and diode Q's gives $\alpha(1\text{-}2\text{-}4\text{-}8) = 31.3$ and $\alpha(1\text{-}2\text{-}4\text{-}6\text{-}8) = 23.1$, $\beta(1\text{-}2\text{-}4\text{-}8) = 0.020$ and $\beta(1\text{-}2\text{-}4\text{-}6\text{-}8) = 0.025$. It is apparent that the extra idler gives improved performance even with idler loss included.

One is tempted to make some fairly general conclusions from the admittedly sparse data obtained thus far. Table XXIX-3 presents the α and β for a group of varactor multipliers. If we extrapolate the results for the quadrupler to the quintupler and sextupler it appears that the addition of the $3\omega_o$ idler to give a 1-2-3-4-5 quintupler and the $3\omega_o$ and $5\omega_o$ idlers to give a 1-2-3-4-5-6 sextupler would result in α's and β's commensurate with the X2, X3 and X4(1-2-3-4) circuits. It is also very tempting to

Table XXIX-2. Comparison of 1-2-4-8 and 1-2-4-6-8 octuplers. In each case idler circuit loss is zero. Values are good for $\omega_{out} < 0.1\,\omega_c$.

PARAMETER	1 - 2 - 4 - 8	1 - 2 - 4 - 6 - 8
EFFICIENCY $\epsilon \simeq e^{-\alpha(\omega_{out}/\omega_c)}$	$\alpha = 21.0$	$\alpha = 14.9$
POWER INPUT $P_{in} \simeq \beta(V_B+\phi)^2 C_{min}\omega_o$	$\beta = 0.0198$	$\beta = 0.0248$
INPUT RESISTANCE $R_{in} \simeq A\,S_{max}/\omega_o$	$A = 0.103$	$A = 0.140$
LOAD RESISTANCE $R_B \simeq B\,S_{max}/\omega_o$	$B = 0.0188$	$B = 0.0251$
BIAS VOLTAGE $\hat{V} = \dfrac{V_0+\phi}{V_B+\phi}$	$\hat{V} = 0.351$	$\hat{V} = 0.347$

estimate that the addition of extra idlers to the octupler to yield a 1-2-3-4-5-6-7-8 octupler would bring the octupler results into line with the rest of the multipliers. But the computational complexity that is required to check such results is extremely high. It is hoped that future work may lead to a unified theory which will predict essentially equivalent efficiencies (in terms of the output frequency to cutoff frequency ratio) and equivalent power-handling capabilities (in terms of the input frequency) for the same diode, regardless of the order of multiplication. In this vein it is interesting to note that the 1-2-4-6-8 octupler is already more efficient than the 1-2-4 quadrupler (for the same output frequency).

3. Overdriven Doublers

An analysis has been carried out here on the overdriven abrupt- and graded-junction doublers.[3] The model chosen for the forward region was exceedingly simple; it was assumed that the diode elastance (C^{-1}) went to zero at charges greater than the charge equivalent to the contact potential, and it was further assumed that the series resistance remained constant in the forward direction. Both of these assumptions, although radical,

Table XXIX-3. Values of α and β for various multipliers.

ORDER	α	β
X2*	9.95	0.0277
X3*	11.6	0.0241
X4(1, 2, 3, 4)	11.4	0.0226
X5(1, 2, 4, 5)*	18.6	0.018
X6(1, 2, 4, 6)*	16.6	0.022
X8(1, 2, 4, 6, 8)	14.9	0.0248

*Data from Penfield and Rafuse.[4]

are fair approximations. The series-loss resistance will, of course, be reduced by conductivity modulation effects in the forward direction, but a good part of the losses in high-quality varactors occurs in the contacts and leads and therefore the total loss will remain essentially constant. The elastance does not actually go to zero but instead simply decreases exponentially (along with an increasing conductance, yielding a very low junction Q); however, at the frequencies of interest the junction impedance level is so low that the diode can be reasonably represented by just the series loss, R_s.

The results for optimum efficiency operation of the optimally overdriven graded- and abrupt-junction doublers are given in Table XXIX-4 along with the results for nominal drive[4] for comparison. The most startling result (although one rather frequently and often embarrassingly observed experimentally) is that the two types of diodes, optimally overdriven, give essentially equal performances. For the same power input, same breakdown voltage and same minimum capacitance, the graded-junction and abrupt-junction diodes are essentially interchangeable in any doubler circuit. The bias voltages are identical, the input and output resistances and reactances are essentially the same, and the efficiencies are practically equal.

It is interesting to note that the graded-junction diode must be overdriven by a factor of 5.8 (in power), whereas the abrupt-junction diode optimizes when overdriven by only a factor of 2.45. Furthermore, the graded junction shows the most improvement in efficiency and actually exceeds the efficiency of an abrupt junction when optimally overdriven.

A second important result, which was not obvious (at least to the author) before the computer derivation of the overdriven doubler was completed, lies in the ratio of fundamental to second-harmonic charge. If the power output is optimized, the low-frequency

Table XXIX-4. Comparison of overdriven and nonoverdriven abrupt-junction and graded-junction diodes. Results are valid for $\omega_{out} < 0.1\,\omega_c$.

PARAMETER	MODE	ABRUPT-JUNCTION	GRADED-JUNCTION
EFFICIENCY $\epsilon \simeq e^{-\alpha(\omega_{out}/\omega_c)}$	OVERDRIVEN	$\alpha = 7.5$	$\alpha = 7.0$
	NOMINAL	$\alpha = 9.95$	$\alpha = 12.8$
POWER INPUT $P_{in} \simeq \beta(V_B+\phi)^2 C_{min}\omega_o$	OVERDRIVEN	$\beta = 0.0680$	$\beta = 0.0680$
	NOMINAL	$\beta = 0.0277$	$\beta = 0.0118$
INPUT RESISTANCE $R_{in} = A\,S_{max}/\omega_o$	OVERDRIVEN	$A = 0.100$	$A = 0.110$
	NOMINAL	$A = 0.080$	$A = 0.0604$
LOAD RESISTANCE $R_2 = B\,S_{max}/\omega_o$	OVERDRIVEN	$B = 0.164$	$B = 0.170$
	NOMINAL	$B = 0.136$	$B = 0.102$
BIAS VOLTAGE $\hat{V} = \dfrac{V_o+\phi}{V_B+\phi}$	OVERDRIVEN	$\hat{V} = 0.258$	$\hat{V} = 0.258$
	NOMINAL	$\hat{V} = 0.349$	$\hat{V} = 0.409$
EFFECTIVE INPUT ELASTANCE $\hat{S}' = S_{in}/S_{max}$	OVERDRIVEN	$\hat{S}' = 0.33$	$\hat{S}' = 0.37$
	NOMINAL	$\hat{S}' = 0.50$	$\hat{S}' = 0.68$
EFFECTIVE OUTPUT ELASTANCE $\hat{S}'' = S_{out}/S_{max}$	OVERDRIVEN	$\hat{S}'' = 0.36$	$\hat{S}'' = 0.40$
	NOMINAL	$\hat{S}'' = 0.50$	$\hat{S}'' = 0.67$

value of the ratio is 2.0, regardless of the diode type or the level of overdriving. One suspects that this result holds true almost universally.

If we assume such a universal behavior, we can calculate the performance for a variety of other diode types. In particular, we can postulate the "ideal" diode characteristic shown in Fig. XXIX-1 and overdrive so that the elastance waveform is a square wave of peak-to-peak value S_{max}. Such a curve is actually approximated by some of the very thin diffused, epitaxial diodes, for which the majority of the elastance change takes place over the first few volts in the back direction and practically no change in elastance occurs for higher voltages until breakdown is reached. If we assume a constant series resistance R_s, we can calculate efficiency, power, input and output resistances, and

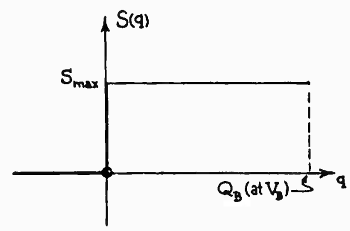

Fig. XXIX-1. Stepwise nonlinear elastance characteristic.

the rest of the necessary parameters with ease.

In Appendix A a detailed derivation of the overdriven stepwise-diode doubler is presented. It should be noted that such a device will not multiply unless it is overdriven, otherwise it appears as a constant elastance. The results are interesting. Presented in Table XXIX-5 are the efficiency, input power, and input and load resistances for such an overdriven doubler, together with the same parameters for the overdriven abrupt- and graded-junction doublers operating under the same conditions (optimum power output, fully driven, average charge equal to zero).

Note that the efficiency increases as the diode becomes, if you wish, more and more nonlinear; although the power-handling capability decreases. In other words, one trades efficiency for power handling. Although the stepwise doubler probably does not have the best achievable efficiency (allowing higher harmonic currents to flow may give better efficiency), it is useful in predicting the behavior of overdriven epitaxial units.

Table XXIX-5. Comparison of efficiency, input power, and input and load resistances for overdriven stepwise-junction, graded-junction, and abrupt-junction doublers. In each case the diode is driven to the breakdown voltage, output power is optimized, and the average charge is zero. (The symbols α, β, A, and B are the same as those in Table XXIX-4.)

PARAMETER	STEPWISE	GRADED	ABRUPT
EFFICIENCY	$\alpha = 4.7$	$\alpha = 8.25$	$\alpha = 10.5$
INPUT POWER	$\beta = 0.063$	$\beta = 0.091$	$\beta = 0.115$
INPUT RESISTANCE	A = 0.212	A = 0.121	A = 0.095
LOAD RESISTANCE	B = 0.212	B = 0.121	B = 0.095

4. Some Observations Concerning $\gamma = 0.45$

Many people still insist on characterizing a varactor as "not quite abrupt" or "not quite graded" with, therefore, exponents that lie between 1/2 and 1/3. The author has never seen one of these "not quite" varactors.

Every diode has associated with it certain parasitic elements. At low frequencies, at which most varactor capacitance measurements are made, the major parasitic is case capacitance. The total capacitance can therefore be written

$$C = C_{case} + C_{min}\left[\frac{V_B + \phi}{v + \phi}\right]^{\gamma}, \tag{1}$$

where $\gamma = 1/2$ for abrupt junctions and $1/3$ for graded. Extremely careful measurements were made on several abrupt- and graded-junction varactors with a three-terminal capacitance bridge (Boonton 75A-S8) and a digital voltmeter.

In no case was a diode found to have an exponent other than 0.500 or 0.333. If careful measurements are made and V_B is determined accurately, three points suffice to determine the three unknowns, ϕ, C_{case}, and C_{min}. For example, careful measurements on a PSI PC-115-10 diode yielded $V_B = 114.0$ volts, $\phi = 0.540$ volts, $C_{min} = 1.81$ pf, and $C_{case} = 0.937$ pf. A plot of $(C-C_{case})^{-2}$ versus v yielded an absolutely straight line with 17 data points lying on the line. The exponent was precisely 0.500.

Other measurements made on epitaxial units yielded straight lines for $(C-C_{case})^{-3}$ versus v, but the values of C_{min}, V_B, and ϕ would change abruptly at some voltage less than breakdown. The characteristic S^3 versus v was composed of two straight segments, one from ϕ to $V_a(<V_B)$, and one of lesser slope from V_a to V_B. In many units with V_B approximately 50 volts, the break voltage V_a was only 6-8 volts. The practice of giving the cutoff frequency of such units at 2, 4 or 6 volts in the reverse direction (depending on the particular manufacturer's crystal ball) can give large errors in extrapolated C_{min} and f_c at breakdown. The errors are unfortunately in the optimistic direction and the units will not perform as expected. If C_{min} and f_c at V_B were given, the units would be far more conservatively characterized, and multiplier performance would be more easily predicted.

Briefly, if the diode is characterizable by an exponent over its entire voltage range (which rules out the so-called hyper-abrupt units) the exponent is either 1/2 or 1/3, not 0.45, 0.36 or some other approximation, arrived at by neglecting the case capacitance or not recognizing the break in the epitaxial units.

5. Circuit Techniques

Some circuit techniques that have been found useful in our laboratory will now be described. At this time, good experimental data on overdriven doublers are not available, but a detailed design of a symmetric two-diode tripler (see Fig. XXIX-2) has been carried out with quite satisfying results.

The tripler was built with two nearly matched PSI PC-117-47 varactors (with measured characteristics of $C_{min} = 6.6$ and 6.9 pf, $V_B + \phi = 138$ v (lowest one of the pair), $\phi = 0.64$ v, $C_{case} = 2.3$ and 1.4 pf). Both the case capacitances and the strays were

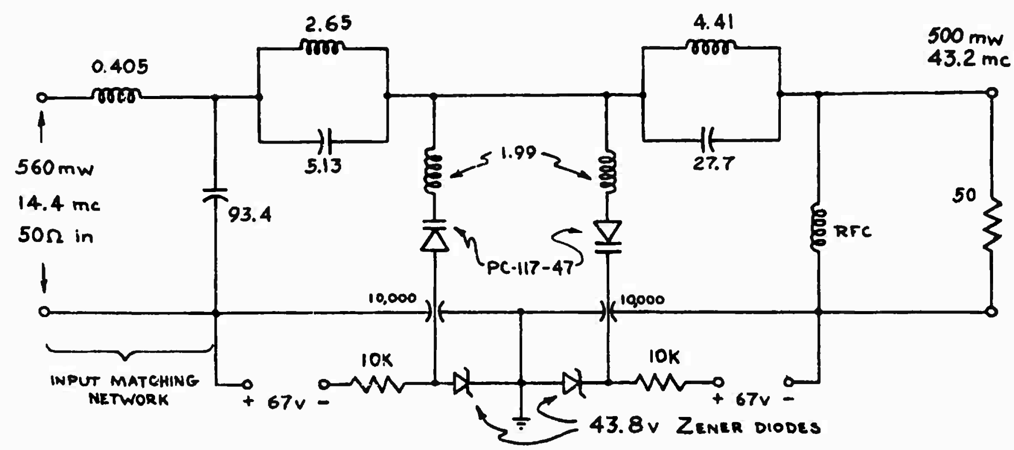

Fig. XXIX-2. Tripler circuit. (Values of the components are in pf, μh, and ohms.)

used to determine the input matching network that is necessary for a match to the 50Ω source at the design power level. The idler at $2\omega_o$ is resonated in the loop formed by the two varactors and the two 1.99-μh coils. Two parallel-resonant traps separate the currents at ω_o and $3\omega_o$ into the input and output circuits, respectively.

The losses in the individual circuits were measured and included in the efficiency calculations. The final operating conditions are compared with the predicted values in Table XXIX-6. The agreement is embarrassingly close, in fact, closer than the accuracy of the measuring instruments. It shows that one can design with care and achieve very close agreement with theory.

Several other interesting observations can be made. First, the multiplier would not operate self-biased (not very much effort was spent trying) and would simply break up

Table XXIX-6. Theoretical and experimental parameters for the symmetric tripler.

PARAMETER	THEOR.	EXPER.
CIRCUIT EFFICIENCY	90%	89.6%
LOAD RESISTANCE	50Ω	50Ω
INPUT RESISTANCE	50Ω	48.5Ω
POWER INPUT	560 mw	558 mw
BIAS VOLTAGE	43.7 v	43.8 v

into spurious oscillations before any appreciable output power could be reached. Second, biased at the proper voltages from potentiometers, the tripler was stable, until the frequency was changed more than 1% or an attempt was made to overdrive; in either case it broke up into spurious oscillations. Third, the majority of the spurious oscillations were identified at their baseband frequency (500-1000 kcps) in the bias circuitry; the addition of the Zener diodes to the bias circuit provided a sufficiently low incremental impedance to swamp the spurious generation mechanism. Under these conditions, the 1-db bandwidth of the tripler became 7% and it could be overdriven up to a factor of 1.5 (limited by the driving source) with no sign of spurious oscillations. In fact, it was very difficult to establish any sort of spurious oscillation; only a radical (20-30%) change in input frequency would excite a divide-by-two or divide-by-three mode. Fourth, a 1-2-3-4-5 quintupler was built as a following stage; it was noted that the output at 216 mc/sec was free of spurious oscillation only if the input of the quintupler was tuned properly and presented a 50Ω load to the tripler. It appears that many of the problems arising during the cascading of multipliers can be cured with careful design of each individual stage.

A spectrum analyzer was used to check the level of the fundamental and unwanted harmonics at the tripler output. The fundamental and all even harmonics were down 40 db. The fifth harmonic was most prevalent, but still 30 db down. Additional filtering can easily be added to reduce the unwanted signals to 80 db below the output, if desired.

6. Conclusions

The major conclusion to draw is that a considerable amount of work remains before parametric multipliers can be considered to be "fully understood." "Jumping to conclusions" in this field is a custom fraught with danger. The author remembers the time when he considered extra idlers to be equal to extra loss. Unfortunately, intuition seems to work only in an a posteriori sense for parametric multipliers.

If we disregard the dangers of intuitive reasoning, it appears from the results of the 1-2-3-4 and 1-2-4-6-8 multipliers that extra idlers can improve both the efficiency and power handling of a varactor multiplier, by nontrivial factors. It also appears (and this is even farther out on a limb) that appropriate idler schemes will yield multipliers with nearly equal efficiencies (for the same diode and the same <u>output</u> frequency) and nearly equal power handling (for the same diode and the same <u>input</u> frequency).

There are two important results from the analysis of the overdriven doublers. The overdriven graded-junction doubler is somewhat more efficient than the overdriven abrupt-junction doubler (precisely the opposite result is found when nominally driving). For identical breakdown voltages and identical minimum capacitances, at the optimal overdrive level the abrupt-junction and graded-junction diodes are indistinguishable in a doubler.

An accompanying result from the overdriven analysis is the charge ratio of 2.0, when the output power is optimized. At low frequencies the ratio holds regardless of the degree of nonlinearity. This allows us to compute the characteristics of an infinite variety of doublers and compare their performances. A particular limiting case, the stepwise doubler, has been analyzed and found more efficient than the graded junction, although of somewhat less power-handling capability. It appears that, as the degree of "nonlinearity" of the varactor characteristic increases, the efficiency, when overdriven, increases and the power handling decreases.

Very careful measurements show that a diode can be characterized by an exponent over its full voltage range, only if the exponent is 1/3 or 1/2. Values of γ in the range 0.500-0.333 are invariably the result of poor measurement procedure or improper subtraction of parasitic-case capacitance. Some epitaxial units may show breaks in the elastance-voltage characteristic, but their exponents do not usually vary. If the diode exponent truly varies with back voltage, it cannot properly be said to have an exponent (even on the "average," whatever that means). Epitaxial units should be characterized by cutoff frequency and capacitance at breakdown, not by some intermediate voltage.

Experimentally it has been observed that careful design will yield multiplier performance essentially as theory predicts. Spurious oscillations can be minimized if the bias-circuit impedance can be kept real and small at frequencies from low audio to an appreciable fraction of the drive frequency. A high-quality Zener diode makes an almost ideal bias source. Oscillations arising during cascading of multipliers can be minimized by insuring that the input impedance of the second multiplier is real and equal to the optimum load resistance for the first multiplier (this is, of course, achievable with an isolator; but such devices, besides being bulky and heavy, just do not exist below 100-200 mc).

APPENDIX A

Derivation of Stepwise-Junction Doublers

If $S(q)$ is S_{max} for $0 < q \leq Q_B$ and zero for $q < 0$ and we assume that the fundamental charge is twice the second-harmonic charge, then, with the junction so driven that the charge wave just reaches the breakdown charge Q_B and averages to zero, we have

$$q(t) = \frac{2}{3\sqrt{3}} Q_B (2 \sin \omega_o t + \sin 2\omega_o t) \tag{2}$$

if the currents are assumed to be "in phase."

The current is given by

$$i(t) = \frac{4}{3\sqrt{3}} Q_B \omega_o (\cos \omega_o t + \cos 2\omega_o t), \tag{3}$$

under the assumption that all higher harmonic currents are open-circuited. The resultant square wave of elastance becomes

$$S(t) = \frac{S_{max}}{2}\left[1 + \sum_{k=1}^{\infty} \frac{4}{\pi}\,\frac{1-(-1)^k}{2k}\sin k\omega_o t\right]. \tag{4}$$

The equation of motion for the junction is

$$v(t) = \int S(t)\; i(t)\; dt \tag{5}$$

and substituting Eqs. 3 and 4 in Eq. 5 and integrating, we have the fundamental and second-harmonic components of v(t).

$$v(t) = \frac{8}{9\sqrt{3}\pi} S_{max}\, Q_B(\cos\omega_o t - \cos 2\omega_o t). \tag{6}$$

Then

$$P_{in} = \frac{1}{2} I_1 V_1 = \frac{16}{81\pi} S_{max}\, Q_B^2 \omega_o. \tag{7}$$

For the stepwise junction, however,

$$Q_B = V_B/S_{max}, \tag{8}$$

so

$$P_{in} = 0.0628\, V_B^2 C_{min}\omega_o, \tag{9}$$

where $C_{min} = S_{max}^{-1}$.

Now we assume a series-loss resistance, R_s, and obtain a cutoff frequency

$$\omega_c = S_{max}/R_s. \tag{10}$$

At low frequencies the dissipated power is

$$P_{diss} = \frac{1}{2}\left(I_1^2 + I_2^2\right) R_s = \frac{16}{27} Q_B^2 \omega_o^2 R_s, \tag{11}$$

and the efficiency is

$$\epsilon \approx 1 - \frac{P_{diss}}{P_{in}} = 1 - 3\pi\frac{\omega_o}{\omega_c}. \tag{12}$$

We can write (12) in the same form as for the other multipliers

$$\epsilon \approx e^{-\frac{3\pi}{2}(\omega_{out}/\omega_c)}. \tag{13}$$

Therefore $\alpha = 4.7$, and $\beta = 0.0628$. The input and load resistances are equal, and are

$$R_{in} = \frac{V_1}{I_1} = R_2 = \frac{V_2}{I_2} = \frac{2}{3\pi} \frac{S_{max}}{\omega_o}, \tag{14}$$

so A = B = 0.212. The average elastance is the same at ω_o and $2\omega_o$, and is simply $S_{max}/2$.

The author wishes to thank Bliss L. Diamond, of Lincoln Laboratory, M.I.T., for allowing the use of his computations on the 1-2-3-4 quadrupler and the 1-2-4-6-8 octupler. Others who contributed to the work are Jon A. Davis, of Microwave Associates, Inc., Burlington, Massachusetts, who carried out the computer solutions for the overdriven graded-junction and abrupt-junction doublers, and Daniel L. Smythe, Jr., who performed the experimental work on the tripler in our laboratory.

R. P. Rafuse

References

1. B. L. Diamond, Some Results for Higher-Order Varactor Frequency Multipliers, Group Report 47G-5, Lincoln Laboratory, M.I.T., 21 March 1963.

2. B. L. Diamond, personal communication, 1963.

3. J. A. Davis, A Forward-Driven Varactor Frequency Doubler, S.M. Thesis, Department of Electrical Engineering, M.I.T., May 1963.

4. P. Penfield, Jr. and R. P. Rafuse, Varactor Applications (The M.I.T. Press, Cambridge, Mass., 1962).

5. A. Uhlir, Jr., Similarity considerations for varactor multipliers, Microwave Journal, Vol. 5, pp. 55-59, July 1962.

XXX. NETWORK SYNTHESIS

Prof. H. B. Lee
Prof. W. C. Schwab
J. Anderson
V. K. Prabu

RESEARCH OBJECTIVES

Our group aims to achieve an improved understanding of lumped, linear, finite, passive, bilateral networks. During the coming year we shall be concerned primarily with the following problems:

1. Determination of fundamental properties of transformerless networks.
2. Development of new methods for synthesizing lossless driving-point impedances.
3. Implications of time-domain power conservation.
4. Extension of known synthesis procedures to include new types of circuit elements.

Research is now under way on all four problems.

H. B. Lee

A. NON SERIES PARALLEL REALIZATION FOR LOSSLESS DRIVING-POINT IMPEDANCES

The purpose of this report is to call attention to a new method for realizing lossless driving-point impedances. The method enables one to realize impedances of the form

$$Z = \sum_{i=1}^{n} k_i \frac{s}{s^2 + \omega_i^2} \tag{1}$$

upon the network N shown in Fig. XXX-1. The final realization contains one more

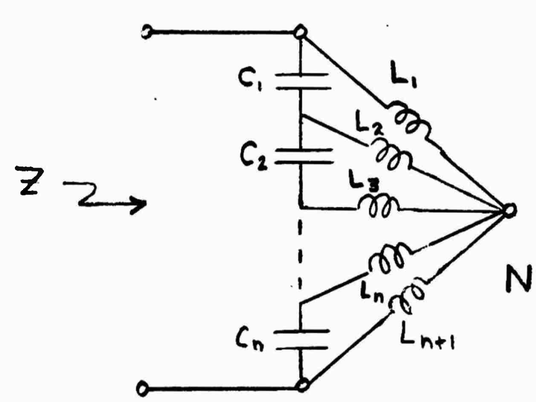

Fig. XXX-1.

than the minimum number of circuit elements; thus the realization procedure is not canonic. Because of the superfluous circuit element, the realization procedure involves one independently specifiable parameter.

The synthesis method can best be explained if one redraws the network N as shown in Fig. XXX-2. It is evident from this figure that N consists of a ladder network driven from an unconventional entry. In the synthesis procedure, one assumes that the network of Fig. XXX-2 realizes the impedance Z. One then determines the corresponding impedance z_{11} shown in Fig. XXX-2. Once z_{11} is known, one realizes Z by developing z_{11} into a ladder. The details of the determination of z_{11} are as follows.

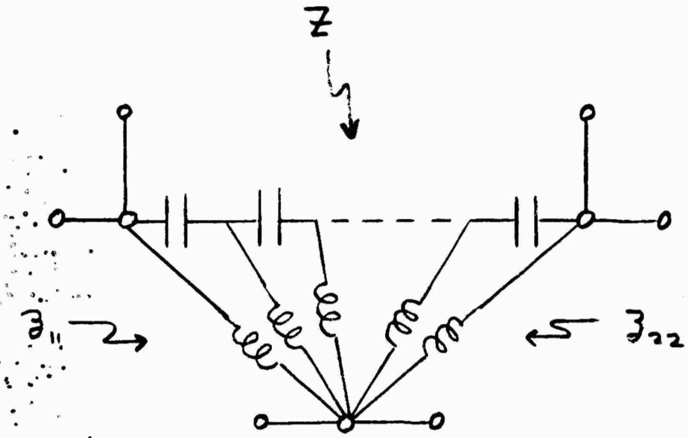

Fig. XXX-2.

If the network of Fig. XXX-2 is to realize the impedance (1), then the impedance z_{11} must have the form

$$z_{11} = As + \sum_{i=1}^{n} a_i \frac{s}{s^2 + \omega_i^2}. \tag{2}$$

Moreover, the transfer impedance of the ladder must take the form

$$z_{12} = A \frac{s^{2n+1}}{\prod_{i=1}^{n} \left(s^2 + \omega_i^2\right)}. \tag{3}$$

Because z_{12} is determined within the multiplier A, z_{12} can be rewritten as follows:

$$z_{12} = As + \sum_{i=1}^{n} A\rho_i \frac{s}{s^2 + \omega_i^2}; \tag{4}$$

the ρ_i in (4) are completely determined, and are given by

$$\rho_i = \lim_{\Omega \to \omega_i} \left[\frac{(s^2 + \Omega^2)\, s^{2n}}{\prod_{j=1}^{n} \left(s^2 + \omega_j^2\right)} \right]. \tag{5}$$

If one assumes that $\omega_1 < \omega_2 \ldots < \omega_n$, then it follows from (5) that the signs of successive ρ_i alternate, the sign of each ρ_i being the same as that of $(-1)^{n-i+1}$. The alternation of sign may be made explicit by rewriting (4) as follows:

$$z_{12} = As + \sum_{i=1}^{n} (-1)^{n-i+1} A|\rho_i| \frac{s}{s^2 + \omega_i^2}. \tag{6}$$

The expression for the impedance z_{22} of the ladder is a simple consequence of (2), (6), and the fact that the z_{ij} are compact.[1] The expression is

$$z_{22} = As + \sum_{i=1}^{n} \frac{A^2|\rho_i|^2}{a_i} \frac{s}{s^2 + \omega_i^2}. \tag{7}$$

Expressions (2), (6), and (7) enable one to express the (given) impedance Z in terms of the parameters of the (desired) impedance z_{11}. Reference to the Tee equivalent of the ladder shows that

$$Z = z_{11} + z_{22} - 2z_{12}. \tag{8}$$

Substitution of (2), (6), and (7) in (8) leads to the following expression for Z

$$Z = \sum_{i=1}^{n} \frac{1}{a_i} \left[a_i + (-1)^{n-i} A|\rho_i| \right]^2 \frac{s}{s^2 + \omega_i^2}. \tag{9}$$

If the impedance Z that results when z_{11} is developed into a ladder is to coincide with the (given) impedance (1), then (9) must coincide with (1). Thus the parameters of z_{11} must satisfy the equations

$$\frac{1}{a_i} \left[a_i + (-1)^{n-i} A|\rho_i| \right]^2 = k_i \qquad \text{for } i = 1, 2, \ldots n. \tag{10}$$

The requirement for Z to be realizable as shown in Fig. XXX-2 is that Eqs. 10 admit of positive real solutions for A and the a_i.

Equations 10 may explicitly be solved for the a_i in terms of the parameter A, through use of the quadratic formula. The resulting expressions are

$$a_i = \left[\frac{k_i}{2} + (-1)^{n-i+1} A|\rho_i|\right] \pm \sqrt{\frac{k_i^2}{4} + (-1)^{n-i+1} A|\rho_i|\, k_i} \qquad \text{for } i = 1, 2, \ldots n. \tag{11}$$

Examination of the expressions (11) reveals that all of the a_i are real and positive, provided

$$0 < A \leq \min. \left[\frac{k_n}{4|\rho_n|}, \frac{k_{n-2}}{4|\rho_{n-2}|}, \frac{k_{n-4}}{4|\rho_{n-4}|}, \text{ etc.}\right]. \tag{12}$$

Thus Eqs. 10 indeed admit of positive real solutions for the a_i and A, and, consequently, any impedance of the form (1) is realizable by N.

To realize a given impedance Z, one need only to

(i) select A in the interval (12),

(ii) determine the a_i from (11), and

(iii) develop (2) into a ladder.

Because (12) permits an infinite number of possible choices for A, the impedance Z always can be realized in an infinite number of ways. Further realization possibilities are introduced by the sign option in each of Eqs. 11.

To illustrate the procedure, we realize the impedance

$$Z = \frac{s}{s^2+1} + \frac{s}{s^2+2}. \tag{13}$$

Substitution of the values $k_1 = 1$, $k_2 = 1$, $\omega_1^2 = 1$, and $\omega_2^2 = 2$ in (5) leads to the values $\rho_1 = 1$ and $\rho_2 = -4$. Thus (12) amounts to the requirement

$$0 < A \leq \frac{1}{16}. \tag{14}$$

If A is chosen to be the maximum value allowed by (12), then (11) shows that

$$a_1 = \frac{9 \pm 4\sqrt{5}}{16} \quad \text{and} \quad a_2 = \frac{1}{4}. \tag{15}$$

If one elects the positive sign in the expression for a_1, and substitutes A, a_1, and a_2 in (2), the following expression results.

$$z_{11} = \frac{s^5 + [16+4\sqrt{5}]\, s^3 + [24+8\sqrt{5}]\, s}{16s^4 + 48s^2 + 32}. \tag{16}$$

When z_{11} is developed into a ladder, the realization of Z shown in Fig. XXX-3 is obtained.

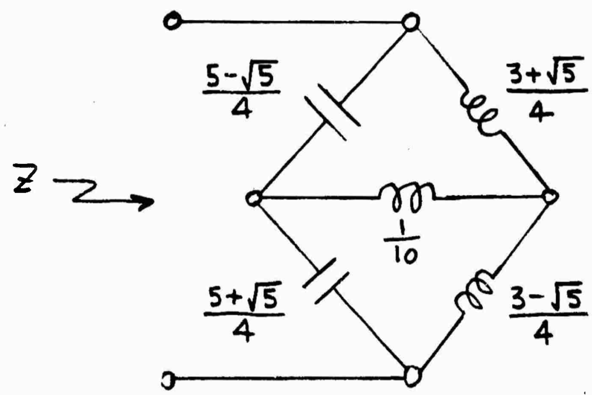

Fig. XXX-3.

By employing the same general approach that has just been described, and slightly varying the details, one can develop a number of related synthesis procedures. For example, one can develop synthesis procedures

(i) for the network that results when the inductors and capacitors of Fig. XXX-1 are interchanged;

(ii) for the dual of the network shown in Fig. XXX-1; and

(iii) for the dual of the network described in (i).

H. B. Lee

References

1. H. B. Lee, The physical meaning of compactness, IEEE Trans., Vol. CT-10, pp. 255-261, June 1963.

XXXI. COMPUTER RESEARCH*

Prof. J. B. Dennis
N. Kerllenevich
R. J. Levy

RESEARCH OBJECTIVES

The purpose of this group, which is operated jointly by the Research Laboratory of Electronics, the Electronic Systems Laboratory, and the Department of Electrical Engineering, M.I.T., is threefold:

1. To provide a flexible and readily accessible computation facility oriented toward the Laboratory's research goals.
2. To develop computation techniques, especially in the sense of increasing the convenience with which operating programs for particular tasks may be produced, and of allowing the scientist easy communication with the machine about tasks that are being performed for him.
3. To provide an education facility where students may learn the principles of automatic computation, and undergraduate and graduate theses and projects may be carried out.

Multi-user Computer Facility

During the past year, a multi-user computation facility built around the PDP-1 computer, which was given to the Department of Electrical Engineering, M. I. T., by the Digital Equipment Corporation, has been placed in operation. At present, the installation permits three persons to encode, test, and operate programs from individual typewriter stations using symbolic languages. A flexible arrangement for the operation of external equipment by time-sharing programs has been included in the system. One application of this feature is the guidance of a high-gain antenna in celestial coordinates for experiments of the Radio Astronomy Group of the Research Laboratory of Electronics (see "Research Objectives," Sec. III). The tracking computation may proceed in parallel with use of the machine by the three on-line users.

A paper that presents the philosophy of the system and many details of its design has been prepared.[1] Information on the use of the facility is contained in internal memoranda[2-7] which are available at the computer room.

J. B. Dennis

References

1. J. B. Dennis, A multi-user computation facility for education and research, September 1963 (submitted for publication to Communs. ACM).

2. Memorandum PDP-6, Time-Shared Operation of the Electrical Engineering PDP-1 Computer, May 22, 1962.

3. Memorandum PDP-11-1, Programming the PDP-1 Computer, July 29, 1963.

4. MACRO Assembly Program for Programmed Data Processor-1 (PDP-1), Digital Equipment Corporation, Maynard, Massachusetts, n. d.

*This work is supported in part by the National Science Foundation (Grant G-16526), the National Institutes of Health (Grant MH-04737-03), and the National Aeronautics and Space Administration (Grant NsG-496).

XXXII. ADVANCED COMPUTATION SYSTEMS

Prof. H. M. Teager
Prof. T. G. Stockham, Jr.
A. L. Scherr
D. U. Wilde

RESEARCH OBJECTIVES

The objectives of this group are to develop and evaluate devices, languages, and programming systems in order to facilitate on-line communication and creative interaction between researchers and computers.

Although the effort is meant to provide results that are generally applicable to many research areas, present study is centered about the specific application areas of linear systems analysis, discrete systems analysis, and plasma physics simulations.

Device development is proceeding on a graphical input table for entry and recognition of hand-drawn symbols and figures. Study continues on a multiplexed display and reproduction system for storage and retrieval of analogue and digital pictorial data, with television and facsimile reproduction technique utilized.

To round out the picture, studies are under way on issues of definition of computer capacity, and translation of problem statements into information processing requirements.

Doctoral thesis work is also under way on computer-system simulation techniques and program analysis.

H. M. Teager

XXXIII. STROBOSCOPIC RESEARCH

Prof. H. E. Edgerton
J. F. Carson
J. A. McMorris II

RESEARCH OBJECTIVES

The goal of our work with electronic flash is twofold. First, there is an intense desire to know more about the fundamental processes that occur in flash lamps so that faster, brighter, special lamps can be designed for all sorts of performance. Second, there is an unending demand for electronic flash sources to help obtain data and radiation for all sorts of research and production problems. To properly design the flash equipment, the designer must go into the problem at hand so that he can obtain useful important data in an efficient or accurate manner.

For several years there has been intense interest in the laser device. We are furnishing flash lamps that are specially designed for good optical coupling to the ruby crystal.

There is also interest in photographing small, high-velocity particles such as those that will be encountered by space ships. The duration required for this photography is approximately 10^{-8} second. Some work has been accomplished with such a short flash, and further work is under way.

For more than ten years we have worked on many applications of electronic flash-lighting equipment to underwater research with partial financial help from the National Geographic Society and interested individuals. This work has been greatly stimulated by the addition of a pressure-testing facility in Room 20D-009, M. I. T. We have assisted with the photographic devices for both existing bathyscaphes, and we have helped with the design of new photographic gear for the French bathyscaphe that is being built for ultimate depths.

H. E. Edgerton

Author Index